

**PHOTOPHYSICAL STUDIES OF SMALL
LIGANDS AND THEIR INTERACTION WITH
BIOLOGICAL MACROMOLECULES**

THESIS

**SUBMITTED FOR THE DEGREE OF
DOCTOR OF PHILOSOPHY (SCIENCE)**

OF

JADAVPUR UNIVERSITY

2008

BY

DEBAPRIYA BANERJEE

**DEPARTMENT OF CHEMICAL, BIOLOGICAL AND
MACROMOLECULAR SCIENCES,
S. N. BOSE NATIONAL CENTRE FOR BASIC SCIENCES,
BLOCK JD, SECTOR III, SALT LAKE,
KOLKATA 700 098, INDIA**

*To My Parents
and Aunt*

Acknowledgements

The thesis encompasses the work done as a research fellow (CSIR) of Satyendranath Bose National Centre for Basic Sciences, (SNBNCBS) Saltlake, Kolkata under the guidance of Dr. Samir Kumar Pal. I take this opportunity to express my sincere gratitude to Dr. Pal for the excellent academic guidance, care and concern bestowed upon me during my tenure as a research fellow. The eye for the minutest details regarding experimental work and the strict sense of discipline that he instilled in me as his student are surely the qualities which would be of immense importance in my academic and personal life in years to come.

I would also like to acknowledge the Director, SNBNCBS for providing the ambience and facilities for successful research activities undertaken at the centre. Thanks are also due to the faculty and staff of the institute whose activities and assistance at several instances were of great help in my research career. I would also acknowledge the Council of Scientific and Industrial Research, India for the fellowship.

I would like to acknowledge the past and present members of our research group (Dr. Rajib Kumar Mitra, Rupa, Ajay, Shankar, Nurul, Sudarson, Sachin, Protiti, Pramod, Abhinandan, Swati and Shantanu) for providing a homely and cheerful environment and also assisting me in research. Specially I would like to acknowledge Rupadi for introducing me to the experimental techniques, Sudarson for help in experiments and Rajibda for helpful discussions. I would also like to thank my classmates (PBIR Chem 2005 and Post M.Sc. 2005) and faculty associated with the course work I had to undertake as a part of the centre's PhD programme.

Acknowledgements are also due to the teachers of The Future Foundation School, Kolkata, for providing the foundations of my education. I would also like to thank my friends whose academic and moral support proved crucial in many critical junctures of my academic career.

Last but not the least I would like to thank my family for encouraging me to ascend the higher rungs of education. Without their sacrifices, moral support and blessings the thesis would not have taken its shape.

Dated:

*Department of Chemical, Biological
and Macromolecular Sciences,
S. N. Bose National Centre for Basic Sciences,
Salt Lake, Kolkata 700098,
India.*

(Debapriya Banerjee)

CONTENTS

Chapter 1: Introduction	Page
1.1. Scope of the Photophysical Studies on Small Ligands and their Interaction with Biological Macromolecules	1
1.2. Objective	2
1.3. Summary of the Work Done	5
I. Studies on Interaction of a Ligand to DNA: Exploration of Minor Groove Dynamics	5
A. Ultrafast Charge Transfer and Solvation of DNA Minor Groove Binder: Hoechst 33258 in Restricted Environments.	5
B. Direct Observation of Essential DNA Dynamics: Melting and Reformation of the DNA Minor Groove.	5
II. Exploration of Sequence Dependent Binding Modes of DNA	6
A. Excited State Solvation and Proton Transfer Dynamics of DAPI in Biomimetics and Genomic DNA.	6
B. Dynamics in the DNA Recognition by DAPI: Exploration of the Various Binding Modes.	7
III. Studies on the Special Binding Modes of DNA: Simultaneous Binding of Two Ligands in the Same Region of DNA	7
A. Simultaneous Binding of Minor Groove Binder and Intercalator to Dodecamer DNA: Importance of Relative Orientation of Donor and Acceptor in FRET.	7

	Page
IV. Studies on Noncovalent Interactions of Small Ligands with Protein	8
A. Spectroscopic Studies on Ligand-Enzyme Interactions: Complexation of α -Chymotrypsin by 4',6-Diamidino-2-phenylindole (DAPI).	8
B. Solvation Dynamics of LDS 750 in Micelles, Reverse Micelles and Proteins.	8
C. Molecular Recognition in Partially Folded States of a Transporter Protein: Temperature-Dependent Specificity of Bovine Serum Albumin.	9
V. Specific Interaction of a Small Ligand with an Enzyme: Relevance of Environmental Dynamics at the Active Site to Enzymatic Activity	9
A. Conformational Dynamics at the Active Site of α -Chymotrypsin and Enzymatic Activity.	10
VI. Role of Hydration Barrier in the Biomolecular Recognition by Small Ligands	10
A. Interplay between Hydration and Electrostatic Attraction in Ligand Binding: Direct Observation of Hydration Barrier at Reverse Micellar Interface.	10
1.4. Plan of Thesis	11
References	13
Chapter 2: An Overview of Steady-State and Dynamical Tools and Systems	17
2.1. Steady-State and Dynamical Tools	17
2.1.1. Solvation Dynamics	17
(i) Theory	17

	Page
(ii) Experimental methods	22
2.1.2. Fluorescence Anisotropy	25
(i) Theory	26
(ii) Experimental methods	28
2.1.3. Arrhenius Theory of Activation Energy	30
2.1.4. Förster Resonance Energy Transfer (FRET)	31
2.1.5. Enzyme Kinetics	34
2.1.6. Adiabatic Compressibility	36
2.2. Systems	36
2.2.1. Organized Assemblies (Biomimetics)	36
A. Micelles	36
B. Reverse Micelles	37
2.2.2. Proteins	40
A. Bovine Serum Albumin (BSA)	40
B. α -Chymotrypsin (CHT)	41
2.2.3. Deoxyribonucleic Acids (DNAs)	42
2.2.4. Molecular Probes	44
A. 2'-(4-hydroxyphenyl)-5-[5-(4-methylpiperazine-1-yl)- -benzimidazo-2-yl-benzimidazole (Hoechst 33258, H258)	44
B. 4',6-diamidino-2-phenylindole (DAPI)	44
C. 2-[4-[4-(dimethylamino) phenyl]-1,3-butadienyl]-3-ethyl -naphtho [2,1-d] thiazolium perchlorate (LDS 750)	44
D. Coumarin 500 (C-500)	44
E. Ala-Ala-Phe-7-amido-4-methylcoumarin (AAF-AMC)	45
F. 2- <i>p</i> -toluidinonaphthalene-6-sulfonate (TNS)	45
G. 1-anilino-8-naphthalenesulfonic acid, ammonium salt (ANS)	47
H. Ethidium Bromide (EB)	47
I. 4-(dicyanomethylene)-2-methyl-6-(<i>p</i> -dimethylaminostyryl) 4H-pyran (DCM)	48

	Page
J. Proflavin	48
K. <i>p</i> -nitrophenyl anthranilate	48
References	49

Chapter 3: Instrumentation and Sample Preparation

3.1. Instrumental Setup	55
3.2. Sample Preparation	63
3.2.1. Preparation of Reverse Micellar Solution	64
3.2.2. Preparation of Synthetic and Genomic DNA Solutions	64
3.2.3. Preparation of Dye-Protein Complexes	64
3.2.4. Preparation of Dye-DNA Complexes	65
3.2.5. Measurement of Enzymatic Activity of α -Chymotrypsin (CHT)	65
3.2.6. Preparation of Anthraniloyl-CHT (ANT-CHT) complex	65
References	66

Chapter 4: Studies on Interaction of a Ligand to DNA:

Exploration of Minor Groove Dynamics

4.1. Introduction	67
4.2. Results and Discussion	67
4.2.1. Ultrafast Charge Transfer and Solvation of DNA Minor Groove Binder: Hoechst 33258 in Restricted Environments.	67
4.2.2. Direct Observation of Essential DNA Dynamics: Melting and Reformation of the DNA Minor Groove.	76
4.3. Conclusion	85
References	87

	Page
Chapter 5: Exploration of Sequence Dependent Binding	
Modes of DNA	
5.1. Introduction	90
5.2. Results and Discussion	91
5.2.1 Excited State Solvation and Proton Transfer	
Dynamics of DAPI in Biomimetics and Genomic DNA.	91
5.2.2 Dynamics in the DNA Recognition by DAPI:	
Exploration of the Different Binding Modes.	108
5.3. Conclusion	114
References	115
Chapter 6: Studies on the Special Binding Modes of DNA:	
Simultaneous Binding of Two Ligands in the Same	
Region of DNA	
6.1. Introduction	120
6.2. Results and Discussion	121
6.2.1. Simultaneous Binding of Minor Groove Binder	
and Intercalator to Dodecamer DNA: Importance of Relative	
Orientation of Donor and Acceptor in FRET.	121
6.3. Conclusion	130
References	131
Chapter 7: Studies on Noncovalent Interactions of Small	
Ligands with Protein	
7.1. Introduction	134
7.2. Results and Discussion	134

	Page
7.2.1. Spectroscopic Studies on Ligand-Enzyme Interactions: Complexation of α -chymotrypsin by 4',6-diamidino-2-phenylindole (DAPI).	134
7.2.2. Solvation Dynamics of LDS 750 in Micelles, Reverse Micelles and Proteins.	144
7.2.3. Molecular Recognition in Partially Folded States of a Transporter Protein: Temperature- Dependent Specificity of Bovine Serum Albumin.	151
7.3. Conclusion	197
References	167

**Chapter 8: Specific Interaction of a Small Ligand with an
Enzyme: Relevance of Environmental Dynamics
at the Active Site to Enzymatic Activity**

8.1. Introduction	173
8.2. Results and Discussion	174
8.2.1 Conformational Dynamics at the Active Site of α -Chymotrypsin and Enzymatic Activity.	174
8.3. Conclusion	185
References	187

**Chapter 9: Role of Hydration Barrier in the Biomolecular
Recognition by Small Ligands**

9.1 Introduction	190
9.2. Results and Discussion	191
9.2.1. Interplay between Hydration and Electrostatic Attraction in Ligand Binding: Direct Observation of Hydration Barrier at Reverse Micellar Interface.	191

	Page
9.3. Conclusion	198
References	200
List of Publications	203

Chapter 1

Introduction

1.1. Scope of the Study on Photophysical Studies of Small Ligands and their Interaction with Biological Macromolecules:

Evolution has produced chemical compounds exquisitely organized to accomplish the most complicated and delicate of tasks [1]. Molecular interactions form the basis of highly specific recognition, reaction, transport and regulation, which are fundamental to all life processes [2,3]. The binding of substrates to receptor proteins, enzymatic reactions, immunological antigen-antibody association, intermolecular reading, translation and transcription of the genetic code [4-6], signal induction by neurotransmitters [7], and cellular recognition are representative examples where a small ligand binds to biological macromolecules like proteins and DNA. A thorough knowledge of the structural, dynamical and energetic parameters that dictate such molecular interactions can find immense use in the modulations of the ligand-macromolecule interaction [8-10] which can have tremendous application in medicine [11]. These ligand-macromolecule interaction are quite subtle and complex, calling for a successful integration of multidisciplinary research. In this respect, experimental biophysics forms a very strong pillar on which the foundations of the studies of ligand-macromolecule interaction are based on and photophysical studies are undoubtedly its efficient tools [12]. In photophysics, the fate of a target molecule is monitored consequent to the absorption of radiation of appropriate frequency. The results of photophysical studies provide a wealth of information not only about the target molecule but also on the environment it resides. By the exploitation of sophisticated photophysical techniques like solvchromism [13], fluorescence anisotropy, temporal evolution of the emission spectrum [14], Förster resonance energy transfer [15] and fluorescence detected circular dichroism, the interactions of ligands with macromolecules can be characterized with ease and considerable accuracy.

The focus of this thesis is to exploit the photophysics of suitable target molecules using steady-state and time-resolved absorption and fluorescence spectroscopic techniques to study the interaction of ligands with biological macromolecules like proteins and DNA. Important aspects of ligand-DNA interaction including sequence dependence of the binding modes of same ligand, simultaneous binding of an intercalator and minor groove binder in the same region of DNA have been explored. The specificity of noncovalent ligand-protein interaction in native and in the different unfolded states of a transporter protein is also explored. The contributions of macromolecular dynamics in the interaction of ligands with macromolecules have been established in relation to DNA minor groove binding and the enzymatic activity of the proteolytic enzyme α -chymotrypsin. We have also demonstrated the interplay of hydration and electrostatic interactions in ligand binding at a charged macromolecular surface. We have used conventional fluorophores as target molecules and the above mentioned photophysical tools to characterize the recognition of macromolecules by ligands. The secondary and tertiary structures of the proteins and DNAs used in our studies have been adjudged from steady-state absorption, circular dichroism (CD) and dynamic light scattering (DLS) techniques.

1.2. Objective:

Interaction of small ligands with biological macromolecules like proteins and DNA are crucial for vital life processes. The double helical DNA binds various ligands like proteins, mutagenic agents and drug molecules. There are two principal modes of ligand DNA interaction, namely, intercalation and minor groove binding. The binding of ligands to DNA are associated with the structural complementarity and favorable electrostatic interactions: the planar ligands sandwich themselves between adjacent base pairs as intercalators, whereas crescent shaped molecules snugly fit into the minor groove of the double helical DNA [16,17]. Recently Zewail et al. [18] have established that the dynamics of hydration is crucial for the recognition of the DNA minor groove by small ligands. However, due to the limited experimental window (200 ps) used in the study, the contributions of the internal twisting and bending motions of DNA to the recognition process have not been identified. One of our studies [19] summarizes the attempt to use

the fluorescent antihelminthic minor groove binder Hoechst 33258 (H258) to report the contribution of DNA dynamics in minor groove ligand binding. The suitability of H258 to report the slower DNA dynamics is confirmed from a study of its internal photophysics in bulk solvents and representative biomimetic systems. The study has been continued to decouple the dynamics which is crucial to the minor groove from the overall DNA dynamics [20], thus establishing the correlation between the structure and dynamics of the minor groove, which is extremely important for minor groove recognition by ligands.

The design of molecules that recognize specific sequences of the DNA can provide new tools to control gene expression and a rational basis for fresh approaches in drug development. The same drug/ligand can bind differently to different DNA sequences [21,22]. Of the two modes of ligand binding to double helical DNA, namely intercalative and minor groove binding, the minor groove binding is the more sequence selective owing to its greater exposure to the base pairs [16]. These different binding modes of a ligand to DNA might leave its signature in the excited state photophysics of the ligand in the different environments. The sequence dependent principal binding modes of the phenylindole derivative DAPI have been explored through photophysical and solvation studies [23].

In addition to the sequence dependent binding modes, certain special binding modes of dyes to DNA are clinically important. Given the interesting observation that mutagens are DNA intercalators [24] and anticancer drugs are mainly bound in the minor groove [25], exploration of the distance of closest approach of these two types of drugs can open new areas in cancer therapy. However, the possibility of simultaneous binding of anticancer drugs and mutagens to the same region of DNA has not been previously explored. Since the intercalator and minor groove binder are expected to bind to the same region of DNA having a specific geometry, the possibility of energy transfer from one system to the other needs to be considered. Our studies on the potential intercalator Ethidium Bromide (EB) and the minor groove binder H258 [26] attempt to explore the above possibilities.

Noncovalent interactions between ligands and macromolecules are perhaps best exemplified in the case of transporter proteins like serum albumins [27]. Although the

serum albumins in the mammalian blood stream are primarily associated with lipid transport, these proteins are also carrier of several important drugs like diazepam, ibuprofen and warfarin [27]. The binding of these drugs to the protein are primarily through electrostatic, van der Waals and hydrophobic interactions. The specific ligand binding in transporter proteins can be exploited for the selective transport of substances and the exploration of the specificity of ligand binding in the different unfolded states of the proteins is indicative of the robustness of the transport mechanism. The binding of the fluorescent dyes DCM and LDS 750 to a specific site in bovine serum albumin (BSA) in native form and in the different unfolded states have been studied [28] to understand the specificity of ligand binding in the transporter protein. Similarly, the noncovalent attachment of the phenylindole derivative DAPI to different sites in structurally analogous serine proteases trypsin and α -chymotrypsin [29] also exemplifies specificity of noncovalent interaction in proteins.

One of the most specific reaction in the physiological milieu is the catalysis of substrates by enzymes. Enzymes specifically catalyze the hydrolysis, oxidation and reduction reactions of various substrates. The specificity of enzyme catalysis was proposed to rest on the induced fit of the substrate in the active site of the enzyme. The positioning of the substrate in the active site of the enzyme was such that it allowed favorable interactions with the protein side chain residues in the active site. However, in recent years it has been proposed that the intrinsic dynamics of proteins are also responsible for the enzymatic activity [30]. Conformational changes in the protein active site assist the catalytic process and a new coordinate, called the conformational coordinate have been proposed in addition to the reaction coordinate to describe the catalytic process [31]. In one of our studies [32] we have shown how the dynamics of a serine residue present at the active site of the enzyme assists the temperature dependent enzymatic activity.

Electrostatic interactions and hydration plays an important role in the interactions of a ligand molecule at a bio-interface. The charge at the bio-interface leaves impression on the hydration structure [33] and dynamics [34]. In turn, the hydration at the biomolecular interface dilutes the electrostatic interaction between the charged interface and the oppositely charged ligand, preventing approach of the latter towards the interface.

Although the effect of interfacial charge to surface hydration have been studied [34], but the interplay of charge and hydration in molecular recognition remains unexplored. In this work, the interplay between electrostatic attraction and hydration at the interface of the negatively charged reverse micelle at different temperatures has been addressed [35].

1.3. Summary of the Work Done:

I. Studies on the Interaction of a Ligand to DNA: Exploration of Minor Groove Dynamics:

A. Ultrafast Charge Transfer and Solvation of DNA Minor Groove Binder Hoechst 33258 in Restricted Environments [19].

In this study, picosecond resolved photophysical studies on a DNA minor groove binder, Hoechst 33258 (H258) in bulk buffer and various restricted media including DNA reveal excited state charge transfer as an important mode of excited state relaxation. The charge transfer is found to be essentially associated with intramolecular twisting of the probe, being absent in SDS micellar environment and in DNA where twisting is hindered. Solvation and rotational dynamics of the probe in various restricted media including DNA are explored. A significantly longer component (8.5 ns) in DNA dynamics, which is well known to be associated with δ -relaxation of the DNA, is identified.

B. Direct Observation of Essential DNA Dynamics: Melting and Reformation of the DNA Minor Groove [20].

In this section, the dynamics of bound water and ions present in the minor groove of a dodecamer DNA has been decoupled from that of the long range twisting/bending of DNA backbone, using the minor groove binder H258 as a fluorescence reporter in the picosecond resolved time window. The bound water and ions are an essential structural component of the minor groove and are destroyed with the destruction of the minor groove when the dodecamer melts at high temperatures and reforms on subsequent cooling of the melted DNA. The melting and rehybridization of the DNA has been monitored by the changes in secondary structure using CD spectroscopy. The change in the relaxation dynamics of the DNA has been studied with picosecond resolution at

different temperatures, following the temperature dependent melting and rehybridization profile of the dodecamer, using time resolved emission spectra (TRES). At room temperature, the relaxation dynamics of DNA is governed by 40 ps(30%) and 12.3 ns(70%) components. The dynamics of bound water and ions present in the minor groove is characterized by the 40 ps component in the relaxation dynamics of the probe bound in the minor groove of the dodecamer DNA. Analyses of the TRES taken at different temperatures show that this component ultimately vanishes with the destruction of the minor groove. The dynamics again reappears with the reformation of the groove.

II. Exploration of Sequence Dependent Binding Modes of DNA:

A. Excited State Solvation and Proton Transfer Dynamics of DAPI in Biomimetics and Genomic DNA [36].

The fluorescent probe DAPI (4',6 Diamidino-2-phenylindole) is an efficient DNA binder. Studies on the DAPI-DNA complexes show that the probe exhibits a wide variety of interaction of different strength and specificity with DNA. Recently, the probe has been used to report the environmental dynamics of a DNA minor groove. However, the use of the probe as a solvation reporter in restricted environments is not straightforward. This is due to the presence of two competing relaxation processes (intramolecular proton-transfer and solvation stabilization) in the excited state, which can lead to erroneous interpretation of the observed excited state dynamics. In this study, the possibility of using DAPI to unambiguously report the environmental dynamics in restricted environments including DNA is explored. The dynamics of the probe is studied in bulk solvents, micelles, reverse micelles and genomic DNA using steady-state and picosecond resolved fluorescence spectroscopy.

B. Dynamics in the DNA Recognition by DAPI: Exploration of the Various Binding Modes [23].

In this study, the dynamics of solvation have been utilized to explore the binding of DAPI to DNA oligomers of different sequences. Picosecond resolved fluorescence and polarization gated anisotropy have been used to characterize the binding of DAPI to the different oligomers. In the double stranded dodecamer of sequence CGCGAATTCGCG

(oligo1), the solvation relaxation dynamics of the probe reveals time constants of 0.130 ns(75%) and 2.35 ns(25%). In the double stranded dodecamer (oligo2) having the sequence GCGCGCGCGCGC, where intercalation has been reported in literature, no solvation is observed in our experimental window. DAPI bound to oligo2 shows quenching of fluorescence compared to that of DAPI in buffer. The quenching of fluorescence of DAPI intercalated in DNA is also borne out by the appearance of a fast component of 30 ps in the fluorescence lifetime, revealing electron transfer to DAPI from GC base pairs, between which it intercalates. In addition to this, the excited state lifetime of the probe in the DAPI-DNA complex also shows a time constant similar to that of the dye in buffer, indicating that the excited state photoprocesses associated with the free dye are also operative in this binding mode, consistent with the binding geometry of DAPI in DNA. Our studies clearly explore the structure-dynamics correlation of DAPI-DNA complex and the two distinct modes of binding of DAPI with DNA.

III. Studies on the Special Binding Modes of DNA: Simultaneous Binding of Two Ligands in the Same Region of DNA:

A. Simultaneous Binding of Minor Groove Binder and Intercalator to Dodecamer DNA: Importance of Relative Orientation of Donor and Acceptor in FRET [26].

In the study, steady-state, picosecond resolved fluorescence and polarization gated anisotropy have been used to establish simultaneous binding of an intercalator EB and a minor groove binder H258 to a dodecamer DNA of specific sequence. The Förster resonance energy transfer (FRET) studies between the dyes H258 (donor) and EB (acceptor) bound to the dodecamer, where the ligands have a particular relative orientation of the transition dipoles, in contrast to the cases in SDS micelle and larger genomic DNA, where the orientations are random, reveal the effect of binding geometry of the ligands in the constrained environment. Our study establishes that reconsideration of the value of orientation factor, κ^2 is crucial for correct estimation of the donor-acceptor distance when the ligands are simultaneously bound to a specific region of biological macromolecule.

IV. Studies on the Noncovalent Interactions of Small Ligands with Protein:

A. Spectroscopic Studies on Ligand-Enzyme Interactions: Complexation of α -Chymotrypsin by 4',6-Diamidino-2-phenylindole (DAPI) [29].

Here, the effect of structural modifications in molecular recognition of two structurally related proteolytic enzymes trypsin and α -chymotrypsin (CHT) by 4',6-Diamidino-2-phenylindole (DAPI) has been addressed. The binding of DAPI to CHT has been characterized by steady-state and picosecond resolved spectroscopic techniques. Enzymatic activity of CHT in the presence of DAPI and binding of the well known inhibitor proflavin (PF) in the presence of DAPI clearly rule out the possibility of DAPI binding at the catalytic site of the enzyme. The spectral overlap between the emission of DAPI and absorption of PF offers the opportunity to explore the binding site of DAPI using FRET. FRET studies between DAPI and PF indicate that DAPI is bound to CHT with its transition dipole nearly perpendicular to that of PF. Competitive binding of DAPI with another fluorescent probe 2,6-*p*-Toluidinonaphthalene sulfonate (TNS), having well defined binding site, indicates that DAPI and TNS bind at the same hydrophobic site of CHT.

B. Solvation of LDS 750 in Micelles, Reverse Micelles and Proteins [37].

In this work, the interaction of the probe LDS 750 (LDS) with biomimetics and the transporter protein bovine serum albumin (BSA) have been characterized through steady-state, picosecond resolved fluorescence and polarization-gated anisotropy. Competitive binding studies with well known BSA binding drugs warfarin and diflunisal shows that LDS binds in domain III of the protein. TRES have been used to explore the environmental dynamics in the different systems. The dynamics of the environmental relaxation suggest that the LDS resides at the interface of the micelles and has an affinity for the water pool in the reverse micelles. The time resolved area normalized spectra (TRANES) of LDS in BSA suggest that the probe has a single binding site in the protein.

C. Molecular Recognition in Partially Folded States of a Transporter Protein: Temperature-Dependent Specificity of Bovine Serum Albumin [28].

The specificity of molecular recognition of bovine serum albumin (BSA) in its different partially folded states has been reported in this section. In order to avoid complications due to chemical denaturation, we have prepared thermally induced partially folded states of the protein. The partially folded states have been structurally characterized by CD and differential thermal analysis (DTA) techniques. The change in the globular structure of the protein as a consequence of thermal unfolding has also been characterized by DLS. Steady-state, picosecond resolved fluorescence and polarization gated anisotropy on the ligands (DCM, LDS) in the protein reveal the dynamics of the binding sites and the specificity of ligand binding in BSA. Picosecond resolved FRET studies on the DCM (donor) and LDS (acceptor) confirm that the specificity of ligand binding in the binding site is maintained up to 70⁰C. At 75⁰C, the protein loses its specificity of recognition at the aforesaid site.

V. Specific Interactions of a Small Ligand with an Enzyme: Relevance of Environmental Dynamics at the Active Site to Enzymatic Activity:

A. Conformational Dynamics at the Active Site of α -Chymotrypsin and Enzymatic Activity [32].

In this study, the role of dynamical flexibility at the active site of a proteolytic enzyme CHT has been correlated with its catalytic activity. The temperature dependent catalytic efficiency reveals a bell-shaped feature with a peak at 37⁰C, the typical body temperature of homeothermal animals. The overall structural integrity of the enzyme in our experimental temperature range have been confirmed from DLS and CD studies. We have followed the dynamical evolution at the active site of CHT with temperature using picosecond resolved fluorescence anisotropy of anthraniloyl probe (covalently attached to the serine-195 residue) and a substrate mimic (inhibitor) proflavin. The conformational dynamics at the active site is found to have direct correlation with the enzyme functionality. The conformational flexibility of the enzyme is also evidenced from the compressibility studies on the enzyme. The site selective fluorescence detected

circular dichroism (FDCD) studies reveal that the conformational flexibility of the enzyme has effect in the structural perturbation at the active site. We have also proposed the possible implications of the dynamics in the associated energetics.

VI. Role of Hydration Barrier in the Biomolecular Recognition by Small Ligands:

A. Interplay between Hydration and Electrostatic Attraction in Ligand Binding: Direct Observation of Hydration Barrier at Reverse Micellar Interface [35].

The recognition of a charged biomolecular surface by an oppositely charged ligand is governed by electrostatic attraction and surface hydration. In this study, the interplay between electrostatic attraction and hydration at the interface of a negatively charged reverse micelle (RM) at different temperatures has been addressed. Temperature dependent solvation dynamics of the probe H258 at the reverse micellar interface explore the nature of hydration at the interface. The interfacial dynamics becomes progressively faster with increasing temperature upto 45⁰C and follows the Arrhenius model. Above 45⁰C, the observed dynamics slows down with increasing temperature, thus deviating from the Arrhenius model. The slower dynamics at higher temperatures is due to the increasing contributions from the motions of the surfactant head groups, indicating the proximity of the probe to the interface at higher temperatures. This suggests an increased electrostatic attraction between the ligand and interface at higher temperatures and is attributed to the change in hydration. Densimetric and acoustic studies, indeed, show a drastic increase in the apparent specific adiabatic compressibility of the water molecules present in RMs after 45⁰C, revealing the existence of a softer hydration shell at higher temperatures. Our study indicates that the hydration layer at a charged interface, act both as physical and energetic barrier, to the electrostatic interactions of small ligands at the interface.

1.4. Plan of Thesis:

The plan of the thesis is as follows:

Chapter 1: This chapter gives a brief introduction to the scope and motivation behind the thesis work. A brief summary of the work done is also included in this chapter.

Chapter 2: This chapter provides an overview of the dynamical and steady-state tools, the structural aspects of biologically important systems (proteins, DNAs and biomimetics) and probes used in the research.

Chapter 3: Details of instrumentation, data analysis and experimental procedures have been discussed in this chapter.

Chapter 4: In this chapter, the study of the photophysical properties and solvation of the probe H258 in restricted environments including micelles, reverse micelles and genomic DNA have been reported. The use of this probe to explore the temperature dependent environmental dynamics associated with melting and reformation of the DNA minor groove is also included.

Chapter 5: The possibility of using the probe DAPI to unambiguously report environmental dynamics in restricted environments have been explored. The sequence dependent binding modes and proton transfer of the probe DAPI have been established through solvation techniques.

Chapter 6: In this chapter, we have discussed the possibility of simultaneous binding of the minor groove binder ligand H258 and the intercalator EB to the same region of the DNA, using FRET techniques. The importance of the binding geometry of the ligands acting as donor and acceptors, i.e. the relative orientation of the transition dipoles of the donor and acceptor in FRET has also been addressed.

Chapter 7: This chapter deals with the noncovalent binding modes of ligands with proteins. Here, the interaction of the ligand DAPI with the serine protease CHT has been addressed. The interactions of the probe LDS with micelles, reverse micelles and the transporter protein BSA have been studied. Simultaneous binding of ligands DCM and LDS in the native and the different folded states of BSA have also been studied.

Chapter 8: In this chapter, the role of conformational dynamics of the active site residues in the temperature dependent enzymatic activity of the protein CHT has been discussed.

Chapter 9: The role of the hydration barrier in the molecular recognition of a charged interface by small ligands has been included in this chapter.

References

- (1) R.M. Hazen, *Genesis: The scientific quest for life's origin*, Joseph Henry Press, 2005.
- (2) X. Luo, D. Zhang, H. Weinstein, Ligand-induced domain motion in the activation mechanism of a G-protein-coupled receptor, *Prot. Eng.* 7 (1994) 1441.
- (3) J.R. Warner, R. Soeiro, Involvement of RNA in protein synthesis, *New England Journal of Medicine* 276 (1967) 563.
- (4) J.M. Gottesfeld, L. Neely, J.W. Trauger, E.E. Baird, P.B. Dervan, Regulation of gene expression by small molecules, *Nature* 387 (1997) 202.
- (5) M.T. McManus, P.A. Sharp, Gene silencing in mammals by small interfering RNAs, *Nat. Rev. Genetics* 3 (2002) 737.
- (6) D.A. Koster, K. Palle, E.S.M. Bot, M.A. Bjornsti, N.H. Dekker, Antitumour drugs impede DNA uncoiling by topoisomerase I, *Nature* 448 (2007) 213.
- (7) C.R. Kahl, A.R. Means, Regulation of cell cycle progression by calcium/calmodulin-dependent pathways, *Endocr. Rev.* 24 (2003) 719.
- (8) S. White, J.W. Szewczyk, J.M. Turner, E.E. Baird, P.B. Dervan, Recognition of the four Watson-Crick base pairs in the DNA minor groove by synthetic ligands, *Nature* 391 (1998) 468.
- (9) P.B. Dervan, Design of sequence-specific DNA-binding molecules, *Science* 232 (1986) 464.
- (10) P.E. Nielsen, Design of sequence-specific DNA-binding ligands, *Chemistry Eur. J.* 3 (1997) 505.
- (11) C. Rodriguez-Galindo, K. Radomski, C.F. Stewart, W. Furman, V.M. Santana, P.J. Houghton, Clinical use of topoisomerase I inhibitors in anticancer treatment, *Med. Pediatr. Oncol.* 35 (2000) 385.
- (12) J.R. Lakowicz, Principles of fluorescence spectroscopy, *Kluwer Academic/Plenum*, New York, 1999.
- (13) R. Jin, K.J. Breslauer, Characterization of the minor groove environment in a drug-DNA complex: Bisbenzimidazole bound to the poly[d(AT)]·poly[d(AT)]duplex, *Proc. Natl. Acad. Sci. USA* 85 (1988) 8939.

- (14) S.K. Pal, A.H. Zewail, Dynamics of water in biological recognition, *Chem. Rev.* 104 (2004) 2099.
- (15) G.E. Plum, K.J. Breslauer, Fluorescence energy transfer monitored competitive equilibria of nucleic acids: Applications in thermodynamics and screening, *Biopolymers* 61 (2002) 214.
- (16) C. Helene, Reading the minor groove, *Nature* 436 (1998) 436.
- (17) K.J. Edwards, D.G. Brown, N. Spink, J.V. Skelly, S. Neidle, Molecular structure of the B-DNA dodecamer d(CGCAAATTTGCG)₂ : An examination of propeller twist and minor-groove water structure at 2.2 Å resolution, *J. Mol. Biol.* 226 (1992) 1161.
- (18) S.K. Pal, L. Zhao, A.H. Zewail, Water at DNA surfaces: Ultrafast dynamics in minor groove recognition, *Proc. Natl. Acad. Sci. USA* 100 (2003) 8113.
- (19) D. Banerjee, S.K. Pal, Ultrafast charge transfer and solvation of DNA minor groove binder: Hoechst 33258 in restricted environments, *Chem. Phys. Lett.* 432 (2006) 257.
- (20) D. Banerjee, S.K. Pal, Direct observation of essential DNA dynamics: Melting and reformation of the DNA minor groove, *J. Phys. Chem. B* 111 (2007) 10833.
- (21) N. Spink, D.G. Brown, J.V. Skelly, S. Neidle, Sequence-dependent effects in drug-DNA interaction: The crystal structure of Hoechst 33258 bound to the d(CGCAAATTTGCG)₂ duplex, *Nucl. Acids Res.* 22 (1994) 1607
- (22) W.D. Wilson, F.A. Tanious, H.K. Barton, R.L. Jones, K. Fox, R.L. Wydra, L. Strekowski, DNA sequence dependent binding modes of 4',6-Diamidino-2-phenylindole (DAPI), *Biochemistry* 29 (1990) 8452.
- (23) D. Banerjee, S.K. Pal, Dynamics in the DNA recognition by DAPI: Exploration of the various binding modes, *J. Phys. Chem. B* 112 (2007) 1016.
- (24) T.D. Sakore, S.C. Jain, C.C. Tsai, H.M. Sobell, Mutagen-nucleic acid intercalative binding: Structure of a 9-Amino-acridine: 5-iodocytidylyl(3'-5') guanosine crystalline complex, *Proc. Natl. Acad. Sci. USA* 74 (1977) 188.
- (25) Y. Hashimoto, K. Shudo, Chemical modification of DNA with mutagenic carcinogens. II. Base sequence-specific binding to DNA of 2-Amino-6-methyl-

- dipyrido [1,2-a:3',2'-d] imidazole (Glu-P-1), *Environ. Health Perspect.* 62 (1985) 215.
- (26) D. Banerjee, S.K. Pal, Simultaneous binding of minor groove binder and intercalator to dodecamer DNA: Importance of relative orientation of donor and acceptor in FRET, *J. Phys. Chem. B* 111 (2007) 5047.
- (27) J. Ghuman, P.A. Zunszain, I. Petitpas, A.A. Bhattacharya, M. Otagiri, S. Curry, Structural basis of the drug-binding specificity of human serum albumin, *J. Mol. Biol.* 363 (2005) 38.
- (28) D. Banerjee, S.K. Pal, Molecular recognition in partially folded states of a transporter protein: Temperature-dependent specificity of bovine serum albumin, *Photochem. Photobiol.* 84 (2008) 750.
- (29) D. Banerjee, S.K. Srivastava, S.K. Pal, Spectroscopic studies on ligand-enzyme interactions: Complexation of α -chymotrypsin with 4',6-Diamidino-2-phenylindole (DAPI), *J. Phys. Chem. B* 112 (2008) 1828.
- (30) E.Z. Eisenmesser, O. Millet, W. Labeikovsky, D.M. Korzhnev, M. Wolf-Watz, D.A. Bosco, J.J. Skalicky, L.E. Kay, D. Kern, Intrinsic dynamics of an enzyme underlies catalysis, *Nature* 438 (2005) 117.
- (31) W. Min, X.S. Xie, B. Bagchi, Two-dimensional reaction free energy surfaces of catalytic reaction: Effects of protein conformational dynamics on enzyme catalysis, *J. Phys. Chem. B* 112 (2008) 454.
- (32) D. Banerjee, S.K. Pal, Conformational dynamics at the active site of α -chymotrypsin and enzymatic activity, *Langmuir* 24 (2008) 8163.
- (33) V.M. Dadarlat, C.B. Post, Decomposition of protein experimental compressibility into intrinsic and hydration shell contributions, *Biophys. J.* 91 (2006) 4544.
- (34) A.V. Benderskii, K.B. Eisenthal, Aqueous solvation dynamics at the anionic surfactant air/water interface, *J. Phys. Chem. B* 105 (2001) 6698.
- (35) D. Banerjee, S.S. Sinha, S.K. Pal, Interplay between hydration and electrostatic attraction in ligand binding: Direct observation of hydration barrier at reverse micellar interface, *J. Phys. Chem. B* 111 (2007) 14239.
- (36) D. Banerjee, S.K. Pal, Excited-state solvation and proton transfer dynamics of DAPI in biomimetics and genomic DNA, *J. Phys. Chem. A* 112 (2008) 7314.

- (37) D. Banerjee, S.K. Pal, Solvation dynamics of LDS 750 in micelles, reverse micelles and proteins, *Chem. Phys. Lett.* 451 (2008) 237.

Chapter 2

An Overview of Steady-state and Dynamical Tools and Systems

In order to investigate the various processes involved in the course of study on photophysics of small ligands and their interaction with biological macromolecules, different steady-state and dynamical tools have been employed. These include solvation dynamics, fluorescence anisotropy, Förster resonance energy transfer (FRET), densimetric and acoustic measurements, enzyme kinetics and determination of activation energy using Arrhenius theory. In this chapter, we have included a brief discussion about the above mentioned dynamical tools. Overviews of the various systems and the fluorescent probes used in the studies have also been provided.

2.1. Steady-State and Dynamical Tools:

2.1.1. Solvation Dynamics: Almost all biological macromolecules, proteins (enzymes) and DNAs are inactive in the absence of water. Hydration of a protein/enzyme/DNA is particularly important for their structural stability and function, especially their recognition by ligand molecules. This role of hydration in enzymatic activity and molecular recognition of biomolecules [1-4] have recently been reviewed in a number of publications.

(i) Theory: Solvation dynamics refer to the process of reorganization of solvent dipoles around a dipole created instantaneously or an electron/proton injected suddenly in a polar liquid. In order to understand the meaning and scope of solvation dynamics, let us first visualize the physical essence of the dynamical process involved for a solute molecule in a polar solvent [5-7]. A change in the probe (solute) is made at time $t=0$, by an excitation pulse, which leads to the creation of a dipole. This dipole gives rise to an instantaneous electric field on the solvent molecules. The interaction of permanent dipoles of the solvent with the instantaneously created electric field, shifts the free energy minimum of the solvent to a non-zero value of the polarization. The solvent motion is crucial (figure 2.1).

Since the probe is excited instantaneously (a Franck-Condon transition as far as the nuclear degrees of freedom are concerned), the solvent molecules at $t=0$ find themselves in a relatively high-energy configuration. Subsequently, the solvent molecules begin to move and rearrange themselves to reach their new equilibrium positions (figure 2.2). The nuclear motion involved can be broadly classified into rotational and translational motions.

When the solvent is bulk water, rotational motion would also include hindered rotation, libration, while translation would include the intermolecular vibration due to the extensive hydrogen bonding. The two specific motions, libration and intermolecular vibration, are relatively high in frequency and are expected to play a dominant role in the initial part of solvation [8]. The molecular motions involved are shown schematically in

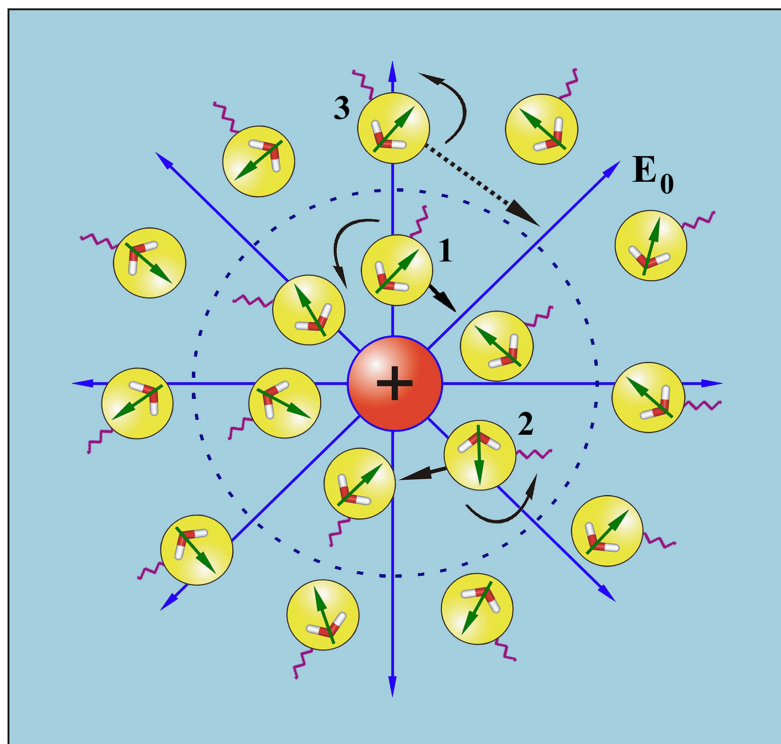


Figure 2.1. Schematic illustration of solvation of an ion (or dipole) by water. The neighboring molecules (numbered 1 and 2) can either rotate or translate to attain the minimum energy configuration. On the other hand, distant water molecule 3 can only rotate to attain minimum energy configuration. The field is shown as E_0 . The springs connected to the molecules are meant to denote hydrogen bonding.

figure 2.1, and in figure 2.3 we show a typical solvation time correlation function. For clarity, we approximate the motions responsible for the decay in different regions.

A simple way to address the dynamics of polar solvation is to start with the following expression for the solvation energy, $E_{\text{solv}}(t)$, [9]

$$E_{\text{solv}}(t) = -\frac{1}{2} \int d\mathbf{r} \mathbf{E}_0(\mathbf{r}) \cdot \mathbf{P}(\mathbf{r}, t) \quad (2-1)$$

where $\mathbf{E}_0(\mathbf{r})$ is the instantaneously created, position-dependent electric field from the ion or the dipole of the solute and $\mathbf{P}(\mathbf{r}, t)$ is the position and time-dependent polarization.

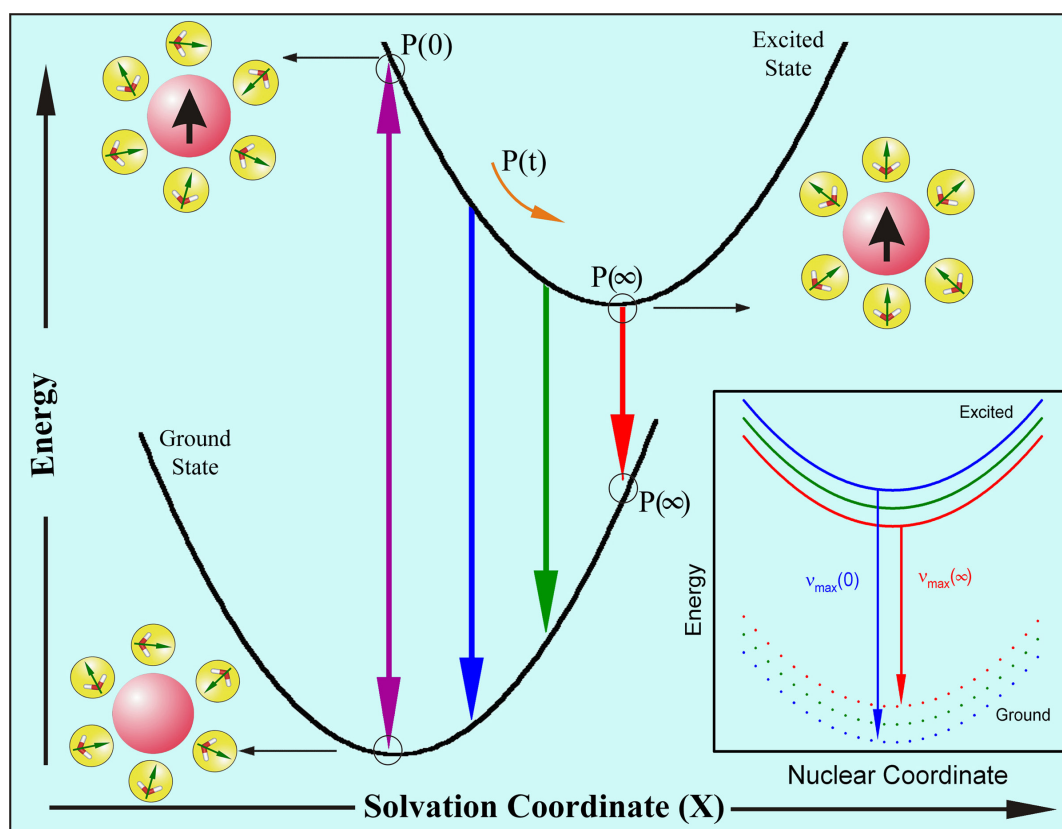


Figure 2.2. Schematic representation of the potential energy surfaces involved in solvation dynamics showing the water orientational motions along the solvation coordinate together with instantaneous polarization P . In the inset we show the change in the potential energy along the intramolecular nuclear coordinate. As solvation proceeds the energy of the solute comes down giving rise to a red shift in the fluorescence spectrum. Note the instantaneous P , e.g., $P(\infty)$, on the two connected potentials.

The latter is defined by the following expression,

$$\mathbf{P}(\mathbf{r},t) = \int d\Omega \boldsymbol{\mu}(\Omega) \rho(\mathbf{r},\Omega,t) \quad (2-2)$$

where $\boldsymbol{\mu}(\Omega)$ is the dipole moment vector of a molecule at position \mathbf{r} , and $\rho(\mathbf{r},\Omega,t)$ is the position, orientation and time-dependent density. Therefore, the time dependence of the solvation energy is determined by the time dependence of polarization that is in turn

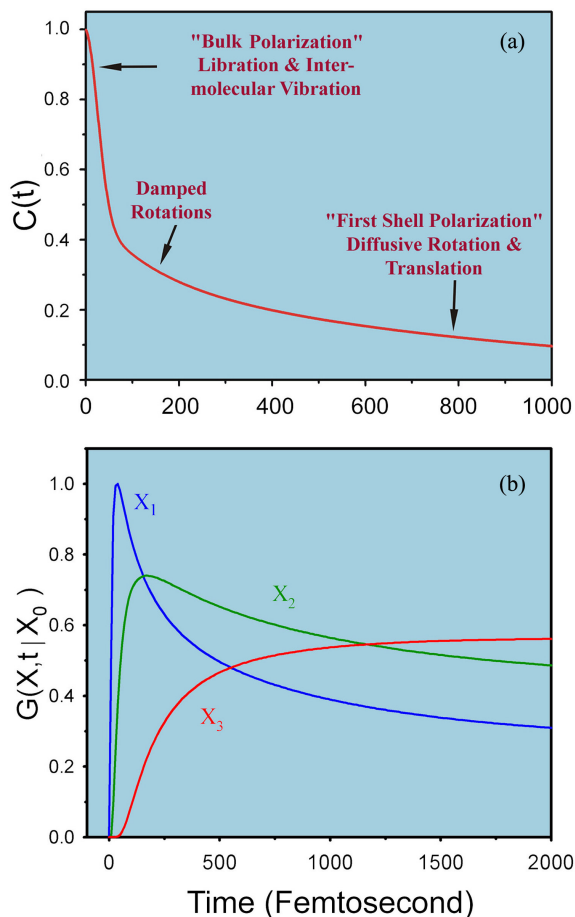


Figure 2.3. (a) A typical solvation time correlation function for water is shown here. The time correlation function exhibits three distinct regions: The initial ultrafast decay, an intermediate decay of about 200 fs and the last slow decay with time constant of 1 ps. The physical origin of each region is indicated on the plot itself; see text. (b) Green's function $G(X,t|X_0)$ for population relaxation along the solvation coordinate (X) is plotted against time in femtosecond. In G , X_0 is the initial position at $t=0$. This figure shows the position and time dependence of the population fluorescence intensity. At early times (when the population is at X_1) there is ultrafast rise followed by an ultrafast decay. At intermediate times (when the population is at X_2) there is a rise followed by a slow decay as shown by the green line. At long times when the population is nearly relaxed (position X_3 , red line) we see only a rise.

determined by the time dependence of the density. If the perturbation due to the probe on dynamics of bulk water is negligible, then the time dependence of polarization is dictated by the natural dynamics of the liquid.

The theoretical analysis of the time-dependent density is usually carried out using a molecular hydrodynamic approach that is based on the basic conservation (density, momentum and energy) laws and includes the effects of intermolecular (both spatial and orientational) correlations. The latter provides the free energy surface on which solvation proceeds. The equation of motion of the density involves both orientational and translational motions of the solvent molecules. The details of the theoretical development are reported in literature [5]; here we shall present a simple physical picture of the observed biphasic solvation dynamics.

Within linear response theory, the solvation correlation function is directly related to the solvation energy as,

$$C(t) = \frac{\langle \delta E(0) \cdot \delta E(t) \rangle}{\langle \delta E^2 \rangle} = \frac{\langle E(t) \rangle - \langle E(\infty) \rangle}{\langle E(0) \rangle - \langle E(\infty) \rangle} \quad (2-3)$$

where δE is the fluctuation of solvation energy from the average, equilibrium value. Note that the equality in equation (2-3) indicates the direct relation for the average of the fluctuations over the equilibrium distribution (left) and the non-equilibrium function (right) which relates to observables; without $\langle E(\infty) \rangle$ the correspondence is clear, and $\langle E(\infty) \rangle$ is rigorously the result of the equilibrium term in the numerator and for normalization in the denominator.

The ultrafast component in the solvation time correlation function (see figure 2.3(a)), originates from the initial relaxation in the steep collective solvation potential. The collective potential is steep because it involves the total polarization of the system [5,6]. This initial relaxation couples mainly to the hindered rotation (i.e., libration) and the hindered translation (i.e., the intermolecular vibration), which are the available high frequency modes of the solvent; neither long amplitude rotation nor molecular translation are relevant here. The last part in the decay of the solvation correlation function involves larger amplitude rotational and translational motions of the nearest neighbor molecules in the first solvation shell. In the intermediate time, one gets contributions from the moderately damped rotational motions of water molecules. In a sense, with the above

description one recovers the famous Onsager’s “inverse snow-ball” picture of solvation [10]. The slowest time constant is ~ 1 ps, which is determined by the individual rotational and translational motions of the molecules in the “first solvation shell” nearly close to the probe. The femtosecond component is dominated by the high frequency hindered rotational and translational (vibration) [8,11,12] polarization.

Figure 2.2 shows a schematic of the solvation potential and the orientational motions for the water molecules involved. From the shape of the potential, it can be seen that the transient behavior for the population during solvation should be a decay function on the blue edge of the spectrum and a rise function on the red edge. These wavelength-dependent features can be explained nicely within a generalized model of relaxation in which a Gaussian wave packet relaxes on a harmonic surface. The relaxation is non-exponential and a Green’s function can describe the approach of the wave packet along the solvation coordinate, X , to its equilibrium value. For the general non-Markovian case it is given by [13],

$$G(X, t|X_0) = \frac{1}{\sqrt{2\pi\langle X^2 \rangle [1 - C^2(t)]}} \exp \left[-\frac{[X - X_0 C(t)]^2}{2\langle X^2 \rangle [1 - C^2(t)]} \right] \quad (2-4)$$

where $\langle X^2 \rangle$ is the equilibrium mean square fluctuation of the polarization coordinate in the excited state surface, $C(t)$ is the solvation correlation function described in equation (2-3) and X_0 is the initial value of the packet on the solvation coordinate. Equation (2-4) describes the motion of the wave packet (polarization density) beginning at $t=0$ (X_0) as a delta function and according to the solvation time correlation function. As $t \rightarrow \infty$, $C(t) \rightarrow 0$ and we recover the standard Gaussian distribution. Initially, ($t \rightarrow 0$), the exponential is large, so the decay is ultrafast, but at long times, the relaxation slows down, ultimately to appear as a rise. In figure 2.3(b), we present calculations of $G(X, t|X_0)$ at different positions along the solvation coordinate giving decays at X_1 and X_2 , but with different time constants, and a rise at X_3 , as demonstrated experimentally.

(ii) Experimental Methods: In order to study solvation stabilization of a probe in an environment, a number of fluorescence transients are taken at different wavelengths across the emission spectrum of the probe. As described earlier, blue and red ends of the emission spectrum are expected to show decay and rise, respectively in the transients. The observed

fluorescence transients are fitted by using a nonlinear least square fitting procedure to a function

$$\left(X(t) = \int_0^t E(t')R(t-t')dt' \right) \quad (2-5)$$

comprising of convolution of the IRF (E(t)) with a sum of exponentials

$$\left(R(t) = A + \sum_{i=1}^N B_i \exp(-t/\tau_i) \right) \quad (2-6)$$

with pre-exponential factors (B_i), characteristic lifetimes (τ_i) and a background (A).

Relative concentration in a multi-exponential decay is finally expressed as;

$$\alpha_n = \frac{B_n}{\sum_{i=1}^N B_i} \quad (2-7)$$

The relative contribution of a particular decay component (f_n) in the total fluorescence is defined as,

$$f_n = \frac{\tau_n B_n}{\sum_{i=1}^N B_i \tau_i} \times 100 \quad (2-8)$$

The quality of the curve fitting is evaluated by reduced chi-square (0.9-1.1) and residual data. The purpose of the fitting is to obtain the decays in an analytical form suitable for further data analysis.

To construct time resolved emission spectra (TRES) we follow the technique described in references [14,15]. As described above, the emission intensity decays are analyzed in terms of the multi-exponential model,

$$I(\lambda, t) = \sum_{i=1}^N \alpha_i(\lambda) \exp(-t/\tau_i(\lambda)) \quad (2-9)$$

where α_i(λ) are the pre-exponential factors, with Σα_i(λ)=1.0. In this analysis we compute a new set of intensity decays, which are normalized so that the time-integrated intensity at each wavelength is equal to the steady-state intensity at that wavelength. Considering F(λ) to be the steady-state emission spectrum, we calculate a set of H(λ) values using,

$$H(\lambda) = \frac{F(\lambda)}{\int_0^{\infty} I(\lambda, t) dt} \quad (2-10)$$

which for multiexponential analysis becomes,

$$H(\lambda) = \frac{F(\lambda)}{\sum_i \alpha_i(\lambda) \tau_i(\lambda)} \quad (2-11)$$

Then, the appropriately normalized intensity decay functions are given by,

$$I'(\lambda, t) = H(\lambda)I(\lambda, t) = \sum_{i=1}^N \alpha'_i(\lambda) \exp\left(-t/\tau_i(\lambda)\right) \quad (2-12)$$

where $\alpha'_i(\lambda) = H(\lambda)\alpha_i(\lambda)$. The values of $I'(\lambda, t)$ are used to calculate the intensity at any wavelength and time, and thus the TRES. The values of the emission maxima and spectral width are determined by nonlinear least-square fitting of the spectral shape of the TRES. The spectral shape is assumed to follow a lognormal line shape [14],

$$I(\bar{\nu}) = I_0 \exp\left\{-\left[\ln 2 \left(\frac{\ln(\alpha + 1)}{b}\right)^2\right]\right\} \quad (2-13)$$

with $\alpha = \frac{2b(\bar{\nu} - \bar{\nu}_{\max})}{\Delta} - 1$ where I_0 is amplitude, $\bar{\nu}_{\max}$ is the wavenumber of the emission

maximum and spectral width is given by, $\Gamma = \Delta \left[\frac{\sinh(b)}{b} \right]$. The terms b and Δ are asymmetry and width parameters, respectively and equation (2-9) reduces to a Gaussian function for $b=0$.

The time-dependent fluorescence Stokes shifts, as estimated from TRES are used to construct the normalized spectral shift correlation function or the solvent correlation function $C(t)$ and is defined as,

$$C(t) = \frac{\bar{\nu}(t) - \bar{\nu}(\infty)}{\bar{\nu}(0) - \bar{\nu}(\infty)} \quad (2-14)$$

where, $\bar{\nu}(0)$, $\bar{\nu}(t)$ and $\bar{\nu}(\infty)$ are the emission maxima (in cm^{-1}) of the TRES at time zero, t and infinity, respectively. The $\bar{\nu}(\infty)$ value is considered to be the emission frequency beyond which insignificant or no spectral shift is observed. The $C(t)$ function represents

the temporal response of the solvent relaxation process, as occurs around the probe following its photoexcitation and the associated change in the dipole moment.

2.1.2. Fluorescence Anisotropy: Anisotropy is defined as the extent of polarization of the emission from a fluorophore. Anisotropy measurements are commonly used in biochemical applications of fluorescence. It provides information about the size and shape of proteins or the rigidity of various molecular environments. Anisotropy measurements have also been used to measure protein-protein associations, fluidity of membranes and for immunoassays of numerous substances. These measurements are based on the principle of photoselective excitation of those fluorophore molecules whose absorption transition dipoles are parallel to the electric vector of polarized excitation light. In an isotropic solution, fluorophores are oriented randomly. However, upon selective excitation, partially oriented population of fluorophores with polarized fluorescence emission results. The relative angle between the absorption and emission transition dipole moments determines the maximum measured anisotropy (r_0). The fluorescence anisotropy (r) and polarization (P) are defined by,

$$r = \frac{I_{\parallel} - I_{\perp}}{I_{\parallel} + 2I_{\perp}} \quad (2-15)$$

$$P = \frac{I_{\parallel} - I_{\perp}}{I_{\parallel} + I_{\perp}} \quad (2-16)$$

where I_{\parallel} and I_{\perp} are the fluorescence intensities of vertically and horizontally polarized emission when the fluorophore is excited with vertically polarized light. Polarization and anisotropy are interrelated as,

$$r = \frac{2P}{3 - P} \quad (2-17)$$

$$\text{and} \quad P = \frac{3r}{2 + r} \quad (2-18)$$

Although polarization and anisotropy provides the same information, anisotropy is preferred since the latter is normalized by total fluorescence intensity ($I_T = I_{\parallel} + 2I_{\perp}$) and in case of multiple emissive species anisotropy is additive while polarization is not. Several phenomena, including rotational diffusion and energy transfer, can decrease the measured anisotropy to values lower than maximum theoretical values. Following a pulsed excitation the fluorescence anisotropy, $r(t)$ of a sphere is given by,

$$r(t) = r_0 \exp(-t/\phi) \quad (2-19)$$

where r_0 is the anisotropy at time $t=0$ and ϕ is the rotational correlation time of the sphere.

(i) Theory: For a radiating dipole, the intensity of light emitted is proportional to the square of the projection of the electric field of the radiating dipole onto the transmission axis of the polarizer. The intensity of parallel and perpendicular projections are given by,

$$I_{\parallel}(\theta, \psi) = \cos^2 \theta \quad (2-20)$$

$$I_{\perp}(\theta, \psi) = \sin^2 \theta \sin^2 \psi \quad (2-21)$$

where θ and ψ are the orientational angles of a single fluorophore relative to the z and y-axes, respectively (figure 2.4(a)). In solution, fluorophores remain in random distribution and the anisotropy is calculated by excitation photoselection. Upon photoexcitation by polarized light, the molecules having absorption transition moments aligned parallel to the electric vector of the polarized light have the highest probability of absorption. For the excitation polarization along z-axis, all molecules having an angle ψ with respect to the y-axis will be excited. The population will be symmetrically distributed about the z-axis. For experimentally accessible molecules, the value of ψ will be in the range from 0 to 2π with equal probability. Thus, the ψ dependency can be eliminated.

$$\langle \sin^2 \psi \rangle = \frac{\int_0^{2\pi} \sin^2 \psi d\psi}{\int_0^{2\pi} d\psi} = \frac{1}{2} \quad (2-22)$$

$$\text{and } I_{\parallel}(\theta) = \cos^2 \theta \quad (2-23)$$

$$I_{\perp}(\theta) = \frac{1}{2} \sin^2 \theta \quad (2-24)$$

Consider a collection of molecules oriented relative to the z-axis with probability $f(\theta)$.

Then, measured fluorescence intensities for this collection after photoexcitation are,

$$I_{\parallel} = \int_0^{\pi/2} f(\theta) \cos^2 \theta d\theta = k \langle \cos^2 \theta \rangle \quad (2-25)$$

$$I_{\perp} = \int_0^{\pi/2} f(\theta) \sin^2 \theta d\theta = \frac{k}{2} \langle \sin^2 \theta \rangle \quad (2-26)$$

where $f(\theta)d\theta$ is the probability that a fluorophore is oriented between θ and $\theta+d\theta$ and is given by,

$$f(\theta)d\theta = \cos^2 \theta \sin \theta d\theta \quad (2-27)$$

k is the instrumental constant. Thus, the anisotropy (r) is defined as,

$$r = \frac{3\langle \cos^2 \theta \rangle - 1}{2} \quad (2-28)$$

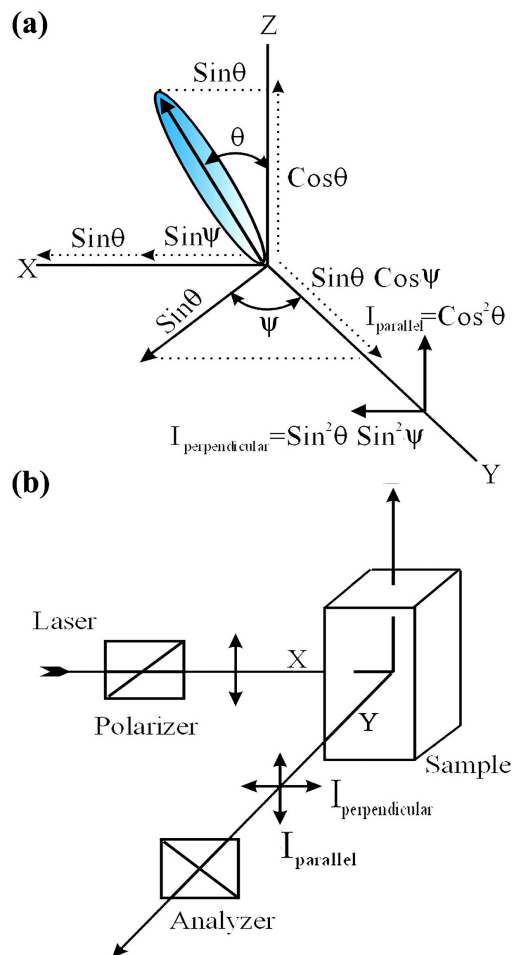


Figure 2.4. (a) Emission intensity of a single fluorophore (blue ellipsoid) in a coordinate system. (b) Schematic representation of the measurement of fluorescence anisotropy.

when $\theta=54.7^\circ$ i.e. when $\cos^2 \theta=1/3$, the complete loss of anisotropy occurs. Thus, the fluorescence taken at $\theta=54.7^\circ$ with respect to the excitation polarization is expected to be

free from the effect of anisotropy and is known as magic angle emission. For collinear absorption and emission dipoles, the value of $\langle \cos^2 \theta \rangle$ is given by the following equation,

$$\langle \cos^2 \theta \rangle = \frac{\int_0^{\pi/2} \cos^2 \theta f(\theta) d\theta}{\int_0^{\pi/2} f(\theta) d\theta} \quad (2-29)$$

Substituting equation (2-27) in equation (2-29) one can get the value of $\langle \cos^2 \theta \rangle = 3/5$ and anisotropy value to be 0.4 (from equation (2-28)). This is the maximum value of anisotropy obtained when the absorption and emission dipoles are collinear and when no other depolarization process takes place. However, for most fluorophores, the value of anisotropy is less than 0.4 and it is dependent on the excitation wavelength. It is demonstrated that as the displacement of the absorption and emission dipole occurs by an angle γ relative to each other, it causes further loss of anisotropy (reduction by a factor 2/5) [15] from the value obtained from equation (2-28). Thus, the value of fundamental anisotropy, r_0 is given by,

$$r_0 = \frac{2}{5} \left(\frac{3 \cos^2 \gamma - 1}{2} \right) \quad (2-30)$$

For any fluorophore randomly distributed in solution, with one-photon excitation, the value of r_0 varies from -0.2 to 0.4 for γ values varying from 90° to 0° .

(ii) Experimental Methods: For time resolved anisotropy ($r(t)$) measurements (figure 2.4(b)), emission polarization is adjusted to be parallel and perpendicular to that of the excitation polarization. Spencer and Weber [16] have derived the relevant equations for the time dependence of $I_{\parallel}(t)$ (equation (2-31)) and $I_{\perp}(t)$ (equation (2-32)) for single rotational and fluorescence relaxation times, ϕ and τ_f , respectively,

$$I_{\parallel}(t) = \exp(-t/\tau_f) (1 + 2r_0 \exp(-t/\phi)) \quad (2-31)$$

$$I_{\perp}(t) = \exp(-t/\tau_f) (1 - r_0 \exp(-t/\phi)) \quad (2-32)$$

The total fluorescence is given by,

$$F(t) = I_{\parallel}(t) + 2I_{\perp}(t) = 3 \exp(-t/\tau_f) = F_0 \exp(-t/\tau_f) \quad (2-33)$$

The time dependent anisotropy, $r(t)$ is given by,

$$r(t) = \frac{I_{\parallel}(t) - I_{\perp}(t)}{I_{\parallel}(t) + 2I_{\perp}(t)} = r_0 \exp(-t/\phi) \quad (2-34)$$

$F(t)$ depends upon τ_f and $r(t)$ only upon ϕ so that these two lifetimes can be separated. This separation is not possible in steady-state measurements. It should be noted that the degree of polarization (P) is not independent of τ_f and is therefore not as useful as r . For reliable measurement of $r(t)$, three limiting cases can be considered,

- (a) If $\tau_f < \phi$, the fluorescence decays before the anisotropy decays, and hence only r_0 can be measured.
- (b) If $\phi < \tau_f$, in contrast to steady-state measurements, ϕ can be measured in principle. The equations (2-31) and (2-32) show that the decay of the parallel and perpendicular components depends only upon ϕ . The experimental disadvantage of this case is that those photons emitted after the lapse of a few rotational correlation times, ϕ can not contribute to the determination of ϕ , but can be avoided with a good signal-to-noise ratio.
- (c) If $\phi \approx \tau_f$, then it becomes the ideal situation since almost all photons are counted within the time (equal to several rotational relaxation times) in which $r(t)$ shows measurable changes.

For systems with multiple rotational correlation times, $r(t)$ is given by,

$$r(t) = r_0 \sum_i \beta_i e^{-t/\phi_i} \quad (2-35)$$

where $\sum_i \beta_i = 1$. It should be noted that the instrument monitoring the fluorescence, particularly the spectral dispersion element, responds differently to different polarizations of light, thus emerging the need for a correction factor. For example, the use of diffraction gratings can yield intensities of emission, which depend strongly upon orientation with respect to the plane of the grating. It is necessary when using such instruments to correct for the anisotropy in response. This instrumental anisotropy is usually termed as G-factor (grating factor) and is defined as the ratio of the transmission efficiency for vertically polarized light to that for horizontally polarized light ($G = I_{\parallel} / I_{\perp}$). Hence, values of fluorescence anisotropy, $r(t)$ corrected for instrumental response, would be given by [17],

$$r(t) = \frac{I_{\parallel}(t) - GI_{\perp}(t)}{I_{\parallel}(t) + 2GI_{\perp}(t)} \quad (2-36)$$

The G-factor at a given wavelength can be determined by exciting the sample with horizontally polarized excitation beam and collecting the two polarized fluorescence decays, one parallel and other perpendicular to the horizontally polarized excitation beam. G-factor can also be determined following longtime tail matching technique [17]. If $\phi < \tau_f$, it can be seen that the curves for $I_{\parallel}(t)$ and $I_{\perp}(t)$ should become identical. If in any experiment they are not, it can usually be assumed that this is due to a non-unitary G-factor. Hence normalizing the two decay curves on the tail of the decay eliminates the G-factor in the anisotropy measurement.

2.1.3. Arrhenius Theory of Activation Energy: The dynamics of solvation at a biomolecular interface can be exploited to give information about the energetics of the participating water molecules [9]. As mentioned above, we consider two types of water, those bound to the surface and those that are free. In the water layer around the protein surface, the interaction with water involves hydrogen bonding to the polar and charged groups of the surface. The strength of this bonding varies from group to group. When strongly bonded to the protein, the water molecules cannot contribute to solvation dynamics because they can neither rotate nor translate. But the hydrogen bonding is transient, and there is a dynamic equilibrium between the free and the bound water molecules. The potential of interaction can be represented by a double-well structure to symbolize the processes of bond breaking and bond forming. In general, the bonded water molecules become free by translational and rotational motions. The experimental observations of a biphasic behavior of hydration indicated the presence of bound and free water in the surface layer.

bound \leftrightarrow free (rotating and translating)

The slow component of the solvation, is related to the rate constant for bound to free water interconversion k_{bf} as,

$$\frac{1}{\tau_{solv}} \approx k_{bf} = \frac{k_B T}{h} e^{-\frac{\Delta G_{bf}^0}{RT}} \quad (2-37)$$

where, ΔG_{bf}° is the binding energy for bound to free water interconversion, k_B is the Boltzmann constant, T , the absolute temperature and h is the Planck constant. This dynamic equilibrium is found to be dependent on external parameters like temperature, pressure etc. The temperature dependence of the solvation follows the Arrhenius equation and yields the activation energy needed for the conversion of bound and free forms [18].

2.1.4. Förster Resonance Energy Transfer: Förster resonance energy transfer (FRET) is an electrodynamic phenomenon involving the non-radiative transfer of the excited state energy from the donor dipole (D) to an acceptor dipole (A) in the ground state (figure 2.5(a)). FRET has got wide applications in all fluorescence applications including medical diagnostics, DNA analysis and optical imaging. Since FRET can measure the size of a protein molecule or the thickness of a membrane, it is also known as “spectroscopic ruler” [19]. FRET is very often used to measure the distance between two sites on a macromolecule. Basically, FRET is of two types: (a) Homo-molecular FRET and (b) Hetero-molecular FRET. In the former case the same fluorophore acts both as energy donor and acceptor, while in the latter case two different molecules act as donor and acceptor.

Each donor-acceptor (D-A) pair participating in FRET is characterized by a distance known as Förster distance (R_0) i.e., the D-A separation at which energy transfer is 50% efficient. The R_0 value ranges from 20 to 60 Å. The rate of resonance energy transfer (k_T) from donor to an acceptor is given by [15],

$$k_T = \frac{1}{\tau_D} \left(\frac{R_0}{r} \right)^6 \quad (2-38)$$

where τ_D is the lifetime of the donor in the absence of acceptor and r is the donor to acceptor (D-A) distance. The rate of transfer of donor energy depends upon the extent of overlap of the emission spectrum of the donor with the absorption spectrum of the acceptor ($J(\lambda)$), the quantum yield of the donor (Q_D), the relative orientation of the donor and acceptor transition dipoles (κ^2) and the distance between the donor and acceptor molecules (r) (figure 2.5(b)). In order to estimate FRET efficiency of the donor and hence to determine distances between donor-acceptor pairs, the methodology described below is followed [15]. R_0 is given by,

$$R_0 = 0.211[\kappa^2 n^{-4} Q_D J(\lambda)]^{1/6} \text{ (in \AA)} \quad (2-39)$$

where n is the refractive index of the medium, Q_D is the quantum yield of the donor and $J(\lambda)$ is the overlap integral. κ^2 is defined as,

$$\kappa^2 = (\cos\theta_T - 3\cos\theta_D \cos\theta_A)^2 = (\sin\theta_D \sin\theta_A \cos\phi - 2\cos\theta_D \cos\theta_A)^2 \quad (2-40)$$

where θ_T is the angle between the emission transition dipole of the donor and the absorption transition dipole of the acceptor, θ_D and θ_A are the angles between these dipoles and the vector joining the donor and acceptor and ϕ is angle between the planes of the

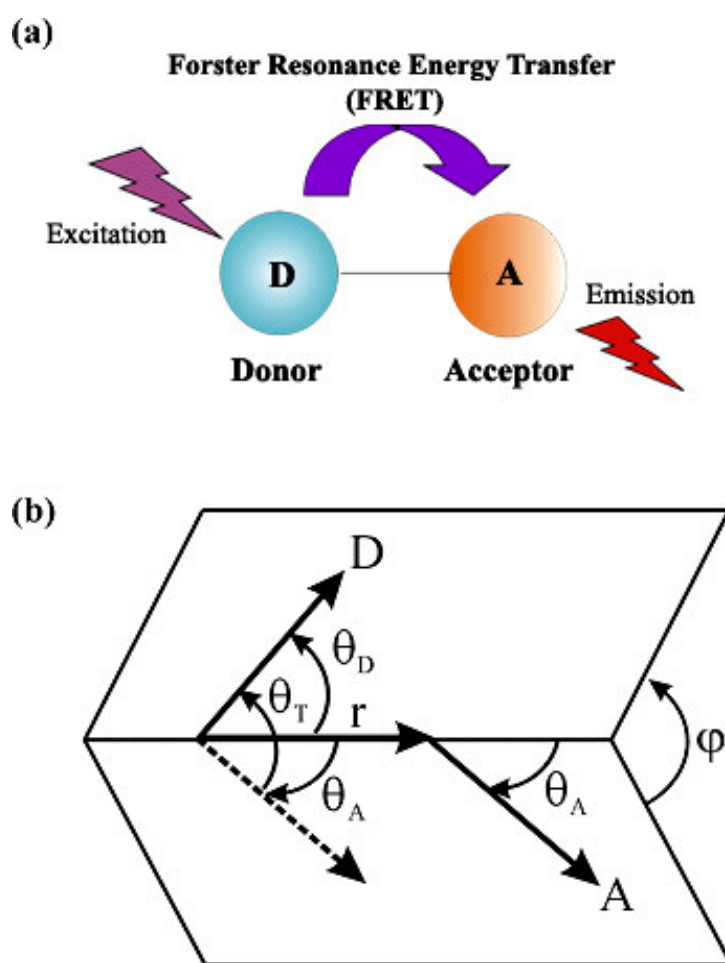


Figure 2.5. (a) Schematic illustration of the Förster resonance energy transfer (FRET) process. (b) Dependence of the orientation factor κ^2 on the directions of the emission and absorption dipoles of the donor and acceptor, respectively.

donor and acceptor (figure 2.5(b)). κ^2 value can vary from 0 to 4. For collinear and parallel transition dipoles, $\kappa^2=4$; for parallel dipoles, $\kappa^2=1$; and for perpendicularly oriented dipoles, $\kappa^2=0$. For donor and acceptors that randomize by rotational diffusion prior to energy transfer, the magnitude of κ^2 is assumed to be 2/3. However, in systems where there is a definite site of attachment of the donor and acceptor molecules, to get physically relevant results, the value of κ^2 has to be estimated from the angle between the donor emission and acceptor absorption dipoles [20]. $J(\lambda)$, the overlap integral, which expresses the degree of spectral overlap between the donor emission and the acceptor absorption, is given by,

$$J(\lambda) = \frac{\int_0^{\infty} F_D(\lambda) \epsilon_A(\lambda) \lambda^4 d\lambda}{\int_0^{\infty} F_D(\lambda) d\lambda} \quad (2-41)$$

where $F_D(\lambda)$ is the fluorescence intensity of the donor in the wavelength range of λ to $\lambda+d\lambda$ and is dimensionless. $\epsilon_A(\lambda)$ is the extinction coefficient (in $M^{-1}cm^{-1}$) of the acceptor at λ . If λ is in nm, then $J(\lambda)$ is in units of $M^{-1}cm^{-1}nm^4$.

Once the value of R_0 is known, the efficiency of energy transfer can be calculated. The efficiency of energy transfer (E) is the fraction of photons absorbed by the donor which are transferred to the acceptor and is defined as,

$$E = \frac{k_T(r)}{\tau_D^{-1} + k_T(r)} \quad (2-42)$$

or

$$E = \frac{R_0^6}{r^6 + R_0^6} \quad (2-43)$$

The transfer efficiency is measured using the relative fluorescence intensity of the donor, in absence (F_D) and presence (F_{DA}) of the acceptor as,

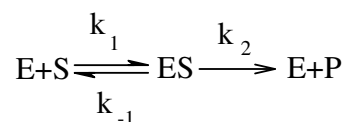
$$E = 1 - \frac{F_{DA}}{F_D} \quad (2-44a)$$

For D-A systems decaying with multiexponential lifetimes, E is calculated from the amplitude weighted lifetimes $\langle \tau \rangle = \sum_i \alpha_i \tau_i$ of the donor in absence (τ_D) and presence (τ_{DA}) of the acceptor as,

$$E = 1 - \frac{\tau_{DA}}{\tau_D} \quad (2-44b)$$

The D-A distances can be measured using equations (2-43), (2-44a) and (2-44b). The distances measured using equations (2-44a) and (2-44b) are revealed as R^S (steady-state measurement) and R^{TR} (time-resolved measurement), respectively. In one of recent studies from our group [21], we have shown that the energy transfer efficiency E , calculated from steady-state experiment (equation 2-44a) might be due to re-absorption of donor emission, but not due to dipole-dipole interaction (FRET).

2.1.5. Enzyme Kinetics: In order to measure enzymatic activity of CHT in various environments, we follow a mechanism originally proposed by Michaelis and Menten. According to this mechanism, a simple enzymatic reaction might be written as,



where E, S and P represent the enzyme, substrate and product, respectively. ES is the transient complex of the enzyme with the substrate. The scheme assumes the following facts:

- i) Enzyme first combines with substrate to form enzyme-substrate complex in a relatively fast reversible step.
- ii) The ES complex then breaks down in a slower second step to yield free enzyme and reaction product P.

As the breakdown of ES to product is the slowest step, rate of reaction,

$$v_0 = k_2[ES] \quad (2-45)$$

Total enzyme concentration at any instant $[E_t]$ = sum of free and substrate bound enzyme.

$$\text{Free enzyme at any instant} = [E_t] - [ES] \quad (2-46)$$

$$\text{Rate of formation of ES} = k_1[E][S] = k_1\{[E_t] - [ES]\}[S] \quad (2-47)$$

$$\text{Rate of breakdown of ES} = (k_{-1} + k_2)[ES] \quad (2-48)$$

Applying steady-state concept,

$$k_1\{[E_t] - [ES]\}[S] = (k_{-1} + k_2)[ES] \quad (2-49)$$

or
$$k_1[E_t][S] - k_1[ES][S] = k_{-1}[ES] + k_2[ES]$$

$$\begin{aligned}
\text{or} \quad & k_1[E_t][S] = \{k_{-1}[S] + (k_{-1} + k_2)\}[ES] \\
\text{or} \quad & [ES] = k_1[E_t][S] / \{k_{-1} + k_2 + k_1[S]\} \\
\text{or} \quad & [ES] = [E_t][S] / \{((k_{-1} + k_2)/k_1) + [S]\} \\
\text{or} \quad & [ES] = [E_t][S] / (K_M + [S]) \quad (2-50)
\end{aligned}$$

$$K_M \text{ is called Michaelis constant, } K_M = (k_{-1} + k_2) / k_1 \quad (2-51)$$

$$\text{Now, } v_0 = k_2[ES] = k_2([E_t][S]) / (K_M + [S])$$

At high [S], [S] >> K_M, v₀ = v_{max}

$$\begin{aligned}
\therefore v_0 = v_{\max} &= k_2[E_t][S] / [S] = k_2[E_t] \\
\therefore v_0 &= \frac{v_{\max}[S]}{K_M + [S]} \quad (2-52)
\end{aligned}$$

This equation is known as Michaelis-Menten equation. It is the rate equation for one-substrate catalyzed reaction. At v₀ = 0.5v_{max}, it is found that K_M = [S]. Hence, K_M is the substrate concentration at which v₀ = 0.5v_{max}. If we take the reciprocal of both sides of Michaelis-Menten equation, we get,

$$\begin{aligned}
\frac{1}{v_0} &= \frac{K_M + [S]}{v_{\max}[S]} \\
\text{or} \quad \frac{1}{v_0} &= \frac{K_M}{v_{\max}[S]} + \frac{1}{v_{\max}} \quad (2-53)
\end{aligned}$$

This form of Michaelis-Menten Equation is known as Lineweaver-Burk equation. For enzymes obeying Michaelis-Menten Equation, a plot of 1/v₀ vs 1/[S] would be a straight line.

The quantity v_{max} varies greatly from enzyme to enzyme. For two-step enzyme reaction, v_{max} = k₂[E_t] where k₂ is the rate limiting step. If for three-step mechanism, k₃ is rate limiting, then v_{max} = k₃[E_t]. Therefore, it is more general to designate rate constant of rate limiting step as k_{cat}. For two steps, k₂ = k_{cat}; for three steps, k₃ = k_{cat}. Therefore, Michaelis-Menten equation becomes,

$$v_0 = v_{\max} [S] / (K_M + [S]) = k_{\text{cat}} [E_t][S] / (K_M + [S]) \quad (2-54)$$

k_{cat} is a first order rate constant and has units of reciprocal time. To compare catalytic efficiencies of enzymes the ratios of k_{cat}/K_M of different enzymes are to be compared. It is

called specificity constant, which is the rate constant for the conversion of (E+S) to (E+P). When $[S] \ll K_M$,

$$v_0 = \frac{k_{cat}}{K_M} [E_t][S] \quad (2-55)$$

where k_{cat} =second order rate constant. v_0 depends on $[E_t]$ and $[S]$.

2.1.6. Adiabatic Compressibility: Adiabatic compressibility, (β_s) of a solution ($w_0=5$) can be determined by measuring the solution density (ρ_s) and the sound velocity (u_s) and applying the Laplace's equation,

$$\beta_s = \frac{1}{\rho_s u_s^2} \quad (2-56)$$

The apparent specific volume of solubilized water ϕ_v is given by,

$$\phi_v = \frac{1}{\rho_{solv}} + \frac{\rho_{solv} - \rho_s}{c_w \rho_{solv}} \quad (2-57)$$

where c_w is the concentration of the water molecules in the micellar solution, ρ_{solv} and ρ_s are the densities of the solvent and the solution respectively. The partial apparent adiabatic compressibility (ϕ_k) of the solubilized is obtained from the following relation,

$$\phi_k = \beta_s (2\phi_v - 2[u] - \frac{1}{\rho_{solv}}) \quad (2-58)$$

$[u]$ is the relative specific sound velocity increment given by,

$$[u] = \frac{u_s - u_{solv}}{u_{solv} c_w} \quad (2-56)$$

u_{solv} and u_w are the sound velocities in solvent and solubilized water respectively.

2.2. Systems:

2.2.1. Organized Assemblies (Biomimetics): Amphiphilic molecules, such as surfactants, aggregate to form macromolecular assemblies like micelles and reverse micelles. Since these assemblies closely resemble certain structural and dynamical properties of biomolecules, they are widely used as mimics of the actual biological systems. In the following section we will discuss about these systems.

A. Micelles: Micelles are spherical or nearly spherical aggregates of amphiphilic surfactant molecules formed in aqueous solution above a concentration known as critical micellar

concentration (CMC). Micelles are formed above a critical temperature called “Kraft point” which is different for different surfactants. Micellar aggregates have diameter varying within 10 nm and the aggregation number, i.e., the number of surfactant molecules per micelle, ranges from 20 to 200. Israelachvili et al. [22] have proposed that surfactant molecular packing considerations are determinant in the formation of large surfactant aggregates. In particular, it is considered that the surfactant packing parameter θ , defined by, $\theta=v/\sigma l$, where v is the surfactant molecular volume; σ , the area per polar head; and l , the length of hydrophobic part; gives a good idea of the shape of aggregates which will form spontaneously. It is considered that normal or direct rod-like micelles are formed when $2<\theta<3$ [23]. Micelles can be neutral (Triton X-100) or ionic (sodium dodecyl sulfate, SDS (anionic) and cetyltrimethylammonium bromide, CTAB (cationic)). The structure of a typical micelle is schematically shown in figure 2.6(a). The core of a micelle is essentially “dry” and consists of the hydrocarbon chains with the polar and charged head groups projecting toward the bulk water. The Stern layer, surrounding the core, comprises of the ionic or polar head groups, bound counter ions and water molecules. Between the Stern layer and the bulk water there is a diffused Guoy-Chapman (GC) layer (figure 2.6(a)), which contains the free counter ions and water molecules. In non-ionic polyoxyethylated surfactants e.g. Triton X-100 (TX-100), the hydrocarbon core is surrounded by a palisade layer, which consists of the polyoxyethylene groups hydrogen-bonded to water molecules. Small angle X-ray and neutron scattering have provided detailed information on the structure of the CTAB micelles [24]. According to these studies, CMC and aggregation number of CTAB micelle are 0.8 mM and 52, respectively and the thickness of the Stern layer is 6-9 Å. The overall radius of CTAB micelle is about 50 Å. For TX-100 micelle, the CMC, thickness of the palisade layer and overall radius of the hydrophobic core are reported to be 0.1 mM, 51 Å and 25-27 Å, respectively and that of SDS micelles are 8.6 mM, 33 Å and 5 Å, respectively [25].

B. Reverse Micelles: Reverse micelles (RMs) or water-in-oil microemulsions (figure 2.6(b)) are nanopools of polar solvent protected by a monolayer of surfactant molecules at the periphery with polar head groups pointing inward into the polar solvent, and the hydrocarbon tails directed toward the non-polar organic solvents [26,27]. RMs with water nanopools resemble the water pockets found in various bioaggregates such as proteins,

membranes and mitochondria. Thus, these systems are very often considered as templates for the synthesis of nanoparticles and as excellent biomimetics for exploration of biological membranes and biologically confined water molecules [28,29]. Aqueous RMs are generally characterized by the degree of hydration (w_0), which is the ratio of molar

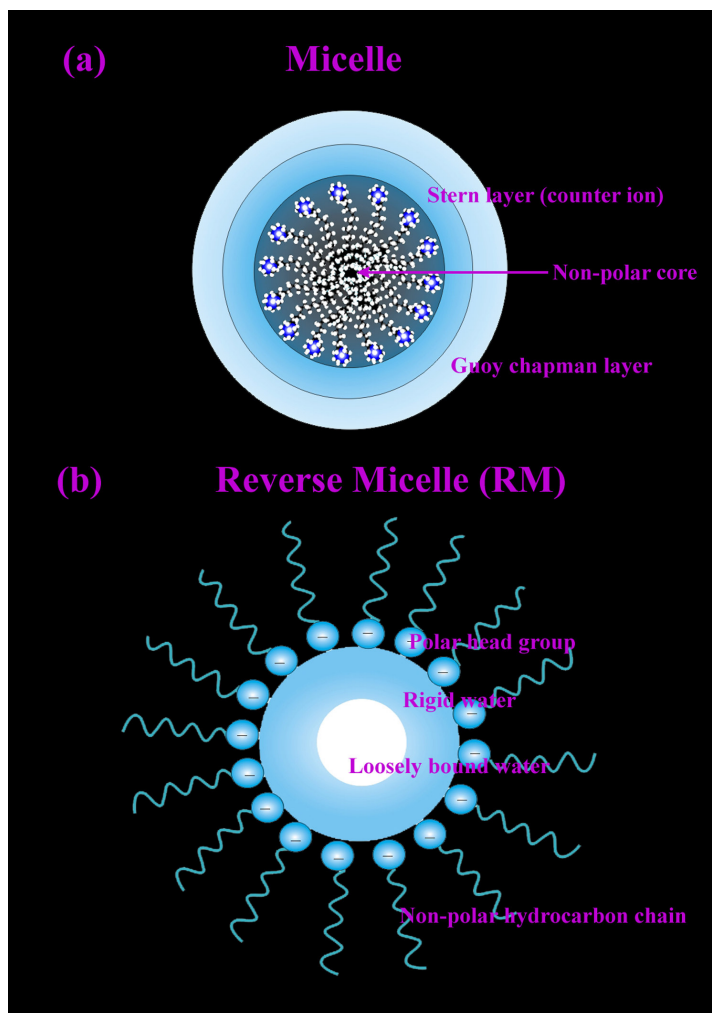


Figure 2.6. Schematic representation of the structure of (a) micelle (b) reverse micelle.

concentration of water to that of surfactant, where the radius of the water pool (r in Å) is empirically defined as, $r=2 \times w_0$ [30]. Shapes and sizes of the surfactant aggregates depend strongly on the type and concentration of the surfactant, and on the nature of counterion [31] and external solvent. In principle, reverse micelles can be formed in the presence and in the absence of solubilized water. However, it has generally been proposed that if the

medium is completely water-free, there is not a well defined CMC and the aggregates formed are very small and polydisperse, indicating minimum cooperativity in the surfactant association. This has been particularly established for surfactant bis (2-ethylhexyl) sulfosuccinate sodium salt (AOT) in several organic solvents [32]. RMs with w_0 values less than 20 are stable and monodisperse over a wide range of temperatures. The AOT-alkane-water system is interesting as the solution is homogeneous and optically transparent over a wide range of temperature, pressure and pH. The AOT-RM can compartmentalize a large amount of water in its central core, and the nanoscale aggregation process is fairly well-characterized with respect to size and shape at various water contents. The CMC of AOT in hydrocarbon solvent is about 0.1 mM [33]. In liquid alkanes, AOT-RMs ($w_0=0$) are completely associated and each micelle contains 23 monomers. The structures of these RMs are slightly asymmetric and are of round cylindrical nature. Spherical RMs are generally formed by surfactants with high values of the packing parameter, $\theta > 3$. AOT RMs can dissolve large amounts of water, being able to reach w_0 values as large as 40-60, depending on the surrounding non-polar organic medium and temperature [34]. At low w_0 values, the systems are usually referred to as reverse micelle, whereas the term water-in-oil microemulsion is frequently used for higher w_0 values. Fluorescence spectroscopy has been extensively used to study the AOT-RM system. Fluorescent probes have been used to determine the viscosity, binding site, rigidity and proximity within the water pool. These studies have shown that water inside the RM is generally of two types: i) interfacial (bound) and ii) core (free) water. One of the studies [35] has shown the existence of third type of water (trapped) molecules present between the polar head groups of the individual surfactant molecules. Thus, the interior of RMs is extremely heterogeneous. Dielectric relaxation studies [36] indicate the presence of 7 ns component for bound water in RM, very similar to those of water molecules in the close vicinity of biological macromolecules (biological water). In contrast to AOT which does not require any cosurfactant to form reverse micelles, cationic surfactant do not form RMs in the absence of cosurfactants [37]. Several non-ionic or neutral surfactant (TX-100) have been reported to form RMs in pure and mixed hydrocarbon solvents [38]. Reverse micelles also have been extensively employed as media to synthesize different metal and semiconductor nanoparticles.

2.2.2. Proteins: Two types of model proteins; Bovine Serum Albumin (BSA) and α -chymotrypsin (CHT) have been used in our studies.

A. Bovine Serum Albumin (BSA): Serum albumins are multi-domain proteins forming the major soluble protein constituent (60% of the blood serum) of the circulatory system. BSA (molecular weight 66,479 Da) is a heart-shaped tridomain protein, similar to that of its human counterpart human serum albumin (HSA) (figure 2.7) comprising of two identical subdomains A and B with each domain depicting specific structural and functional characteristics. BSA having 585 amino acid residues assumes solid equilateral triangular shape with sides ~ 80 Å and depth ~ 30 Å [39]. Its amino acid sequence comprises of 17 disulfide bridges distributed over all domains, one free thiol (cysteine34) in domain I. About 67% of BSA is α -helical while the rest of the structure being turns and extended polypeptides. Each domain contains 10 principle helices (h1-h10). Subdomains A and B share a common motif that includes h1, h2, h3 and h4 for subdomain A, and h7, h8, h9, h10 for subdomain B. The non-existence of disulfide linkage connecting h1 and h3 in subdomain IA is an exception. BSA is engaged with various physiological functions involving maintenance of osmotic blood pressure, transportation of a wide variety of ligands in and out of the physiological system [40]. The protein binds various kinds of ligands including photosensitizing drugs. The principal binding regions are located in subdomains IIA and IIIA of which IIIA binding cavity is the most active one and binds digitoxin, ibuprofen and tryptophan [41]. Warfarin, however, occupies a single site in domain-IIA. It is known that BSA undergoes reversible conformational transformation with change in pH of the protein solution, which is very essential for picking up and releasing the drugs at sites of differing pH inside the physiological system. At normal pH (pH=7), BSA assumes the normal form (N) which abruptly changes to fast migrating form (F) at pH values less than 4.3, as this form moves “fast” upon gel electrophoresis. Upon further reduction in pH to less than 2.7 the F-form changes to the fully extended form (E). On the basic side of the normal pH (above pH=8), the N-form changes to basic form (B) and above pH=10, the structure changes to the aged form (A). Serum albumins undergo ageing when stored at low ionic strength at alkaline pH. The ageing process is catalyzed by the free sulfhydryl group and involves sulfhydryl-disulfide interchange that results in the conservation of the sulfhydryl at its original position.

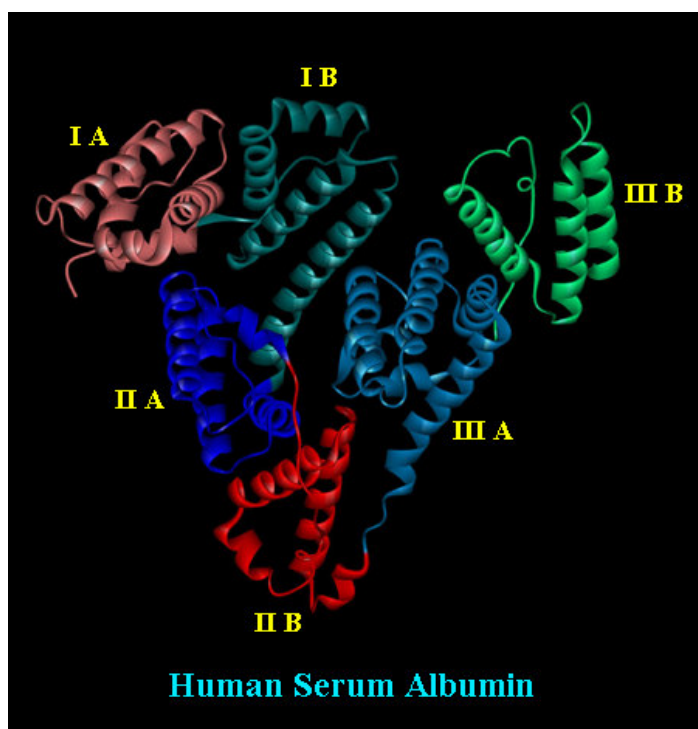


Figure 2.7. X-ray crystallographic structure (PDB code: 1N5U) of human serum albumin depicting the different domains.

B. α -Chymotrypsin (CHT): α -chymotrypsin (CHT) (figure 2.8) isolated from bovine pancreas is a member of the family serine endopeptidase (molecular weight of 25,191 Da) [42] catalyzing the hydrolysis of peptides in the small intestine. The three dimensional structure of CHT was solved by David Blow [43]. The molecule is a three dimensional ellipsoid of dimensions 51x40x40 Å and comprises of 245 amino acid residues. CHT contains several antiparallel β -pleated sheet regions and little α -helix. All charged groups are on the surface of the molecule except the *catalytic triad* of histidine57 (His57), aspartate102 (Asp102) and serine195 (Ser195) which are essential for catalysis. The Ser195 residue is hydrogen bonded to His57 residue, which in turn is H-bonded to β -carboxyl group of Asp102. An oxyanion hole is formed by amide nitrogens of glycine193 and Ser195. It is selective for hydrolyzing peptide bonds on the carboxyl side of the aromatic side chains of tyrosine, tryptophan, and phenylalanine and of large hydrophobic residues such as methionine. It also catalyzes the hydrolysis of ester bonds. CHT enhances the rate of peptide hydrolysis by a factor of 10^9 . The reaction has two distinct phases,

acylation and deacylation of the enzyme. Upon binding of the substrate, the hydroxyl group of the Ser195 attacks the carbonyl group of peptide bond to generate a tetrahedral

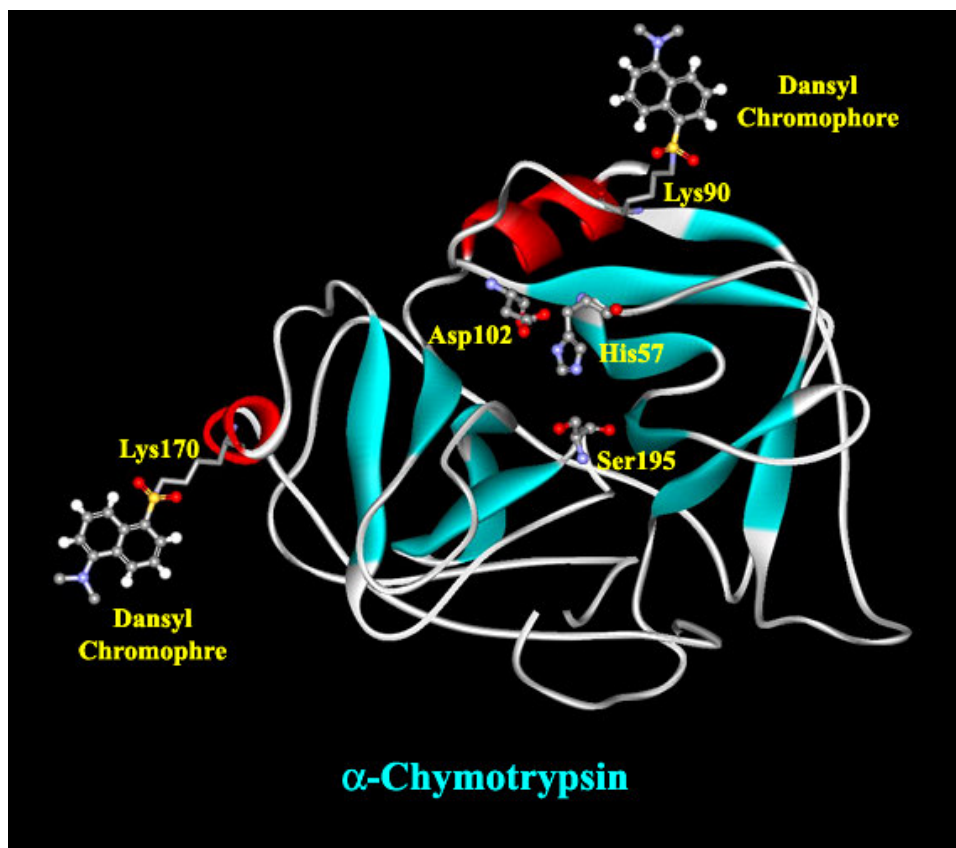


Figure 2.8. X-ray crystallographic structure (PDB code: 2CHA) of α -chymotrypsin depicting the catalytic triad (His57, Asp102 and Ser195) and two dansyl chromophore binding sites (Lys170 and Lys90).

intermediate. In this transient structure, the oxygen atom of the substrate now occupies the oxyanion hole. The acyl-enzyme intermediate now forms, assisted by proton donation of His57. The N-terminal portion is now released and replaced by water. The acyl-enzyme intermediate subsequently undergoes hydrolysis and the enzyme is regenerated.

2.2.3. Deoxyribonucleic Acids (DNAs): Nucleic acids form the central molecules in transmission, expression and conservation of genetic information. DNA serves as carrier of genetic information [44]. The classic example of how biological function follows from biomolecular structure comes from the elucidation of double helical structure of DNA by

Watson and Crick [45]. DNAs are polynucleotides with each nucleotide comprising of deoxyribose sugar, purine and pyrimidine bases and phosphate groups. The main bases whose intermolecular hydrogen bonding holds the DNA strands together are adenine, guanine, thymine and cytosine. There are generally three forms of DNA: the A, B and Z-

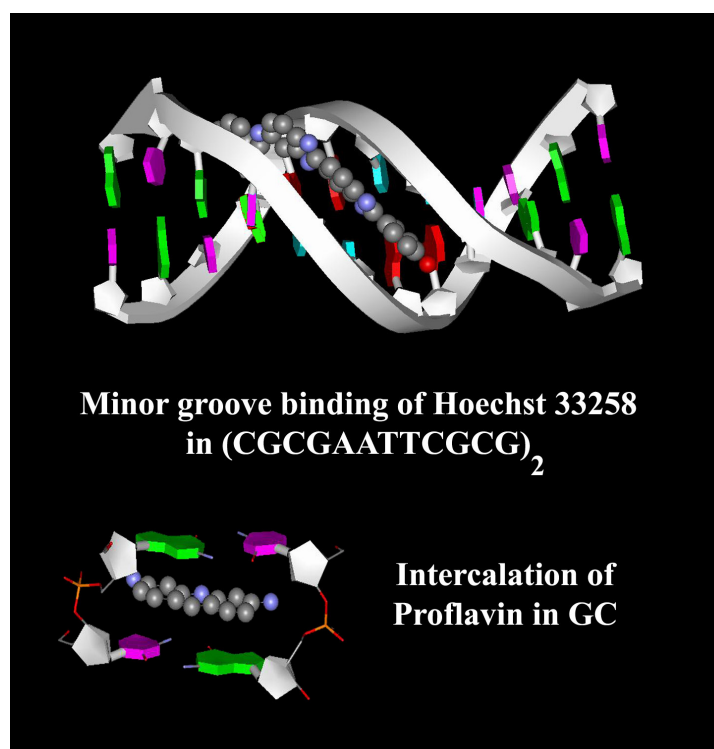


Figure 2.9. Schematic representation of minor groove binding and intercalation of Hoechst 33258 and proflavin, respectively. The DNA structures are downloaded from the nucleic acid data bank and handled using the Weblab viewerlite program.

form. Native DNA, however, exists in B-form. Native DNA is about a metre long and comprises of hundreds of base pairs. The distance between two base pairs in B-DNA is 3.4 Å [42]. In about 4 M NaCl, B-form is converted into Z-form. DNA structures consist of major and minor grooves and intercalation spaces through which DNA interacts with ligands. There are two modes of interaction of DNA with ligands: (i) intercalation, where the planar polycyclic heteroaromatic ligands occupy the space in between the base pairs of DNA and interact through π - π interaction [46], and (ii) groove binding where the ligands

bind in the major and minor grooves of DNA (figure 2.9) [47]. The water molecules at the surface of DNA are critical to the structure and to the recognition by other molecules, proteins and drugs [1].

2.2.4. Molecular Probes: In this section we will discuss about the different probe molecules that have been used in the course of study.

A. 2'-(4-hydroxyphenyl)-5-[5-(4-methylpiperazine-1-yl)-benzimidazo-2-yl]-benzimidazole, Hoechst 33258 (H258): The commercially available probe H258 is widely used as fluorescent cytological stain of DNA. Since it has affinity for the double stranded DNA H258 can affect transcription/translation, and block topomerase/helicase activities. The dye is also used as a potential antihelminthic drug. X-ray crystallographic and NMR studies of the dye bound to a dodecamer DNA shows that the dye is bound to A-T rich sequence of the DNA minor groove. The binding constant of the dye to double stranded DNA at low [dye]:[DNA] ratio is found to be $5 \times 10^5 \text{ M}^{-1}$. The solvchromic properties of the dye [48] can be used to report the hydration dynamics [49] as well as the dynamics of restricted systems [50].

B. 4',6-Diamidino-2-phenylindole (DAPI): The dye DAPI is another commercially available fluorescent cytological stain for DNA. Studies on the DAPI-DNA complexes show that the probe exhibits a wide variety of interactions of different strength and specificity with DNA [51]. The dye exhibits intramolecular proton transfer as an important mode of excited state relaxation at physiological pH [52], which takes place from the amidino to the indole moiety. Suppression of this excited state pathway leads to enhancement of fluorescence quantum yield and hence the fluorescence intensity in hydrophobic restricted environments.

C. 2-[4-[4-(dimethylamino) phenyl]-1,3-butadienyl]-3-ethyl-naphtho [2,1-d] thiazolium perchlorate (LDS 750): The laser dye LDS 750 is a polar styryl derivative. The dye is soluble in methanol, sparingly soluble in water and almost insoluble in isooctane. The dye possesses characteristics of being a good solvation probe and has been used to report the solvation dynamics in liquid aniline [53]. However, the involvement of internal photoprocesses to the excited state relaxation of the probe cannot be ruled out.

D. Coumarin 500 (C500): The solvation probe C500 is sparingly soluble in water and shows reasonably good solubility in isooctane. In bulk water the absorption peak (400 nm)

is significantly red shifted compared to that in isoctane (360 nm). The emission peak of C500 in bulk water (500 nm) also shows a 90 nm red shift compared to that in isoctane (excitation at 350 nm). The significantly large solvochromic effect (solvation) in the absorption and emission spectra of C500 makes the dye an attractive solvation probe for microenvironments. The photophysics of the probe have also been studied in detail [54].

E. Ala-Ala-Phe-7-amido-4-methylcoumarin (AAF-AMC): AAF-AMC is a fluorescent aromatic tripeptide substrate (figure 2.10) suitable for cleavage by serine protease. Its concentration is determined using extinction coefficient, $\epsilon=16 \text{ mM}^{-1}\text{cm}^{-1}$ at 325 nm. The rate of catalytic activity is determined by monitoring absorbance of cleaved product (7-amido-4-methylcoumarin) having $\epsilon=7.6 \text{ mM}^{-1}\text{cm}^{-1}$ at 370 nm in aqueous buffer solution [55].

F. 2-p-toluidinonaphthalene-6-sulfonate (TNS): TNS is a well known probe for many biological systems [56] (see figure 2.10). In aqueous solution, the emission quantum yield of TNS is very small (0.001) with emission peak at ~490 nm and the lifetime is also very short (60 ps) [57]. TNS has multiple absorption peaks at 270, 320 and 360 nm. Its molar extinction coefficient at 350 nm is $6640 \text{ M}^{-1}\text{cm}^{-1}$. On binding to the less polar interior of the organized media, the emission intensity increases markedly by about 200 fold with huge blue shift [56]. The fluorescence enhancement of TNS in organized media is attributed to suppression of the main nonradiative pathway, namely, intramolecular charge transfer (ICT) in the relatively nonpolar interior of the organized assemblies [58]. In 1,4-dioxane (dielectric constant ~2.2), TNS shows emission peak at 412 nm. This concomitant blue shift and fluorescence enhancement has made TNS an efficient probe for reporting the polarity of its immediate environment. TNS has been used to study solvation dynamics in many biological systems. Zhong et al. detected subpicosecond components in the solvation dynamics of TNS in histone [59]. On the other hand, Pierce and Boxer [60] and Bashkin et al. [61], reported solvation dynamics of TNS on a 10 ns timescale in other proteins.

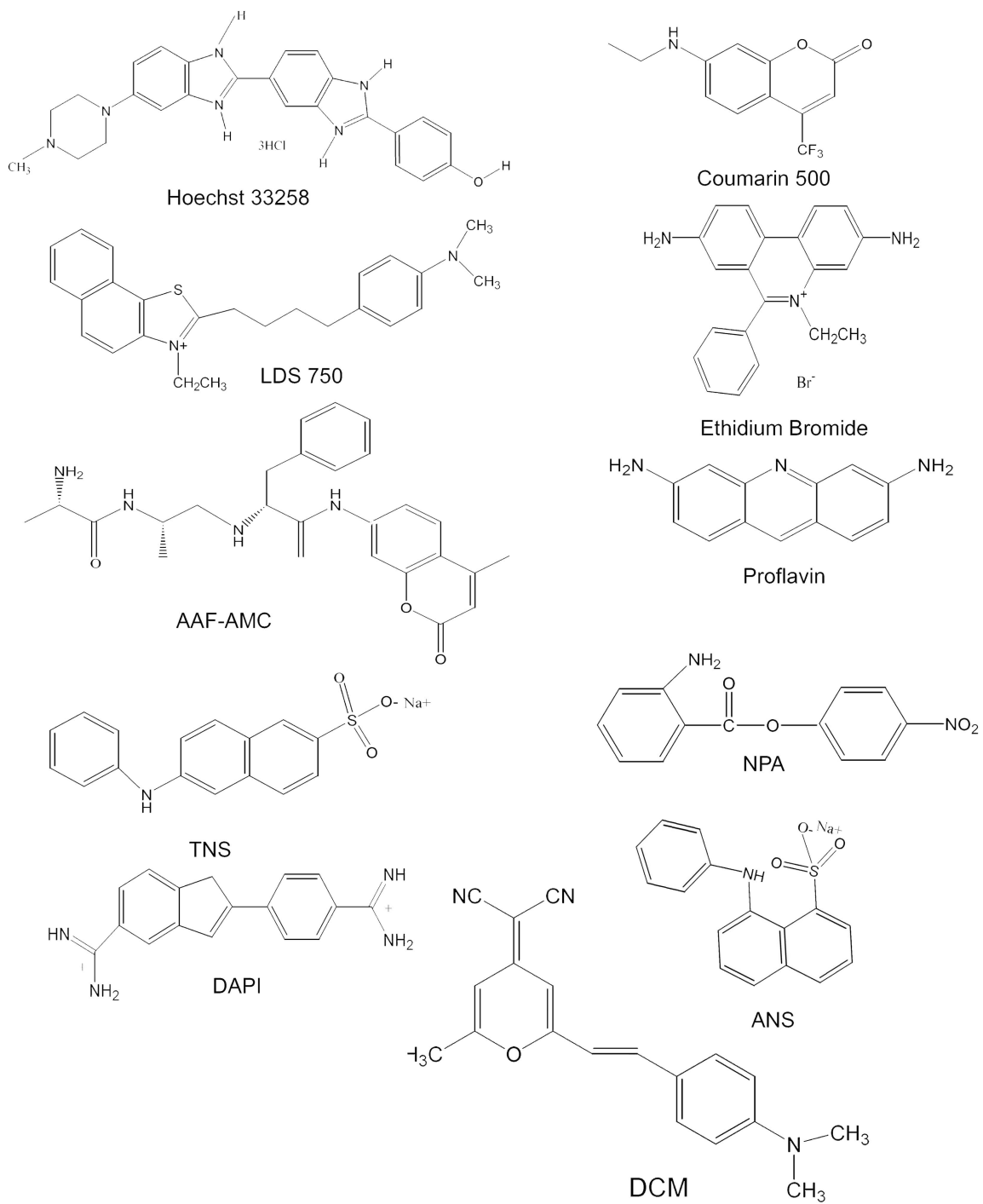


Figure 2.10. Schematic representation of the fluorescent probes used.

G. 1-anilino-8-naphthalenesulfonic acid, ammonium salt (ANS): ANS is a well known solvation probe [62] which binds selectively to the native state of certain proteins and enzymes in their hydrophobic as well as polar sites (figure 2.10). In aqueous solution, the emission quantum yield of ANS is very small (0.004) with emission peak at ~520 nm and a lifetime of ~0.25 ns. The steady-state emission is quenched dramatically in polar solvents. Because of its bichromophoric structure, ANS is known to undergo charge transfer (CT) from one aromatic moiety to the other ring and solvation. In steady-state, in nonpolar solvents, the emission is strong and is mostly from the locally excited state, i.e., before charge separation. In polar solvents, the fluorescence decreases and is dominated by emission from the CT state. The solvent polarity and rigidity determine the wavelength and yield of emission and that is why ANS is a useful biological probe. In the protein solutions, the steady-state fluorescence intensity is much larger than in the water solution. ANS is known to bind rigidly at a single site on the surface of the enzyme protein bovine pancreatic α -chymotrypsin (CHT) near the cysteine-1–122 disulfide bond. This ANS binding site is almost opposite in position to the enzymatic center of CHT. With femtosecond time-resolution, Zewail and coworkers have reported ultrafast hydration dynamics at the surface of the enzyme CHT, when the protein is in its physiologically active or inactive states using ANS as the fluorescent probe [63].

H. Ethidium Bromide (EB): Ethidium Bromide (EB) is a well known fluorescent probe (figure 2.10) for DNA, which readily intercalates into the DNA double helix [64]. Compared to the case of bulk water, the emission intensity and lifetime of EB increase nearly 11 times when EB intercalates into the double helix of DNA. This remarkable fluorescence enhancement of EB is utilized to study the motion of DNA segments, significantly enhanced quenching of DNA bound EB by various agents, and the interaction of DNA with surfactants and drug [65]. The photophysical processes of the fluorescence enhancement have recently been explored. The emission intensity of EB is low in highly polar, protic solvents, such as alcohol and water, compared to polar, aprotic solvents, e.g., acetone or pyridine. EB is insoluble in nonpolar, aprotic solvents like alkanes or dioxane. Compared to the case of water, the emission intensity and lifetime of EB increase nearly 5 times in acetone. Addition of water to acetone is found to quench fluorescence of EB, while deuterated solvents enhance emission of EB.

I. 4-(dicyanomethylene)-2-methyl-6-(p-dimethylamino-styryl) 4H-pyran (DCM): The laser dye DCM, is completely insoluble in water, and has selective binding affinity to the micellar surface [66]. The dye is completely hydrophobic (nonpolar) in the ground state. However, UV excitation increases dipole moment of the probe making it polar and hence increases its hydrophilicity in the excited state. Thus the excited DCM diffuses from the micellar surface (relatively nonpolar) towards polar bulk water phase revealing a fluorescence emission signature (temporal line width) of the excursion through multiple environments in the excited state [67].

J. Diaminoacridine (Proflavin, PF): The fluorescent dye PF is an acriflavine derivative, a disinfectant bacteriostatic against many gram-positive bacteria. It has been used in the form of the dihydrochloride and hemisulfate salts as a topical antiseptic, and was formerly used as a urinary antiseptic. PF is also known to have a mutagenic effect on DNA by intercalating between nucleic acid base pairs [68]. It differs from most other mutagenic components by causing basepair-deletions or basepair-insertions and not substitutions. The dye also inhibits the activity of the serine protease α -chymotrypsin [69]. PF absorbs strongly in the blue region at 445nm (in water at pH=7) with molar extinction coefficient of 40,000.

K. *p*-nitrophenyl anthranilate (NPA): The fluorescent probe NPA finds wide application as a precursor for labeling proteins [70] and nucleic acid bases [71] with the fluorescent anthraniloyl group. The probe is soluble in acetonitrile. NPA acts as a substrate for the proteolytic enzyme CHT and this forms the basis of the covalent anthraniloyl labeling at the active site of the protein.

References

- (1) S.K. Pal, A.H. Zewail, Dynamics of water in biological recognition, *Chem. Rev.* 104 (2004) 2099.
- (2) J.A. Rupley, G. Careri, Protein hydration and function, *Adv. Prot. Chem.* 41 (1991) 37.
- (3) J.A. Kornblatt, M.J. Kornblatt, Water as it applies to the function of enzymes, *Int. Rev. Cytol.* 215 (2002) 49.
- (4) Y. Pocker, Water in enzyme reaction: Biophysical aspects of hydration-dehydration processes, *Cell. Mol. Life Sci.* 57 (2000) 1008.
- (5) B. Bagchi, R. Biswas, Polar and nonpolar solvation dynamics, ion diffusion and vibrational relaxation: Role of biphasic solvent response in chemical dynamics, *Adv. Chem. Phys.* 109 (1999) 207.
- (6) B. Bagchi, Dynamics of solvation and charge transfer in dipolar liquids, *Ann. Rev. Phys. Chem.* 40 (1989) 115.
- (7) G.R. Fleming, M. Cho, Chromophore-solvent dynamics, *Ann. Rev. Phys. Chem.* 47 (1996) 109.
- (8) R. Jimenez, G.R. Fleming, P.V. Kumar, M. Maroncelli, Femtosecond solvation dynamics of water, *Nature* 369 (1994) 471.
- (9) S.K. Pal, J. Peon, B. Bagchi, A.H. Zewail, Biological water: Femtosecond dynamics of macromolecular hydration, *J. Phys. Chem. B* 106 (2002) 12376.
- (10) L. Onsager, Comments on "Effects of phase density on ionization process and electron localization in fluids" by J. Jortner and A. Gathon, *Can. J. Chem.* 55 (1977) 1819.
- (11) R.M. Stratt, M. Maroncelli, The emerging molecular view of solvation dynamics and vibrational relaxation, *J. Phys. Chem.* 100 (1996) 12981.
- (12) C.-P. Hsu, X. Song, R.A. Marcus, Time-dependent stokes shift and its calculation from solvent dielectric dispersion data, *J. Phys. Chem. B* 101 (1997) 2546.
- (13) J.T. Hynes, Outer-sphere electron-transfer reactions and frequency-dependent friction, *J. Phys. Chem.* 90 (1986) 3701.

- (14) M.L. Horng, J.A. Gardecki, A. Papazyan, M. Maroncelli, Subpicosecond measurements of polar solvation dynamics: coumarin 153 revisited, *J. Phys. Chem.* 99 (1995) 17311.
- (15) J.R. Lakowicz, Principles of fluorescence spectroscopy, *Kluwer Academic/Plenum*, New York, 1999.
- (16) R.D. Spencer, G. Weber, Measurement of subnanosecond fluorescence lifetimes with a cross-correlation phase fluorometer, *Ann. N. Y. Acad. Sci.* 158 (1969) 361.
- (17) D.V. O'Connor, D. Philips, Time correlated single photon counting, *Academic Press*, London, 1984.
- (18) R.K. Mitra, S.S. Sinha, S.K. Pal, Temperature-dependent hydration at micellar surface: Activation energy barrier crossing model revisited, *J. Phys. Chem. B* 111 (2007) 7577.
- (19) L. Stryer, Fluorescence energy transfer as a spectroscopic ruler, *Ann. Rev. Biochem.* 47 (1978) 819.
- (20) D. Banerjee, S.K. Pal, Simultaneous binding of minor groove binder and intercalator to dodecamer DNA: Importance of relative orientation of donor and acceptor in FRET, *J. Phys. Chem. B* 111 (2007) 5047.
- (21) P. Majumder, R. Sarkar, A.K. Shaw, A. Chakraborty, S.K. Pal, Ultrafast dynamics in a nanocage of enzymes: Solvation and fluorescence resonance energy transfer in reverse micelles, *J. Coll. Interf. Sci.* 290 (2005) 462–474.
- (22) J.N. Israelachvili, D.J. Mitchell, B.W. Ninham, Theory of self assembly of hydrocarbon amphiphiles into micelles and bilayers, *J. Chem. Soc. Faraday Trans.* 272 (1976) 1525.
- (23) D.J. Mitchell, B.W. Ninham, Micelles, vesicles and microemulsions, *J. Chem. Soc. Faraday Trans.* 2 (1981) 601.
- (24) S.S. Berr, E. Caponetti, J.S. Johnson, J.R.R.M. Jones, L.J. Magid, Small-angle neutron scattering from hexadecyltrimethylammonium bromide micelles in aqueous solutions, *J. Phys. Chem.* 90 (1986) 5766.
- (25) N.J. Turro, X.-G. Lei, K.P. Anantapadmanabhan, M. Aronson, Spectroscopic probe analysis of protein-surfactant interactions: The BSA/SDS system, *Langmuir* 11 (1995) 2525.

- (26) P.L. Luisi, M. Giomini, M.P. Pileni, B.H. Robinson, Reverse micelles as hosts for proteins and small molecules, *Biochim. Biophys. Acta* 947 (1988) 209.
- (27) T.K. De, A. Maitra, Solution behavior of aerosol OT in non-polar solvents, *Adv. Coll. Interf. Sci.* 59 (1995) 95.
- (28) K. Bhattacharyya, Solvation dynamics and proton transfer in supramolecular assemblies, *Acc. Chem. Res.* 36 (2003) 95.
- (29) B.E. Cohen, D. Huppert, K.M. Solntsev, Y. Tsfadia, E. Nachiel, M. Gutman, Excited state proton transfer in reverse micelles, *J. Am. Chem. Soc.* 124 (2002) 7539.
- (30) M.P. Pileni, Water in oil colloidal droplets used as microreactors, *Adv. Coll. Interf. Sci.* 46 (1993) 139.
- (31) F. Caboi, P. Capuzzi, P. Baglioni, M. Monduzzi, Microstructure of Ca-AOT/water/deacane w/o microemulsions, *J. Phys. Chem. B* 101 (1997) 10205.
- (32) M. Zulauf, H.-F. Eicke, Inverted micelles and microemulsions in the ternary system H₂O/aerosol-OT/isooctane as studied by photon correlation spectroscopy, *J. Phys. Chem.* 83 (1979) 480.
- (33) Y.-C. Jean, H.J. Ache, Determination of critical micelle concentrations in micellar and reverse micellar systems by positron annihilation techniques, *J. Am. Chem. Soc.* 100 (1978) 984.
- (34) C. Petit, P. Lixon, M.P. Pileni, Structural study of divalent metal bis(2-ethylhexyl) sulfosuccinate aggregates, *Langmuir* 7 (1991) 2620.
- (35) T.K. Jain, M. Varshney, A. Maitra, Structural studies of aerosol OT reverse micellar aggregates by FT-IR spectroscopy, *J. Phys. Chem.* 93 (1989) 7409.
- (36) M.A. Middleton, R.S. Schetchter, K.P. Johnston, Dielectric properties of anionic and nonionic surfactant microemulsions, *Langmuir* 6 (1990) 920.
- (37) J. Lang, N. Lalem, R. Zana, Quarternary water in oil microemulsions. 1. Effect of alcohol chain length and concentration on droplet size and exchange of material between droplets, *J. Phys. Chem.* 95 (1991) 9553.
- (38) D.-M. Zhu, X. Wu, Z.A. Schelly, Reverse micelles and water in oil microemulsions of Triton X-100 in mixed solvents of benzene and n-hexane, *Langmuir* 8 (1992) 1538.

- (39) X.M. He, D.C. Carter, Atomic structure and chemistry of human serum albumin, *Nature* 358 (1992) 209.
- (40) T.J. Peters, All about albumin: Biochemistry, genetics and medical applications, *Academic Press*, San Diego, CA, 1996.
- (41) J. Ghuman, P.A. Zunszai, I. Petitpas, A.A. Bhattacharya, M. Otagiri, S. Curry, Structural basis of the drug-binding specificity of human serum albumin, *J. Mol. Biol.* 353 (2005) 38.
- (42) D.L. Nelson, M.M. Cox, *Lehninger Principles of Biochemistry*, *Worth*, New York, 2000.
- (43) J.J. Birktoft, D.M. Blow, The structure of crystalline α -chymotrypsin: V. The atomic structure of tosyl- α -chymotrypsin at 2\AA resolution, *J. Mol. Biol.* 68 (1972) 187.
- (44) O. Avery, C. Macleod, M. McCarty, Studies on the chemical nature of the substances inducing transformation of the substances inducing transformation of pneumococcal types, *J. Expt. Med.* 7 (1944) 137.
- (45) J.D. Watson, F.H.C. Crick, Molecular structure of nucleic acids, *Nature* 171 (1953) 737.
- (46) L.S. Lerman, The structure of DNA-acridine complex, *Proc. Natl. Acad. Sci. USA* 49 (1963) 94.
- (47) P.B. Dervan, Molecular recognition of DNA by small molecules, *Bioorg. Med. Chem.* 9 (2001) 2215.
- (48) R. Jin, K.J. Breslauer, Characterization of the minor groove environment in a drug-DNA complex: Bisbenzimidazole bound to the poly[d(AT)]-poly[d(AT)]duplex, *Proc. Natl. Acad. Sci. USA* 85 (1988) 8939.
- (49) S.K. Pal, L. Zhao, A.H. Zewail, Water at DNA surfaces: Ultrafast dynamics in minor groove recognition, *Proc. Natl. Acad. Sci. USA* 100 (2003) 8113.
- (50) D. Banerjee, S.K. Pal, Ultrafast charge transfer and solvation of DNA minor groove binder: Hoechst 33258 in restricted environments, *Chem. Phys. Lett.* 432 (2006) 257.

- (51) W.D. Wilson, F.A. Tanious, H.K. Barton, R.L. Jones, K. Fox, R.L. Wydra, L. Strekowski, DNA sequence dependent binding modes of 4',6-Diamidino-2-phenylindole (DAPI), *Biochemistry* 29 (1990) 8452.
- (52) M.L. Barcellona, E. Gratton, A molecular approach to 4',6-Diamidino-2-phenylindole (DAPI) photophysical behaviour at different pH values, *Biophys. Chem.* 40 (1991) 223.
- (53) N.A. Smith, S.R. Meech, I.V. Rubtsov, K. Yoshihara, LDS-750 as a probe of solvation dynamics: A femtosecond time-resolved fluorescence study in liquid aniline, *Chem. Phys. Lett.* 303 (1999) 209.
- (54) S. Nad, H. Pal, Photophysical properties of coumarin 500 (C500): Unusual behaviour in nonpolar solvents, *J. Phys. Chem. A* 107 (2003) 501.
- (55) R. Biswas, S.K. Pal, Caging enzyme function: α -chymotrypsin in reverse micelle, *Chem. Phys. Lett.* 387 (2004) 221.
- (56) W.O. McClure, G.M. Edelman, Fluorescent probes for conformational states of proteins. I. Mechanism of fluorescence of 2-p-toluidinylnaphthalene-6-sulphonate, a hydrophobic probe, *Biochemistry* 5 (1966) 1908.
- (57) S. Mukherjee, P. Sen, A. Halder, S. Sen, P. Dutta, K. Bhattacharyya, Solvation dynamics in a protein-surfactant aggregate. TNS in HSA-SDS, *Chem. Phys. Lett.* 379 (2003) 471.
- (58) K. Bhattacharyya, M. Chowdhury, Environmental and magnetic field effects on exciplex and twisted charge transfer emission, *Chem. Rev.* 93 (1993) 507.
- (59) D. Zhong, S.K. Pal, A.H. Zewail, Femtosecond studies of protein-DNA binding and dynamics: Histone I, *CHEMPHYSCHEM* 2 (2001) 219.
- (60) D.W. Pierce, S.G. Boxer, Dielectric relaxation in a protein matrix, *J. Phys. Chem.* 96 (1992) 5560.
- (61) J.S. Bashkin, G. Mcledon, S. Mukamel, J. Marohn, Influence of medium dynamics on solvation and charge separation reactions: Comparison of a simple alcohol and protein solvent, *J. Phys. Chem.* 94 (1990) 4757.
- (62) R.P. DeToma, J.H. Easter, L. Brand, Dynamic interactions of fluorescence probes with the solvent environment, *J. Am. Chem. Soc.* 98 (1976) 5001.

- (63) S.K. Pal, J. Peon, A.H. Zewail, Ultrafast surface hydration dynamics and expression of protein functionality: α -chymotrypsin, *Proc. Natl. Acad. Sci. USA* 99 (2002) 15297.
- (64) D.P. Millar, R.J. Robbins, A.H. Zewail, Torsion and bending of nucleic acids studied by subnanosecond time resolved fluorescence depolarized of intercalated dyes, *J. Chem. Phys.* 76 (1982) 2080.
- (65) S.K. Pal, D. Mandal, K. Bhattacharyya, Photophysical processes of ethidium bromide in Micelles and Reverse micelles, *J. Phys. Chem. B* 102 (1998) 11017.
- (66) S.K. Pal, D. Sukul, D. Mandal, S. Sen, K. Bhattacharyya, Solvation dynamics of DCM in micelles, *Chem. Phys. Lett.* 327 (2000) 91.
- (67) R. Sarkar, A.K. Shaw, M. Ghosh, S.K. Pal, Ultrafast photoinduced deligation and ligation dynamics: DCM in micelle and micelle-enzyme complex, *J. Photochem. Photobiol. B: Biology* 83 (2006) 213.
- (68) S. Neidle, L.H. Pearl, P. Herzyk, H.M. Berman, A molecular model for proflavine-DNA intercalation, *Nucl. Acids Res.* 16 (1988) 8999–9016.
- (69) S.A. Bernhard, B.L. Lee, Z.H. Tashjian, On the interaction of α -chymotrypsin with chromophores: Proflavin binding and enzyme conformation during catalysis, *J. Mol. Biol.* 18 (1966) 405.
- (70) J. Schlessinger, I.Z. Steinberg, Circular polarization of fluorescence of probes bound to chymotrypsin. Change in asymmetric environment upon electronic excitation, *Proc. Nat. Acad. Sci. USA* 69 (1972) 769.
- (71) A. Giovane, C. Balestrieri, M.L. Balestrieri, L. Servillo, Interaction studies between elongation factor Tu and anthraniloyl fluorescent analogues of guanyl nucleotides, *Eur. J. Biochem.* 227 (1995) 428.

Chapter 3

Instrumentation and Sample Preparation

In this chapter the details of instrumental setup and sample preparation techniques used in our studies have been described.

3.1. Instrumental Setups: Steady-state UV-Vis absorption and emission spectra of the probe molecules were measured with Shimadzu UV-2450 spectrophotometer and Jobin

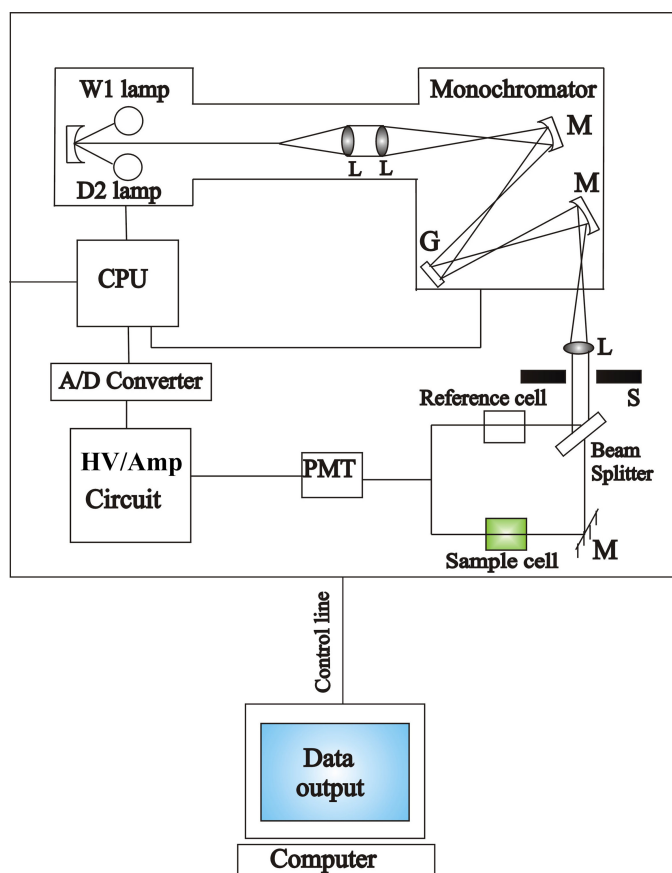


Figure 3.1. Schematic ray diagram of an absorption spectrophotometer. Tungsten halogen (W1) and Deuterium lamps (D2) are used as light sources in the visible and UV regions, respectively. M, G, L, S, PMT designate mirror, grating, lens, shutter and photomultiplier tube, respectively. CPU, A/D converter and HV/Amp indicate central processing unit, analog to digital converter and High-voltage/Amplifier circuit, respectively.

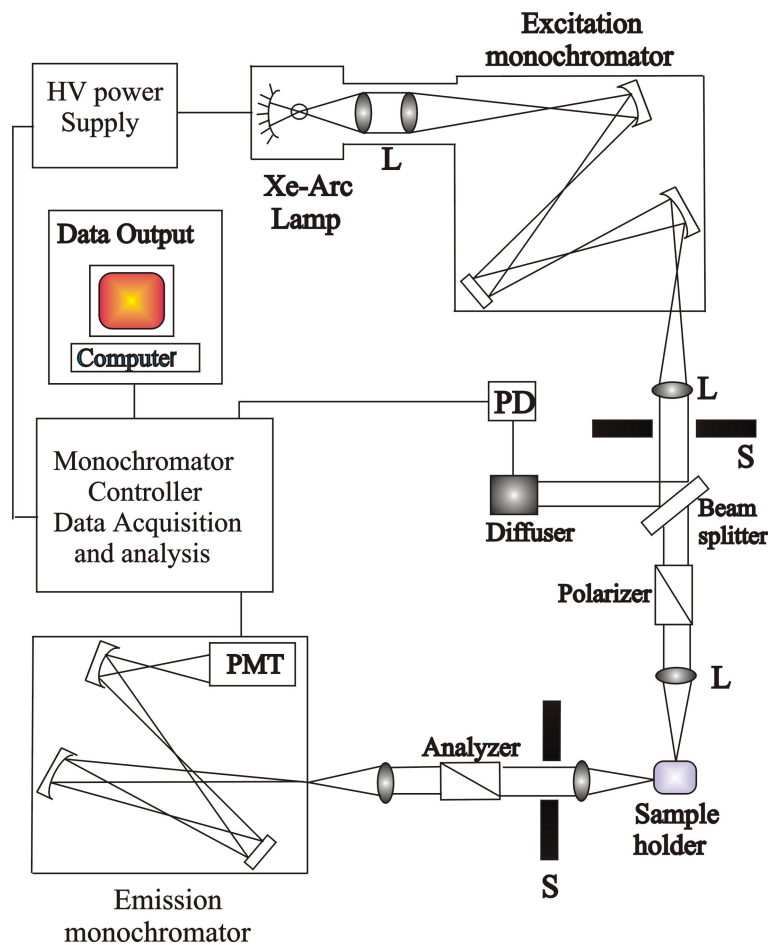


Figure 3.2. Schematic ray diagram of an emission spectrofluorimeter. M, G, L, S, PMT and PD represent mirror, grating, lens, shutter, photomultiplier tube and reference photodiode, respectively.

Yvon Fluoromax-3 fluorimeter, respectively. Schematic ray diagrams of these two instruments are shown in figures 3.1 and 3.2.

Circular dichroism (CD) is a form of spectroscopy based on the differential absorption of left and right-handed circularly polarized light. It can be used to determine the structure of macromolecules (including the secondary structure of proteins and the handedness of DNA). The CD measurements were done in a JASCO spectropolarimeter with a temperature controller attachment (Peltier) (figure 3.3). The CD spectra were acquired using a quartz cell of 1 cm path length. For proteins, the typical concentration used for CD measurements were within 10 μM while that for DNA were about 60 μM . The

secondary structural data of the CD spectra were analyzed using CDNN deconvolution program.

The working principle of CD measurement is as follows: when a plane polarized light passes through an optically active substance, not only do the left (L) and right (R) circularly polarized light rays travel at different speeds, $c_L \neq c_R$, but these two rays are absorbed to different extents, i.e. $A_L \neq A_R$. The difference in the absorbance of the left and right circularly polarized light, i.e., $\Delta A = A_L - A_R$, is defined as circular dichroism [1]. CD spectroscopy follows Beer-Lambert law. If I_0 is the intensity of light incident on the cell, and I , that of emergent light, then absorbance is given by,

$$A = \log_{10} \left(\frac{I_0}{I} \right) = \epsilon cl \quad (3-1)$$

i.e., A is proportional to concentration (c) of optically active substance and optical path length (l). If ' c ' is in moles/litre and ' l ' is in cm, then ϵ is called the molar absorptivity or molar extinction coefficient. In an optically active medium, two absorbances, A_L and A_R are considered, where $A_L = \log_{10} (I_0/I_L)$ and $A_R = \log_{10} (I_0/I_R)$. At the time of incidence on the sample, intensity of left and right circularly polarized light are same, i.e. $I_0 = I_L = I_R$. Any micrograph passes periodically changing light through the medium, oscillating between left and right circular polarization, and the difference in absorbances are recorded directly [2].

$$\Delta A = A_L - A_R = \log_{10} \left(\frac{I_0}{I_L} \right) - \log_{10} \left(\frac{I_0}{I_R} \right) = \log_{10} \left(\frac{I_R}{I_L} \right) \quad (3-2)$$

or
$$\Delta A = (\Delta \epsilon) cl \quad (3-3)$$

As seen from equation (3-2), I_0 does not appear in this final equation, so there is no need for a reference beam. The instruments are, therefore, of single beam type. Most of the CD spectropolarimeters, although they measure differential absorption, produce a CD spectrum in units of ellipticity (θ) expressed in millidegrees versus λ , rather than ΔA versus λ . The relation between ellipticity and CD is given by,

$$\theta = \frac{2.303 \times 180 \times (A_L - A_R)}{4\pi} \text{ degrees} \quad (3-4)$$

To compare the results from different samples, optical activity is computed on a molar or residue basis. Molar ellipticity, $[\theta]$ is defined as,

$$[\theta] = \frac{\theta}{cl} \quad (3-5)$$

where ‘ θ ’ is in degrees, ‘ c ’ is in moles per litre and ‘ l ’ is in cm. The unit of molar ellipticity is $\text{deg M}^{-1} \text{cm}^{-1}$.

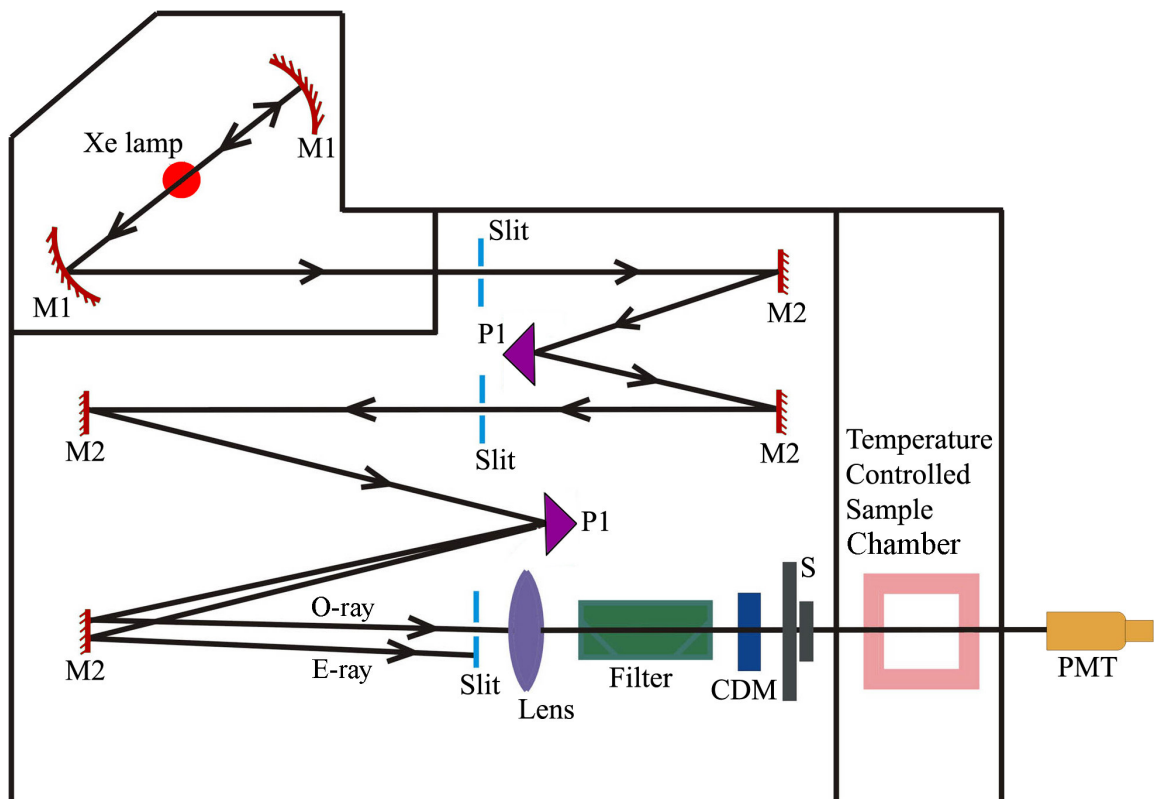


Figure 3.3. Schematic ray diagram of a Circular Dichroism (CD) spectropolarimeter. M1, M2, P1, S, PMT, CDM, O-ray and E-ray represent concave mirror, plain mirror, reflecting prism, shutter, photomultiplier tube, CD-modulator, ordinary ray and extraordinary ray, respectively.

All the picosecond-resolved fluorescence transients were recorded using time correlated single photon counting (TCSPC) technique. The schematic block diagram of a TCSPC system is shown in figure 3.4. TCSPC setup from Edinburgh instruments, U.K. was used during fluorescence decay acquisitions. The instrument response functions (IRFs) of the laser sources at different excitation wavelengths varied between 60 ps to 100 ps. The fluorescence from the sample was detected by a photomultiplier after dispersion through a

grating monochromator [3]. For all transients, the polarizer in the emission side was adjusted to be at 54.7° (magic angle) with respect to the polarization axis of excitation beam. In order to measure anisotropy, fluorescent transients were taken with emission polarizer aligned in parallel and perpendicular directions with respect to vertical polarization of excitation light.

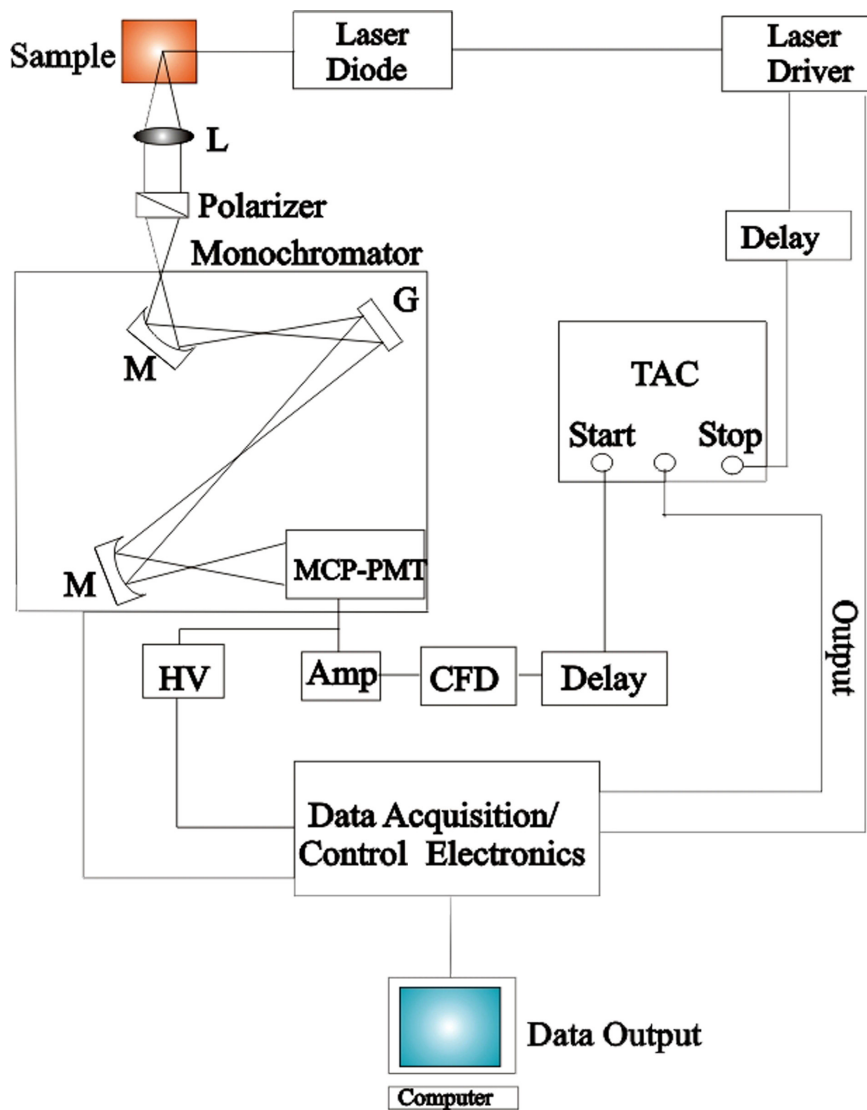


Figure 3.4. Schematic ray diagram of a time correlated single photon counting (TCSPC) spectrophotometer. A signal from microchannel plate photomultiplier tube (MCP-PMT) is amplified (Amp) and connected to start channel of time to amplitude converter (TAC) via constant fraction discriminator (CFD) and delay. The stop channel of the TAC is connected to the laser driver via a delay line. L, M, G and HV represent lens, mirror, grating and high voltage source, respectively.

Dynamic light scattering (DLS) also known as photon correlation Spectroscopy (PCS) or quasi-elastic light Scattering (QELS) is one of the most popular techniques used to determine the hydrodynamic size of the particle. DLS measurements were performed on a Nano S Malvern instrument, U.K. employing a 4 mW He-Ne laser ($\lambda=632.8$ nm) and equipped with a thermostatted sample chamber. The instrument allows DLS measurements in which all the scattered photons are collected at 173° scattering angle (figure 3.5). The instrument measures the time-dependent fluctuation in intensity of light scattered from the particles in solution at a fixed scattering angle [4].

It has been seen that particles in dispersion are in a constant, random Brownian motion and this causes the intensity of scattered light to fluctuate as a function of time. The correlator used in a DLS instrument constructs the intensity autocorrelation function $G(\tau)$ of the scattered intensity,

$$G(\tau) = \langle I(t)I(t + \tau) \rangle \quad (3-6)$$

where τ is the time difference (the sample time) of the correlator. For a large number of monodisperse particles in Brownian motion, the correlation function (given the symbol G) is an exponential decaying function of the correlator time delay τ ,

$$G(\tau) = A[1 + B \exp(-2\Gamma\tau)] \quad (3-7)$$

where A is the baseline of the correlation function, B is the intercept of the correlation function. Γ is the first cumulant and is related to the translational diffusion coefficient as, $\Gamma = Dq^2$, where q is the scattering vector and its magnitude is defined as,

$$q = \left(\frac{4\pi n}{\lambda_0} \right) \sin\left(\frac{\theta}{2}\right) \quad (3-8)$$

where n is the refractive index of dispersant, λ_0 is the wavelength of the laser and θ , the scattering angle. For polydisperse samples, the equation can be written as,

$$G(\tau) = A \left[1 + B |g^{(1)}(\tau)|^2 \right] \quad (3-9)$$

where the correlation function $g^{(1)}(\tau)$ is no longer a single exponential decay and can be written as the Laplace transform of a continuous distribution $G(\Gamma)$ of decay times,

$$g^{(1)}(\tau) = \int_0^{\infty} G(\Gamma) \exp(-\Gamma\tau) d\Gamma \quad (3-10)$$

The scattering intensity data in DLS are processed using the instrumental software to obtain the hydrodynamic diameter (d_H) and the size distribution of the scatterer in each sample. In a typical size distribution graph from the DLS measurement, X-axis shows a distribution of size classes in nm, while the Y-axis shows the relative intensity of the scattered light. The diffusion coefficient (D) can be calculated using the hydrodynamic diameter (d_H) of the particle by using the Stoke-Einstein relation,

$$D = \frac{k_B T}{3\pi\eta d_H} \quad (3-11)$$

where k_B , T , d_H , η are Boltzmann constant, temperature in Kelvin, hydrodynamic diameter and viscosity, respectively. The ray diagram of the DLS setup is shown in figure 3.5.

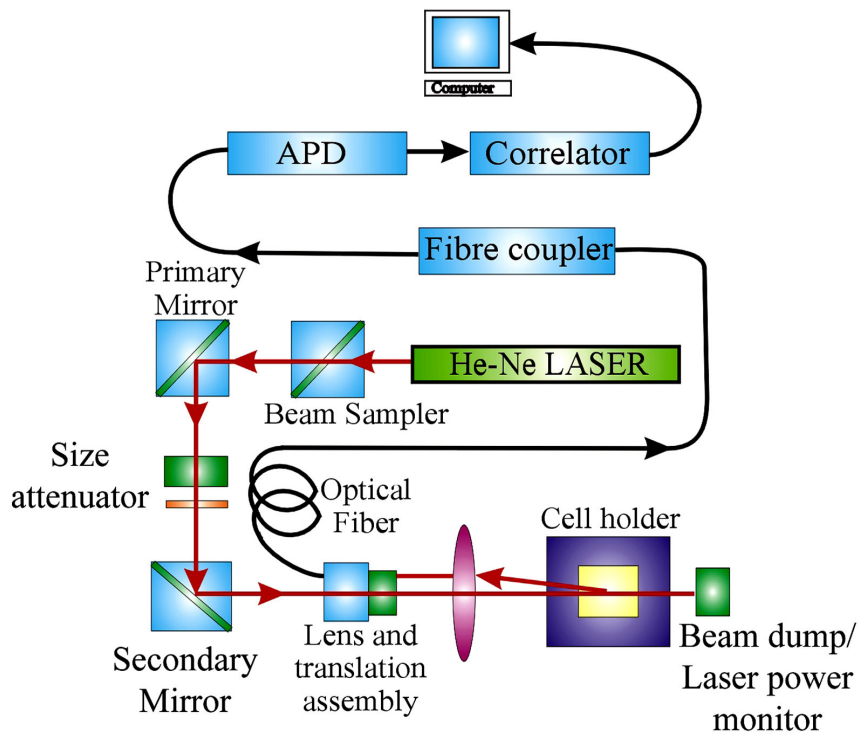


Figure 3.5. Schematic ray diagram of Dynamic Light Scattering (DLS) instrument. The Avalanche Photo Diode (APD) is connected to preamplifier/amplifier assembly and finally to correlator. It has to be noted that lens and translational assembly, laser power monitor, size attenuator, laser are controlled by the computer.

The density and sound velocity measurements were done in DSA 5000 from Anton Paar. The instrument measures density and sound velocity with accuracies of 5×10^{-3} and 1×10^{-6} respectively. The density and velocity are measured according to the following measuring principle. A U-shaped glass tube of known volume and mass is filled with the liquid sample and excited electronically by a Piezo element (figure 3.6). The U-tube is kept oscillating continuously at the characteristic frequency f . Optical pick-ups record the oscillation period P as $P=1/f$. This frequency is inversely proportional to the density ρ of the filled-in sample. The reference oscillator speeds up the measurements when aiming at various measuring temperatures.

The density is calculated as,

$$\rho = AxP^2 - B \quad (3-12)$$

where A and B are parameters. Once the instrument has been adjusted with air and water, the density of the sample can be determined. Hence related parameters can be calculated from the density.

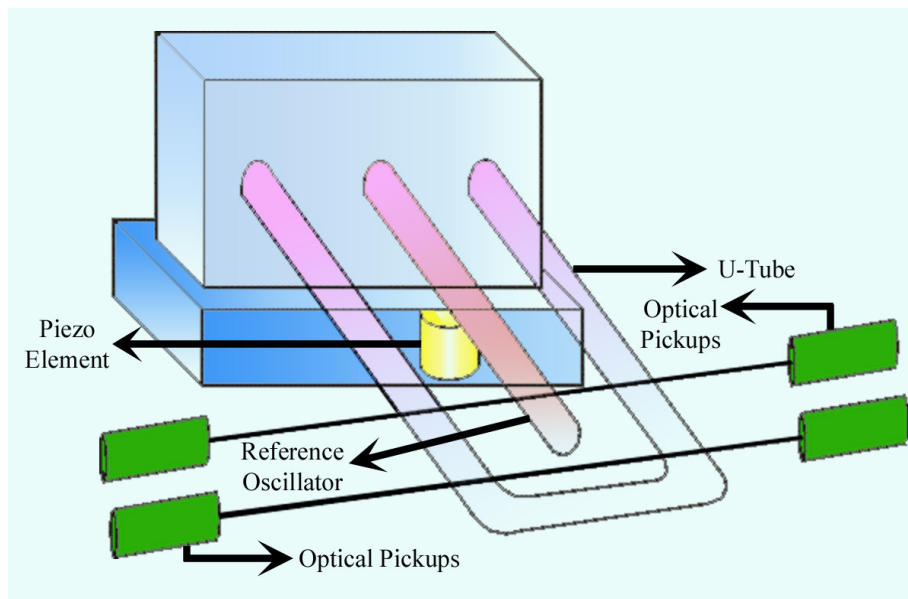


Figure 3.6. Schematic representation of the densimeter.

To determine the unfolding of the protein, we have carried out the differential temperature analysis. This was carried out using Diamond thermogravimetric

(TG)/differential thermal analyzer (DTA) from Perkin Elmer. The TG determines the weight change of a sample whereas the DTA measures the change in temperature between a sample and the reference as a function of temperature and/or time. The schematic of the TG/DTA is shown in figure 3.7. When a weight change occurs on the sample side, the beam holding the platinum pans is displaced. This movement is detected optically and the driving coil current is changed to return the displacement to zero. The detected driving coil current change is proportional to the sample weight change and the output is the TG signal. The DTA detects the temperature difference between the sample holder and the reference holder using the electromotive force of thermocouples, which are attached to the holders. This difference is as the DTA signal.

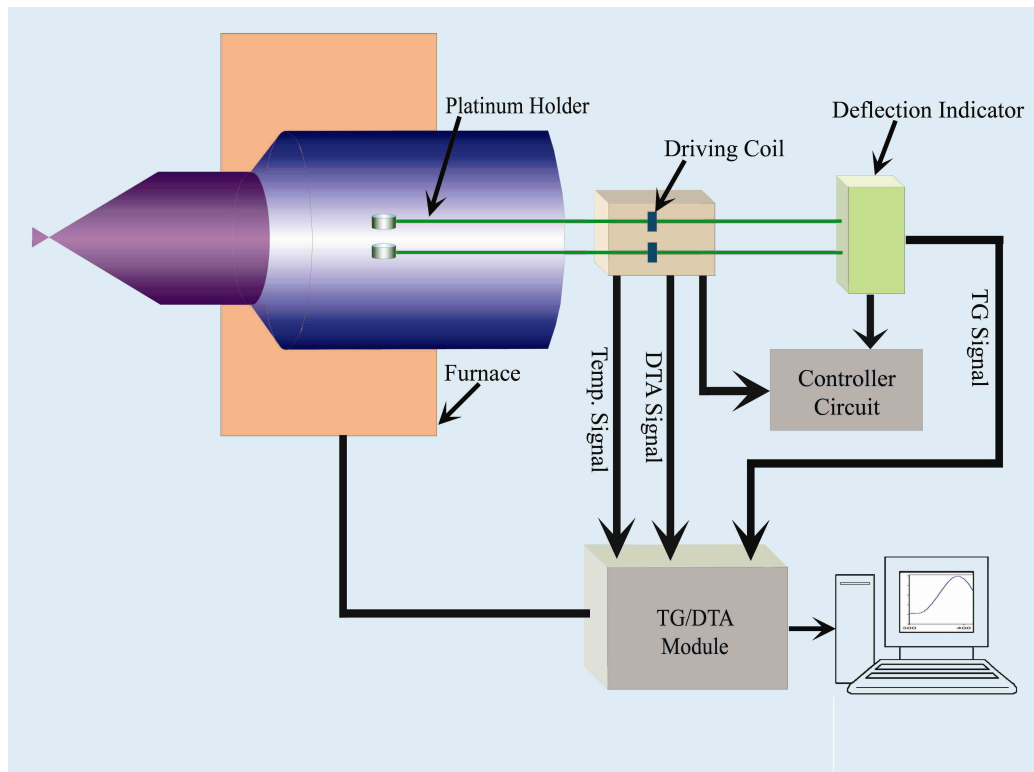


Figure 3.7. The schematic representation of TG/DTA setup.

3.2. Sample Preparation: In this section the different sample preparation methods have been discussed.

Chemicals used: The chemicals, spectroscopic probes, proteins, genomic DNA and synthetic oligonucleotides were procured from the following sources.

Deionized water, used to prepare all aqueous solutions is obtained from Millipore. The chemicals phosphate buffer (disodium hydrogen phosphate, monosodium hydrogen phosphate), sodium bis(2-ethylhexyl)sulfosuccinate (AOT) and isooctane, the fluorescent probes *p*-nitrophenyl anthranilate (NPA), Ala-Ala-Phe 7-amido-4-methyl coumarin (AAF-AMC), sodium salt of 2,6-*p*-toluidinonaphthalene sulfonate (TNS), 1-anilino-8-naphthalenesulfonic acid, ammonium salt (ANS), the proteins bovine serum albumin (BSA) and α -chymotrypsin (CHT), genomic calf thymus and salmon sperm DNAs are obtained from Sigma Aldrich. The surfactants sodium dodecyl sulphate (SDS), and Cetyltrimethylammonium Bromide (CTAB) are from Fluka and the surfactant Triton -X 100 is from Romil: The fluorescent probes Coumarin 500 (C500), LDS 750, DCM are from Exciton while Hoechst 33258 (H258), 4',6-Diamidino-2-phenylindole (DAPI) and Ethidium bromide (EB) are from Molecular Probes. The synthetic oligonucleotides having sequences CGCAAATTTGCG, CGCGAATTCGCG and GCGCGCGCGCGC are obtained from Gene Link.

3.2.1. Preparation of Reverse Micellar solution: Reverse micellar solutions of specific degree of hydration (w_0) were prepared by addition of calculated volume of aqueous solution of the probe in known volume of 100 mM AOT solution in isooctane. In order to ensure that each reverse micelle contains not more than one probe molecule, the overall probe concentration was kept less than that of reverse micellar concentration.

3.2.2. Preparation of Synthetic and Genomic DNA solutions: In order to reassociate the single strand DNA into self-complimentary double stranded DNA (ds DNA), thermal annealing was performed as per the methodology prescribed by the vendor. The aqueous solutions of ds DNA were then dialyzed exhaustively against Millipore water prior to further use. Aqueous sample solutions of genomic DNA were prepared in phosphate buffer (pH ~7). The nucleotide concentrations were determined by absorption spectroscopy using the average extinction coefficient per nucleotide of the DNA ($6,600 \text{ M}^{-1}\text{cm}^{-1}$ at 260 nm) [5].

3.2.3. Preparation of Dye-Protein complex: In order to prepare dye-protein complexes, aqueous solution of dyes (DAPI, TNS, C500, ANS, and LDS 750) were mixed with the

protein solutions (prepared in 50 mM/100 mM buffer) so as to maintain a [dye]:[protein] ratio of 1:50. The solutions were stirred for about 30 mins to ensure complete complexation of the dyes with the proteins. For FRET studies, the concentration of the acceptor dye was kept equal to the protein concentration.

3.2.4. Preparation of Dye-DNA complex: In order to prepare dye-DNA complexes, aqueous solutions of the dyes (H258, DAPI, EB) were added to the genomic DNA/synthetic oligonucleotides and stirred for 1 hour to ensure complete complexation of the dye. For steady state and solvation studies the [dye]:[DNA] ratio was kept low to ensure complete complexation of the probe. For FRET studies, the concentration of the acceptor dye was kept equal to the macromolecular concentration.

3.2.5. Measurement of Enzymatic Activity of α -Chymotrypsin (CHT): For the measurement of the enzymatic activity of CHT, AAF-AMC was used as the substrate. The concentration of the substrate was kept an order of magnitude higher than that of the enzyme. The rate of formation of product was followed by measuring the absorbance of product at 370 nm. The absorbance of the product was converted to molar concentration term by using the extinction coefficients of the product at 370 nm wavelength.

3.2.6. Preparation of Anthraniloyl-CHT (ANT-CHT) complex: To label CHT with the anthraniloyl group, we followed the procedure of Haughland and Stryer [6]. A stock solution of NPA in acetonitrile was added in small aliquots to CHT solution at 4°C with continuous stirring, until the concentration of the probe in solution exceeds that of the protein by an order of magnitude. The reaction was allowed to complete by overnight stirring of the NPA-CHT solution at 4°C. The resultant solution is filtered and dialyzed extensively to remove the free probes in solution.

References:

- (1) A. Rodger, B. Norden, Circular dichroism and linear dichroism, *Oxford University Press*, 1997.
- (2) G. Snatzke, Circular dichroism principles and applications, *Wiley-VCH*.
- (3) D.V. O'Connor, D. Philips, Time correlated single photon counting, *Academic Press*, London, 1984.
- (4) R. Pecora, Dynamic light scattering: Applications of photon correlation spectroscopy, *Plenum Press*, 1985.
- (5) G. Cosa, K.-S. Focsaneanu, J.R.N. McLean, J.P. McNamee, J.C. Scaiano, Photophysical properties of fluorescent DNA dyes bound to single and double stranded DNA in aqueous buffered solution, *Photochem. Photobiol.* 73 (2001) 585.
- (6) R.P. Haugland, L. Stryer, in *Conformation of Biopolymers* (Ramachandran, G. M., ed.; *Academic press, New York*) Vol. I (1967) 321.

Chapter 4

Studies on Interaction of a Ligand to DNA:

Exploration of Minor Groove Dynamics

4.1. Introduction:

The minor groove of a double helical DNA is the host of large number of ligands. An important category of such ligands are drugs which possess anticancer and antitumor properties. Majority of these drugs are crescent shaped molecules which fit into the AT rich region of the DNA minor groove [1]. The binding of the minor groove drugs is enthalpy driven. Pioneering studies by Zewail et al. [2] have shown that apart from favorable electrostatic and hydrogen bonded interactions, the dynamics of hydration associated with the DNA minor groove are crucial for minor groove recognition. However, due to the limited experimental window, the possible contribution of the overall DNA dynamics to minor groove recognition by drugs, cannot be explored. This chapter summarizes the attempt to utilize the photophysical properties of the fluorescent antihelminthic minor groove binder Hoechst 33258 (H258) to report the contribution of the DNA dynamics in minor groove recognition. The suitability of H258 to report the slower DNA dynamics is confirmed from a study of its internal photophysics in bulk solvents and representative biomimetic systems. The study has been continued to decouple the dynamics crucial to the minor groove from the overall DNA dynamics, thus establishing the correlation between the structure and dynamics of the minor groove, which is crucial for minor groove recognition by ligands.

4.2. Results and Discussion:

4.2.1. Ultrafast Charge Transfer and Solvation of DNA Minor Groove Binder: Hoechst 33258 in Restricted Environments [3].

Figure 4.1(a) shows the absorption and emission spectra of H258 in various environments. The emission spectrum of the dye in buffer shows a peak at 505 nm, which

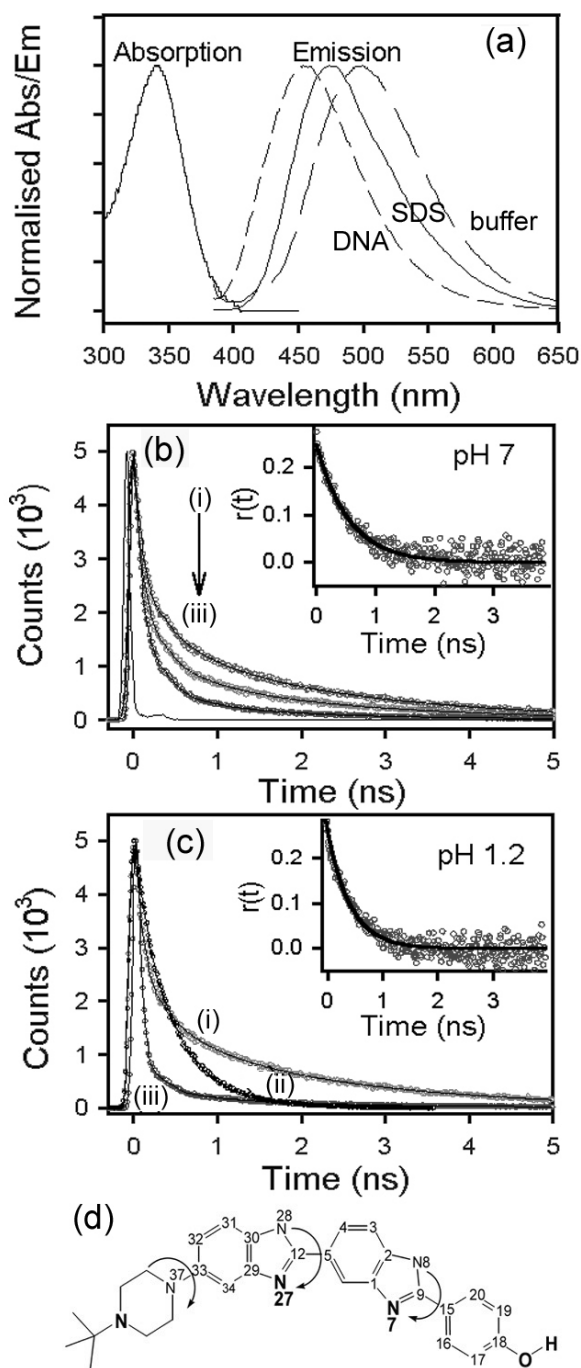


Figure 4.1. (a) Absorption and emission spectra of H258 in buffer, 100 mM SDS and DNA. (b) Fluorescence transients of H258 at various concentrations (i) 1 μM , (ii) 10 μM and (iii) 100 μM . Instrument response function (IRF) is also shown for comparison. (c) Fluorescence transients of H258 at (i) pH=7 (ii), pH=127 and (iii) pH=1.2). Insets show fluorescence anisotropies of H258 in the respective media. (d) Schematic diagram of H258 showing the protonation centres (bold) and twisting axes (arrows).

becomes blue shifted in hydrophobic environments (475 nm in SDS micelles and 457 nm in DNA). The probe notoriously undergoes dimerization in bulk water. A decay component of time constant <80 ps (indicative of dimer formation) decreases (from 29% to 10%) with dilution (100 μ M to 1 μ M, figure 4.1(b)). It is found that the concentration of the probe where no significant dimerization occurs is 1 μ M. In order to avoid complications due to dimer emission we maintained 1 μ M concentration of the probe in all sample solutions.

Figure 4.1(c) shows fluorescence transients of the probe in buffer solutions of various pH values. The transients of H258 in buffer at pH=1.2 with a systematic series of wavelength detection (data not shown) show three distinct time scales of 50 ps(95% at 610 nm and 40% at 460 nm), 550-950 ps (550 ps(21%) at 460 nm and 950 ps(5%) at 610 nm) and \sim 3 ns (40% at 460 nm, vanishes at 610 nm). It is known that in the ground state the probe at pH=1.2 is protonated at both the nitrogens (N27 and N7, figure 4.1(d)) of benzimide rings, the latter being at a torsional angle of 43°. Upon photoexcitation, charge transfer occurs from phenyl to the distant benzimidazole moiety resulting in a stronger and planar bond between two benzimidazole units [4,5]. The possibility of charge transfer from phenyl to its nearest benzimidazole moiety is ruled out because there is a significant increase in the basicity of the N7 atom in the excited state of the probe compared to that of N27. Thus, for the charge transfer reaction twisting of two benzimidazole planes is essential for the required planarity.

The experimental observations are in agreement with excited state intramolecular charge transfer (TICT) of the probe as detailed for similar dye molecules [6]. The nanosecond component (\sim 3 ns) predominant in the blue end is consistent with the lifetime of the locally excited (LE) state. In case of the probe in restricted media including DNA (see below) the excited state dynamics is essentially dominated by LE state nanosecond decay. The faster 50 ps component present in the transients (heavily at the red side) is assigned to the population decay of the charge transferred (CT) state coupled with an underlying triplet state of the probe [7] and/or radiationless transition to ground state [4]. This component is absent in higher pH solutions (pH=7 and pH=12) where the possibility of CT state formation is vanishingly small [5]. The observed 550-950 ps components represent the twisting motion of H258 in a barrier crossing from

initial to the final state of charge separation. The molecule twists toward the CT state and is stabilized by the polar solvents [6]. The total available energy in the molecule above the twisting barrier decreases with time. The resulting twisting time becomes longer, consistent with the gradual increase in the decay time from the blue side (550 ps) to the red side (950 ps) of the emission. The $r(t)$ of the probe in the solution (pH=1.2) shows a decay constant of 500 ps (inset, figure 4.1 (b) and (c)), further confirming rotational motion of the probe due to twisting in the solution.

As evidenced in the fluorescence decays, at pH=7 (decay components 110 ps(14%), 480 ps(13%) and 2.24 ns(72%)) and at pH=12 (decay components 100 ps(9.7%), 350 ps(46.5%) and 710 ps(43.8%)) and in the $r(t)$ s (0.53 ns in pH=7 and 0.45 ns in pH=12) of the probe in high pH solutions, the twisting relaxation still exists in the absence of the CT state. Higher quantum yields and similarity of temporal decays in the blue and red ends of the emission spectra of the probe in higher pHs are also in agreement with the absence of CT state. In order to study the contribution of the LE and CT states in the overall steady-state fluorescence spectrum, we constructed decay associated spectra (DAS, data not shown) of the slower and faster components of the TRES of the probe at pH=1.2. DAS studies for the faster component (50 ps) associated with CT state population dynamics gives a peak around 18600 cm^{-1} (537 nm) close to the steady-state peak value of 18720 cm^{-1} (534 nm) obtained in buffer solution of pH=1.2. The DAS for the slower decay components responsible for LE state emission shows a peak at 19900 cm^{-1} (502 nm) close to the steady-state peak values of the probe in buffer solutions of pH=7 (502 nm) and pH=12 (500 nm).

In order to investigate the geometrical restriction on the charge transfer reaction, we studied temporal fluorescence dynamics of the probe in anionic SDS micelles at various pH conditions. The affinity of the probe towards the micellar environment is established by a post-CMC (8 mM) blue shift in the steady-state emission spectra in SDS solution at pH=7 (data not shown). Time resolved fluorescence studies are carried out in the 100 mM SDS prepared in different pH values (figure 4.2(a)). At the surface of an ionic micelle the effective pH can be calculated using the formula, $C_s = C_b \exp(-e\psi/k_B T)$ [8], C_s , C_b , ψ , k_B and T being hydrogen ion concentrations in bulk and at the micellar surface, surface potential, Boltzmann constant and absolute temperature, respectively.

Thus the pH at the surface of the SDS micelle at pH=1.2 should acquire a value lower

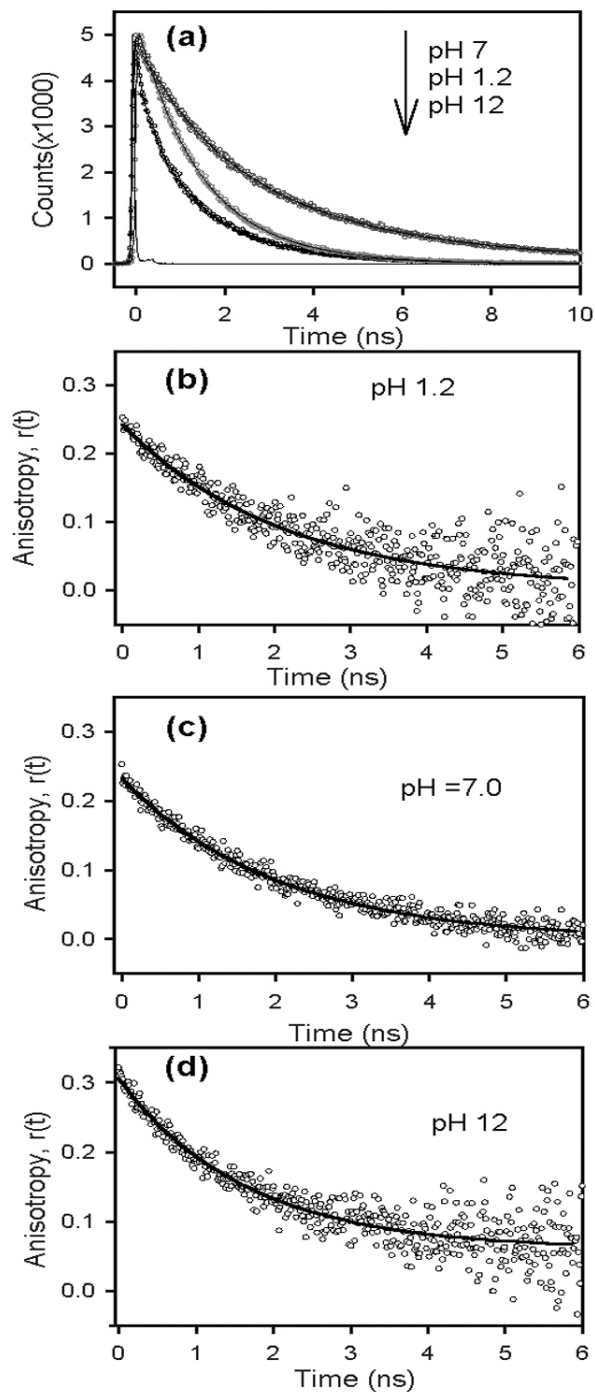


Figure 4.2. (a) Fluorescence transients of H258 in 100mM SDS at different pHs. (b)-(d) show fluorescence anisotropies of H258 in 100mM SDS at various pHs.

than 1.2. At the micellar surface the probe does not show either 50 ps component reflective of CT species or the components around 550 ps indicative of intramolecular twisting relaxation. The observations indicate that the twisting, which is essentially hindered at the micellar surface is prerequisite for the formation of CT state in the restricted environment even at pH=1.2.

The temporal nature of $r(t)$ s in 100 mM SDS solutions at different pH (figures 4.2(b)-(d)) are similar, being around 2 ns, which is in good agreement with the values reported for other dyes in SDS micellar environment [9]. The observations confirm the residence of the probe at the micellar surface. The residual anisotropy reflects geometrical restriction of the probe (rotational motion in a cone) in a microenvironment [6]. However, a steady-state emission peak of the probe (18700 cm^{-1}) in the micelles at pH=1.2 is observed to be similar to that in bulk buffer (18720 cm^{-1}) indicating a significant solvchromic shift [10] at the micellar surface with large proton concentration (ionic environment). The solvchromic shift toward red side of the emission spectrum is further confirmed by fluorescence of the probe in the micellar solution (pH=7) in presence of 1M NaCl.

Figures 4.3(a) and 4.3(b) show the steady-state emission spectra and the fluorescence decay profiles of the probe in 100 mM AOT reverse micelles (RM) with $w_0=2.5$ and $w_0=40$, respectively. The $r(t)$ (figures 4.3(c)-(d)) of the probe in $w_0=2.5$ RM (6.2 ns(57%) with a significant residual offset) shows single exponential decay in contrast to biexponential decay in $w_0=40$ RM (1.7 ns(24%), 12.85 ns(76%)) reflecting larger contribution of tumbling motion of the probe in the bigger sized RM. The higher offset in the smaller sized RM is due to incomplete rotation of the host RM, which could be rationalized in terms of higher concentration of micelles in $w_0=2.5$ RMs (aggregation-number<43) compared to that in $w_0=40$ RMs (aggregation-number>800). In the case of $w_0=40$ RM, 12.85 ns decay is due to global motion of the RM. Note that the value of the rotational anisotropy do not approach to that of bulk water (0.53 ns) even at $w_0=40$ RM indicating interfacial affinity of the probe. The probe in $w_0=2.5$ RM shows significantly slower solvation dynamics. The constructed TRES of the probe (figure 4.4(a)) in the RM

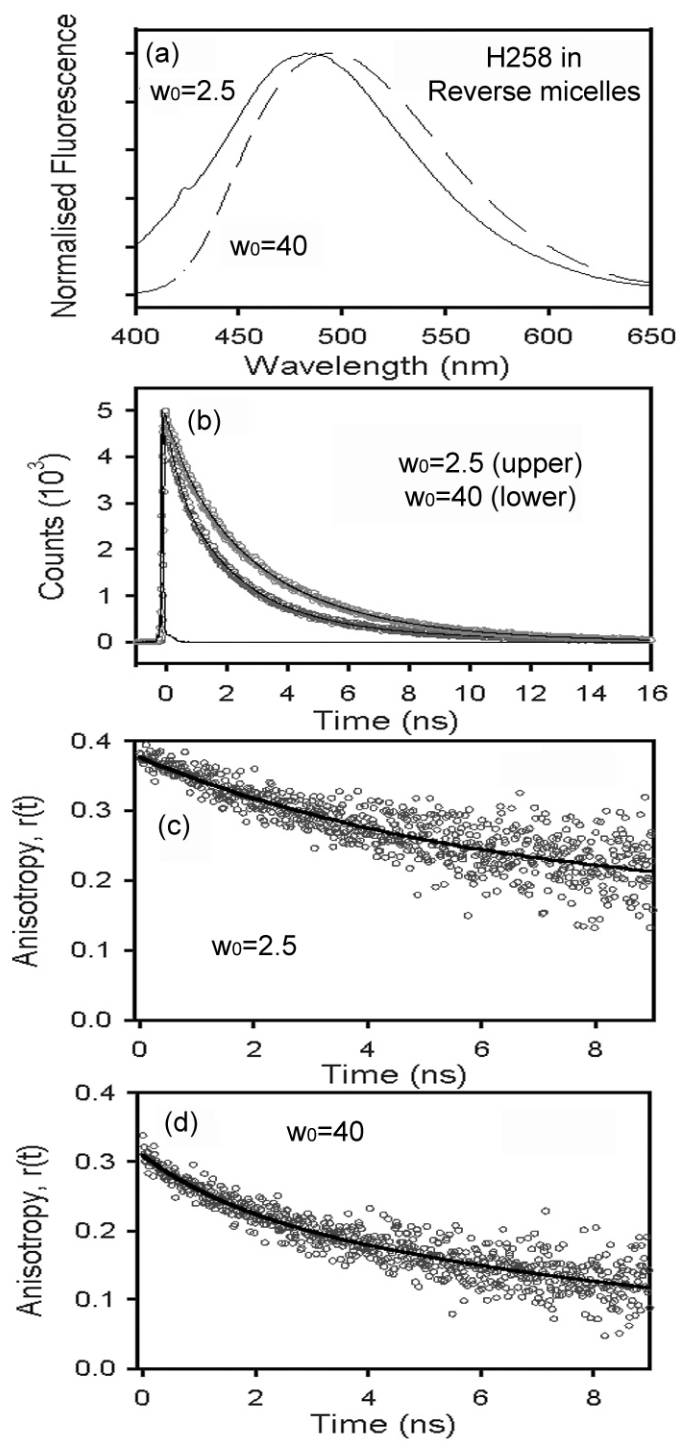


Figure 4.3. (a) The steady-state emission spectra of H258 in RMs. (b) Fluorescence transients of H258 in RMs. (c), (d) show fluorescence anisotropies of H258 in RMs.

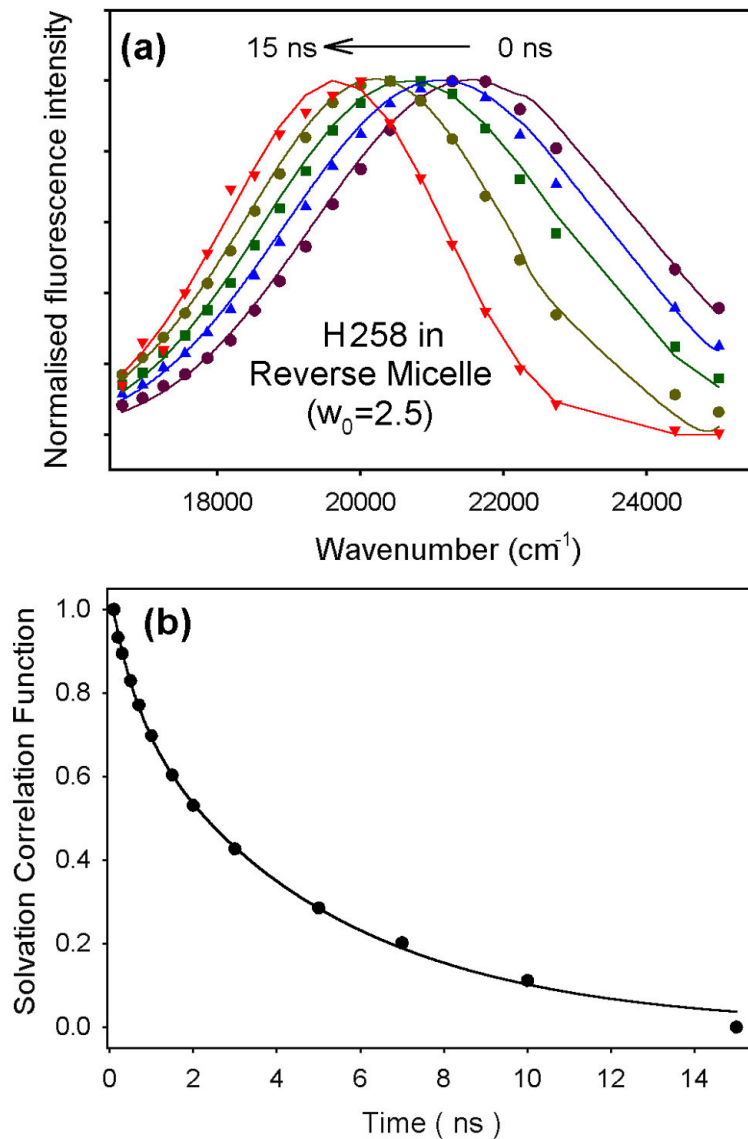


Figure 4.4. TRES (a) and solvation correlation function, $C(t)$ (b) of H258 in $w_0=2.5$ RM.

shows significant shift of 1000 cm^{-1} in 15 ns time window. The $C(t)$ (figure 4.4(b)) shows biexponential decay with time constants 0.59 ns(25%) and 4.9 ns(75%). Slower and faster components might be attributed to those water molecules near the ionic head group and the central region of the water pool respectively. The solvation dynamics in $w_0=40$ RM does not show any slower component.

Upon complexation (minor groove binding) with DNA, the fluorescence decay of the probe shows only nanosecond components in the fluorescence decay reflecting

insignificant role of either twisting or CT type of intramolecular dynamics in the microenvironment. Thus DNA-bound probe is an attractive choice to explore the internal (minor groove) dynamics of the DNA. An attempt to use the probe has already been made to explore the dynamics of hydration of genomic and synthesized DNA by using femtosecond resolved fluorescence spectroscopy [2]. However, limited experimental window (upto 200 ps) restricts the exploration of relatively slower dynamics due to local reorganizational motion of the DNA environment. Recently, studies of solvation

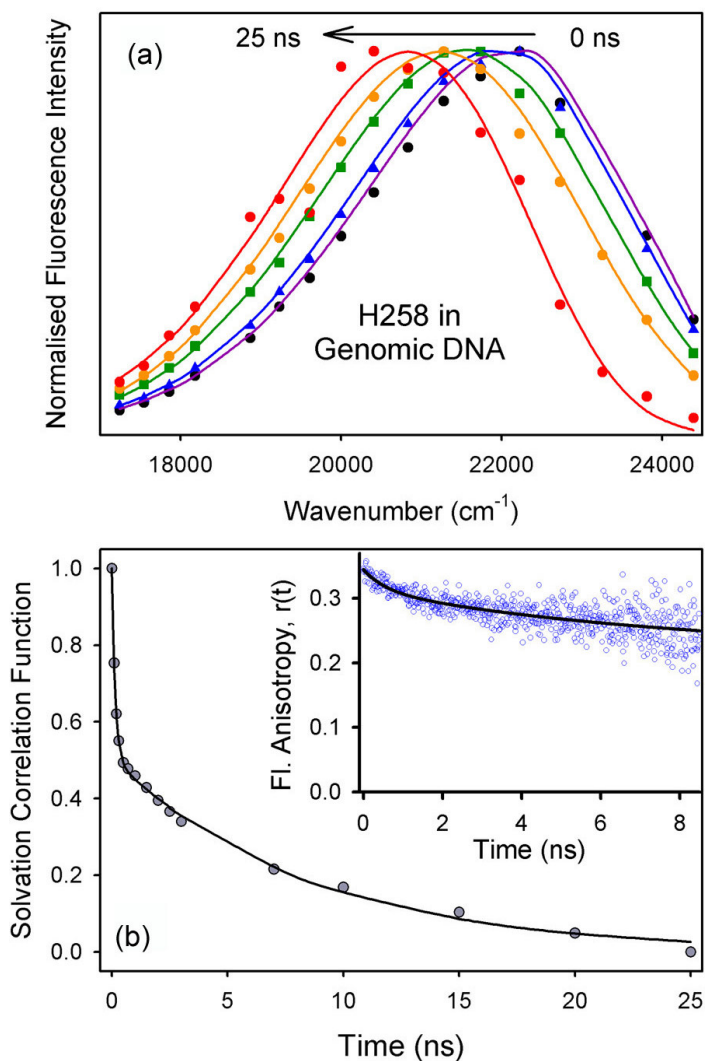


Figure 4.5. TRES (a) and solvation correlation function, $C(t)$ (b) of H258 in DNA. Restricted physical motion of the probe is evident from $r(t)$ (inset).

dynamics have been reported for extrinsic chromogenic probes, inserted into DNA either by covalent adduction of coumarin dye [11] or hydrophobic intercalation of acridine dye [12]. The fluorescence results [11] give two relaxation time constants of 300 ps(47%) and 13 ns(53%), both measured with 100 ps time resolution and attributed to the local reorganization in the modified DNA.

In order to explore the reorganizational motion of a genomic DNA by using H258, solvation studies are carried out in 100 μ M salmon sperm DNA. Figure 4.5(a) shows the constructed TRES giving a shift of 800 cm^{-1} in a 25 ns time window, essentially indicating that the probe in the excited state is stabilized due to the solvation by the DNA. The plot of C(t) (figure 4.5(b)) is fitted with a biexponential curve yielding decay components of 150 ps(49%) and 8.5 ns(51%). The temporal decay of the C(t) is similar to that of a coumarin molecule embedded in DNA [11]. The time constant of 8.5 ns obtained in our experiment is slow for even low frequency vibrational motion of the DNA or quasiharmonic oscillation of the fluorophore [11]. However, the longer time constant (8.5 ns) is consistent with the solvation due to the δ -relaxation of the DNA environment, which is attributed to the diffusion of counter ions along the DNA chain [11,13].

4.2.2. Direct Observation of Essential DNA Dynamics: Melting and Reformation of the DNA Minor Groove [14].

The B-form of DNA is a right-handed helix. The average secondary structure of DNA gives a positive peak at 277 nm and a negative peak around 250 nm in the far UV spectrum. The melting of DNA is accompanied by structural changes involving unwinding of the helix, destruction of major and minor grooves and finally the separation of the two strands resulting in the formation of two single strands of complementary sequence [15]. This is reflected by a change in the secondary structure of the DNA and the change in molar ellipticity of the DNA can be utilized to construct the melting profile of the DNA. Figure 4.6(a) shows the overall secondary structure of the dodecamer at different temperatures. It is clear that the peak at 250 nm is mostly affected by the temperature-induced melting of the DNA. The change in the molar ellipticity associated with this peak has been monitored to construct the temperature-induced melting and

rehybridization profiles of the dodecamer, as shown in figure 4.6(b). The figure shows that the dodecamer is rehybridized into the original form accompanied by a modest hysteresis effect. The melting and rehybridization temperatures have been estimated to be 50°C and 42°C, respectively in the dodecamer. In contrast, the melting and rehybridization of a genomic DNA do not follow the same pathway and there is a considerable hysteresis involved. This is consistent with the fact that under our

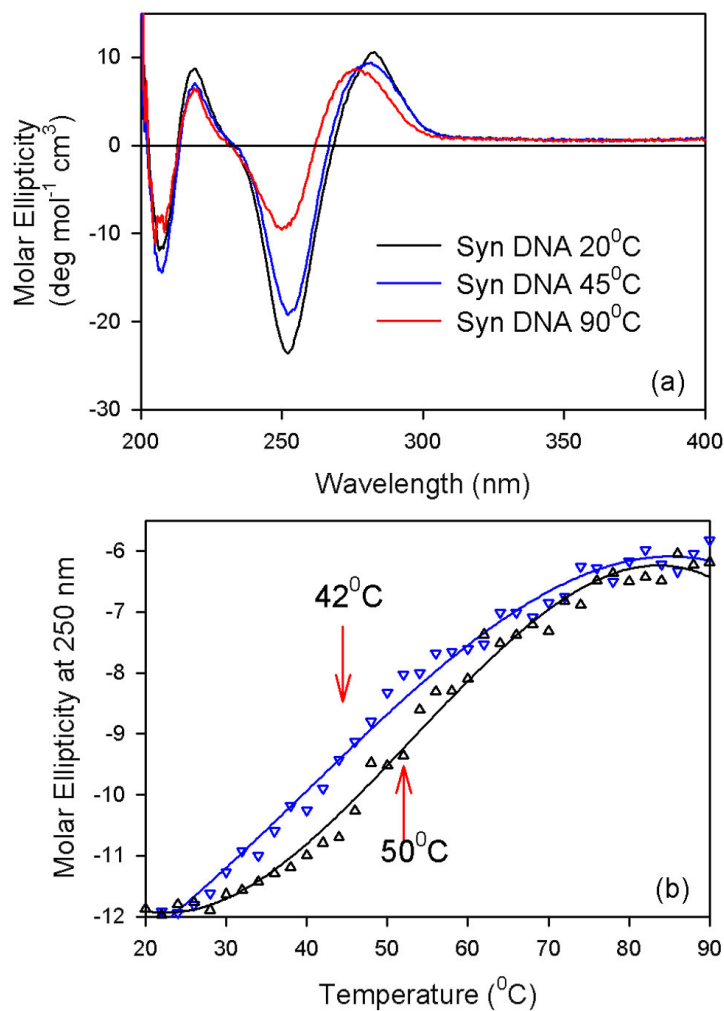


Figure 4.6. (a) The circular dichroism spectra of dodecamer DNA (labeled as Syn DNA in the figure) at various temperatures. (b) The melting (black triangles) and rehybridization (blue inverted triangles) profiles of dodecamer DNA. Solid lines are cubic polynomial fits.

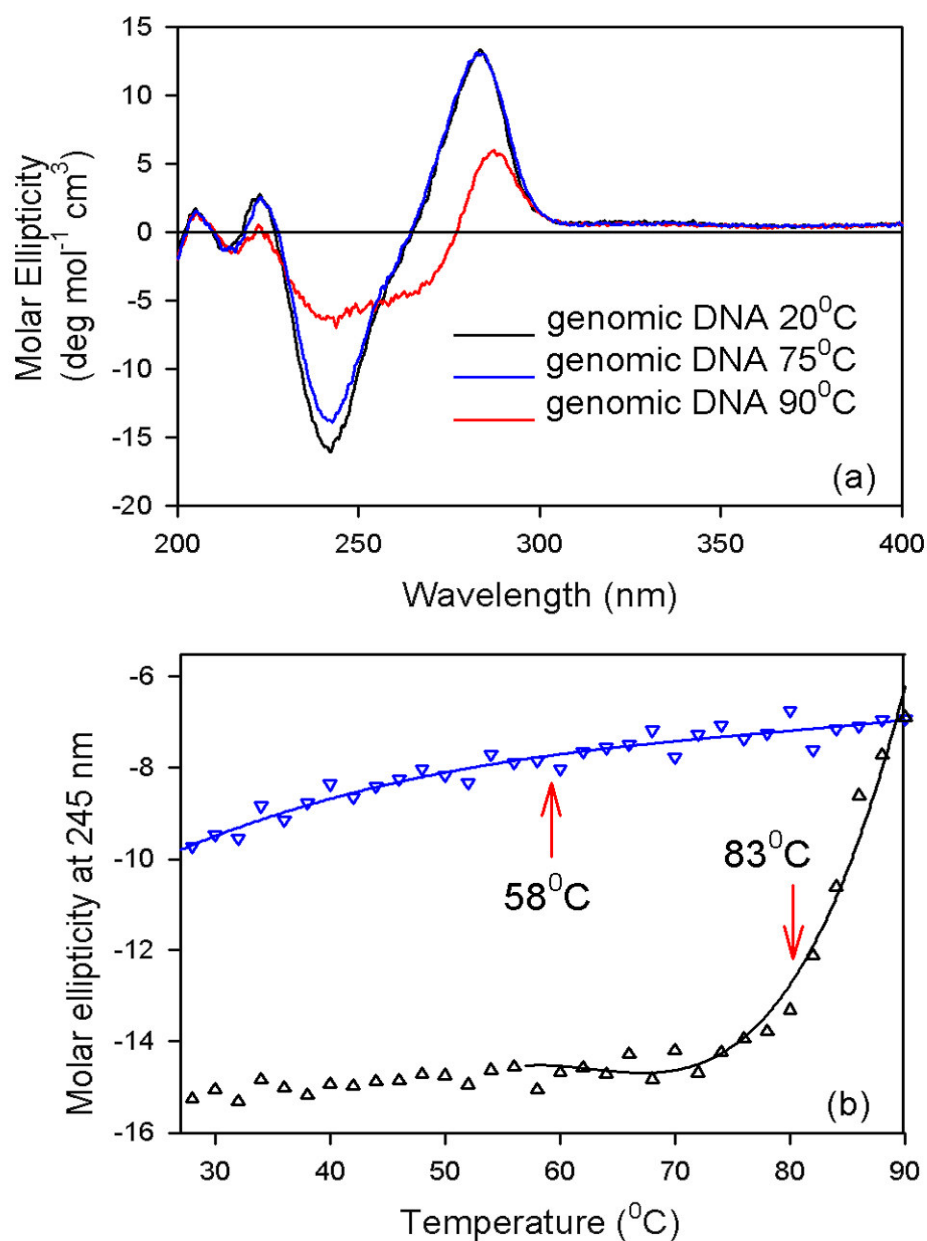


Figure 4.7. (a) The circular dichroism spectra of genomic DNA at various temperatures. (b) The melting (black triangles) and rehybridization (blue inverted triangles) profiles of genomic DNA. Solid lines are the cubic polynomial fits.

experimental conditions, the rehybridization of a long strands can be erroneous due to intrastrand loop formation [16]. Figure 4.7(a) shows the change in molar ellipticity of the genomic DNA at three different temperatures while figure 4.7(b) shows the change in molar ellipticity at 245 nm with the melting and rehybridization of the genomic DNA.

The melting and the rehybridization temperatures of genomic DNA are found to be 83⁰C and 58⁰C respectively. It is evident from the CD studies that the melting of the DNA is associated with structural changes in both the dodecamer and genomic DNA. Since the structure of a biomolecule is strongly correlated with its dynamics [17], a change in the structure of the biomolecule is likely to find reflection in the associated dynamics. A comparison of the dynamics of the macromolecule in the native and melted states brings out the essential dynamics associated with the structure of the macromolecule.

The solvation dynamics of the environment, constructed from the TRES measurements is an efficient technique to characterize the dynamics of a macromolecule [17]. To compare the dynamics of the native and single stranded DNA, it is essential that the fluorescence reporter remains an integral part of the DNA in both the conditions. The antihelminthic bisbenzimidazole drug H258 has affinity for both single stranded and double stranded DNA [5] and hence can effectively be used as a probe to report the dynamics of DNA all along its melting profile of the DNA. The drug binds to the minor groove of the DNA as characterized by X-ray crystallographic and NMR studies [18,19]. The DNA bound drug experiences a rigidity of environment as evidenced by increase in the time constant associated with the decay of the fluorescence anisotropy of the drug-DNA complex compared to that of the drug in bulk buffer [3]. Figure 4.8 shows the temporal decay of fluorescence anisotropy of the drug bound to genomic and dodecamer DNA at room temperature and above the melting temperatures. The fluorescence anisotropy of the drug in bulk buffer is also shown for comparison. The fluorescence anisotropy of the drug in bulk buffer (figure 4.8(a)) decays with a time constant of 500 ps characterizing the twisting motion of the probe in bulk buffer. When bound to the dodecamer at 20⁰C, the absence of any 500 ps component suggests that the twisting motions of H258 are frozen in the dodecamer. The temporal decay of fluorescence anisotropy of the drug at

20⁰C in the dodecamer (figure 4.8(b)) shows a long component of 5 ns associated

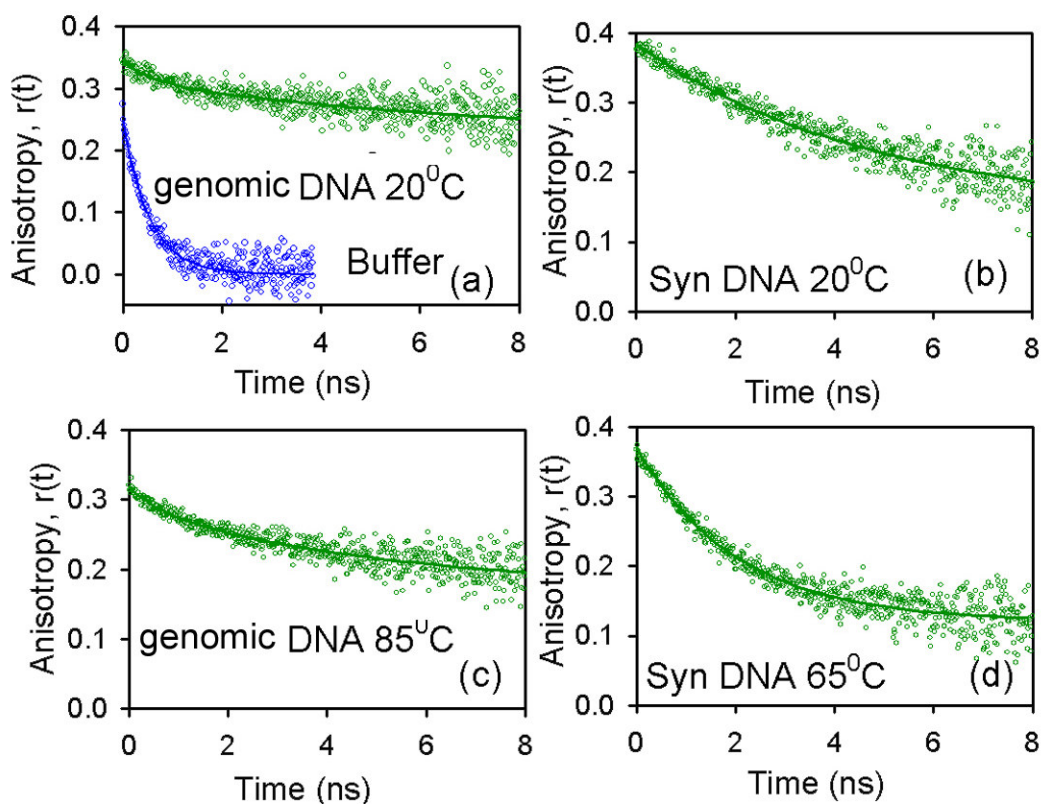


Figure 4.8. The fluorescence anisotropy of the H258 in buffer, genomic and synthesized DNAs (Syn DNA in the figures) at different temperatures. Solid lines indicate exponential fittings of the experimental data points.

with the restricted motion of the probe in the DNA. At the higher temperature (65⁰C), the time constant associated with the temporal decay of the fluorescence anisotropy decreases from 5 ns to 2 ns consistent with the faster rotational motions in the single stranded DNA at high temperature. The temporal decays of the rotational anisotropies of H258 bound to genomic DNA at 20⁰C and at 85⁰C also show similar time constants to that of the dodecamer. In addition, the temporal decay of fluorescence anisotropy in the genomic DNA shows a huge residual offset, indicating the overall motion of the DNA, which does not decay in the experimental time window. However, at the higher temperatures, in both the dodecamer and the genomic DNA temporal decay of

fluorescence anisotropy does not show time constants characteristic of probe in buffer.

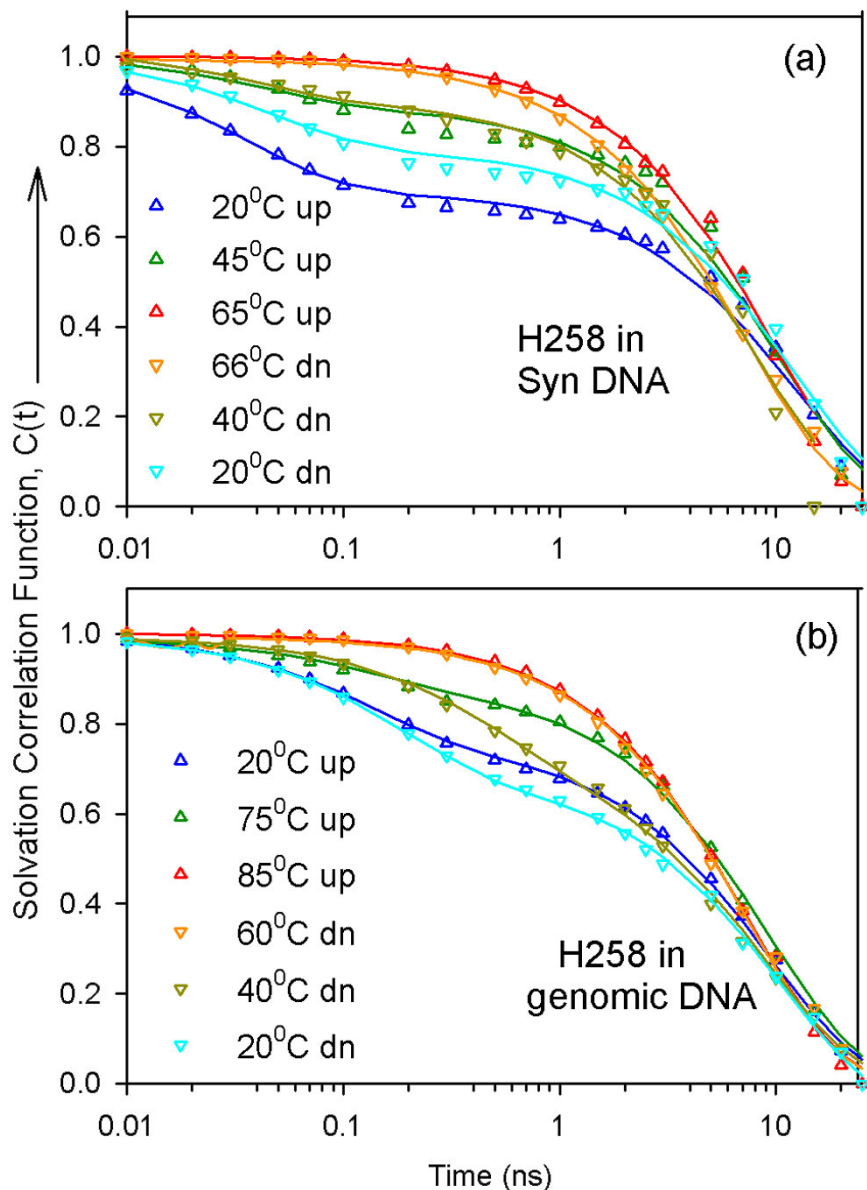


Figure 4.9. The temporal decay of the solvation correlation function at different temperatures for the synthesized dodecamer (labeled Syn DNA in the figure) (a) and genomic (b) DNA. The time has been plotted on a logarithmic scale. Solid lines indicate exponential fittings of the experimental data points.

The result clearly shows that the probe is associated with the DNA even at higher temperatures and therefore, can report the dynamics of the DNA both in the native and melted state.

Figure 4.9(a) shows the temporal decay of the solvation correlation function for the probe in dodecamer DNA at various temperatures. At 20⁰C, the solvation correlation function decays with a time constant of 40 ps(30%) and 12.3 ns(70%). At 45⁰C, the temporal decay of the solvation correlation function shows time constants of 40 ps(11%) and 12.0 ns(89%). On the completion of melting, the dynamics of solvation reported by the drug shows only the nanosecond component. The retention of this component even at high temperatures when the DNA is single stranded, strongly suggest that this long component is associated with the bending and twisting motions of the DNA backbone, and strongly associated water molecules and counterions which are an integral part of the backbone [3,11]. With increase in temperature, the value of the nanosecond component decreases from 12.3 ns to 8.2 ns. The decrease in the time constant associated with this nanosecond relaxation at higher temperatures could be rationalized considering the fact that with the increase in temperature, the bending/twisting motions of the DNA become faster.

It should be noted that the short component of 40 ps is not associated with the local motion of the H258 molecule. The rotational dynamics of the dye in bulk buffer is associated with a time constant of 500 ps [3]. The time constant of 500 ps is an order of magnitude slower than the observed time component of 40 ps. It is also to be noted that when bound to the dodecamer, the rotational motion of the dye is completely frozen as indicated by the absence of any subnanosecond component in the decay of the rotational anisotropy in the H258 bound dodecamer. The short component of 40 ps, is therefore, associated with the relaxation dynamics of DNA environment at lower temperature, which vanishes at the high temperatures, where the DNA is essentially single stranded. This component, therefore reflects the dynamics unique to the structure associated with the double stranded DNA, namely, the base pairs and the grooves. The results from femtosecond-resolved transient absorption [12] suggest an ultrafast (within 200 fs) inertial “repolarization” of nuclear degrees of freedom of the DNA pocket. In another recent study, the temperature dependent Stokes shift of acridine dye intercalated in the DNA show that the DNA dynamics are essentially diffusive in nature [20]. So, the possible contribution of the fast repolarization of base pairs to the 40 ps component in the solvation correlation function in our study can safely be ruled out. NMR studies [21]

have shown that the timescales associated with the opening of base pairs fall in the millisecond range, therefore, the contribution due to the opening of base pairs can also be ruled out. This leads to the conclusion that the observed dynamics are associated with the minor groove of the dodecamer. Femtosecond resolved solvation studies [2] of H258, bound to the dodecamer of the same sequence shows a 1 ps component associated with bulk water. Picosecond resolved studies, with our instrumental resolution; on the dye in bulk water shows no solvation, indicating that the experimental window, associated with our studies is, indeed, blind to the dynamics of the bulk water molecules. Thus, the dynamics of free water makes no contribution to the 40 ps component in our experimental window.

The study [2], also reveals a 20 ps component associated with solvation due to bound water present in the minor groove. In a recent theoretical study, [22] atomistic molecular dynamics simulations have been employed to determine the orientational time correlation function of water molecules bound to the minor groove in a 38mer DNA. The study reveals that the average orientation time associated with the ordered water molecules in the minor groove is 25.8 ps. It is to be considered that the experimental window of 50 ns used in our studies is chosen to simultaneously report both the fast and slow dynamics of the DNA. To achieve this, the resolution of the faster components has been sacrificed. Since femtosecond time resolved studies do not report any component in addition to the 20 ps component in a 200 ps window, it can be concluded that the 40 ps component obtained in our study is essentially the 20 ps component associated with the dynamics of bound waters in the minor groove. Therefore, the 40 ps component, in our experimental time resolution, reflects the dynamics of the bound water in the hydration spine in the minor groove [23]. It is worthwhile to mention that although the binding of the probe to the minor groove results in the expulsion of 55 water molecules from the groove [24], the spine of hydration is still present in the dodecamer-probe complex [25]. A high resolution crystallographic study [23] has demonstrated that monovalent cations are an intrinsic part of minor groove structure and solvation. Therefore, the possible contribution from the reorientation of these cations, present in the hydration spine of the minor groove to this 40 ps component cannot be ruled out [23].

In order to investigate the nature of variation of this component, it is useful to summarize the changes associated with the melting of DNA. The melting of DNA has been a subject of study for a long time. Various experimental and computational techniques [26-29] have been employed to characterize the melting of genomic and synthesized DNAs. It is evident from these studies that the melting of a DNA duplex is associated with the unstacking and final separation of the DNA base pairs and the eventual formation of single-stranded DNA [15]. The melting of DNA is associated with a positive ΔC_p value of $64.6 \text{ cal deg}^{-1} \text{ mol}^{-1}$ and accompanied by the loss in the number of water molecules bound to the DNA [29]. In a separate report [26], it has been suggested that the main contribution to the enthalpy of the process of heat denaturation of DNA duplex is the enthalpy of the disruption of the ordered water structure in the hydration shell of the double helix. The melting of DNA also results in the destruction of the minor groove and the spine of hydration associated with it [28]. As the DNA melts, the bound water associated with the 40 ps component to relaxation of DNA attains bulk like character across an energy barrier of $2.3 \text{ kcal mol}^{-1}$ [17]. The observed energy barrier is close to the maximum value of the activation energy (20 kJ mol^{-1} ($4.7 \text{ kcal mol}^{-1}$)) for the diffusion of bound waters of the minor groove from the DNA surface, obtained from NMR and molecular modeling experiments [30].

Thus, the initial decrease and subsequent absence of the 40 ps component at higher temperatures further confirm that this component is associated with the dynamics of the bound water and counterions associated with the spine of hydration in the minor groove. The decrease in the spectral shift (data not shown), of 200 cm^{-1} , associated with solvation at elevated temperatures confirms that we are losing a considerable fraction of solvation due to the conversion of bound water to bulk water. The time constants associated with the temporal decays of the solvation correlation function (figure 4.9(a)) at decreasing temperatures following the rehybridization of the dodecamer DNA show the recovery of the 40 ps component at the onset of structural changes associated with rehybridization. The loss in the percentage contribution of the 40 ps component at 20°C in the rehybridized DNA could be due to the improper formation (not like the native DNA) of the minor groove due to a bound dye molecule. It further confirms that the structure of the minor groove is crucial for the associated dynamics. The observations

show that the 40 ps component associated with the dynamics of bound water molecules and monovalent cations are crucial to the formation of the minor groove and are strongly correlated to the minor groove structure.

To render an interesting comparison, the same probe in genomic DNA is used to monitor the dynamics of the environment with increasing and decreasing temperature. Two widely different solvation timescales, 100 ps and 8 ns again characterizes (figure 4.9(b)) the environment of the minor groove, consistent with the solvation due to the bound waters/ions present in the hydration spine and that due to the motion of the DNA backbone/ion atmosphere. The 100 ps component follows the same general trend as that followed by the 40 ps component in the dodecamer DNA. Densimetric and acoustic measurements, used to estimate the relative change in the number of water molecules associated with a single base pair of the genomic DNA at different temperatures, reveal that there is a loss of 4 water molecules per base pair from 20⁰C to 70⁰C, consistent with other studies [27]. The 100 ps component in this case, can also be said to reflect the contribution of bound water molecules, which are released at high temperatures and reformed at lower temperatures. This consistency in the trend of the picosecond component, characterizing the bound water dynamics, in both synthesized and genomic DNA gives our interpretations a more general basis. It is interesting to observe that although the average secondary structure of native and rehybridized genomic DNA shows a wide disparity (figure 4.7(b)), it is not reflected in the dynamics reported by the dye in the rehybridized genomic DNA. The dye reports the same environment in both the native and rehybridized DNA. This interesting result can be justified considering the fact that among the many minor grooves formed on the rehybridized genomic DNA, the drug chooses a properly formed minor groove. In the dodecamer, however, only one minor groove is formed per DNA and the formation of minor groove is not perfect due to the bound drug.

4.3. Conclusion:

Our present study explores the nature of excited state charge transfer processes of a DNA minor groove binder, H258 in bulk and restricted environments including DNA. The experimental results are consistent with TICT as the dominant mode of relaxation of the

dye in bulk buffer at low pH. It also explores the possibility of using the probe to study slower relaxation dynamics in biomimetics and DNA. The study identifies the nanosecond relaxational dynamics due to δ -relaxation of a genomic DNA crucial for molecular recognition. Also, the dynamics crucial to the minor groove and that due to the DNA backbone have been decoupled. A 40 ps component reflects the environmental relaxation characterizing the minor groove of the dodecamer DNA and is associated with the relaxation dynamics due to the bound water molecules and cations present in the hydration spine associated with the minor groove. The component is distinct from the longer 12 ns component associated with the twisting/bending motions of the sugar phosphate backbone and the rigidly held water molecules and counterions, which are present even in the single stranded DNA. The 40 ps component disappears for the dodecamer DNA with the collapse of the groove and reappears with its formation, and thus can be used to monitor the melting and reformation of the minor groove.

References

- (1) K.J. Edwards, D.G. Brown, N. Spink, J.V. Skelly, S. Neidle, Molecular structure of the B-DNA dodecamer d(CGCAAATTTGCG)₂ : An examination of propeller twist and minor-groove water structure at 2.2 Å resolution, *J. Mol. Biol.* 226 (1992) 1161.
- (2) S.K. Pal, L. Zhao, A.H. Zewail, Water at DNA surfaces: Ultrafast dynamics in minor groove recognition, *Proc. Natl. Acad. Sci. USA* 100 (2003) 8113.
- (3) D. Banerjee, S.K. Pal, Ultrafast charge transfer and solvation of DNA minor groove binder: Hoechst 33258 in restricted environments, *Chem. Phys. Lett.* 432 (2006) 257.
- (4) K.K. Kalninh, D.V. Pestov, Absorption and fluorescence spectra of the probe Hoechst 33258, *J. Photochem. Photobiol. A: Chem.* 83 (1994) 39.
- (5) G. Cosa, K.-S. Focsaneanu, J.R.N. McLean, J.P. McNamee, J.C. Scaiano, Photophysical properties of fluorescent DNA dyes bound to single and double stranded DNA in aqueous buffered solution, *Photochem. Photobiol.* 73 (2001) 585.
- (6) D. Zhong, S.K. Pal, A.H. Zewail, Femtosecond studies of protein-DNA binding and dynamics: Histone I, *CHEMPHYSCHEM* 2 (2001) 219.
- (7) H. Gerner, Direct and sensitized photoprocesses of Bis -benzimidazole dyes and the effect of surfactant and DNA, *Photochem. Photobiol.* 73 (2001) 339.
- (8) D. Roy, K. Karmakar, S.K. Mondal, K. Sahu, K. Bhattacharya, Excited state proton transfer from pyranine to acetate in a CTAB micelle, *Chem. Phys. Lett.* 399 (2004) 147.
- (9) N.C. Maiti, M.M.G. Krishna, P.J. Britto, P. N., Fluorescence dynamics of dye probes in micelles, *J. Phys. Chem. B* 101 (1997) 11051.
- (10) R. Jin, K.J. Breslauer, Characterization of the minor groove environment in a drug-DNA complex: Bisbenzimidazole bound to the poly[d(AT)]·poly[d(AT)]duplex, *Proc. Natl. Acad. Sci. USA* 85 (1988) 8939.

- (11) E.B. Brauns, M.L. Madaras, R.S. Coleman, C.J. Murphy, M.A. Berg, Measurement of local DNA reorganisation on the picosecond and nanosecond time scales, *J. Am. Chem. Soc.* 121 (1999) 11644.
- (12) S. Hess, W.B. Davis, A.A. Voityuk, N. Rosch, M.E. Michel-Beyerle, N.P. Ernstring, S.A. Kovalenko, J.L.P. Lustres, Excited-state photophysics of an acridine derivative selectively intercalated in duplex DNA, *CHEMPHYSCHEM* 3 (2002) 452.
- (13) E.B. Brauns, M.L. Madaras, R.S. Coleman, C.J. Murphy, M.A. Berg, Complex local dynamics in DNA on the picosecond and nanosecond time scales, *Phys. Rev. Lett.* 88 (2002) 158101.
- (14) D. Banerjee, S.K. Pal, Direct observation of essential DNA dynamics: Melting and reformation of the DNA minor groove, *J. Phys. Chem. B* 111 (2007) 10833.
- (15) K. Drukker, G. Wu, G.C. Schatz, Model simulations of DNA denaturation dynamics, *J. Chem. Phys.* 114 (2001) 579.
- (16) S. Semsey, M.Y. Tolstorukov, K. Virnik, V.B. Zhurkin, S. Adhya, DNA trajectory in the gal repressosome, *Genes and Dev.* 18 (2004) 1898.
- (17) S.K. Pal, A.H. Zewail, Dynamics of water in biological recognition, *Chem. Rev.* 104 (2004) 2099.
- (18) M.C. Vega, I.G. Saez, J. Aymami, R. Eritja, G.A.V.D. Marel, J.H. VanBoom, A. Rich, M. Coll, Three-dimensional crystal structure of the A-tract DNA dodecamer d(CGCAAATTTGCG) complexed with the minor groove-binding drug Hoechst 33258, *Eur. J. Biochem.* 222 (1994) 721.
- (19) A. Fede, A. Labhardt, W. Bannwarth, W. Leupin, Dynamics and binding mode of Hoechst 33258 to d(GTGGAATTCCAC)₂ in the 1:1 solution complex as determined by two-dimensional ¹H-NMR, *Biochemistry* 30 (1991) 11377.
- (20) E.B. Brauns, C.J. Murphy, M.A. Berg Local dynamics in DNA by temperature dependent stokes shift of an intercalated dye, *J. Am. Chem. Soc.* 120 (1998) 2449.
- (21) P.K. Bhattacharya, J. Cha, J.K. Barton, ¹H NMR determination of base-pair lifetimes in oligonucleotides containing single base mismatches, *Nucl. Acids Res.* 30 (2002) 4740.

- (22) S. Pal, P.K. Maiti, B. Bagchi, Exploring DNA groove water dynamics through hydrogen bond lifetime and orientational relaxation, *J. Chem. Phys.* 125 (2006) 234903.
- (23) V. Tereshko, G. Minasov, M. Egli, A hydration spine in a B-DNA minor groove, *J. Am. Chem. Soc.* 121 (1999) 3590.
- (24) F. Han, N. Taulier, T.V. Chalikian, Association of the minor groove binding drug Hoechst 33258 with d(CGCGAATTCGCG)₂: Volumetric, calorimetric and spectroscopic characterizations, *Biochemistry* 44 (2005) 9785.
- (25) A. Guerri, I.J. Simpson, S. Neidle, Visualisation of extensive water ribbons and networks in a DNA minor-groove drug complex, *Nucl. Acids Res.* 26 (1998) 2873.
- (26) G.M. Mrevlishvili, A.P.S.M.C. Carvalho, M.A.V.R. da Silva, T.D. Mdzinarashvili, G.Z. Razmadze, T.Z. Tarielashvili, The role of bound water on the energetics of DNA duplex melting, *J. Therm. Anal. Cal.* 66 (2001) 133.
- (27) C.H. Spink, J.B. Chaires, Effects of hydration, ion release and excluded volume on the melting of triplex and duplex DNA, *Biochemistry* 38 (1999) 496.
- (28) Y.Z. Chen, E.W. Prohofsky, Synergistic effect in the melting of the DNA hydration shell: Melting of the minor groove hydration spine in poly(dA).poly(dT) and its effect on base pair stability, *Biophys. J.* 64 (1993) 1385.
- (29) T.V. Chalikian, J. Volker, G.E. Plum, K.J. Breslauer, A more unified picture for the thermodynamics of nucleic acid duplex melting: A characterization by calorimetric and volumetric techniques, *Proc. Natl. Acad. Sci. USA* 96 (1999) 7853.
- (30) A.N. Lane, T.C. Jenkins, T.A. Frenkiel, Hydration and solution structure of d(CGCAAATTTGCG)₂ and its complex with propamidine from NMR and molecular modelling, *Biochim. Biophys. Acta* 1350 (1997) 205.

Chapter 5

Exploration of Sequence Dependent Binding Modes of DNA

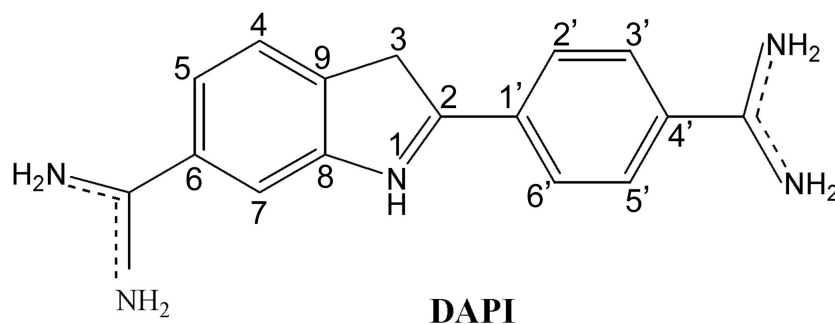
5.1. Introduction:

The interaction of ligands with double helical DNA is highly specific and sequence selective. Differences in DNA sequences can alter the expression or function of proteins that are targeted by drugs thus, can contribute significantly to variation in the responses of individuals to the same drug. The same ligand can bind differently to different DNA sequences. A representative example in this regard is the fluorescent DNA binder 4',6-Diamidino-2-phenylindole (DAPI). Studies on DAPI-DNA complexes have shown that DAPI exhibits a wide array of interaction of varying strength and specificity with DNA [1-12]. Complexes with DAPI bound in the minor groove [1,6], major groove [12] and by intercalation [3,5] have been proposed on the basis of a variety of experimental observations with different DNA samples. In addition to the above mentioned modes of binding to DNA, several unique binding modes like π - π stacking interactions [2], off-centred minor groove binding [7], nonclassical intercalation [9] and allosteric binding [11] of DAPI to DNA have also been reported. In the aforesaid studies [2,3,7,9], a variety of techniques like NMR, DNase footprinting, circular dichroism and electric linear dichroism have been employed. It is to be mentioned that for exploring the binding interaction of a ligand with biological macromolecules including DNA, solvation dynamics study is established to be an efficient tool [13,14]. Since the environmental dynamics of the minor groove, major groove and the interior of the DNA have been well characterized in a number of simulation [15] and spectroscopic studies with femtosecond [16-18] and picosecond [19] resolution, the investigation of the environmental dynamics could be an efficient technique to visualize the environment where the probe resides. However, the use of DAPI as a reporter of the environmental dynamics of restricted environment including DNA is not straightforward. This is due to the presence of two competing relaxation processes (intramolecular proton transfer and solvation

stabilization) in the excited state, which may lead to erroneous interpretation of the observed excited state dynamics. In this chapter, we utilize photophysical properties of DAPI to explore the condition in which, the probe can unambiguously report the dynamics of a restricted environment, and use the results to distinguish two popular sequence selective modes of DAPI-DNA interactions.

5.2. Results and Discussion:

5.2.1. Excited State Solvation and Proton Transfer Dynamics of DAPI in Biomimetics and Genomic DNA [20].



Scheme 5.1. Schematic representation of the probe DAPI.

The probe DAPI (Scheme 5.1) is a positively charged molecule bearing 2 units of positive charge. The results of the photophysical studies [21], mentioned above, suggest that the excited state proton transfer from amidino to the indole ring of DAPI involves the hydration shell surrounding the molecule. In the study [21], the proton transfer has been characterized by a fast component of 190 ps and the absence of proton transfer in DAPI-DNA complex has been attributed to the disruption of the hydration shell in the minor groove of DNA. The disruption of the hydration shell might affect the hydrogen bonding interactions of DAPI with the solvent [22]. To further investigate the effect of hydration/hydrogen bonding/solvent polarity on the nature of the excited state proton transfer, the excited state dynamics of the dye is studied in water-1,4-dioxane (dioxan) mixtures. Figure 5.1(a) shows the emission spectra of the dye in dioxan- water mixture at

different percentages of dioxan. The emission spectrum shows a considerable dependence on the solvent as is expected for a dye exhibiting proton transfer [23]. In bulk water, the emission is much quenched indicative of proton transfer. On the progressive addition of dioxan, there is a gain in the fluorescence intensity without any shift of the emission

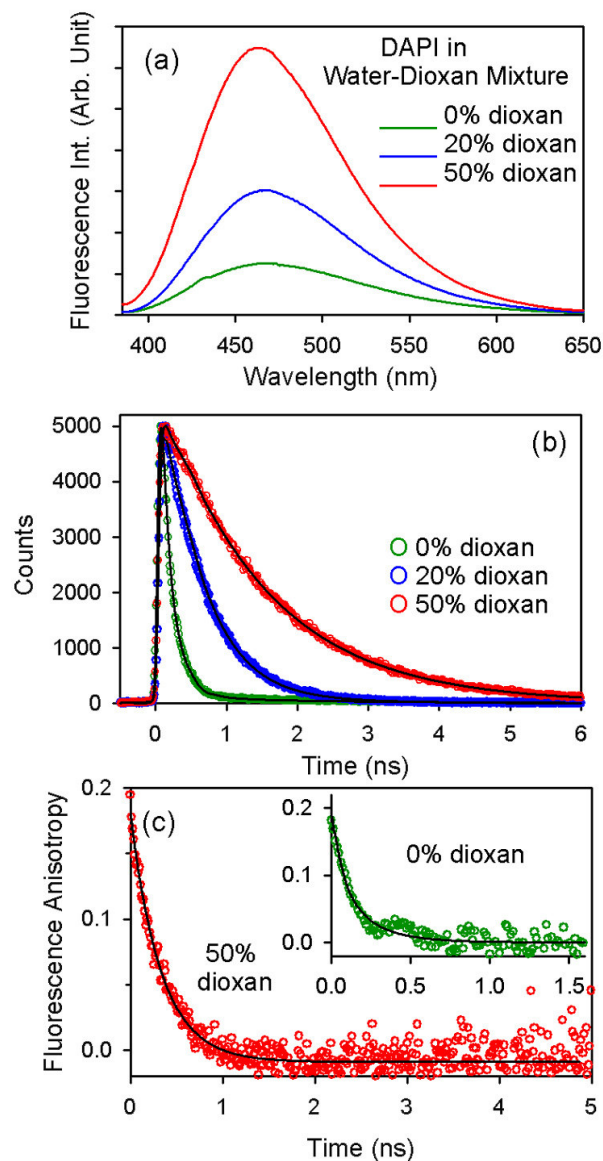


Figure 5.1. The emission (a) of DAPI in water-dioxan mixtures (i)0% dioxan, (ii)20% dioxan, (iii) 50% 1,4 dioxane. The temporal fluorescence decay (b) of DAPI in water-dioxan mixture. The temporal decay of fluorescence anisotropy (c) of DAPI in water-dioxan mixture containing 0% (inset) and 50% dioxan. The lifetime and anisotropies are monitored at their corresponding emission maxima.

Table 5.1: DAPI in Different Environments

Medium	Fluorescence Lifetimes		Rotational Correlation Time Constants		Solvation Corr. Function		Spectral Shift (cm ⁻¹)
	τ_1 (ns)	τ_2 (ns)	τ_1 (ns)	τ_2 (ns)	τ_1 (ns)	τ_2 (ns)	
Buffer	0.120 (98%)	2.2 (2%)	0.100 (100%)	-	-	-	-
Water+ 0%DX*	0.122 (97%)	2.2 (3%)	0.100 (100%)	-	-	-	-
Water+ 20%DX*	0.513 (97%)	1.7 (3%)	0.130 (100%)	-	-	-	-
Water+ 50%DX*	0.800 (77%)	1.3 (23%)	0.150 (100%)	-	-	-	-
SDS	0.120 (13%)	3.1 (87%)	-	2.3 (100%)	1.0 (100%)	-	283
TX-100	0.120 (63%)	3.0 (37%)	0.110 (20%)	2.8 (80%)	-	-	-
CTAB	0.120 (97%)	1.4 (03%)	0.100 (100%)	-	-	-	-
w ₀ =2.5	0.700 (28%)	2.7 (72%)	4.1 (100%)	-	0.227 (51%)	3.1 (49%)	1425
w ₀ =5	0.410 (22%)	2.7 (78%)	5.8 (100%)	-	0.137 (65%)	1.5 (35%)	1164
w ₀ =10	0.320 (19%)	2.7 (81%)	14.0 (50%)	2.8 (50%)	0.080 (69%)	1.1 (31%)	946
w ₀ =20	0.280 (17%)	2.6 (83%)	64.0 (40%)	2.8 (60%)	0.060 (40%)	0.523 (60%)	694
DNA	1.00 (37%)	3.8 (63%)	0.600 (23%)	4.1 (24%)	0.180 (77%)	6.0 (23%)	734

**DX in the table stands for dioxan. The rotational anisotropy of DAPI in DNA contains an additional offset (53%). The fluorescence lifetimes and the rotational anisotropies in different mediums have been monitored at the corresponding emission maxima.*

maximum suggesting that the proton transfer process is hindered. The fast component (120 ps, associated with proton transfer) in the temporal decay of fluorescence in water becomes longer (800 ps) in water-dioxan mixture (water + 50% dioxan) (figure 5.1(b), Table 5.1). The replacement of water by dioxan in the solvation shell decreases its polarity and proticity, both of which can alter solvent assisted proton transfer by affecting the hydrogen bonding interactions of the molecule with the solvation shell. However, the

replacement of water by protic ethanol in the solvation shell, alters the solute-solvent hydrogen bonded interactions due to the polarity effect. Earlier studies have shown that the lifetimes of the dye in ethanol does not show the 120 ps component associated with intramolecular proton transfer [24]. The absence of the 120 ps component in ethanol suggests that the intramolecular proton transfer process depends on the solvent polarity rather than the solvent proticity. The dependence of the excited state photo processes on solvent polarity clearly indicates that the excited state proton transfer involves the role of the solvent surrounding the dye molecule. A similar conclusion is reported in a separate study [21]. Figure 5.1(c) shows the temporal decay of fluorescence anisotropy of the dye in water-dioxan mixture having 50% dioxan. The modest difference of the time constants with that of aqueous buffer (inset of figure 1(c)) suggests that the changes in the excited state photo processes are concerned exclusively with the change in solvent polarity, *not* with solvent viscosity.

The study in the bulk solvents with varying polarity suggests that in the excited state, the proton transfer is a dominant mode of excited state relaxation. The proton transfer of DAPI depends on the polarity and/or presence of water molecules in close vicinity of the probe molecule. The proton transfer process is manifested by a fast decay in the blue end and rise in the red end, similar to solvation stabilization [25]. To explore the possibility of using such a probe as a solvation reporter in biomolecules like DNA and other biomimetics, the proton transfer process in the macromolecules should be considered. Considering the high affinity of the drug to the negatively charged DNA [6,10], SDS micelles with negative charge is the obvious choice of a suitable biomimetic. Figure 5.2(a) shows the absorption and emission spectra of the dye in 40 mM SDS solution. The observed red shift ($\lambda_{\text{abs}}=355$ nm) in the absorption spectrum compared to DAPI in buffer ($\lambda_{\text{abs}}=342$ nm) reflects the ground state stability of the probe in the negatively charged micelle. The emission spectrum shows 8 nm blue shift compared to the emission in buffer, indicative of the destabilization of the excited state of the probe in the nonpolar micellar environment. The temporal decay of the fluorescence of the probe in SDS micelles (figure 5.3(b)) is associated with time constants of 120 ps(13%) and 3.1 ns(87%). The longer component of 3.1 ns reflects the lifetime of the probe in the

hydrophobic environment. The geometrical restriction imposed on the dye is borne out by

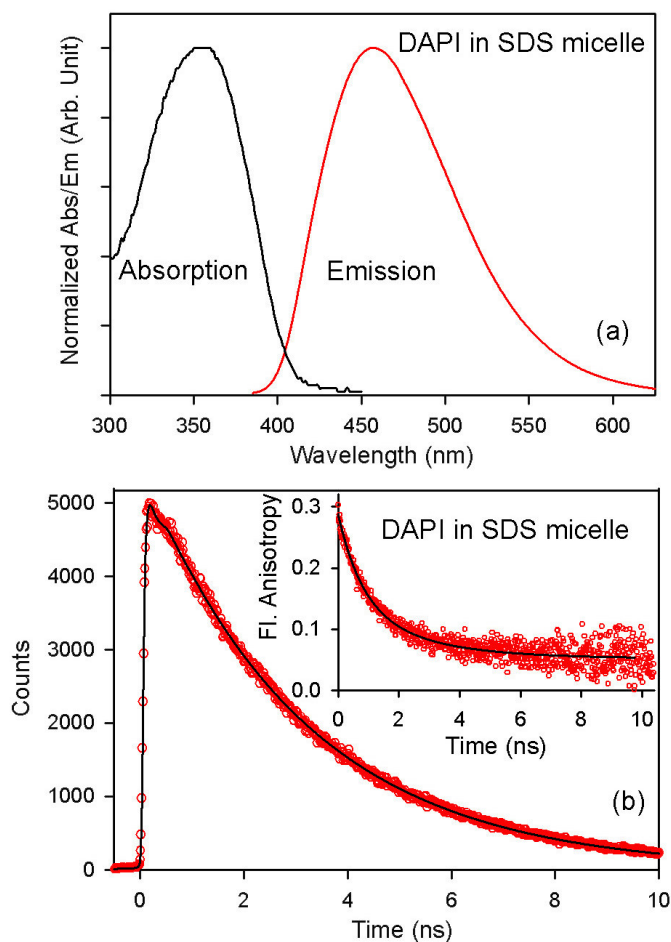


Figure 5.2. The absorption and emission (a), temporal fluorescence decay (b) and fluorescence anisotropy (inset of (b)) of DAPI in SDS micelles. The lifetime and anisotropy is monitored at their corresponding emission maxima.

the slower decay of the fluorescence anisotropy (inset of figure 5.2(b)), compared to that in bulk buffer. The time constant of 2.3 ns, associated with the decay of fluorescence anisotropy is consistent with the location of the dye at the micellar interface [19,26].

In order to investigate the nature of dominant forces that dictate the interaction of the probe with hydrophobic moieties like micelles, we have studied the excited state dynamics of DAPI in neutral TX-100 micelles and positively charged CTAB micelles

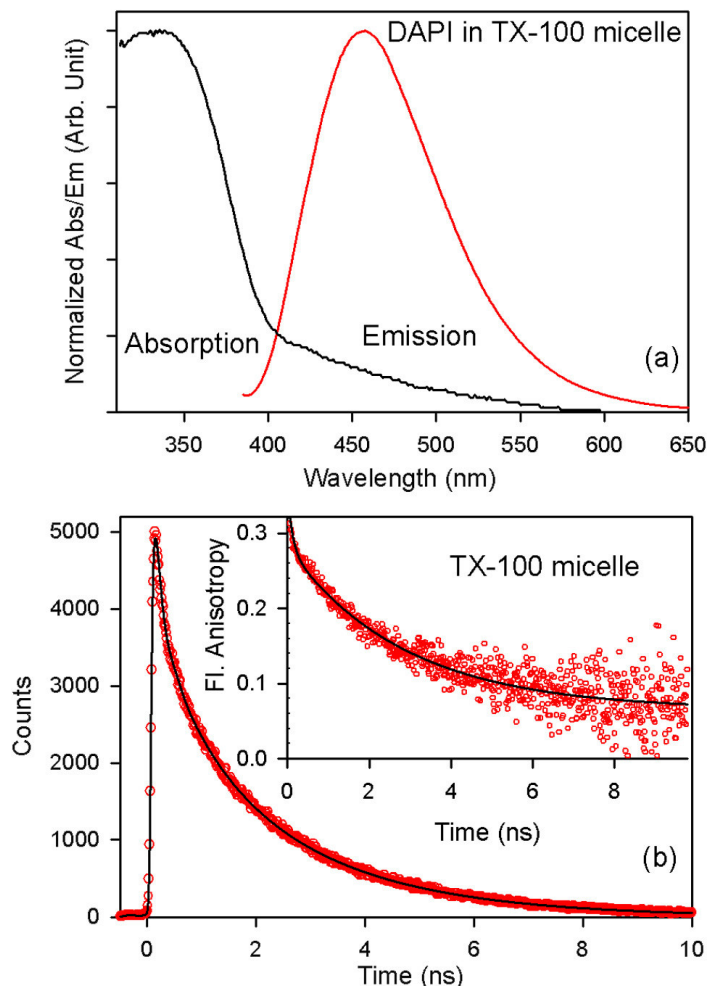


Figure 5.3. The absorption and emission, (a) temporal fluorescence decay (b) and fluorescence anisotropy (inset of (b)) of DAPI in TX-100 micelles. The lifetime and anisotropy is monitored at their corresponding emission maxima.

Figure 5.3(a) shows the absorption and emission spectra of DAPI in TX-100 micelles. The red shift of 13 nm in the absorption spectrum and the blue shift of 7 nm in emission spectrum compared to the absorption and emission spectra of the probe in bulk buffer indicate the interaction of the probe with the micelle. A significant (51%) retention of bulk like decay (120 ps) in the temporal decay of fluorescence (figure 5.3(b)) suggests that a considerable fraction of the molecule undergoes proton transfer. It is to be noted that the fast dynamics is not due to the population of the probe in bulk buffer. This is evidenced from the slower rotational time constant in the rotational anisotropy (figure 5.3(b), inset) suggesting that a significant fraction (80%) of the probe remains bound to

the TX-100 micelles. Thus, the possibility of the polar head groups of TX-100 micelles, involved in hydrogen bonding and proton transfer cannot be ruled out. The dynamics of the probe in CTAB micelles are essentially similar to that in bulk buffer, indicating that the probe does not interact with CTAB micelles. The observations prove beyond doubt that charge interactions overwhelm hydrophobic interactions in the recognition of DAPI by organized assemblies like micelles. The result finds biological relevance in the different molecular recognition of trypsin and α -chymotrypsin by the probe [27].

In order to study the relaxation dynamics of DAPI in SDS micelles, the fluorescence decays are monitored at the blue and red ends of the emission spectrum. The fast decay in the blue end and rise in the red end (figure 5.4(a)) of the probe might be indicative of solvation. The constructed TRES (data not shown), shows a shift of 276 cm^{-1} in a 1.5 ns window. The solvation correlation function decays with a time constant of 1.0 ns. However, it is to be noted that the probe undergoes proton transfer in the excited state. Thus, the decay and the rise in the blue and red ends as well as the observed shift can also represent the excited state proton transfer dynamics. At the surface of an ionic micelle, the effective pH can be calculated using the formula, $C_s = C_b \exp(-e\psi/k_B T)$ [28] C_s , C_b , ψ , k_B and T being hydrogen ion concentrations in bulk and at the micellar surface, surface potential, Boltzmann constant and absolute temperature, respectively. As a result, at the surface of the negatively charged SDS micelle, the actual pH is much less than that of the bulk buffer (pH=7). This suggests that the molecule remains as a dication even at the micellar surface, no anions are present. In order to investigate the exact cause for the observed spectral shift, time resolved area normalized emission spectra (TRANES) are constructed for the probe in SDS micelles (figure 5.4(b), inset). TRANES is an effective technique to study the equilibrium between two species in the system [29-31]. The presence of isoemissive point in TRANES in SDS (figure 5.4(b)) indicates that the observed spectral shift has significant contribution from proton transfer dynamics. The rate of proton transfer in SDS environment using Birks scheme [32] is found to be $3.3 \times 10^6\text{ s}^{-1}$.

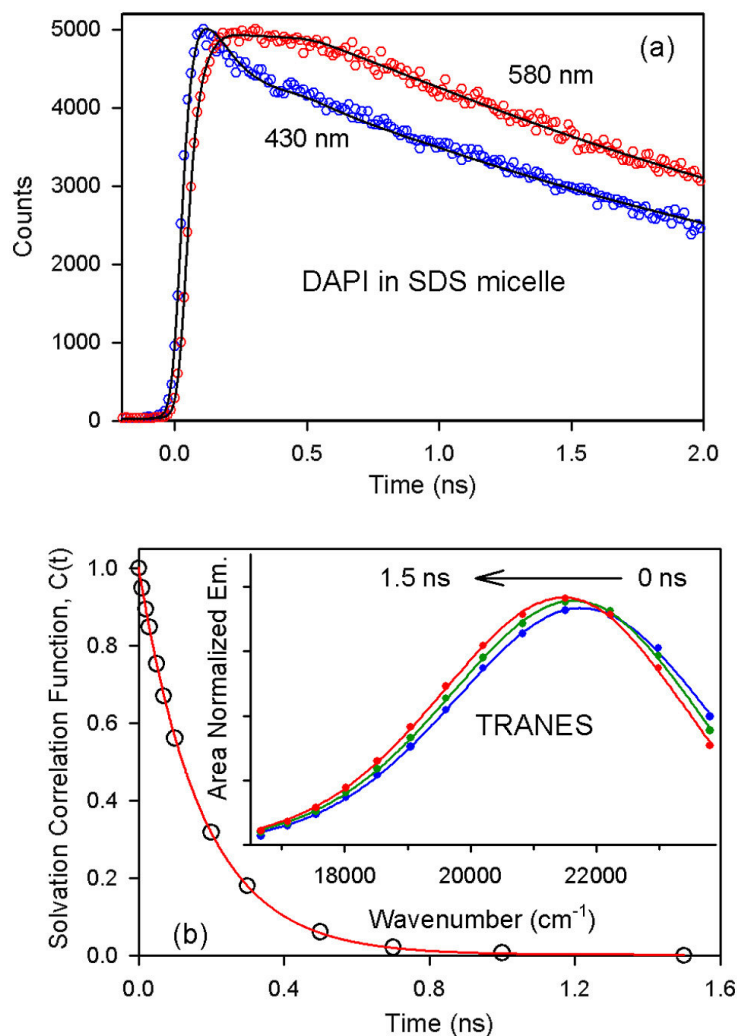


Figure 5.4. The fluorescence transients (a), TRANES ((b), inset) and the solvation correlation function (b) of DAPI in SDS micelles.

In order to study the effect of controlled increase in the number of water molecules in restricted environment, negatively charged AOT/isooctane reverse micelles (RM) with different w_0 values are excellent choices. Figure 5.5(a) shows the absorption and emission spectra of the probe in RM with $w_0=2.5$. The 13 nm red shift in the absorption spectrum compared to that of the probe in buffer indicates ground state stabilization of the positively charged probe in negatively charged AOT. The emission maximum shifts from 465 nm in buffer to 456 nm in the RMs. The blue shift in emission spectrum indicates destabilization of the excited state of DAPI in the hydrophobic

environment of the RM. The time constants associated with the temporal decay of fluorescence (Table 5.1) (figure 5.5(b)) are 700 ps and 2.7ns. In this regard, it is to be noted that lifetime of the probe in less polar water dioxane mixtures comes to be 800 ps and 1.3 ns. Also the lifetimes of the probe in the hydrophobic minor groove of DNA are 1.0 ns and 3.8 ns (Table 5.1). A comparison of the lifetime of DAPI in RMs

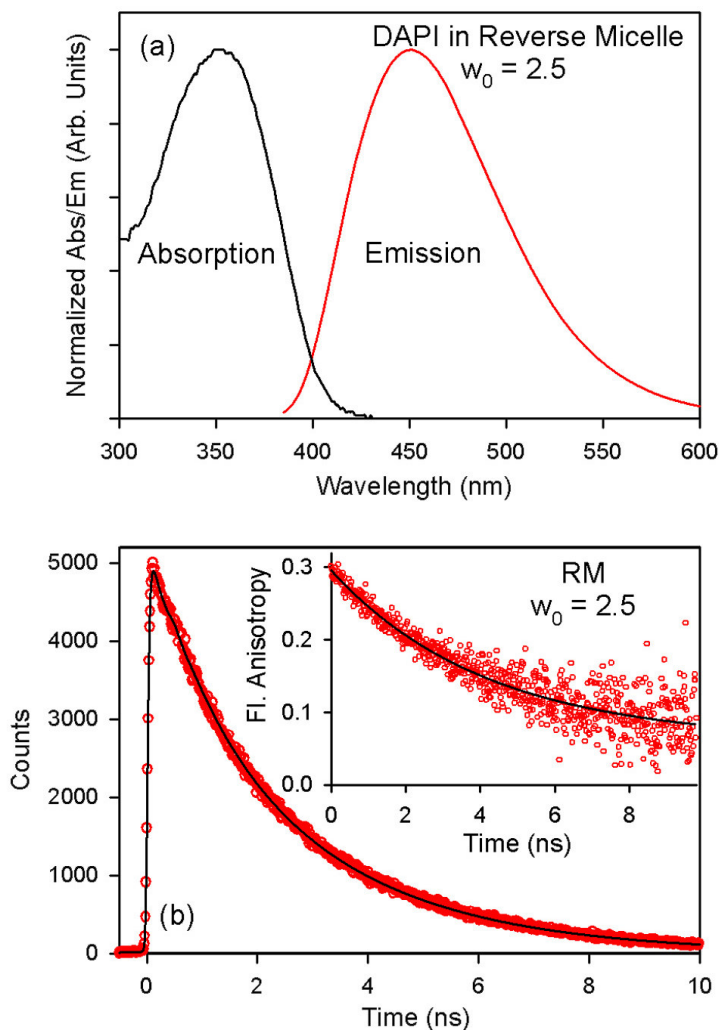


Figure 5.5. The absorption and emission (a) temporal decay of fluorescence (b) and fluorescence anisotropy (inset of (b)) of DAPI in reverse micelles ($w_0=2.5$). The lifetime and anisotropy are monitored at their corresponding emission maxima.

with the lifetimes in other hydrophobic environments reveals that the probe resides in a hydrophobic environment in the RMs. It should be mentioned that the possibility of

residence of the probe in the isooctane phase is negligibly small because of the insolubility of the probe in isooctane. The geometrical restriction of the probe environment is borne out by the decay of fluorescence anisotropy (inset of 5.5(b)). The time constant of 4.1 ns associated with the decay is consistent with the rotational time scale of the RM. The absence of the any additional faster component indicates that the rotational motions of the probe are sufficiently freezed in the RM.

To investigate the location of the probe in the negatively charged reverse micelles, the temporal decays of fluorescence anisotropy of the probe are monitored in reverse micelles with different w_0 values (Table 5.1). A comparison of the obtained results with the global tumbling motion of the RMs, obtained from the Stokes Einstein Debye (SED) [33] equation reveals that the smaller sized RM ($w_0=2.5$ and $w_0=5$), the rotational lifetimes (4.10 and 5.8 ns from experiment, 3.0 and 4.5 ns from SED equation) essentially reflect the global tumbling time of the reverse micelles. In these reverse micelles, the dye's rotation is essentially freezed and masked by the overall motion of the RMs. However, in the bigger sized RM faster rotational motions of the probe, indicated by a component of 2.8 ns are observed in addition to that corresponding to the global tumbling (14 ns and 65 ns for $w_0=10$ and $w_0=20$, respectively). The increased water mobility in the bigger sized RMs is responsible for the faster rotational motion of the probe, the observation being consistent with a recent study [34]. The time constant of 2.8 ns is consistent with the location of the probe at the micellar interface [26]. To investigate whether the probe can report the environmental dynamics of the reverse micelle, decays are taken across the emission spectrum. The probe shows fast decay in the blue end, and a rise in the red end (figure 5.6(a)) in reverse micelle with $w_0=2.5$, which might be reflective of the solvation dynamics. The inset of figure 5.6(b) shows the constructed TRES and figure 5.6(b) shows the decay of the correlation function of the probe in $w_0=2.5$. The time constants of 227 ps(51%) and 3.1 ns(49%) associated with the temporal decay of the correlation function are consistent with the location of the dye in the interface of the reverse micelle. The time constants associated with the decay of the

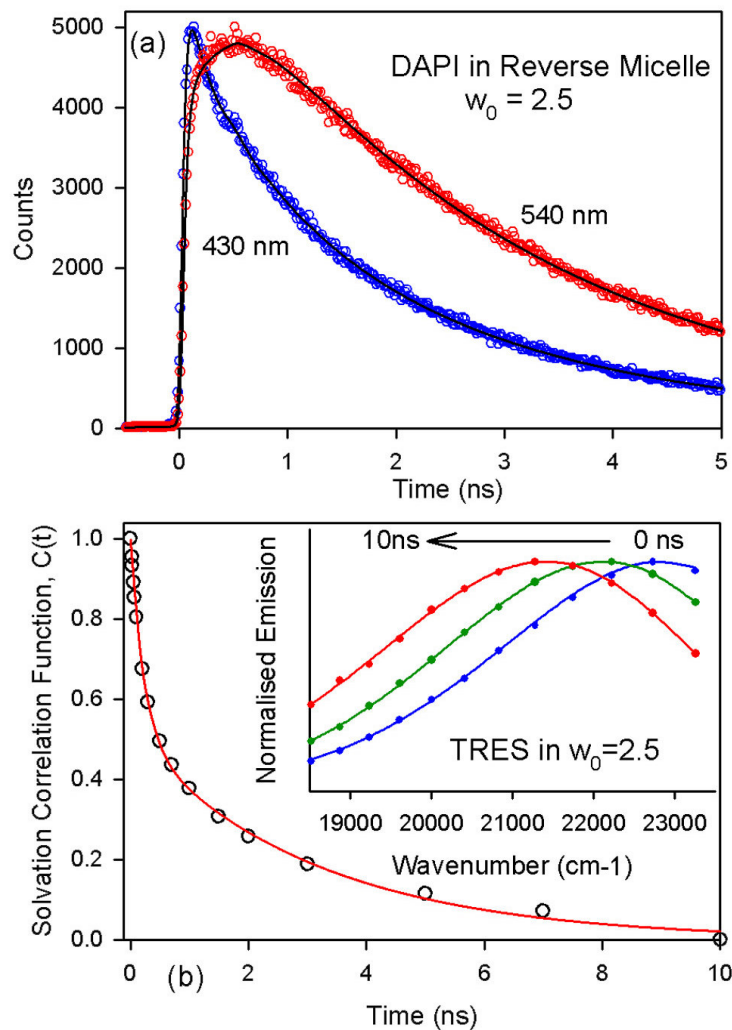


Figure 5.6. The fluorescence transients (a), TRES ((b), inset) and the solvation correlation function, $C(t)$ (b) of DAPI in Reverse Micelle ($w_0=2.5$).

solvation correlation function becomes progressively faster as the size of the RM increases from $w_0=2.5$ to $w_0=20$ (0.057 ns(40%), and 0.523 ns(60%), Table 5.1). The spectral shift associated with the solvation also shows a decrease from $w_0=2.5$ (1425 cm⁻¹) to $w_0=20$ (700 cm⁻¹) (Table 5.1). The decrease in spectral shift is observed because with our instrumental resolution, we are losing a considerable fraction of ultrafast solvation in bigger sized RMs [35]. Similar loss in ultrafast solvation is also evident from spectral shift associated with the TRES in micellar environment. The faster time constants and decrease in spectral shift in our instrumental resolution is consistent

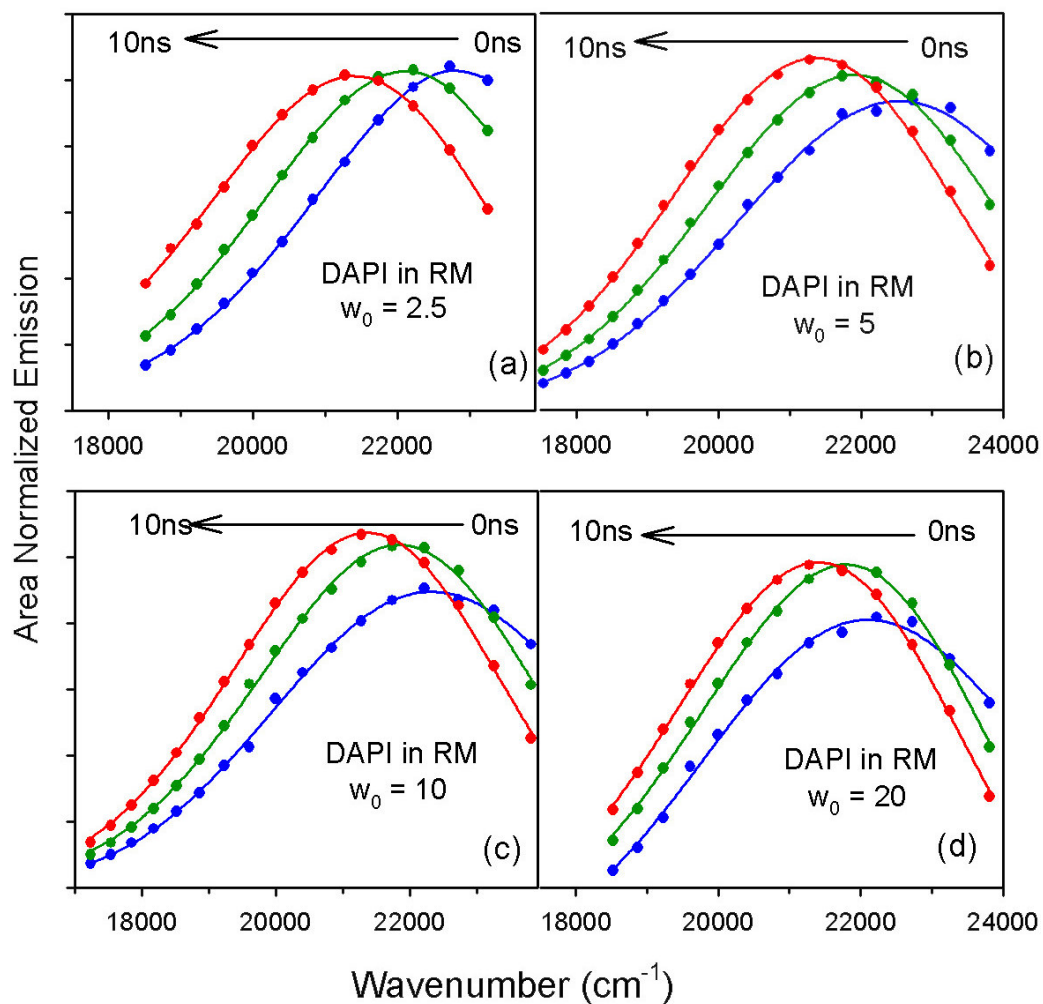


Figure 5.7. The TRANES of DAPI in Reverse Micelles with different w_0 s.

with the increase in the hydrophilicity and lability of the water molecules present at the interface of the RM.

In order to distinguish solvation from intramolecular charge transfer phenomenon, TRANES are constructed in reverse micelles with various w_0 values. None of the spectra (figure 5.7) show isoemissive points. The absence of isoemissive points indicates that the probe reports the dynamics of the environments, the time constants associated with the relaxation of the reverse micellar environments is consistent with a previously reported study [36]. The study shows that the protolysis reaction of acids in the water pool of AOT reversed micelle strongly depends on the localization of the acid in the micelle. The acid

molecules which are located around the centre and at the vicinity of the interface show

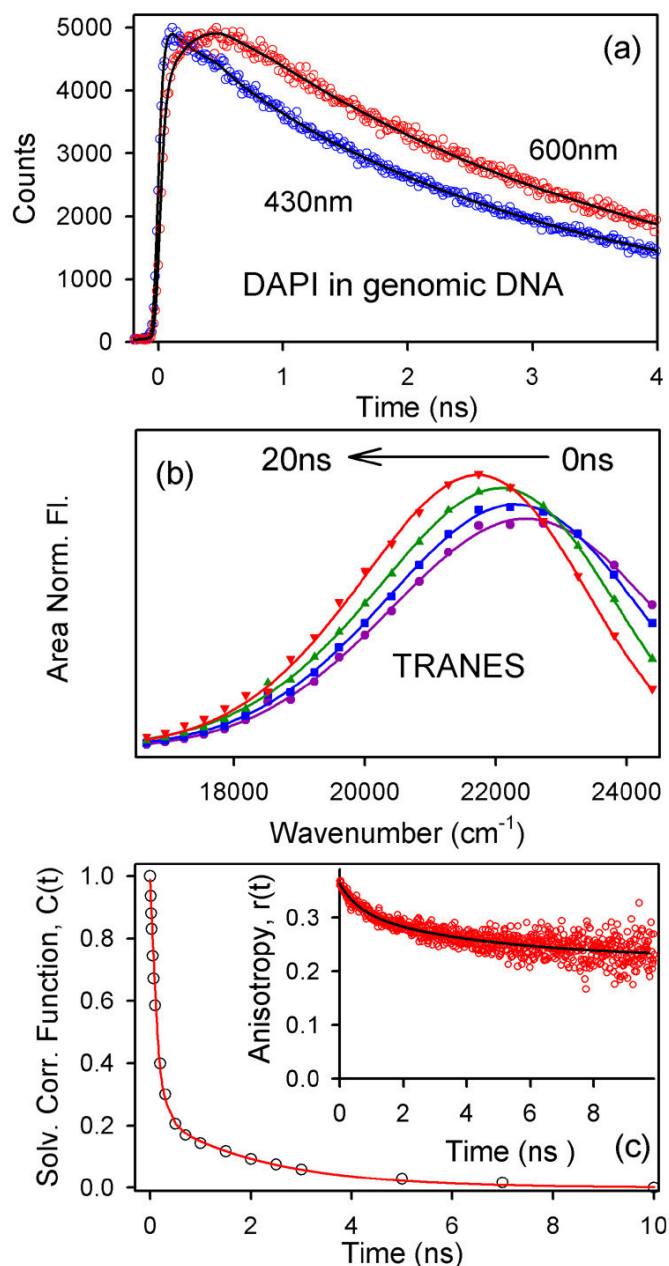


Figure 5.8. The fluorescence transients (a), TRANES (b), solvation correlation function (c), and anisotropy (c, inset) of DAPI in salmon sperm DNA. The anisotropy has been monitored at the fluorescence maxima.

deprotonation similar to bulk water at $w_0=10$ and $w_0=40$, respectively, but the acid molecule located at the interface does not undergo deprotonation at any w_0 value. The absence of the proton transfer could be due to lack of a significant number of water

molecules needed for the proton transfer process [37] or the hydrogen bonded structure of the water at the interface [36].

At this stage, it would be worthwhile to consider the dynamics reported by DAPI in genomic salmon sperm DNA. It is important to mention in this regard that the high concentration of DNA (100 μM base pair) compared to low concentration of DAPI (1 μM), ensures that the probe is bound in the high affinity binding mode (minor groove binding in AT rich sequences). A red shift in the absorption spectrum ($\lambda_{\text{abs}}=356$ nm) (data not shown), compared to that of the probe in buffer ($\lambda_{\text{abs}}=342$ nm), indicates the ground state stabilization of the probe in genomic salmon sperm DNA. The emission spectrum ($\lambda_{\text{em}}=450$ nm) (data not shown) shows a 15 nm blue shift compared to that of DAPI in buffer ($\lambda_{\text{em}}=465$ nm) indicating the excited state destabilization of the probe in the less polar DNA environment. The temporal decay of fluorescence shows time constants in the nanosecond scale. The increase in fluorescence lifetime of the probe compared to that in bulk buffer (120 ps) is consistent with the residence of the probe in the hydrophobic DNA environment. The temporal decay of fluorescence anisotropy (inset of figure 5.8(c)) is associated with time constants of 600 ps(23%) and 4.1 ns(24%), along with a residual offset. The offset indicates incomplete rotation of the genomic DNA in our experimental time window. The fast decay in the blue end and rise in the red end (figure 5.8(a)) coupled with the absence of an isoemissive point in the TRANES (figure 5.8(b)) clearly indicates that the reported dynamics reflects solvation stabilization of the DNA environment. The solvation correlation function (figure 5.8(c)) decays with time constants of 180 ps(77%) and 6.0 ns(23%). The observed time constants are comparable with those reported by other DNA binding dyes in restricted environments [38].

5.2.2. Dynamics in the DNA Recognition by DAPI: Exploration of the Different Binding Modes [39].

Figure 5.9(a) shows absorption and emission spectra of DAPI bound to the synthetic dodecamer duplex (CGCGAATTTCGCG)₂ (oligo1). The absorption spectrum shows a red shift compared to that of the probe in buffer, consistent with the ground state stabilization of a positively charged probe in negatively charged DNA. The emission spectrum shows a blue shift, compared to the emission in bulk buffer, suggesting that the

excited state dipole of the probe is less stabilized in the less polar and hydrophobic

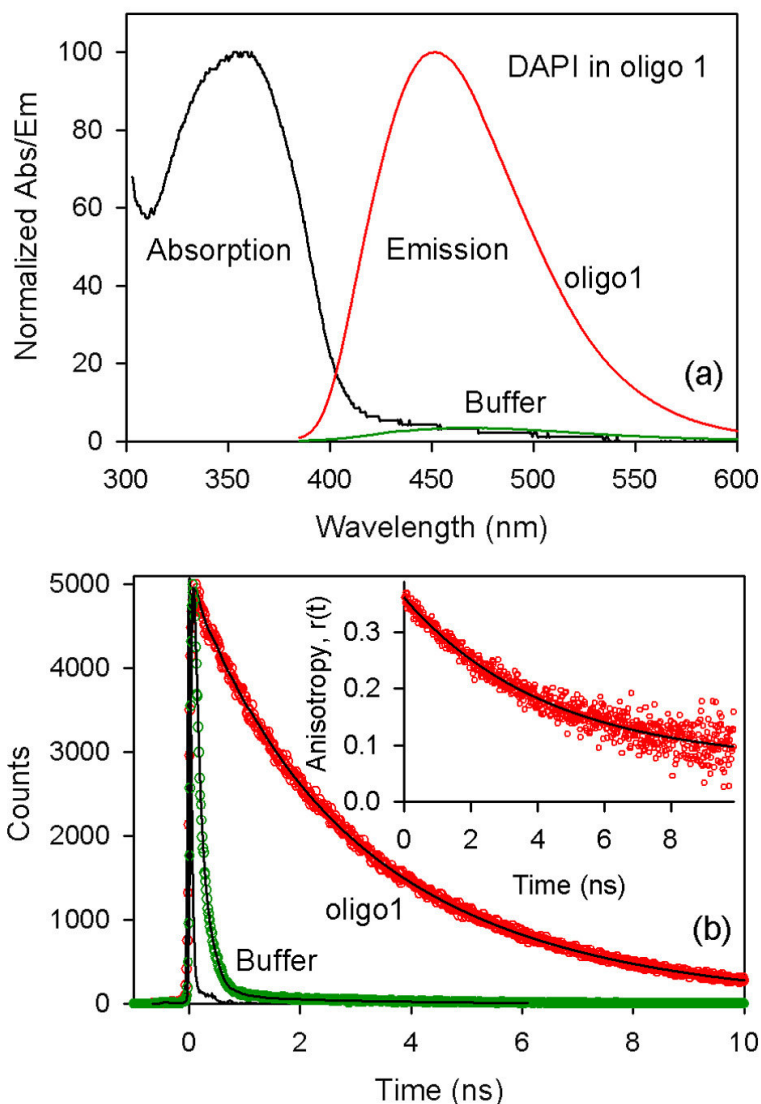


Figure 5.9. The absorption and emission spectra (a), the temporal decay of fluorescence (b), and fluorescence anisotropy (inset) of DAPI bound to the double-stranded dodecamer of sequence CGCGAATTCGCG. The emission spectrum (a) and the temporal decay of fluorescence (b) of DAPI in buffer (50mM phosphate buffer pH=7) are shown for comparison (green). The instrument response function IRF is also shown in black (b).

DNA environment. In this regard, it should be noted that although bound waters hydrate the DNA minor groove, the polarity of the minor groove is less than water [40]. The probe also shows a significant (28 times) increase in the fluorescence intensity when

bound to oligo1 compared to that of DAPI in bulk buffer. The increase of fluorescence is consistent with the high affinity binding in the minor groove, as reported in other studies [3]. The X-ray crystal structure [1] of DAPI bound to the oligomer of the same sequence shows that the probe inserts itself edgewise into the narrow minor groove, displacing the ordered spine of hydration. In this mode of binding, DAPI and a single water molecule together span the four AT base pairs present at the centre of the duplex. The indole nitrogen of the probe (Scheme 5.1) forms a bifurcated hydrogen bond with the thymine oxygen atoms of the two central base pairs, as with netropsin and Hoechst 33258 (H258). Figure 5.9(b) shows the temporal decay of fluorescence of the DAPI-oligo1 complex and that of free DAPI in buffer. The time constants associated with the decay of DAPI in the DAPI-oligo1 are in the order of nanoseconds, compared to the fast decay of the probe (100 ps), in bulk buffer. The inset of figure 5.9(b) shows the temporal decay of fluorescence anisotropy of the DAPI-oligo1 complex. The time constant associated with the decay is 4.5 ns. The observed time constant is in close agreement with the value of 4.6 ns reported by H258 in the minor groove of the same DNA oligomer (see below). It is to be noted that the time constant associated with the decay of rotational anisotropy of the probe in aqueous buffer is 100 ps. The absence of any subnanosecond component in the decay of fluorescence anisotropy in oligo1 shows that DAPI fits tightly into the minor groove of oligo1.

To construct the time resolved emission spectrum (TRES), the fluorescence transients are taken across the emission spectrum. The transients show fast decay in the blue end and rise in the red end (figure 5.10(a)), indicative of solvation [13]. The constructed TRES show spectral shift of 700 cm^{-1} in a 10 ns window. To ascertain whether the associated spectral shift is due to the environmental relaxation or associated with some intramolecular photoprocesses, (e.g formation of excited state species) TRANES are constructed. TRANES is widely used to determine the kind of species present in the system and the environment around the species [30,31]. A useful feature of the method is that an isoemissive point in the spectra involves two emitting species, which are kinetically coupled either irreversibly or reversibly or not coupled at all. In recent literature, various other studies have also used the TRANES technique

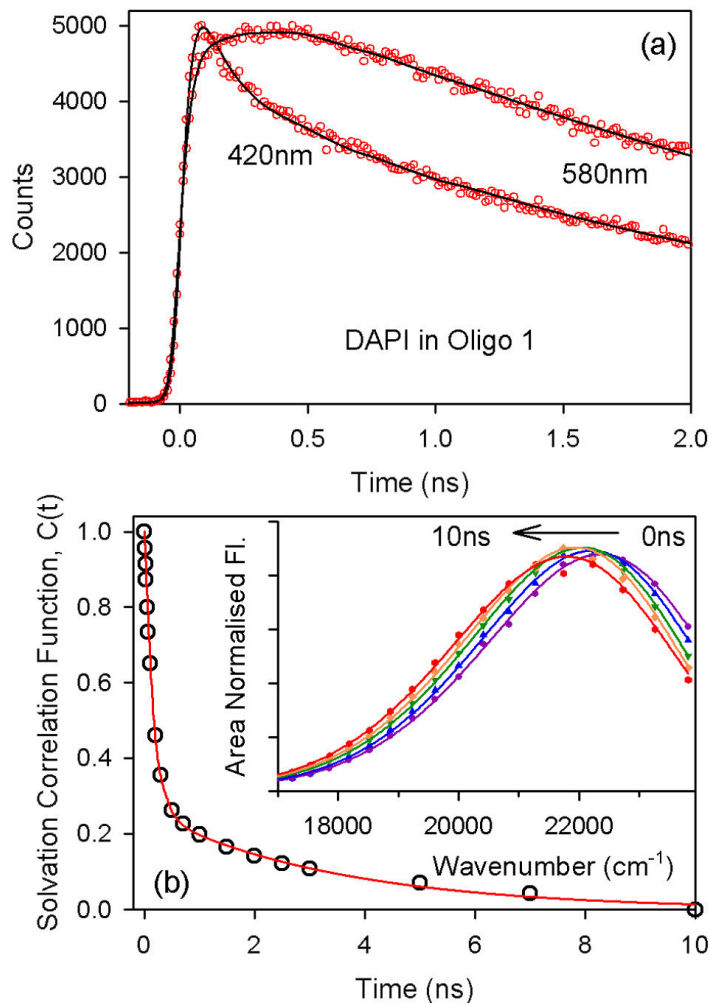


Figure 5.10. The fluorescence transients (a), the solvation correlation function, (b) and TRANES (inset) of DAPI bound to double stranded dodecamer of sequence CGCGAATTCGCG (oligo1).

to confirm different emissive species in micro-heterogeneous environments [30,31]. The inset of figure 5.10(b) shows the constructed TRANES. The absence of isoemissive points in the TRANES show that a single conformer is involved in the relaxation process and the process indeed reflects environmental stabilization. The solvation correlation function (figure 5.10(b)) decays with time constants of 130 ps(75%) and 2.52 ns(25%), which reflect the environmental relaxation of the minor groove of oligo1.

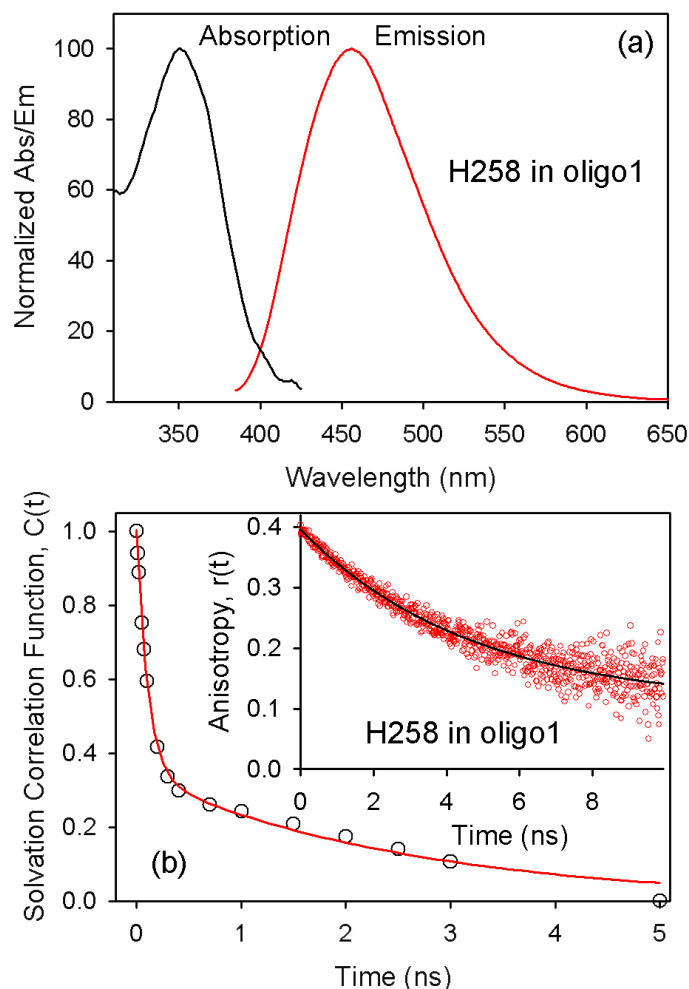


Figure 5.11. The absorption, emission (a), temporal decay of fluorescence anisotropy (inset of b) and solvation correlation function (b) of H258 bound to oligo1.

It is known that the dynamics of solvation represents the environmental stabilization of the excited state of a probe. The environmental stabilization is independent of the nature of the probe molecule. In order to obtain a general picture of the environmental dynamics of the minor groove, we have used the well known minor groove binder H258 to independently probe the dynamics of the minor groove of oligo1. The binding of H258 to oligo1 has been confirmed from X-ray crystallographic studies [41]. Figure 5.11(a) shows the absorption and emission spectrum of H258 in oligo1. The red shift in the absorption spectrum and blue shift in the emission spectrum of H258-oligo1 complex, compared to that of H258 in buffer [19] indicates the binding of the

probe to DNA. The time constant of 4.6 ns in the temporal decay of fluorescence anisotropy (inset of figure 5.11(b)) depicts the overall tumbling motion of oligo1. The

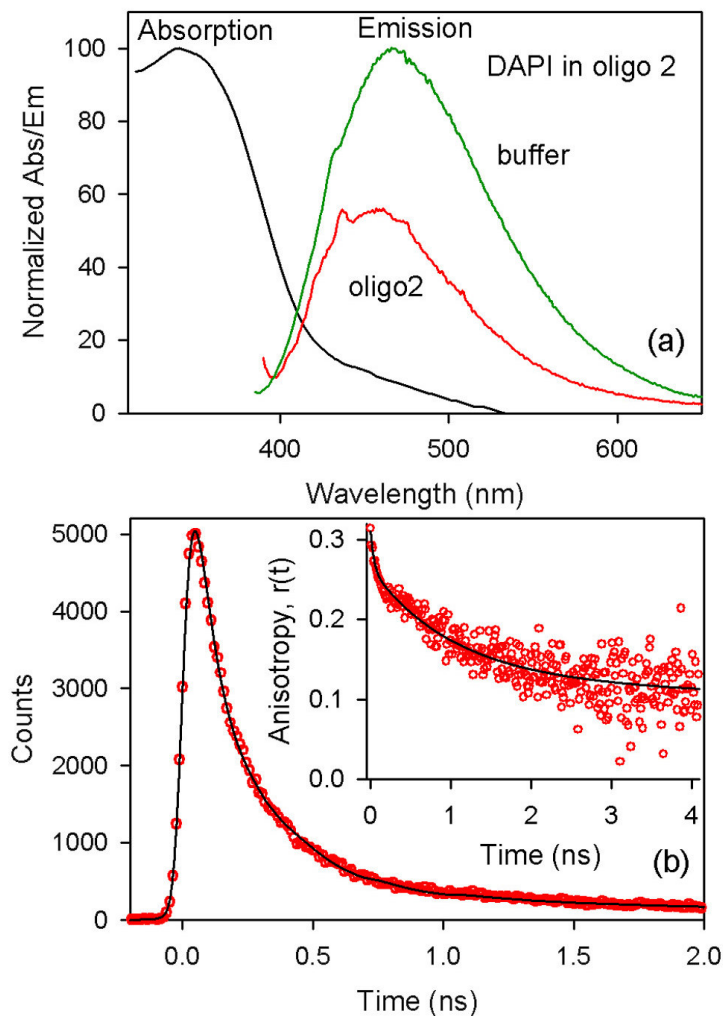


Figure 5.12. The absorption, emission spectra (a), the temporal decay of fluorescence (b) and fluorescence anisotropy (inset) of DAPI bound to double stranded dodecamer of sequence GCGCGCGCGCGC (oligo2). The emission spectrum of DAPI in 50 mM phosphate buffer (green) is shown for comparison.

absence of any subnanosecond component indicates that the probe motion (500 ps in aqueous buffer [19]), is frozen in the H258-oligo1 complex. The solvation correlation function (figure 5.11(b)) decays with time constants of 110 ps(68%) and 2.58 ns(32%). The striking similarity of the time constants associated with environmental stabilization reported by H258 and DAPI clearly shows that both the probes occupy the minor groove

of oligo1. Thus, the dynamics of solvation provides direct evidence of the minor groove binding of DAPI.

Figure 5.12(a) shows the absorption and emission spectra of DAPI bound to synthetic DNA dodecamer having sequence (GCGCGCGCGCGC)₂ (oligo2). As observed earlier with oligo1, the absorption spectrum is red shifted and the emission spectrum is blue shifted compared to that of DAPI in bulk buffer. It is to be noted that the probe in oligo2 shows a much quenched (2 times) fluorescence compared to that of the probe in bulk buffer. According to the existing literature [3], this is consistent with the low affinity intercalative binding mode of the probe to DNA sequences where there are no/nonconsecutive AT regions. The quenching of fluorescence suggests that there is an additional mode of excited state relaxation of DAPI in the DAPI-oligo2 complex, compared to that in buffer. It is known from ab-initio studies, [42] that DAPI is a good electron acceptor and DNA bases, specially guanine are good electron donors. So, electron transfer from DNA bases to DAPI could be a possible mode of excited state relaxation. The electron transfer process is also evident from the appearance of an additional fast component of 30 ps(40%) in the temporal decay of fluorescence of DAPI in oligo2 (figure 5.12(b)). This component is faster than that associated with the free probe in buffer (130 ps) and is indicative of the fast electron transfer from DNA to DAPI. In addition to this 30 ps component, DAPI shows another component of 150 ps, similar to that of DAPI in buffer. The similarity of the relatively slower time constants of 150 ps associated with the fluorescence decay of the probe in the GC dodecamer (oligo2) and buffer is in accordance with a previously reported study [24], where it has been interpreted as nonintercalative electrostatic binding of DAPI to GC DNA. However, perhaps due to limited resolution (phase correlation technique), the faster component of 30 ps has not been reported in the aforesaid study. The 150 ps component in the excited state relaxation of DAPI in the DAPI-oligo2 complex is associated with proton transfer (proton transfer of DAPI in buffer is known from earlier studies [21,43]). This shows that both intramolecular proton transfer and electron transfer from the DNA base to DAPI are associated with the excited state relaxation of DAPI in DAPI-oligo2 complex. Since the proton transfer in DAPI is intramolecular, it involves the redistribution of positive charge density in the molecule itself, hence, concomitant electron transfer can also occur.

Concerted electron transfer and proton transfer processes are reported in literature [44,45]. The temporal decay of fluorescence anisotropy of DAPI in oligo2 (inset of figure 5.12(b)) also shows a fast component of 40 ps(20%) indicative of the electron transfer. The additional time components of 1.3 ns(55%) and 6 ns(25%) associated with the decay of fluorescence anisotropy, indicate restricted motions of the probe and the overall tumbling motion of DNA respectively [46]. The observation of electron transfer from DNA base pairs to DAPI in the DAPI-oligo2 complex gives further support to the intercalative binding mode in DAPI-oligo2 complex and rules out the possibility of major groove binding of DAPI in oligo2. The similarity of the fluorescence transients at the blue and red ends of the spectrum reveals that there is no solvation stabilization in the experimental time window.

To explain the observation of proton transfer for DAPI bound to oligo2, it is essential to have a clear picture of the intercalative binding mode. Molecular modeling studies of DAPI bound to RNA sequence A₈U₈, where the dye intercalates, have been used to determine the binding geometry of the probe in the intercalative binding mode [10]. The results show that in the intercalative binding mode, the indole ring of DAPI is stacked between the adenosines and the phenyl ring of the probe is between uracils. In this binding mode, the DAPI indole-phenyl bond is twisted approximately 8° to match the base pair propeller twist. The amidine groups are rotated 31° with respect to the indole and 32° with respect to the phenyl ring to which they are bound and project out into the major groove in the RNA complex. X-ray crystallographic analysis with intercalation complexes of dinucleotides and modeling studies with intercalators in the segments of RNA and DNA have indicated that the intercalation sites in both types of nucleic acids are quite similar [47]. This model provides rationalization for the time constants associated with the decay of the fluorescence anisotropy. The 1.3 ns component associated with the decay of fluorescence anisotropy in DAPI-oligo2 complex reflects the hindered rotation of the amidino groups projected out in the major groove. It is to be noted that the excited state relaxation of the DAPI in buffer takes place by an intramolecular excited state protontransfer from the 6-amidino group to the ring [43]

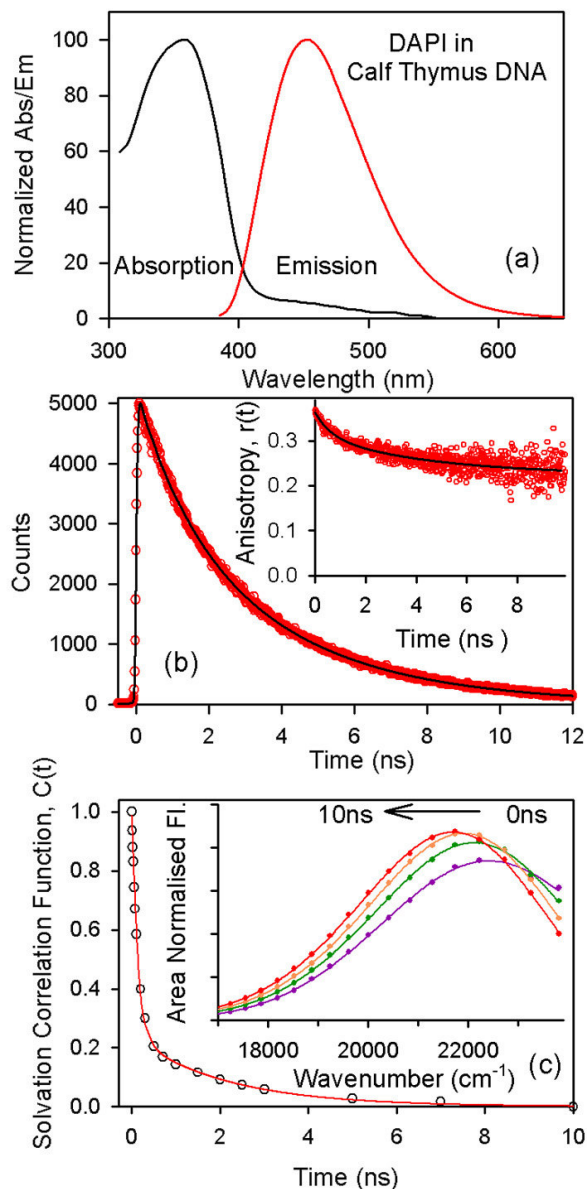


Figure 5.13. The absorption-emission spectra (a), temporal decay of fluorescence (b), fluorescence anisotropy (inset of (b)), the solvation correlation function (c) and TRANES (inset of (c)) of DAPI bound to calf thymus DNA..

through the intervention of the solvation shell surrounding the molecule [21]. In the intercalative binding mode, the amidino groups are projected in the major groove of the oligo2. The orientation times of water present in the shallow major groove (average reorientation time=6 ps) of the DNA are similar to that of free water (average reorientation time=1 ps) [15]. Hence, the proton transfer from 6-amidino group to the

indole ring of DAPI takes place with equal ease. This interpretation rationalizes the observation that a considerable portion of the fluorescence decay of DAPI in GC DNA (oligo2 in the present study) is buffer-like. The absence of solvation in the intercalative binding mode could be due to the fact that the faster solvation, reported for another intercalating dye [48], is beyond our instrumental resolution.

To render an interesting comparison, the environmental dynamics of the probe has been studied in calf thymus DNA having random sequence. The absorption spectrum (figure 5.13(a)), of DAPI bound to calf thymus DNA shows red shift, similar to the probe-oligo1 complex. The blue shift and increase in the fluorescence intensity of DAPI when bound to the genomic DNA, indicates that the dye resides in a hydrophobic environment. However, the increase in fluorescence intensity is less than that of the probe bound to oligo1. This difference could be attributed to difference in binding affinity of DAPI to a random DNA sequence. The possibility of DAPI binding to GC regions is less probable because of the stronger binding of DAPI to AT base pairs (binding constant= $3 \times 10^8 \text{ M}^{-1}$), compared to the binding in GC sequences (binding constant= $1.2 \times 10^5 \text{ M}^{-1}$) [49]. Also, in our study, the concentration of base pairs is 100 times more than that of the probe, ensuring that the probe is bound only in the high affinity mode. Figure 5.13(a) shows the temporal decay of fluorescence intensity of DAPI bound to calf thymus DNA. The time constants associated with the temporal decay of fluorescence shows nanosecond components similar to that of the probe in oligo1, where DAPI is located in the minor groove of the dodecamer. The temporal decay of fluorescence anisotropy (figure 5.13(b)), shows time constants of 0.652 ns(13%) and 4.47 ns(27%) indicating the restricted motions of the probe and a huge residual indicating the overall tumbling motion of the large DNA. The probe in calf thymus DNA shows a fast decay in blue end and rise in the red end indicative of solvation. The constructed TRES shows a spectral shift of 700 cm^{-1} in a 10 ns window, similar to the DAPI-oligo1 complex. To ascertain whether the observed spectral shift is solely due to solvation stabilization, TRANES (inset of figure 5.13(c)) is constructed for DAPI in calf thymus DNA. The absence of any isoemissive point in the TRANES reveals that the dynamics reports the solvation stabilization of the probe in the DNA environment. The time constants associated with the decay of solvation correlation function are 0.150 ps(74%)

and 3.72 ns(24%), similar to that of the probe in oligo1, where the probe is located in the minor groove. The similarity in the dynamical time scales further confirm the groove binding mode in the AT rich region of calf thymus DNA.

5.3. Conclusion:

A wealth of information is available for the interaction of the probe DAPI with DNA. However, the probe has not been previously used to report the dynamics of any restricted environment. The photophysics of the probe in bulk solvents having different polarity suggests that intramolecular proton transfer is an important mode of excited state relaxation, which depends on the solvent polarity and/or the availability of water molecules in close vicinity of the molecule. In order to avoid the misinterpretation of the observed dynamics of the probe due to competing excited state events of solvation and proton transfer, TRANES are constructed for the dynamics of DAPI in micelles and reverse micelles. The results indicate that the probe can report the environmental dynamics in reverse micelles. In SDS micelles, the dynamics has interference from intramolecular proton transfer process. The environmental dynamics of DAPI in double stranded dodecamers having sequences CGCGAATTCGCG (oligo1) and GCGCGCGCGCGC (oligo2) are explored. The dynamics of the probe in oligo1, show solvation timescales of 130 ps(75%) and 2.35 ns(25%), which is consistent with minor groove binding. In oligo2, the probe does not report any environmental relaxation in our experimental window. The absence of solvation, the fluorescence quenching due to electron transfer process (30 ps, in our resolution), and the presence of a ~150 ps component in the fluorescence lifetime of DAPI both in oligo2 and in bulk buffer have been correlated with the intercalative binding mode of the dye. The dynamics of DAPI in calf thymus DNA, having random sequence is similar to that of DNA in the minor groove. Our studies clearly explore the structure-dynamics correlation of DAPI-DNA complex and the two distinct modes of interaction of DAPI with DNA.

References

- (1) T.A. Larsen, D.S. Goodsell, D. Cascio, K. Grzeskowiak, R.E. Dickerson, The structure of DAPI bound to DNA, *J. Biomol. Struct. Dyn.* 7 (1989) 477.
- (2) E. Trotta, E. D'Ambrosio, G. Ravagnan, M. Paci, Simultaneous and different binding mechanisms of 4',6-Diamidino-2-phenylindole to DNA hexamer (d(CGATCG))₂: A ¹H NMR study, *J. Biol. Chem.* 271 (1996) 27608.
- (3) E. Trotta, E. D'Ambrosio, G. Ravagnan, M. Paci, Evidence of DAPI intercalation in CG sites of DNA oligomer [d(CGACGTCG)]₂: A ¹H NMR study, *Nucl. Acids Res.* 23 (1995) 1333.
- (4) K. Jansen, B. Norden, M. Kubista, Sequence dependence of 4',6-Diamidino-2-phenylindole (DAPI)-DNA interactions, *J. Am. Chem. Soc.* 115 (1993) 10527.
- (5) W.D. Wilson, F.A. Tanious, H.K. Barton, R.L. Jones, K. Fox, R.L. Wydra, L. Streckowski, DNA sequence dependent binding modes of 4',6-Diamidino-2-phenylindole (DAPI), *Biochemistry* 29 (1990) 8452.
- (6) E. Trotta, M. Paci, Solution structure of DAPI selectively bound in the minor groove of a DNA T.T mismatch containing site: NMR and molecular dynamics studies, *Nucl. Acids Res.* 26 (1998) 4706.
- (7) D. Vlieghe, J. Sponer, L.V. Meervelt, Crystal structure of d(GGCCAATTGG) complexed with DAPI reveal novel binding mode, *Biochemistry* 38 (1999) 16443.
- (8) D.L. Boger, B.E. Fink, S.R. Brunette, W.C. Tse, M.P. Hedrick, A simple, high resolution method for establishing DNA binding affinity and sequence selectivity, *J. Am. Chem. Soc.* 123 (2001) 5878.
- (9) P. Colson, C. Bailly, C. Houssier, Electric linear dichroism as a new tool to study sequence preference in drug binding to DNA., *Biophys. Chem.* 58 (1996) 125.
- (10) F.A. Tanious, J.M. Veal, H. Buczak, L.S. Ratmeyer, W.D. Wilson, DAPI (4',6-Diamidino-2-phenylindole) binds differently to DNA and RNA: Minor-groove binding at AT sites and intercalation at AU sites, *Biochemistry* 31 (1992) 3103.
- (11) S. Eriksson, S.K. Kim, M. Kubista, B. Norden, Binding of 4',6-Diamidino-2-phenylindole (DAPI) to AT regions of DNA: Evidence for an allosteric conformational change, *Biochemistry* 32 (1993) 2987.

- (12) S.K. Kim, S. Eriksson, M. Kubista, B. Norden, Interaction of 4',6-Diamidino-2-phenylindole(DAPI) with Poly[d(G-C)₂] and Poly[d(G-mSC)₂]: Evidence for major groove binding of a DNA probe, *J. Am. Chem. Soc.* 115 (1993) 3441.
- (13) S.K. Pal, A.H. Zewail, Dynamics of water in biological recognition, *Chem. Rev.* 104 (2004) 2099.
- (14) D. Zhong, A. Douhal, A.H. Zewail, Femtosecond studies of protein-ligand hydrophobic binding and dynamics: Human serum albumin, *Proc. Natl. Acad. Sci. USA* 97 (2000) 14056.
- (15) S. Pal, P.K. Maiti, B. Bagchi, Exploring DNA groove water dynamics through hydrogen bond lifetime and orientational relaxation, *J. Chem. Phys.* 125 (2006) 234903.
- (16) S.K. Pal, L. Zhao, T. Xia, A.H. Zewail, Site and sequence selective ultrafast hydration of DNA, *Proc. Natl. Acad. Sci. USA* 100 (2003) 13746
- (17) S.K. Pal, L. Zhao, A.H. Zewail, Water at DNA surfaces: Ultrafast dynamics in minor groove recognition, *Proc. Natl. Acad. Sci. USA* 100 (2003) 8113.
- (18) E.B. Brauns, M.L. Madaras, R.S. Coleman, C.J. Murphy, M.A. Berg, Measurement of local DNA reorganisation on the picosecond and nanosecond time scales, *J. Am. Chem. Soc.* 121 (1999) 11644.
- (19) D. Banerjee, S.K. Pal, Ultrafast charge transfer and solvation of DNA minor groove binder: Hoechst 33258 in restricted environments, *Chem. Phys. Lett.* 432 (2006) 257.
- (20) D. Banerjee, S.K. Pal, Excited-state solvation and proton transfer dynamics of DAPI in biomimetics and genomic DNA, *J. Phys. Chem. A* 112 (2008) 7314.
- (21) M.L. Barcellona, E. Gratton, A molecular approach to 4',6-Diamidino-2-phenylindole (DAPI) photophysical behaviour at different pH values, *Biophys. Chem.* 40 (1991) 223.
- (22) X. Zhang, M.M. Cunningham, R.A. Walker, Solvent polarity at polar solid surfaces: The role of solvent structure, *J. Phys. Chem. B* 107 (2003) 3183
- (23) S.M. Andrade, S.M.B. Costa, Hydrogen bonding effects in the photophysics of a drug, piroxicam, in homogeneous media and dioxane-water mixtures, *Phys. Chem. Chem. Phys.* 1 (1999) 4213.

- (24) M.L. Barcellona, G. Cardiel, E. Gratton, Time-resolved fluorescence of DAPI in solution and bound to polydeoxynucleotides, *Biochem. Biophys. Res. Comm.* 170 (1990) 270.
- (25) T.K. Mukherjee, D. Panda, A. Datta, Excited-state proton transfer of 2-(2'-Pyridyl)benzimidazole in microemulsions: Selective enhancement and slow dynamics in Aerosol OT reverse micelles with an aqueous core, *J. Phys. Chem. B* 109 (2005) 18895.
- (26) N.C. Maiti, M.M.G. Krishna, P.J. Britto, P. N., Fluorescence dynamics of dye probes in micelles, *J. Phys. Chem. B* 101 (1997) 11051.
- (27) D. Banerjee, S.K. Srivastava, S.K. Pal, Spectroscopic studies on ligand-enzyme interactions: Complexation of α -chymotrypsin with 4',6-Diamidino-2-phenylindole (DAPI), *J. Phys. Chem. B* 112 (2008) 1828.
- (28) D. Roy, K. Karmakar, S.K. Mondal, K. Sahu, K. Bhattacharya, Excited state proton transfer from pyranine to acetate in a CTAB micelle, *Chem. Phys. Lett.* 399 (2004) 147.
- (29) A.S.R. Koti, M.M.G. Krishna, N. Periasamy, Time-resolved area-normalized emission spectroscopy (TRANES): A novel method for confirming emission from two excited states, *J. Phys. Chem. A* 105 (2001) 1767.
- (30) R. Sarkar, S.K. Pal, Ligand-DNA interaction in a nanocage of reverse micelle, *Biopolymers* 83 (2006) 675.
- (31) A.K. Shaw, S.K. Pal, Fluorescence relaxation dynamics of acridine orange in nanosized micellar systems and DNA, *J. Phys. Chem. B* 111 (2007) 4189.
- (32) S. Kapelle, W. Rettig, R. Lapouyade, Dual fluorescent polyaniline model compounds: steric and temperature effects on excited state charge separation, *Photochem. Photobiol. Sci.* 1 (2002) 492.
- (33) S.S. Narayanan, R. Sarkar, S.S. Sinha, F. Dias, A. Monkman, S.K. Pal, Luminescence depolarization dynamics of quantum dots: Is it hydrodynamic rotation or exciton migration?, *J. Phys. Chem. C* 112 (2008) 3423.
- (34) A. Douhal, G. Angulo, M. Gil, J.A. Organero, M. Sanz, L. Tormo, Observation of three behaviors in confined liquid water within a nanopool hosting proton-transfer reactions, *J. Phys. Chem. B* 111 (2007) 5487.

- (35) R.E. Riter, D.M. Willard, N.E. Levinger, Water immobilization at surfactant interfaces in reverse micelles, *J. Phys. Chem. B* 102 (1998) 2705.
- (36) E. Bardez, E. Monnier, B. Valeur, Dynamics of excited-state reactions in reverse micelles. 2. Proton transfer involving various fluorescent probes according to their sites of solubilization., *J. Phys. Chem.* 89 (1985) 5031.
- (37) R. Krishnan, T.G. Fillingim, G.W. Robinson, Solvent structural effects on proton dissociation, *J. Am. Chem. Soc.* 112 (1990) 1353.
- (38) D. Banerjee, S.K. Pal, Direct observation of essential DNA dynamics: Melting and reformation of the DNA minor groove, *J. Phys. Chem. B* 111 (2007) 10833.
- (39) D. Banerjee, S.K. Pal, Dynamics in the DNA recognition by DAPI: Exploration of the various binding modes, *J. Phys. Chem. B* 112 (2007) 1016.
- (40) R. Jin, K.J. Breslauer, Characterization of the minor groove environment in a drug-DNA complex: Bisbenzimidazole bound to the poly[d(AT)]-poly[d(AT)]duplex, *Proc. Natl. Acad. Sci. USA* 85 (1988) 8939.
- (41) P.E. Pjura, K. Grzeskowiak, R.E. Dickerson, Binding of hoechst 33258 to the minor groove of B-DNA, *J. Mol. Biol.* 197 (1987) 257.
- (42) D. Reha, M. Kabelac, F. Ryjacek, J. Sponer, J.E. Sponer, M. Elstner, S. Suhai, P. Hobza, Intercalators. 1. Nature of stacking interactions between intercalators (ethidium, daunomycin, ellipticine, and 4',6-Diaminido-2-phenylindole) and DNA base pairs. Ab initio quantum chemical, density functional theory, and empirical potential study, *J. Am. Chem. Soc.* 124 (2002) 3366.
- (43) A. Mazzini, P. Cavatorta, M. Iori, R. Favilla, G. Sartor, The binding of 4',6-Diamidino-2-phenylindole to bovine serum albumin, *Biophys. Chem.* 42 (1992) 101.
- (44) R.M. Haddox, H.O. Finklea, Proton-coupled electron transfer of an osmium aquo complex on a self-assembled monolayer on gold, *J. Phys. Chem. B* 108 (2004) 1694.
- (45) J.J. Concepcion, M.K. Brennaman, J.R. Deyton, N.V. Lebedeva, M.D.E. Forbes, J.M. Papanikolas, T.J. Meyer, Excited state quenching by proton-coupled electron transfer, *J. Am. Chem. Soc.* 129 (2007) 6968.

- (46) A.K. Shaw, S.K. Pal, Activity of subtilisin carlsberg in macromolecular crowding, *J. Photochem. Photobiol. B: Biol.* 86 (2007) 199.
- (47) H. Shieh, H.M. Berman, D. M., S. Neidle, The structure of drug-deoxydinucleoside phosphate complex; generalized conformational behavior of intercalation complexes with RNA and DNA fragments, *Nucl. Acids Res.* 8 (1980) 85.
- (48) A. Furstenberg, M.D. Julliard, T.G. Deligeorgiev, N.I. Gadjev, A.A. Vallisov, E. Vauthey, Ultrafast excited state dynamics of DNA fluorescent intercalators: New insight into the fluorescence enhancement mechanism, *J. Am. Chem. Soc.* 128 (2006) 7661.
- (49) W.D. Wilson, F.A. Tanious, H.J. Barton, L. Strekowski, D.W. Boykin, Binding of 4',6-Diamidino-2-phenylindole(DAPI) to GC and mixed sequences in DNA: Intercalation of a classical groove-binding molecule, *J. Am. Chem. Soc.* 111 (1990) 5008.

Chapter 6

Studies on the Special Binding Modes of DNA: Simultaneous Binding of Two Ligands in the Same Region of DNA

6.1. Introduction:

The recognition of DNA by small molecules [1] is of special importance in the design of new drugs. There are three specific modes of interaction of small ligands with DNA, namely intercalation, minor groove binding and major groove binding. The binding of these ligands to DNA is highly sequence specific. A number of techniques like X-ray crystallography [2], NMR [3,4], Raman spectroscopy [5] along with theoretical calculations [6] have been used to characterize a variety of these ligands in their specific DNA environments. However, simultaneous binding of various ligands to DNA is an area that has not been sufficiently explored. Simultaneous binding of different ligands to DNA has importance in drug designing since it provides information on the compatibility of various drugs and the effect of drugs on mutagen-bound DNA. Since the majority of the mutagens and anticancer/antihelminthic drugs are intercalators and minor groove binders respectively [7,8], simultaneous binding of an intercalator and minor groove binder to DNA is worth investigation. The nature of binding of an intercalator and minor groove binder to genomic DNA and mammalian cells have been reported [9,10] in the literature. In a recent report [9], Förster resonance energy transfer (FRET) has been used to study the distance between the bound ligand molecules in genomic DNA. The study [9] shows that the region where intercalation takes place is not suited for minor groove binding in genomic DNA. It has to be noted that in normal conditions, both the ligands do not compete for a particular site. The condition, where both the ligands are forced to occupy the same site is hard to achieve in genomic DNA solutions with very high concentration of ligands because the aforesaid condition triggers DNA condensation [11,12]. An alternative route to study simultaneous binding of ligands is to use a smaller DNA as the

host for both the ligands. Simultaneous major and minor groove binding [13] of two ligands ruthenium-porphyrin and 4',6-Diamidino-2-phenylindole (DAPI) in a dodecamer DNA has been reported. The above mentioned study has established resonance energy transfer across the DNA stem. In this chapter, we have attempted to study the complexation of a minor groove binding drug Hoechst 33258 (H258) on a DNA with a potent mutagenic intercalator ethidium bromide, (EB) in the same region of a DNA segment.

6.2. Results and Discussion:

6.2.1. Simultaneous Binding of Minor Groove Binder and Intercalator to Dodecamer DNA: Importance of Relative Orientation of Donor and Acceptor in FRET [14].

The dye H258 is extremely sensitive to the polarity of the environment. The absorption spectrum of the dye shows a red shift and the emission spectrum shows a blue shift with the decrease in the polarity of the environment. The strong dependence of the emission spectrum of the dye on the polarity of the environment has been exploited to characterize the polarity of the minor groove of the DNA [15]. The emission spectrum (figure 6.1(a)) clearly shows that the dye resides in the hydrophobic environment of the SDS micelle and that of the DNAs compared to that in bulk buffer. Figure 6.1(b) shows the fluorescence transients of the probe in different environments. The temporal fluorescence decay of the probe in buffer at pH=7 is characterized by time constants of 110 ps(14%), 480 ps(13%) and 2.24 ns(72%). Due to the geometrical restriction imposed on the probe in the SDS micelles, the 480 ps component indicative of the twisting motion of the probe in bulk environment [16], is lost and the fluorescence decays with time constants of 1.15 ns(15%) and 4.10 ns(85%). The geometrical restriction imposed on the dye bound to the minor groove of genomic salmon sperm (SS) DNA and synthesized dodecamer having sequence CGCAAATTTGCG is also evident from the absence of the 480 ps component in the fluorescence decays of the dye in the respective media. The temporal decay of fluorescence of the probe bound to the genomic and dodecamer DNA shows only nanosecond component. The geometrical restrictions characterizing the binding of the probe in the micellar and DNA environments are also borne out by the decays of

fluorescence anisotropies in the different media as shown in figures 6.2(a)-(c).

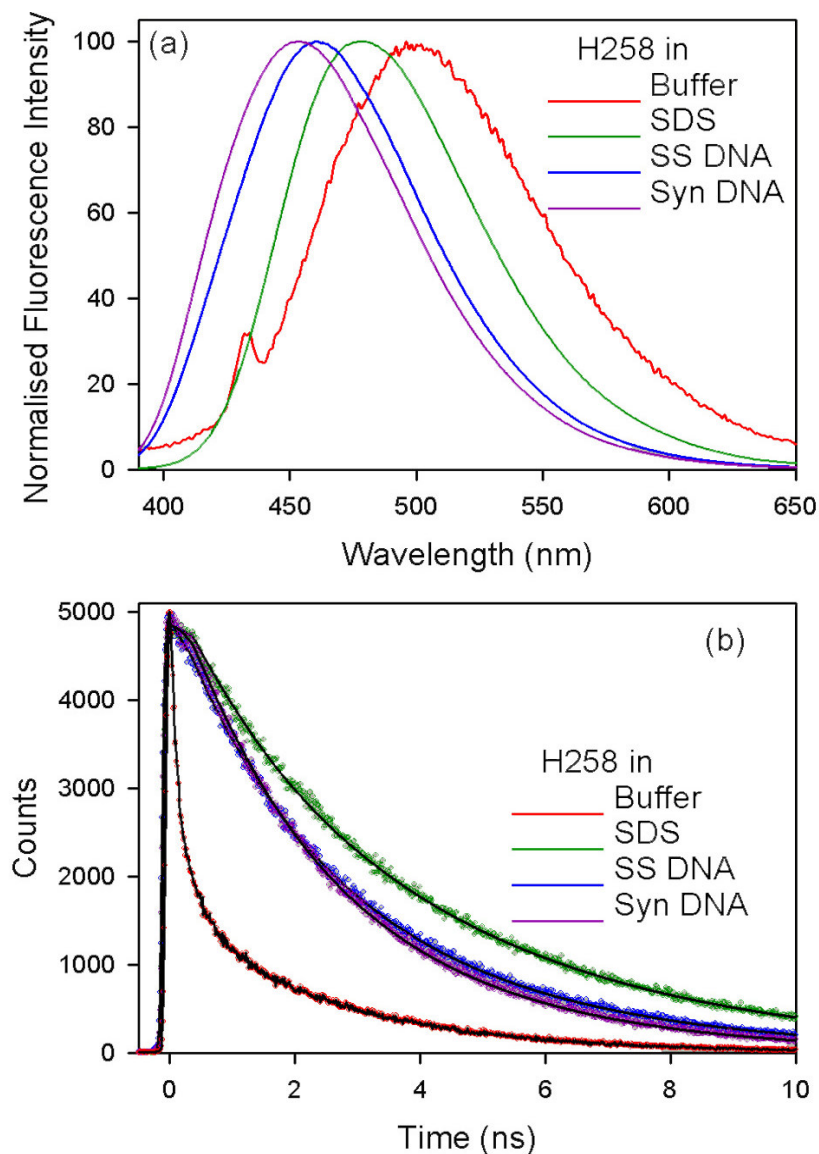


Figure 6.1. The emission (a) and temporal decays of fluorescence (b) of $1\mu\text{M}$ H258 in 50mM phosphate buffer, 50mM SDS, $100\mu\text{M}$ (base pair) SS DNA and $70\mu\text{M}$ (base pair) dodecamer.

Having thus characterized the binding of H258 in different environments, we consider the possibility of the simultaneous binding of H258 and EB in DNA. FRET is an effective technique to find out the distance between two ligands having overlap of their emission and absorption spectrum. We studied the resonance energy transfer between the ligands H258 and EB in SDS micelles. In micelles the donor (H258) and acceptor (EB)

can bind simultaneously without any restriction on the relative orientation of their

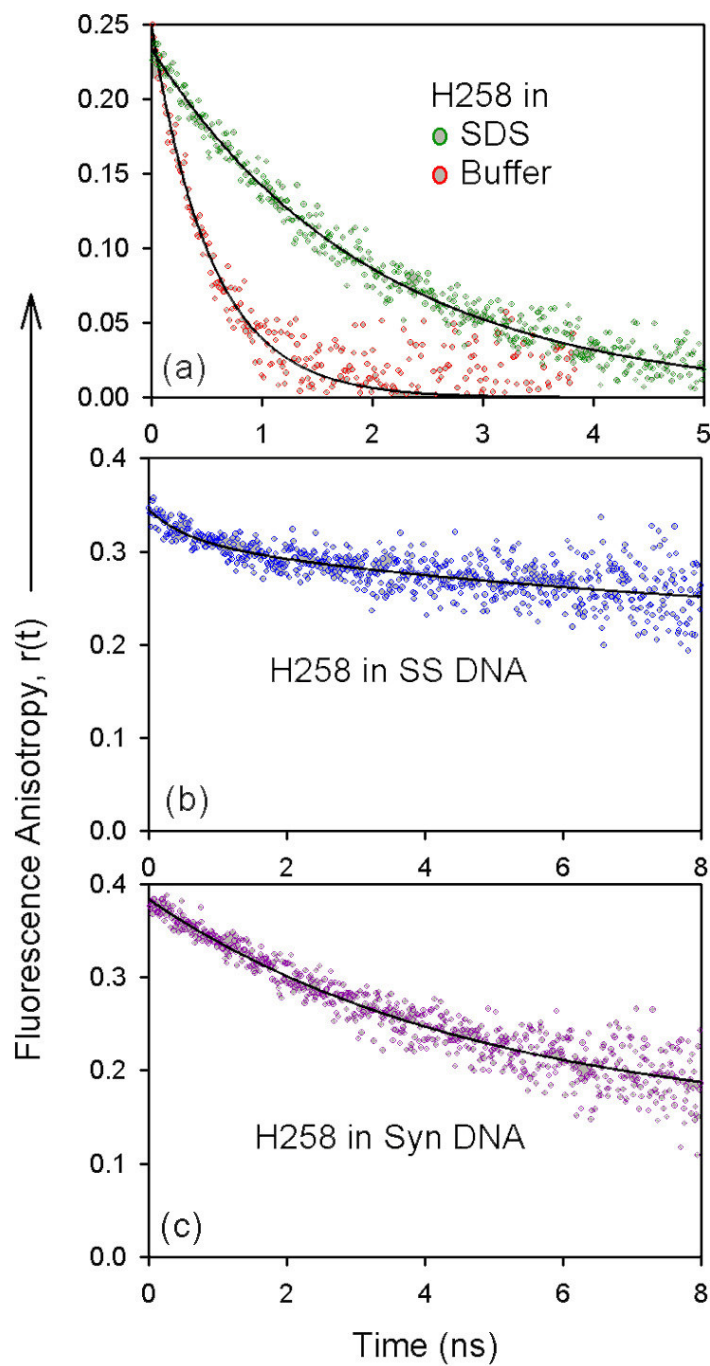


Figure 6.2. The fluorescence anisotropy decays of $1\mu\text{M}$ H258 in 50mM phosphate buffer, 50mM SDS, $100\mu\text{M}$ (base pair) SS DNA and $70\mu\text{M}$ (base pair) dodecamer.

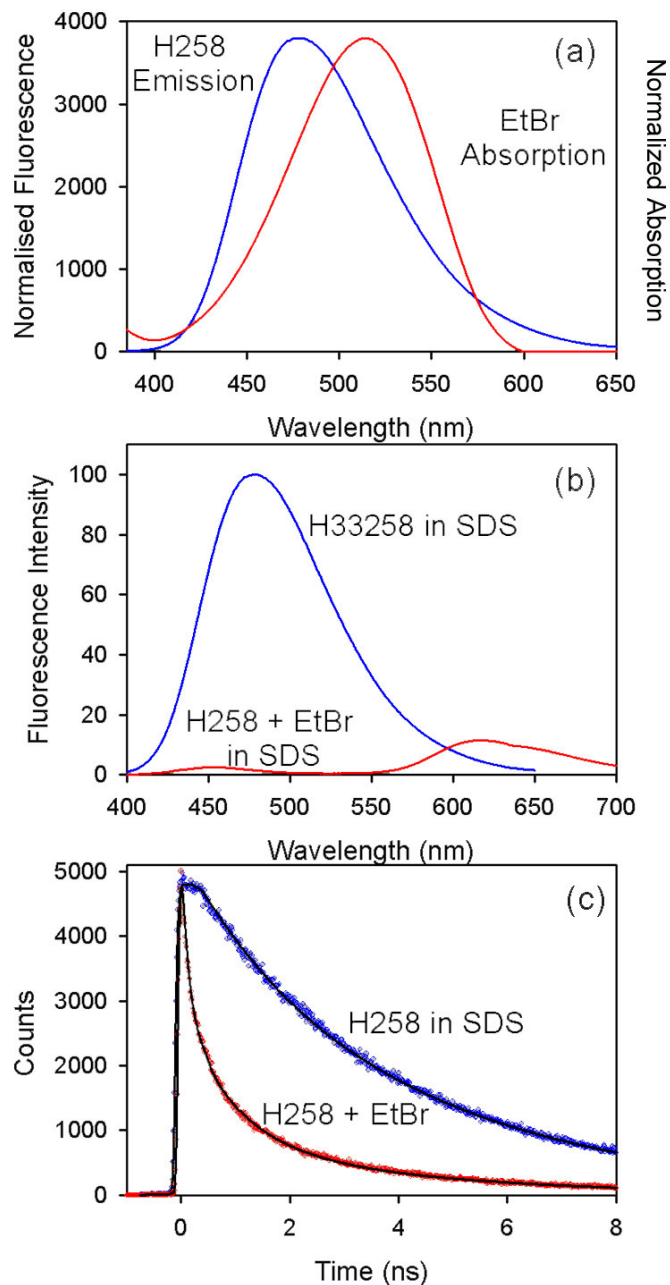


Figure 6.3. (a) The spectral overlap of H258 and EB in 50mM SDS. The emission spectrum (b) and the temporal decay of fluorescence (c) of H258 and H258-EB in 50mM SDS.

transition dipole moments. Thus the orientation parameter κ^2 can be taken as 0.667 [17]. Figure 6.3(a) shows that there is sufficient spectral overlap between the emission spectrum of the H258 and the absorption spectrum of the EB in SDS micelles. In order to prevent homomolecular energy transfer between donor molecules and to ensure efficient

energy transfer between the donor and acceptor, the concentration of donor molecules are kept low and that of the acceptor molecules are comparable to the micellar concentration. Both H258 and EB occupy the micellar interface [16] and the relative orientation of the bound ligands is random in SDS micelles. The energy transfer takes place from the donor to the acceptor as indicated by the quenching of fluorescence intensity (figure 6.3(b)) as well as the faster decay (figure 6.3(c)) of the donor in the donor-acceptor complexes in micelles, compared to that of only donor in the micelles. Analyses of the above mentioned temporal fluorescence decays show that 12% of the donor molecules bound to the micelles do not involve in energy transfer. The population may be reflective of the donor molecules in the micelles without any acceptor. Our studies also reveal that 62% of the donor molecules undergo energy transfer with 97% efficiency and the remaining 26% with an efficiency of 75%. The distances between the donor and the acceptor have been estimated to be 2.07 nm and 3.02 nm, by using R_0 value of 3.67 nm. The observation is consistent with the binding of the donor and acceptor across the chords in the spherical SDS micelle (≈ 4 nm diameter [18]).

Figure 6.4(a) shows the spectral overlap between absorption and emission spectrum of the acceptor and the donor respectively in 100 μM salmon sperm DNA. The concentration of the EB (10 μM) assures maximum intercalation of the dye (considering one EB intercalates per 10 base pairs [19]). On the addition of acceptor (EB) molecules to H258-DNA solution, there is no shift in the emission maxima of the probe H258 compared to that of the H258-DNA complex without EB, indicating that the donor is still bound to the DNA. The binding of the EB to DNA is confirmed by the 22 ns component in its temporal fluorescence decay characterizing the DNA environment [19] (inset of figure 6.4(c)). Circular dichroism spectra (data not shown) show that the simultaneous binding of these two ligands does not alter the average secondary structure of the native DNA. The quenching of the fluorescence intensity (figure 6.4(b)) coupled with the appearance of faster components in the decay (figure 6.4(c)) of H258 in the presence of EB in DNA suggests considerable energy transfer from the donor to the acceptor molecule. It has been suggested in a previous study [9] that the donor and the acceptor molecules in the genomic DNA cannot assume random orientations with respect

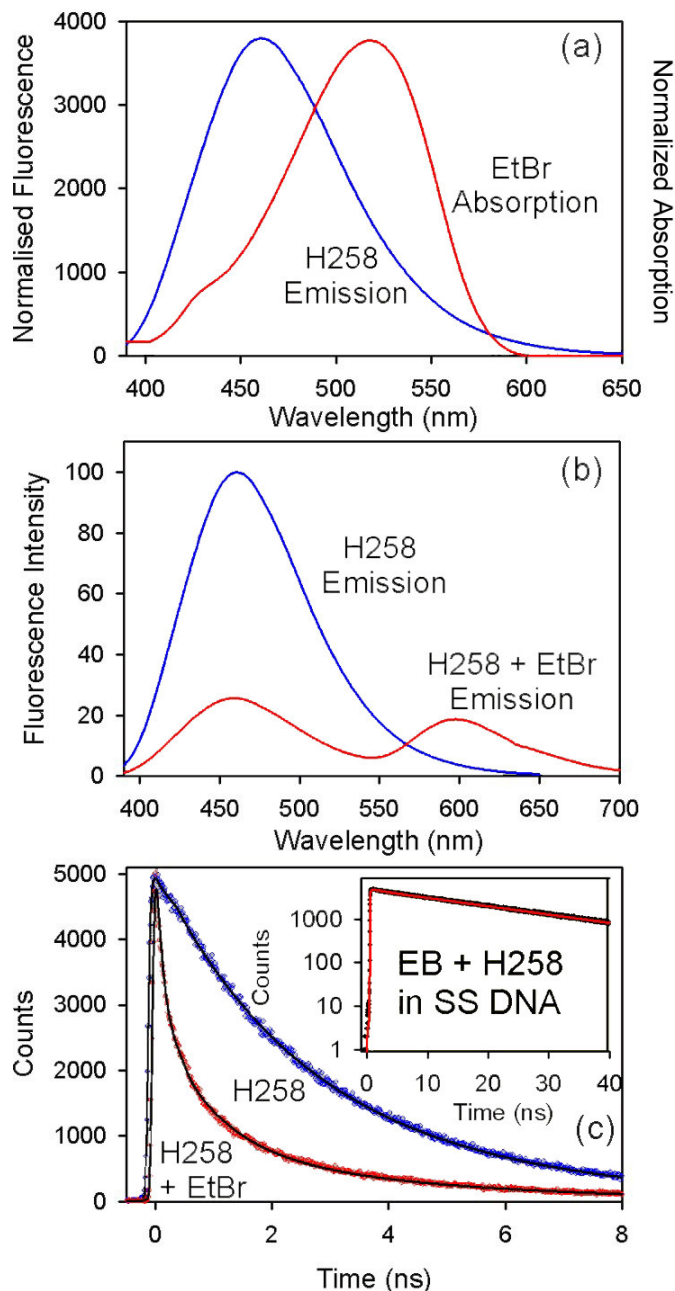


Figure 6.4. (a) The spectral overlap of H258 and EB in 100 μ M (base pair) genomic DNA. The emission spectrum (b) and the temporal decay (c) of H258 and H258-EB in genomic DNA.

to each other [9]. So the value of κ^2 , which takes into account the relative orientation of the donor and acceptor transition dipoles [17], cannot be taken as 0.667, the value in the random orientation condition. In accordance with the above mentioned study, the calculated value of R_0 , using κ^2 value of 1.2 is found to be 3.23 nm.

Analyses of the temporal decays of the donor and the donor-acceptor complex in the genomic DNA show that 5% of the DNA bound donor does not involve in energy transfer, 51% donors transfer energy to the acceptor with an efficiency of 98%, 25% with an efficiency 85% and the remaining 17% undergoes energy transfer with an efficiency of 51%. The corresponding distances between the donor and acceptor molecules are estimated to be 1.77 nm, 2.50 nm and 3.30 nm. It has been shown that the center of the H258 (donor) is situated at a distance of 0.4 nm from the helix axis [20]. The probability of energy transfer between donor and acceptor molecules bound to different DNA strands (inter-DNA energy transfer) has been checked by a control experiment. In the experiment, two separate solutions, one containing the donor (H258) bound to genomic DNA and another containing acceptor (EB) bound to genomic DNA are mixed. The temporal decay of the resultant solution shows no faster component associated with energy transfer. The result indicates that there is no inter-DNA energy transfer. Using this information along with the above mentioned donor-acceptor distances it is estimated that the centres of the H258 and EB molecules are separated by 5, 7 and 10 base pairs respectively within the persistence length of the genomic DNA. The donor-acceptor distance of 3.30 nm can also be assigned to donor and acceptors coming in close proximity due to folding and loop formation in genomic DNA [21]. So this study does not conclude that the donor and acceptor molecules are bound to the same region of the genomic DNA. In order to verify whether the intercalator EB and groove binder H258 can bind to the same region of the DNA, FRET studies are carried out in the dodecamer DNA. Each of the dyes individually binds to the dodecamer as shown in separate studies [2,19]. The X-ray crystal structure of H258 bound to the minor groove of the dodecamer shows that the probe binds in the central A-T rich sequence involving 5 base pairs [2]. In a solution containing both the dyes H258 and EB in dodecamer DNA, H258 shows emission maximum at 460 nm, characteristic of minor groove binding (figure 6.5(b)), whereas the dye EB shows the 22 ns lifetime, indicative of intercalation [19] (inset of figure 6.5(c)). Figure 6.5(a) shows the spectral overlap between the emission

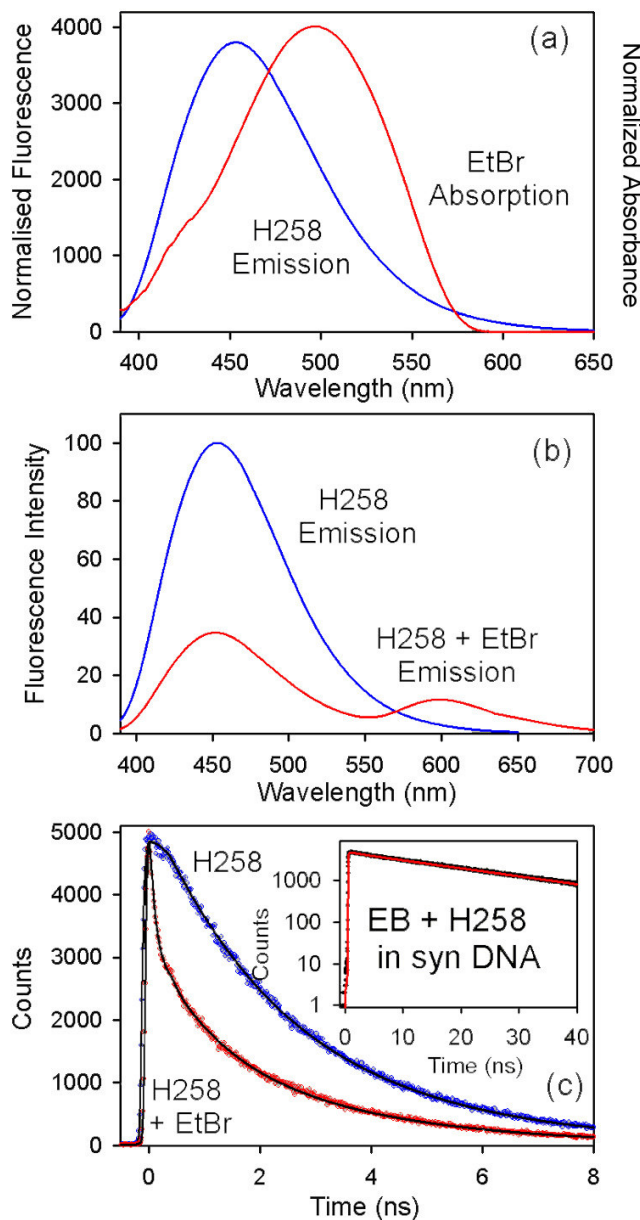


Figure 6.5. (a) The spectral overlap of H258 and EB in $70\mu\text{M}$ (base pair) synthesized DNA. The emission spectrum (b) and the temporal decay (c) of H258 and H258-EB in synthesized DNA.

spectrum of the donor and the absorption spectrum of the acceptor in the dodecamer. The quenching of fluorescence intensity (figure 6.5(b)) along with the faster temporal decay (figure 6.5(c)) in the H258-EB complex relative to that of the H258 in the dodecamer suggests energy transfer between the two molecules. The binding possibility of the intercalator and the minor groove binder to different DNA molecules has been carefully

avoided using EB concentration equal to that of the DNA concentration, indicating that the energy transfer takes place within the same DNA. The X-ray crystallographic studies [2] (solid phase of DNA) along with NMR studies [22] (concentrated solution) on the dodecamer does not report any aggregation or hairpin structure formation. The structure of the dodecamer in the native state and in the presence of both the dyes have been studied by CD spectroscopy. The results (data not shown) show that the simultaneous binding of the two dyes does not bring about a major perturbation in the structure of the dodecamer. The possibility of the energy transfer between the dye molecules bound to different dodecamer units can be ruled out considering that there is no homomolecular energy transfer [23] between the H258/EB molecules bound to the dodecamer. To further confirm that the energy transfer takes place between the dye molecules bound to a single dodecamer, a control experiment is performed. As a control, two separate solutions, one containing the donor (H258) bound to dodecamer DNA and another containing acceptor (EB) bound to dodecamer DNA are mixed. The temporal decay of the resultant solution shows no faster component associated with energy transfer. The result confirms that the energy transfer is indeed intra-DNA.

The difference between the temporal decays of the H258-EB complex in genomic (figure 6.4(c)) and dodecamer (figure 6.5(c)) DNA clearly points out the difference in binding of these two dyes to genomic and synthesized DNAs. This difference could be due to the fact that the relative orientations of the transition dipoles of the donor and the acceptor are different in genomic and synthesized DNA. In the synthesized DNA, the molecules H258 and EB attain a definite geometry relative to each other. The transition dipole moment of EB is inclined 75° with respect to the helix axis [5,24,25]. The transition dipole of the minor groove binding drug, H258 is perpendicular to the long axis of the minor groove, which in turn makes an angle of 51° with the helix axis. The transition dipoles of the donor-acceptor pair thus make an angle of 66° with respect to each other. Using these results, the value of κ^2 is estimated to be 0.04 and the R_0 value is calculated to be 1.91 nm. It is calculated that 21% of the donor molecules does not involve in energy transfer. The loss of efficiency of FRET of the donor in the close proximity of the acceptor in the dodecamer is clear indication of smaller value of κ^2 compared to those in the genomic DNA and SDS micelles. From our studies it is also

clear that 60% of the donor molecules show an energy transfer efficiency of 97% to the acceptors situated at 0.92 nm (2 base pairs away from donor), whereas the remaining 17% transfers energy to acceptors located 1.95 nm with an efficiency of 50%. The distance of 1.95 nm, which is 5 base pairs away from the acceptor reveals that the acceptor molecules are intercalated at the ends of the dodecamer. The small percentage of intercalator binding to the ends (5 base pairs from donor) is consistent with other studies [26]. It is worthwhile to mention that if the value of κ^2 is taken as 1.2 the calculated donor-acceptor distances are 1.92 nm and 3.37 nm. The distance of 3.37 nm indicates that the H258 and EB are separated by a distance of 10 base pairs. The result is unphysical because in the dodecamer DNA the maximum distance from the centre of the helix is 2.07 nm (6 base pairs). Considering the random orientation of the transition dipoles of the donor-acceptor, ($\kappa^2=0.667$) one of the calculated donor-acceptor distance of 3.06 nm, also has no physical significance.

6.3. Conclusion:

Our studies on the dodecamer DNA show that the minor groove binding by H258 and intercalation by EB can independently take place involving a particular site of the dodecamer. The intercalator and the minor groove binder on simultaneous binding to dodecamer DNA have their transition dipoles oriented at 66° with respect to each other. In the dodecamer majority of the acceptor molecules are located at a distance of 0.92 nm from donor (H258) in the centre of the DNA, and a small number of acceptors are intercalated in the ends of the dodecamer at a distance of 1.92 nm. The binding nature is essentially different from the two dyes bound to genomic DNA, where the two dyes are separated by 5 and 7 base pairs along the persistence length or by loop formation by a distance of 3.3 nm. It is also revealed that the use of the calculated value of the orientation parameter ($\kappa^2=0.04$) is crucial for the estimation of the distance between the donor and acceptor bound to the dodecamer. The use of the value of the orientation parameter for the random distribution of acceptor ($\kappa^2=0.667$) as well as that of partially restricted distribution of acceptor ($\kappa^2=1.2$) lead to erroneous results.

References

- (1) P.B. Dervan, Molecular recognition of DNA by small molecules, *Bioorg. Med. Chem.* 9 (2001) 2215.
- (2) M.C. Vega, I.G. Saez, J. Aymami, R. Eritja, G.A.V.D. Marel, J.H. VanBoom, A. Rich, M. Coll, Three-dimensional crystal structure of the A-tract DNA dodecamer d(CGCAAATTTGCG) complexed with the minor groove-binding drug Hoechst 33258, *Eur. J. Biochem.* 222 (1994) 721.
- (3) E. Trotta, M. Paci, Solution structure of DAPI selectively bound in the minor groove of a DNA T.T mismatch containing site: NMR and molecular dynamics studies, *Nucl. Acids Res.* 26 (1998) 4706.
- (4) A. Fede, A. Labhardt, W. Bannwarth, W. Leupin, Dynamics and binding mode of Hoechst 33258 to d(GTGGAATTCCAC)₂ in the 1:1 solution complex as determined by two-dimensional ¹H-NMR, *Biochemistry* 30 (1991) 11377.
- (5) M. Tsuboi, J.M. Benevides, G.J.J. Thomas, The complex of ethidium bromide with genomic DNA: Structure analysis by polarized raman spectroscopy, *Biophys. J.* 92 (2007) 928.
- (6) C. Aleman, A. Adhikary, D. Zanuy, J. Casanovas, On the protonation equilibrium for the benzimidazole derivative Hoechst 33258: An electronic molecular orbital study, *J. Biomol. Struct. Dyn.* 20 (2002) 301.
- (7) T.D. Sakore, S.C. Jain, C.C. Tsai, H.M. Sobell, Mutagen-nucleic acid intercalative binding: Structure of a 9-Amino-acridine: 5-iodocytidylyl(3'-5') guanosine crystalline complex, *Proc. Natl. Acad. Sci. USA* 74 (1977) 188.
- (8) Y. Hashimoto, K. Shudo, Chemical modification of DNA with mutagenic carcinogens. II. Base sequence-specific binding to DNA of 2-Amino-6-methyl-dipyrido [1,2-a:3',2'-d] imidazole (Glu-P-1), *Environ. Health Perspect.* 62 (1985) 215.
- (9) S. Murata, J. Kusba, G. Piszczek, I. Gryczynski, J.R. Lacowicz, Donor fluorescence decay analysis for energy transfer in double helical DNA with various acceptor concentrations, *Biopolymers* 57 (2000) 306.

- (10) R.G. Langlois, R.H. Jensen, Interactions between pairs of DNA-specific fluorescent stains bound to mammalian cells, *J. Histochem. Cytochem.* 27 (1979) 72.
- (11) M. Saito, M. Kobayashi, S. Iwabuchi, Y. Morita, Y. Takamura, E. Tamiya, DNA condensation monitoring after interaction with Hoechst 33258 by atomic force microscopy and fluorescence spectroscopy, *Biotechnology* 136 (2004) 813.
- (12) K. Yuhzaki, H. Hamaguchi, Intercalation induced structural change of DNA by near infrared Raman spectroscopy, Proc. XIX Int. Conf. Raman Spec. CSIRO, Gold Coast, Queensland, Australia, 2004, p. 460.
- (13) B.W. Lee, S.J. Moon, M.R. Youn, J.H. Kim, H.G. Jang, S.K. Kim, DNA mediated resonance energy transfer from 4',6 diamidino phenanthroline to $[\text{Ru}(1,10\text{-phenanthroline})_2 \text{L}]^{2+}$, *Biophys. J.* 85 (2003) 3865.
- (14) D. Banerjee, S.K. Pal, Simultaneous binding of minor groove binder and intercalator to dodecamer DNA: Importance of relative orientation of donor and acceptor in FRET, *J. Phys. Chem. B* 111 (2007) 5047.
- (15) R. Jin, K.J. Breslauer, Characterization of the minor groove environment in a drug-DNA complex: Bisbenzimidazole bound to the poly[d(AT)]-poly[d(AT)]duplex, *Proc. Natl. Acad. Sci. USA* 85 (1988) 8939.
- (16) D. Banerjee, S.K. Pal, Ultrafast charge transfer and solvation of DNA minor groove binder: Hoechst 33258 in restricted environments, *Chem. Phys. Lett.* 432 (2006) 257.
- (17) J.R. Lakowicz, Principles of fluorescence spectroscopy, *Kluwer Academic/Plenum*, New York, 1999.
- (18) A.K. Shaw, S.K. Pal, Activity of subtilisin carlsberg in macromolecular crowding, *J. Photochem. Photobiol. B: Biol.* 86 (2007) 199.
- (19) R. Sarkar, S.K. Pal, Ligand-DNA interaction in a nanocage of reverse micelle, *Biopolymers* 83 (2006) 675.
- (20) P.E. Pjura, K. Grzeskowiak, R.E. Dickerson, Binding of hoechst 33258 to the minor groove of B-DNA, *J. Mol. Biol.* 197 (1987) 257.
- (21) O.V. Tsodikov, R.M. Saecker, S.E. Melcher, M.M. Levandoski, D.E. Frank, M.W. Capp, M.T.J. Record, Wrapping of flanking non-operator DNA in lac

- repressor-operator complexes: Implications for DNA looping, *J. Mol. Biol.* 294 (1999) 639.
- (22) A.N. Lane, T.C. Jenkins, T.A. Frenkiel, Hydration and solution structure of d(CGCAAATTTGCG)₂ and its complex with propamide from NMR and molecular modelling, *Biochim. Biophys. Acta* 1350 (1997) 205.
- (23) A.K. Shaw, R. Sarkar, S.K. Pal, Direct observation of DNA condensation in a nano-cage by using a molecular ruler, *Chem. Phys. Lett.* 408 (2005) 366.
- (24) D.P. Millar, R.J. Robbins, A.H. Zewail, Direct observation of torsional dynamics of DNA and RNA by picosecond spectroscopy, *Proc. Natl. Acad. Sci. USA* 77 (1980) 5593.
- (25) M. Levitt, How many base pairs per turn does DNA have in solution and in chromatin? Some theoretical calculations, *Proc. Natl. Acad. Sci. USA* 75 (1978) 640.
- (26) S.C. Jakeway, U.J. Krull, Consideration of end effects of DNA hybridization in selection of fluorescent dyes for development of optical biosensors, *Can. J. Chem.* 77 (1999) 2083.

Chapter 7

Studies on Noncovalent Interactions of Small Ligands with Protein

7.1. Introduction:

Proteins are like molecular machines, building blocks and arms of a living cell. Protein ligand interactions form the basis of a wide variety of important biological functions like transport of substances in the blood stream [1] and enzymatic activity. Majority of the ligands bind noncovalently in the active site of the proteins through hydrogen bonds and hydrophobic interactions [2]. The noncovalent interactions in proteins are associated with a certain degree of specificity. The diversity of substrate specificity within a single structural motif is well illustrated by the trypsin family of serine proteases [3]. Slight alterations in the chemical structure of ligands shows different effects in the enzymatic activity of related serine proteases [4]. Specificity of ligand binding can also be important in transport proteins like serum albumins for selective drug transport. Retention of the specificity in structurally modified (unfolded) proteins is indicative of the robustness of the transport process. In this chapter, we attempt to study the specificity of noncovalent interactions between ligands and proteins. In this regard, we explore the binding interactions of the trypsin inhibitor DAPI in structurally related protein α -chymotrypsin. We also study the specificity of binding of two model ligands, DCM and LDS to the transporter protein bovine serum albumin in its native form and in the different unfolded states.

7.2. Results and Discussion:

7.2.1. Spectroscopic Studies on Ligand Enzyme Interactions: Complexation of α -Chymotrypsin by 4',6-Diamidino-2-phenylindole (DAPI) [5].

Figure 7.1(a) shows the excitation and emission spectra of DAPI bound to α -chymotrypsin (CHT). It is to be noted that due to the huge absorption tail of CHT (present in high concentration in solution), the exact nature of the peak of DAPI bound to

CHT is not discernible from the absorption spectra. The excitation spectrum is, therefore, reported here for the clarity of presentation. The excitation spectrum shows a

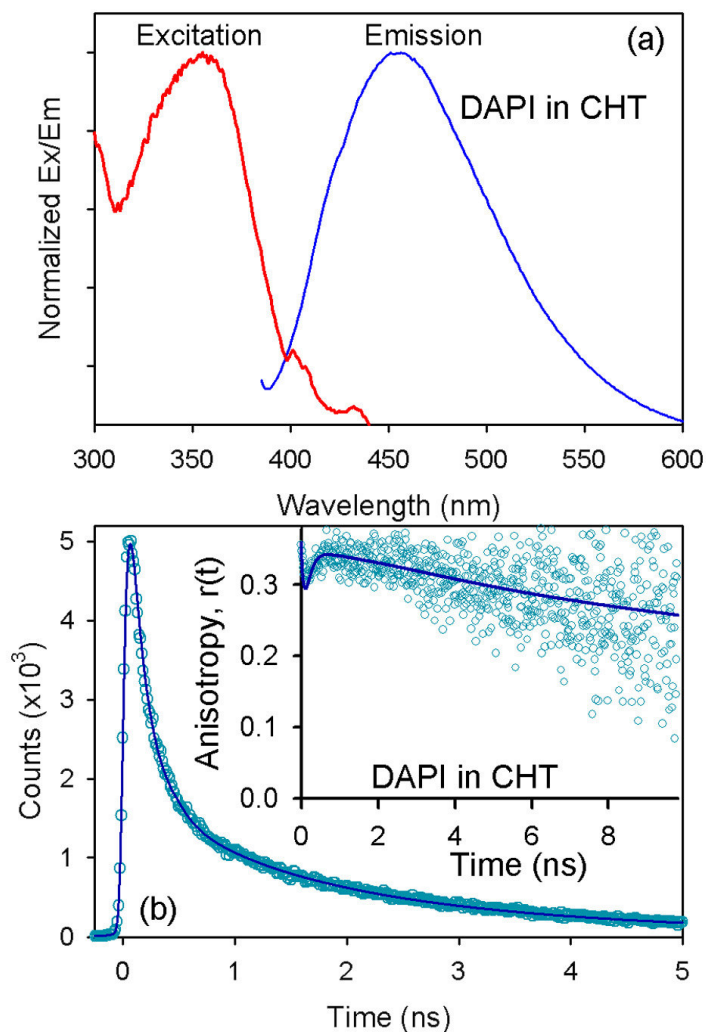


Figure 7.1. The absorption, emission (a), temporal decay of fluorescence (b) and anisotropy (inset b) of DAPI in CHT.

peak at 356 nm corresponding to maximum absorption. The absorption peak of DAPI in CHT is red shifted compared to that of DAPI in buffer and is in accordance with the absorption peak of DAPI in biomimetics/DNA (data not shown). The emission spectrum of DAPI-CHT complex shows a blue shift compared to that in buffer and a concomitant increase in fluorescence intensity. The steady-state results thus indicate interaction of

DAPI with the protein. Figure 7.1(b) shows the temporal decay of fluorescence of DAPI in CHT. The decay has been fitted with time constants of 130 ps(75%), 1.0 ns(12%) and 3.0 ns(13%). The 130 ps component is similar to that obtained when the probe is in buffer [6,7]. In buffer, this 130 ps component represents solvent assisted intramolecular proton transfer process [6], from the amidino to the indole moiety of DAPI [8]. The significant bulk like component in the fluorescence transients is not due to the population of the probe in bulk water as the temporal anisotropy (see below) of the probe in CHT stands against free type probe in the DAPI-CHT complex. Therefore, the presence of a 130 ps component suggests that in the CHT binding mode, the amidinoindole moiety of DAPI is solvent exposed. The longer components in the fluorescence decay are associated with the lifetime of the probe in the hydrophobic environment. The inset of figure 7.1(b) shows the temporal decay of fluorescence anisotropy of the DAPI-CHT complex. The fluorescence anisotropy shows dip and rise in our experimental window. This type of anisotropy decay occurs in a system where there is a juxtaposition of very fast and slow motions of the excited dipole of the fluorophore [9,10]. The decay has been fitted with time constants of 500 ps(16%) and 11 ns(84%) associated with the rotational motions of the enzyme molecule. The faster component of 500 ps is associated with the faster rotation of the solvent exposed group of DAPI molecule and the slow component stands for the slower rotation of the protein bound part.

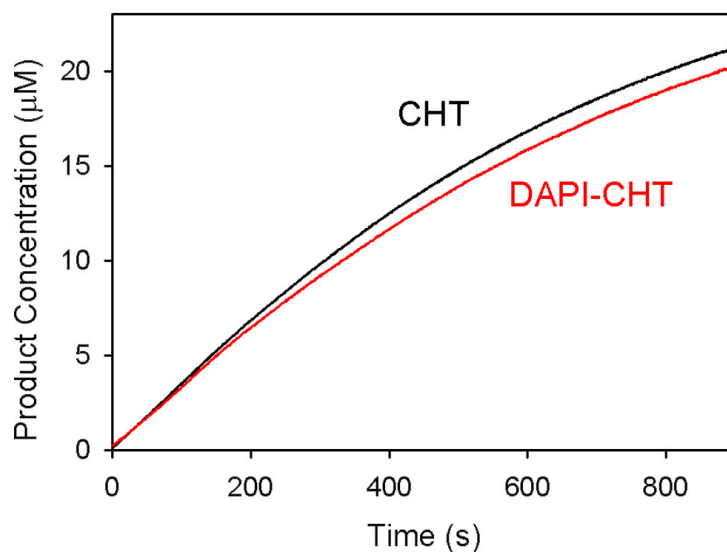


Figure 7.2. The enzymatic activity of DAPI-CHT complex compared to that of CHT.

To explore whether DAPI binds in the S1 pocket as an inhibitor as it does in trypsin, the enzymatic activity of DAPI-CHT complex is compared to that of CHT. Figure 7.2 shows the enzymatic activity of CHT and DAPI-CHT complex in a 900 s time window. The essential similarity (within experimental error) of the plots suggests clearly that DAPI bound to CHT does not act as an inhibitor. The results give an indication that DAPI does not bind to the active site (S1 site) of CHT. Addition of the well established inhibitor PF to DAPI-CHT complex shows that both DAPI and PF simultaneously bind CHT under the experimental conditions (discussed later). The observation further confirms the fact that DAPI does not bind at the active site of the molecule. Simultaneous binding of PF and DAPI to CHT offers a unique opportunity of using Försters resonance energy transfer (FRET) studies between the protein-bound probes. The FRET technique gives accurate distance between two fluorescent probes, one of which acts as a donor and the other an acceptor. In our study DAPI is the donor and proflavin (PF) is the acceptor. The binding of PF to the active site of CHT is well documented in literature [11]. In order to check the suitability of DAPI-PF as donor acceptor pair, FRET between DAPI and PF is studied in SDS micelles having similar size to that of CHT. Figure 7.3(a) shows significant spectral overlap between the emission spectrum of DAPI (donor) and the absorption spectrum of PF (acceptor) in SDS micelles. Both DAPI and PF occupy the micellar interface, and the relative orientation of the bound ligands is random in SDS micelles. The binding of PF to SDS has been indicated by a longer lifetime of PF in the PF-DAPI-SDS complex (inset of figure 7.3(c)). The energy transfer takes place from the donor to the acceptor, as indicated by the quenching of fluorescence intensity (figure 7.3(b)) as well as the faster decay (figure 7.3(c)) of the donor in the donor-acceptor complexes in micelles compared to that of the donor itself in the micelles. The results prove beyond doubt that DAPI and PF is an effective pair for FRET. The distance between the donor and the acceptor has been estimated to be 3.32 nm, by using an estimated R_0 value of 3.87 nm. The observation is consistent with the binding of the donor and acceptor across the chords in the spherical SDS micelle (4 nm diameter [12]).

For DAPI and PF bound to CHT, figure 7.4(a) shows the spectral overlap between the absorption spectrum of PF and emission of DAPI bound to CHT. There is appreciable

spectral overlap indicating that these two probes can serve as good donor-acceptor pair in

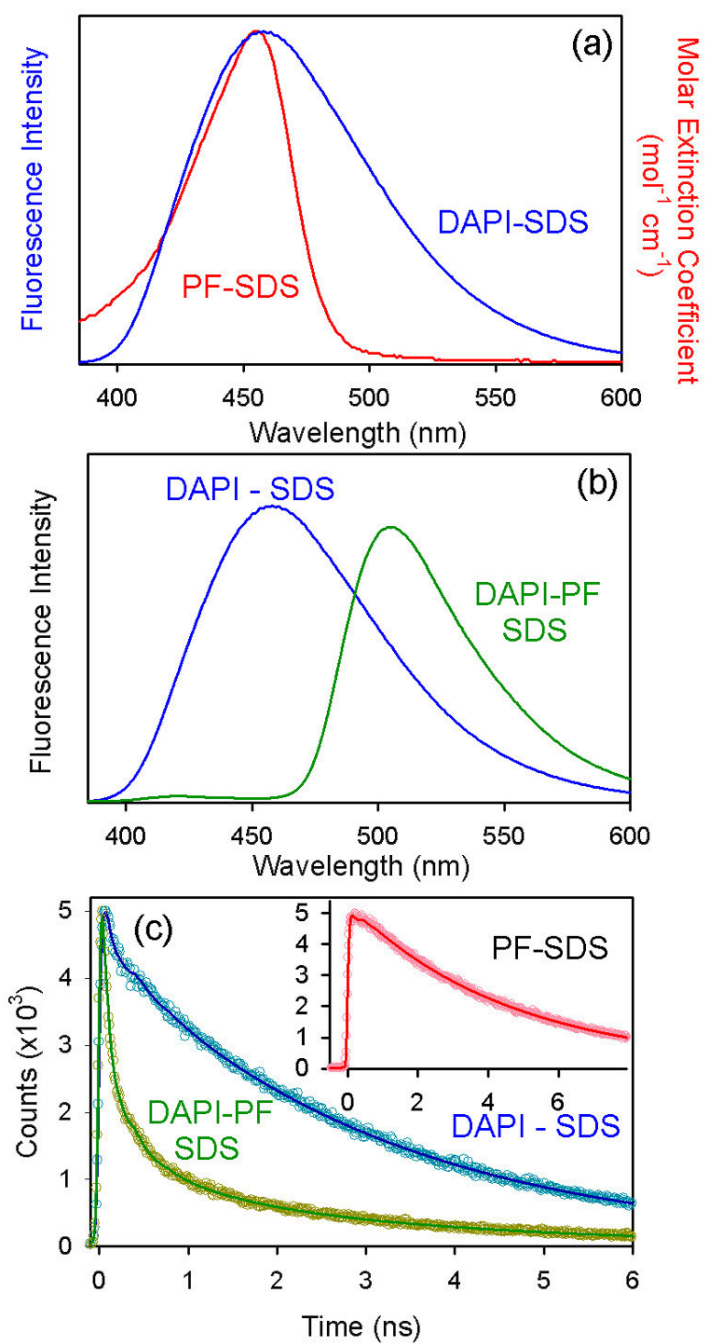


Figure 7.3. (a) The spectral overlap of DAPI and PF in SDS micelles. The emission spectra (b) and the temporal decay of fluorescence (c) of DAPI and DAPI-PF in 20mM SDS.

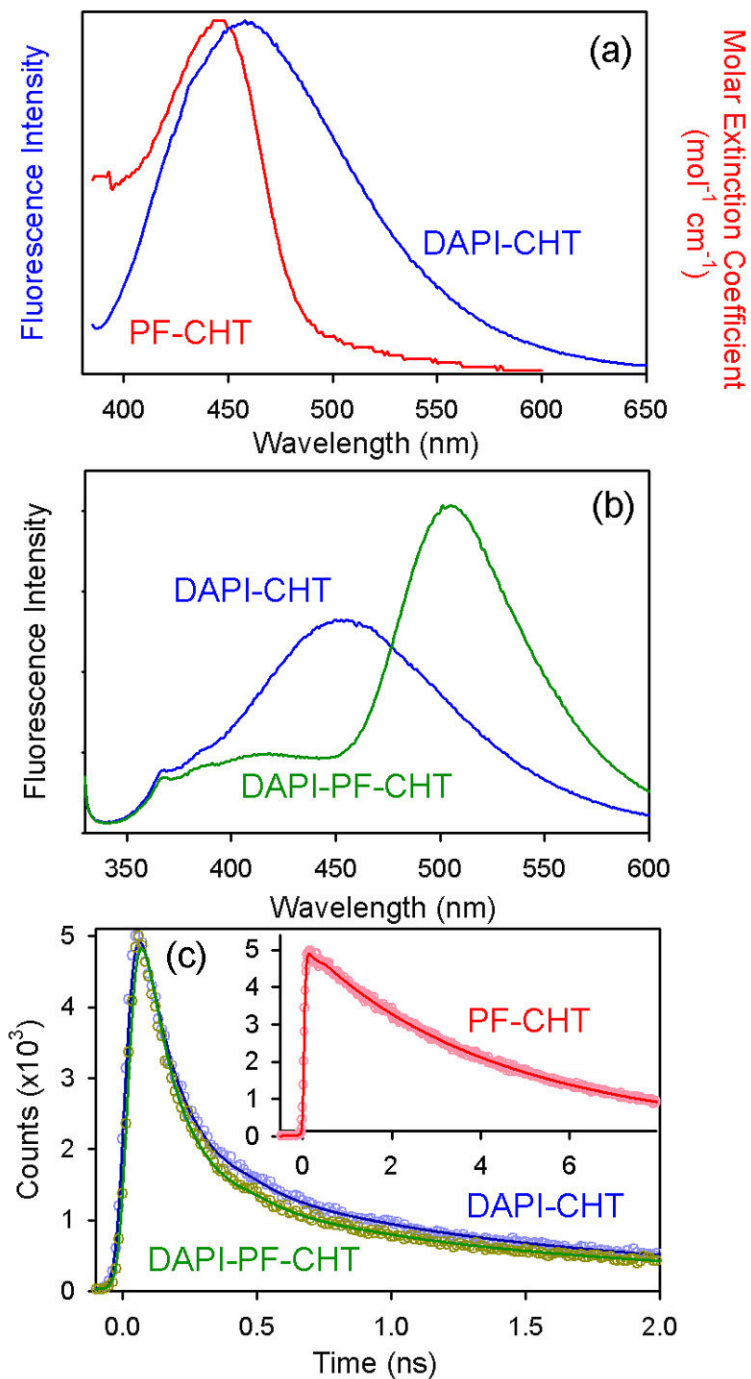


Figure 7.4. (a) The spectral overlap of DAPI and PF in $100\mu\text{M}$ CHT. The emission spectra (b) and the temporal decay of fluorescence (c) of DAPI and DAPI-PF in $100\mu\text{M}$ CHT.

CHT. There is quenching of fluorescence intensity (figure 7.4(b)) in the DAPI-PF-CHT complex relative to that of DAPI-CHT, reflecting energy transfer from DAPI to PF. The binding of PF to CHT in the PF-DAPI-CHT complex under the experimental conditions

is given by the long fluorescence lifetime (inset of figure 7.4(c)) and increased fluorescence intensity (figure 7.4(b)) of PF-CHT complex. However, the temporal fluorescence decays (figure 7.4(c)) of DAPI in DAPI-CHT and DAPI-PF-CHT complexes show very little difference between the observed lifetimes, indicating inefficient dipole-dipole coupling. The observation is also consistent with the reabsorption of donor emission by the acceptor PF as evidenced in the steady-state emission spectra (figure 7.4(b)). Negligible energy transfer can have the following interpretations (i) DAPI and PF are bound at the active site of CHT with unfavorable orientations of their transition dipoles, (ii) DAPI and PF are separated by a distance larger than Förster distance, R_0 , with favorable orientations of transition dipoles, (iii) DAPI and PF are bound at a distance smaller than R_0 , with unfavorable orientations of their transition dipoles. Let us examine the conditions one by one. Enzymatic activity of CHT in the presence of DAPI is similar to that of the native enzyme. This suggests that DAPI is not inhibiting the activity and hence is less likely bound at the active site. Also, had DAPI and PF bound at the active site there would have been a quenching of DAPI fluorescence due to Dexter resonance transfer [13,14].

Therefore, the possibility of PF and DAPI simultaneously occupying the active site of CHT is ruled out. The result is in agreement with the behaviour of DAPI in hydrophobic environments. It is known that the interaction of DAPI with hydrophobic residues is dominated by favorable electrostatic interactions. The replacement of negatively charged aspartate189 in trypsin (where DAPI binds at active site [15]) to serine 189 in CHT creates a more hydrophobic active site. The change in the polarity of the active site of CHT compared to trypsin and the associated structural changes thus accounts for the different molecular recognition of trypsin and CHT by DAPI. The calculated value of R_0 (considering random orientation of dipoles, i.e. a κ^2 value of 0.66) for DAPI and PF in CHT is 3.76 nm, which is less than the distance between the active site and any point within or at the surface of CHT. The observation indicates that both the fluorophores are not bound to CHT at a distance greater than R_0 with favorable orientations of their transition dipoles. The absence of energy transfer, therefore suggests that DAPI and PF are bound to CHT with perpendicular or nearly perpendicular orientation of their respective transition dipoles.

The studies on the enzymatic activity of DAPI-CHT complex along with FRET studies in DAPI-PF-CHT complexes indicate that DAPI binds to CHT at some site other than the catalytic site. In addition to the catalytic binding site, two other sites in CHT, capable of binding ionic hydrophobic dyes are reported in literature. The first one is the hydrophobic binding site proposed by Smith and Hansch [16], which is known to bind the hydrophobic dye TNS [17], and the other is the ANS binding site reported by Johnson et al [18]. The difference in the nature of the binding sites of TNS and ANS are reflected in the pH dependent fluorescence spectra of TNS-CHT and ANS-CHT complexes. The fluorescence of TNS-CHT complex shows a 15 nm red shift and an increase in fluorescence intensity as the pH of the medium is raised from 2.5 to 7.8 [17]. On the other hand, the fluorescence spectra of ANS-CHT complexes show a red shift but concomitant decrease in fluorescence intensity over the same pH range [18], indicating the difference in the nature of binding sites of these two dyes. The fluorescence spectrum of DAPI-CHT shows a 20 nm red shift along with an increase in fluorescence intensity at high pH and is similar the fluorescence behavior of TNS-CHT complex. In order to confirm the exact location of DAPI in CHT, competitive binding studies between DAPI and TNS are performed. Both the dyes show blue shift and increase in fluorescence intensity when bound to CHT. TNS gives a fluorescence maximum at 427 nm whereas DAPI shows an emission peak around 460 nm. However the increase in fluorescence intensity of TNS in CHT ($Q_D=0.6$) is much more than that of DAPI ($Q_D=0.24$).

Figure 7.5(a) shows the fluorescence spectrum of TNS-CHT and TNS-DAPI-CHT complexes. The quenching of fluorescence of TNS in TNS-DAPI-CHT indicates that TNS is being expelled out from the protein on addition of DAPI. Also, TNS in CHT shows a 9 ns lifetime, which is much longer than the longest lifetime component of DAPI in CHT (3 ns). So, this long component can be monitored to characterize the binding of TNS to CHT. In this regard, it is to be noted that both TNS and DAPI absorb the 375 nm light used as our excitation source. This might raise the complicity that the reported fluorescence is actually the average of the fluorescence coming from the two fluorophores. However, the comparison of the emission spectrum of TNS-DAPI-CHT

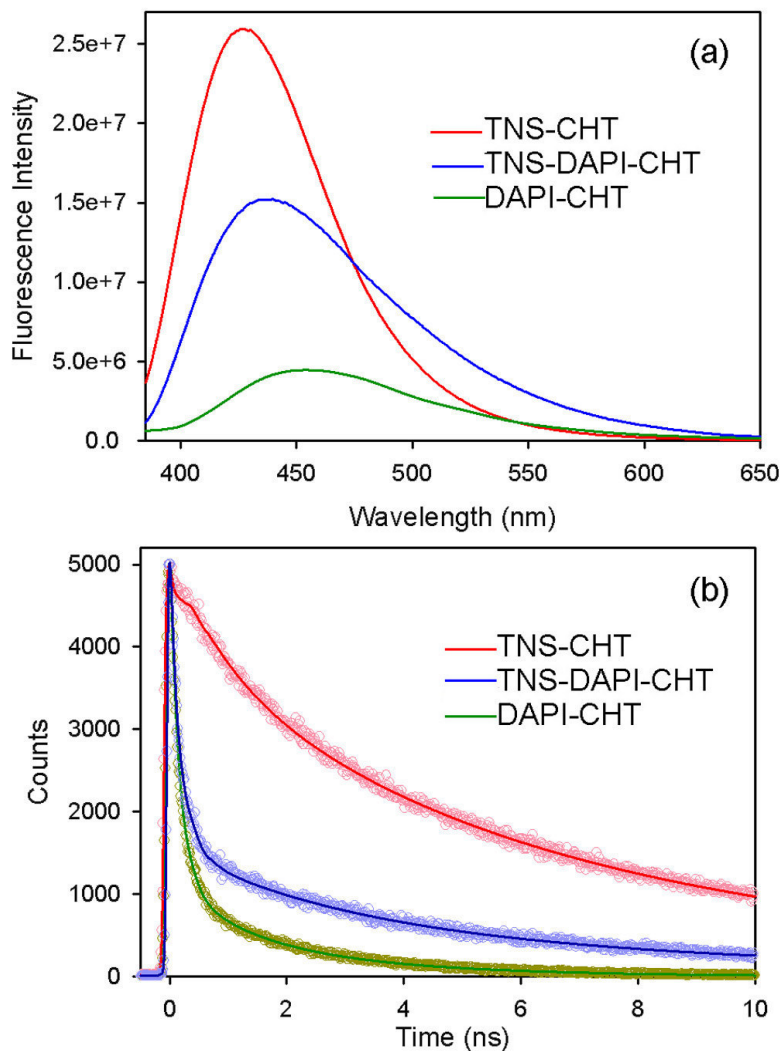
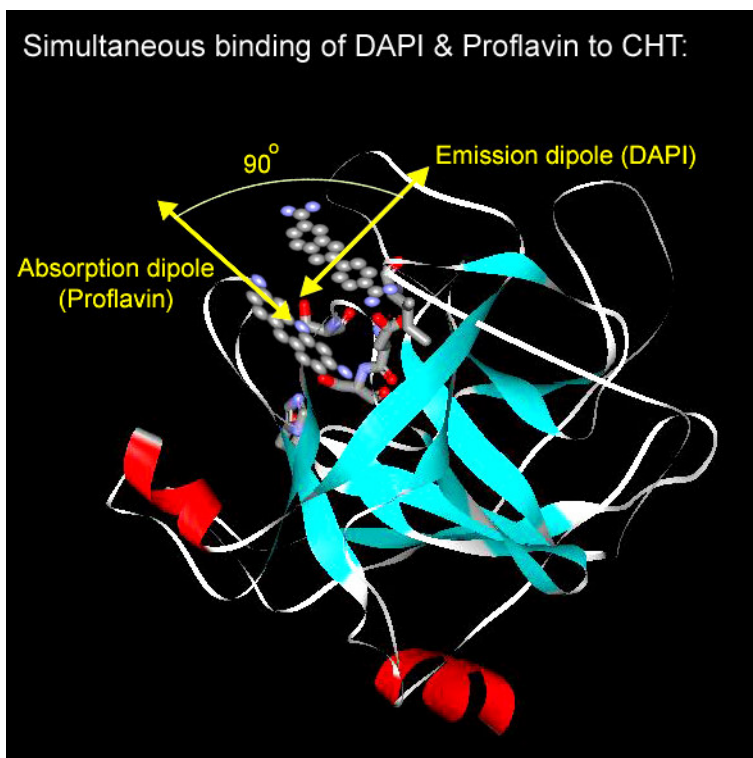


Figure 7.5. (a) The fluorescence spectra and (b) the temporal decay of fluorescence of TNS-CHT, TNS-DAPI-CHT and DAPI-CHT complexes.

and DAPI-CHT (having the same concentration of DAPI as in the TNS-DAPI-CHT complex) shows that at 410 nm, the fluorescence of TNS is 9 times more than that of DAPI. This ensures that at 410 nm, the decay of fluorescence essentially reports the relaxation of the excited TNS molecules, with minimum interference from DAPI. The temporal decays of fluorescence in TNS-CHT and TNS-DAPI-CHT complexes at 410 nm are shown in figure 7.5(b). The fluorescence of DAPI-CHT having the same concentration of DAPI is also forwarded for comparison. Analyses of the decays show that the 9 ns lifetime characteristic of TNS-CHT complex decreases from 50% to 18% in

TNS-DAPI-CHT complex. This gives a clear indication that TNS is expelled on the addition of DAPI. In other words, DAPI competes for the binding site of TNS.



Scheme 7.1. Simultaneous binding of DAPI and Proflavin in CHT. From FRET studies, the relative orientation between the transition dipoles of the donor and acceptor is found to be nearly perpendicular. The molecular structure of CHT (2CHA) is downloaded from the Protein Data Bank and processed with the program Weblab Viewerlite.

It is interesting to observe that although the binding of TNS to CHT affects the enzymatic activity, the binding of DAPI to the same site leaves the enzymatic activity unaltered. The apparent anomaly in the behavior of these two dyes binding at the same site can easily be resolved if one considers the correlation between the ligand binding at this hydrophobic site [16] and the mechanism of enzyme inhibition [19]. The anionic TNS binds in the hydrophobic environment of isoleucine16 (Ile16) and aspartate194 (Asp194) ion pair and through electrostatic repulsion, displaces the Asp194 side chain in such a way that it blocks and inactivates the serine195 (Ser195) and histidine57 (His57) active site. However, the cationic DAPI may form an alternate ion pair with Asp194 and hence does not effectively displace the Asp194, a phenomenon that is crucial for enzyme

deactivation. To estimate the binding geometry of DAPI in the TNS-binding site, we use the result of energy transfer in PF-DAPI-CHT complex. Estimating that the centers of the active site and the DAPI binding site are 1.2 nm apart, the value of the orientation factor κ^2 is calculated to be close to zero. This indicates a perpendicular geometry of the PF and DAPI transition dipoles when PF and DAPI bind at the active site and TNS binding site respectively in CHT (scheme 7.1).

7.2.2. Solvation Dynamics of LDS in Micelles, Reverse Micelles and Proteins [20].

Figure 7.6(a) shows the absorption spectra of the laser dye and solvation probe LDS (LDS) in buffer and in different restricted environments and in the transporter protein bovine serum albumin (BSA). The absorption spectra of the dye in micelles and BSA shows a red shift compared to the absorption of the dye in buffer indicating the ground state stabilization of the dye in the restricted environments. The shift is maximum for micelles (TX-100, CTAB and SDS) indicating maximum ground state stability of the probe in micelles. The proximity of the absorption maxima of LDS in RM ($w_0=2.5$) and BSA suggest comparable ground state stabilization of the dye in both the environments. Figure 7.6(b) shows the emission spectra of LDS in the restricted environments. The emission spectrum of the dye in buffer is also shown for comparison. It is interesting to observe that the emission spectrum of the dye in micelles and reverse micelles are red shifted compared to those of the buffer. The red shift in the emission spectra can be rationalized considering internal Stark effect [21]. The static electric field created due to the presence of charged/polar surfactant head groups affects the excited state of the probe and that is indicated by the red shift in the emission spectra. This shift is expected to be different from that of the polarity dependent solvchromic shift as reported by Maroncelli et al. [22]. Only, the emission of LDS in BSA is blue shifted indicating the destabilization of the excited state in the binding pocket of BSA.

In order to explore the possibility of using LDS as a reporter of the environmental dynamics, fluorescence transients are taken across the emission spectrum in all the restricted environments. Figure 7.7(a) shows the fluorescence transients of LDS in AOT/isooctane reverse micelles (RM) having $w_0=2.5$. The transients show fast decay in

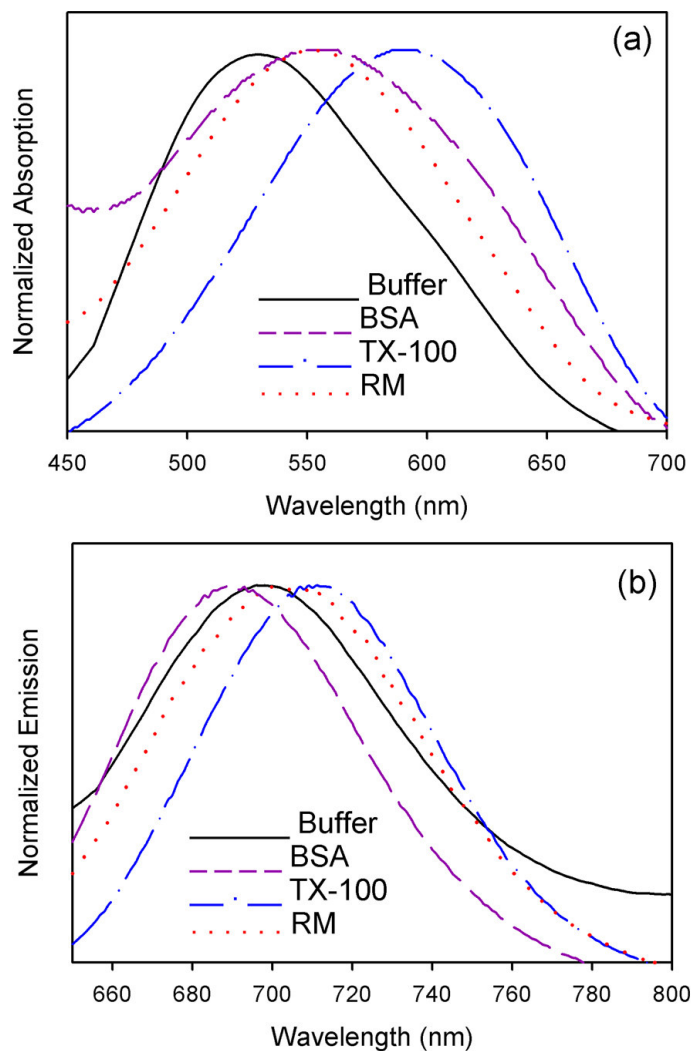


Figure 7.6. The absorption (a) and emission spectra (b) of LDS in different restricted environments. For the sake of clarity only representative micelles (TX-100) and reverse micelles ($w_0=2.5$) are shown.

the blue end and rise in the red end indicative of solvation. The constructed TRES (figure 7.7(b)) gives a shift of 700 cm^{-1} in a 3 ns window. In order to confirm that the observed dynamics represents environmental stabilization, TRANES are constructed. The absence of isoemissive points in TRANES excludes the possibility of interference of any internal dynamics of the probe to the observed relaxation dynamics [23]. Figure 7.7(c) shows the temporal decay of the solvation correlation function ($C(t)$). The time constants of 110 ps(50%) and 650 ps(50%) indicate that the molecule is located in the water pool of the

RM. The restricted rotational motion of the probe is borne out by a long component

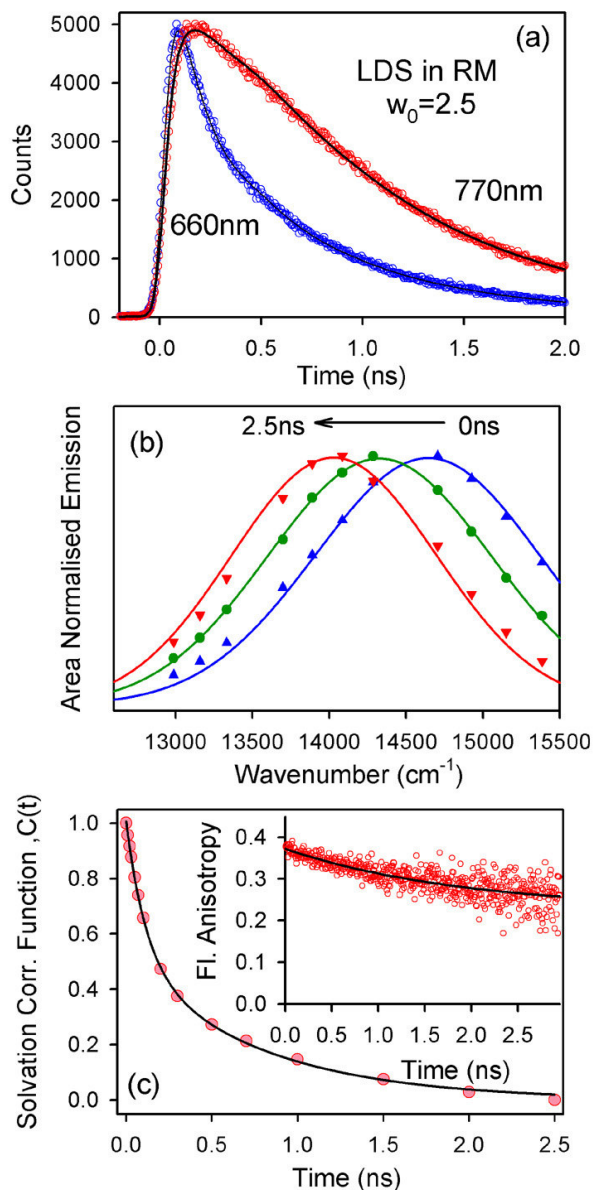


Figure 7.7. The fluorescence transients (a), TRES (b), the temporal decay of solvation correlation function (c) and fluorescence anisotropy (c, inset) of the LDS in reverse micelle ($w_0 = 2.5$).

in the decay of fluorescence anisotropy. In order to see the effect of increase in the pool size of the RM, the dynamics of environmental relaxation are monitored in RMs having different w_0 values. Figure 7.8 shows the decay of the solvation correlation function, $C(t)$ in RM with different w_0 . The insets show the geometrical restriction to rotational motion

of the probe in different environments. The results indicate that the dynamics reported by the probe become faster (corresponding time constants are 110 ps(50%) and 650 ps(50%) in $w_0=2.5$ and 80 ps(80%) and 300 ps(20%) in $w_0=10$) with increasing pool size in the RM. The results are consistent with the fact that the probe moves towards the water pool in the bigger sized RM. The temporal decay of fluorescence anisotropy also indicates faster time scales associated with the increased rotational motion of the probe located in the water pool of the bigger RM.

To study the effect of the surface charge on the recognition of biomimetics by LDS we studied the dynamics of the probe in neutral (TX-100), cationic (CTAB) and anionic (SDS) micelles. As discussed above, the probe shows ground state stability in all the micelles, whereas, the ionic environment created by the charge/polarity of micellar head groups influences the excited state stability of the probe. The inset of figure 7.9(a) shows the geometrical restriction imposed to the rotational motion of the probe in a solution containing TX-100 micelles. The time constant of 1.46 ns associated with the temporal decay of fluorescence, which is considerably slower than the rotational orientational time in buffer (<80 ps) confirms the binding of the probe to TX-100 micelles. Figure 7.9(a) shows the temporal decay of the solvation correlation function in the neutral TX-100 micelles. The fast decay in the blue end and rise in the red end of the emission spectrum of the probe in TX-100 micelles (data not shown) suggests stabilization of the excited state dipole in the micellar environment. The constructed solvation correlation function decays with time constant of 60 ps. This observed time scale of 60 ps matches with the relaxation dynamics of free type of water molecules present at the micellar surface [24]. This suggests that LDS is not deeply embedded in the hydrophobic interior of the micelle but is more solvent exposed. Figure 7.9(b) and the corresponding inset show the temporal decay of the solvation correlation function and rotational anisotropy of LDS in CTAB micelles. The slow component (1.27 ns) in the fluorescence anisotropy suggests the association of the probe with CTAB micelles, whereas environmental dynamics suggests a huge solvent exposure of LDS in CTAB

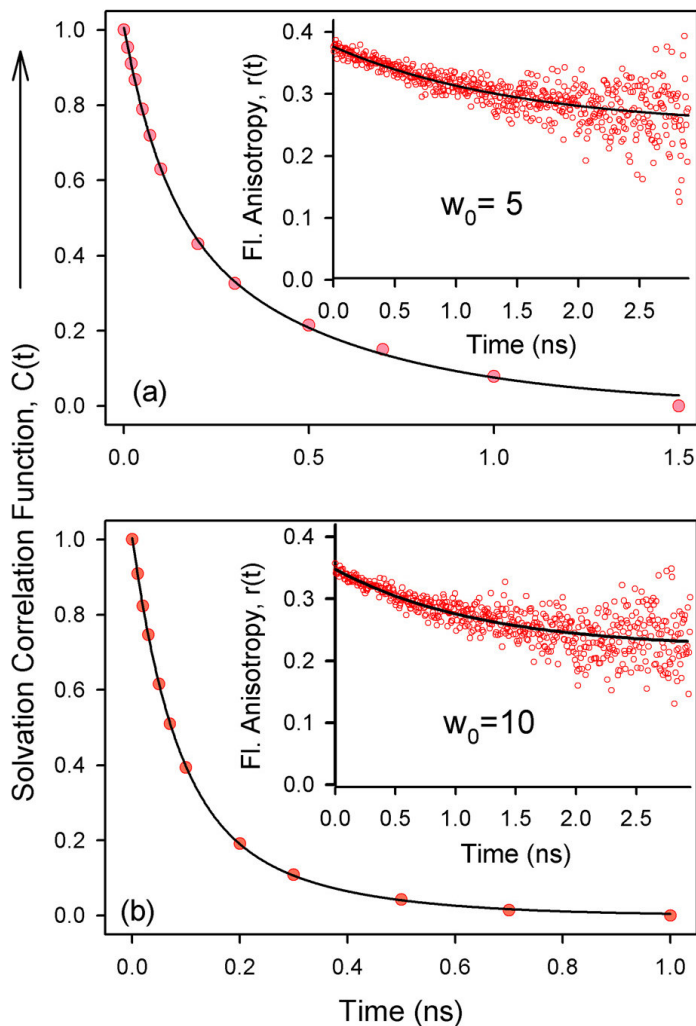


Figure 7.8. The temporal decay of solvation correlation functions and fluorescence anisotropies (corresponding insets) of LDS in reverse micelles of different w_0 values.

micelles, similar to the results obtained for neutral TX-100 micelles. The geometrical restriction to rotational motion (evidenced by a slower component in the decay of fluorescence anisotropy) indicates that the probe interacts with SDS micelles. However, the similarity of the fluorescence transients at the blue and red ends of the emission spectrum suggests the absence of solvation stabilization in our experimental window. The absence of any change may be due to the very fast environmental relaxation of the ionic environment, which is not detectable in our experimental window.

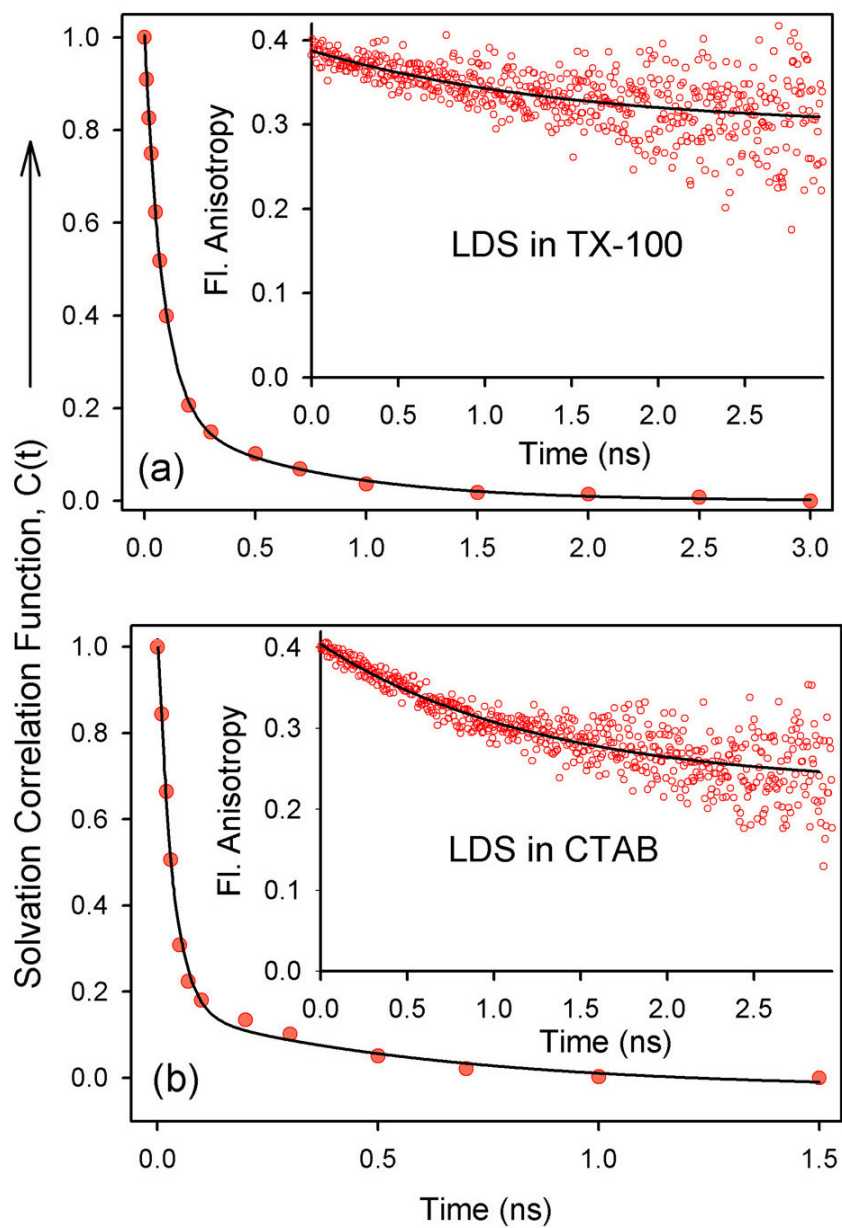


Figure 7.9. The temporal decay of the solvation correlation functions and fluorescence anisotropies (corresponding insets) of LDS in micelles.

It is worthwhile at this stage to extend our studies on LDS in the transporter protein bovine serum albumin (BSA). In order to estimate the exact binding site of LDS

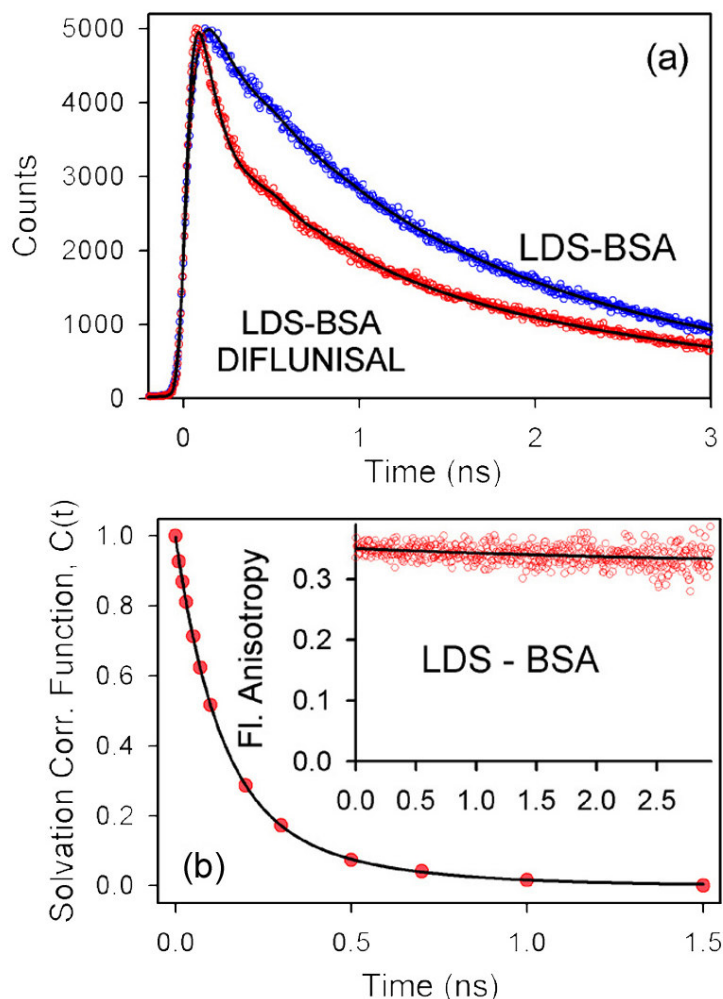


Figure 7.10. (a) The temporal decay of fluorescence of LDS-BSA and LDS-BSA-Diflunisal complexes), temporal decay of the solvation correlation function (b) and fluorescence anisotropy (inset) of LDS in BSA.

in BSA, competitive binding studies are done with well known BSA-binders warfarin and diflunisal. It is known that warfarin specifically binds in subdomain IIA [25] of the protein. Diflunisal on the other hand has the capacity of binding to both domain II and domain III in BSA [26]. It is important to mention here that for the competitive binding studies, the concentration of LDS is maintained an order of magnitude lower than that of BSA, while that of the competitive binder (warfarin/diflunisal) is used in excess. The significant difference in the fluorescence lifetimes of LDS in buffer (< 80 ps) and BSA (3 ns) makes it a very suitable parameter to study competitive binding. On addition of warfarin to LDS-BSA complex, there is no appreciable change in the observed

fluorescence lifetime. This suggests that LDS does not bind to the warfarin-binding site in BSA. However, on the addition of diflunisal, the appearance of a faster component (< 80 ps(50%)) suggests the presence of free LDS molecules in solution (figure 7.10(a)). The results indicate that diflunisal expels LDS from its binding site in domain III of the protein. The severe geometrical restriction to probe rotation in the binding site of BSA (inset, figure 7.10(b)) is exhibited by absence of faster components in the temporal decay of fluorescence anisotropy. The decay of anisotropy shows only a huge offset indicating the global rotational motion of the protein. In order to establish LDS as an environmental reporter of the BSA environment, TRES is constructed in BSA. The average time constant of 0.40 ns associated with the decay of solvation correlation function (figure 7.10(b)) is consistent with the dynamics of protein environments [27]. To ascertain that the observed dynamics actually represents environmental relaxation we have also constructed the TRANES (data not shown). The absence of isoemissive point indicates that the probe can unambiguously report the dynamics of the protein environment [23]. The absence of isoemissive point in TRANES also shows that LDS occupies a specific site in BSA.

7.2.3. Molecular Recognition in Partially Folded States of a Transporter Protein: Temperature-Dependent Specificity of Bovine Serum Albumin [28].

The unfolding of a protein is marked by a change in the secondary and globular structure of the protein. Figures 7.11(a) and 7.11(b) show the change in the hydrodynamic radius and the percent helicity of the protein, respectively at various temperatures. Both the curves show changes in slopes indicating the presence of intermediates in the melting profile of the protein. It is to be noted that the presence of intermediate unfolded states in the thermal and chemical denaturation of bovine serum albumin (BSA) have already been indicated by calorimetric [29] and spectroscopic [30,31] studies. Careful inspection of the curves in figure 7.11(a) and 7.11(b) reveal that there are three unfolded states at three consecutive temperatures around 50°C , 64°C and 75°C , respectively. To obtain a more quantitative picture of the unfolding process and to construct an energy profile of the

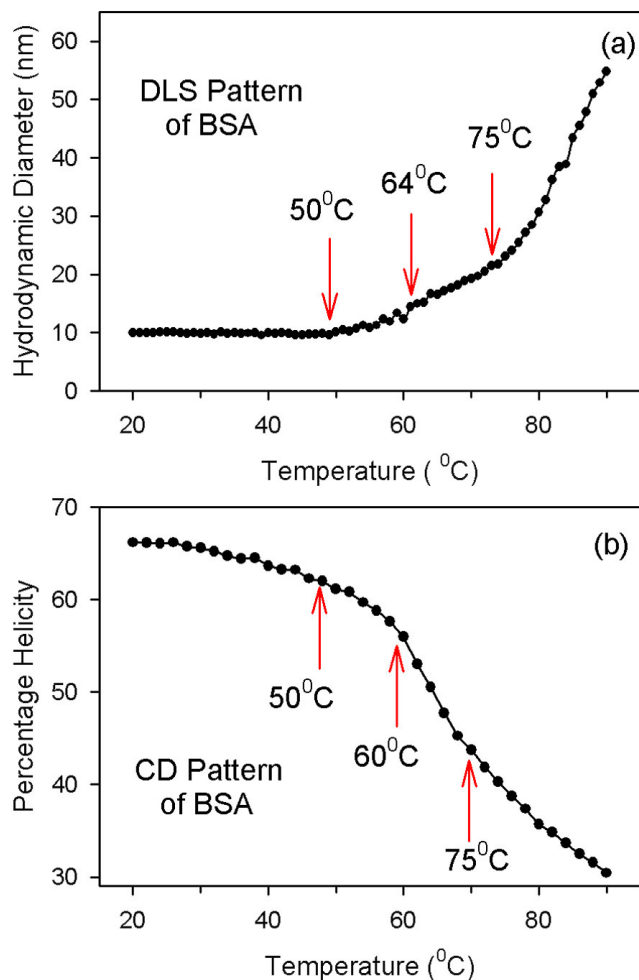


Figure 7.11. The hydrodynamic diameter (a) and the percentage helicity (b) of 100 μ M BSA in phosphate buffer. The arrows indicate the change in slope of the curve reflecting the structural transitions of the protein.

unfolding of the protein, DTA studies are carried out on the protein in buffer. Figure 7.12(a) shows the DTA pattern of 100 μ M of the protein in buffer. Arrows show the onsets of the changes in slope of the thermogram. The total endothermic area under the curve could be resolved into three separate curves (deconvolution) having peaks around 54 $^{\circ}$ C, 64 $^{\circ}$ C and 72 $^{\circ}$ C (figure 7.12(b)), indicating three transitions take place in the protein around these three temperatures. The temperatures obtained from the DTA measurements tally quite well with that obtained from the DLS and CD results (figures 7.11(a) & (b)).

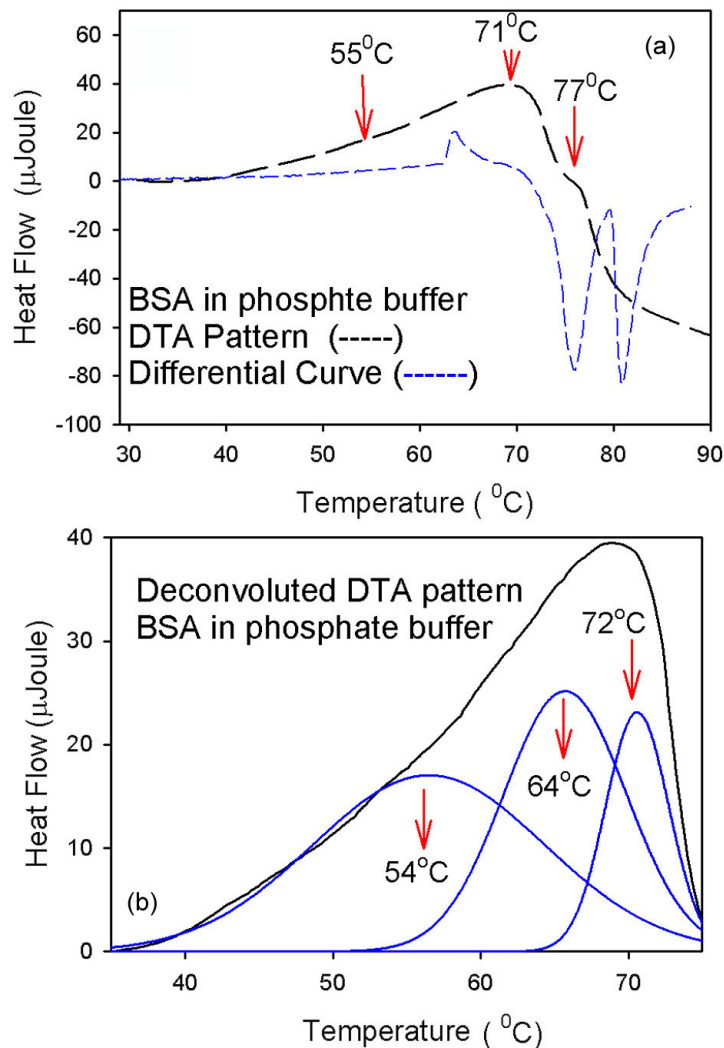


Figure 7.12. The DTA pattern of 100μM BSA in phosphate buffer. The arrows indicate the change in slope of the curve reflecting the structural transitions of the protein. (b) The deconvoluted DTA profile of BSA in phosphate buffer.

The peak coming in the exothermic region at temperatures around 80°C is associated with thermal aggregation of the protein at the higher temperature [32]. The area under each deconvoluted curve gives the heat energy change (ΔH) associated with the corresponding structural transition. The ΔH values associated with the transitions have been tabulated in Table 7.1. The observed ΔH values are in good accordance with previously reported result [29]. The free energy change (ΔG) associated with the transitions have been estimated from the relation [32,33],

$$\Delta G = -RT \ln K \dots \dots \dots (7-1)$$

where K is the equilibrium constant associated with the transition,



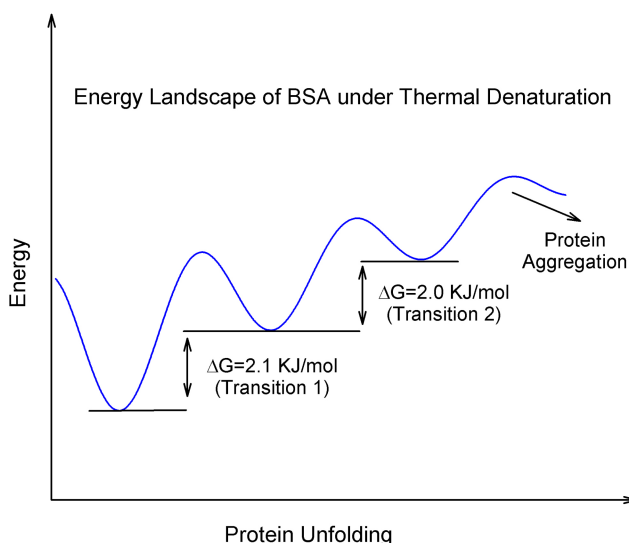
where N denotes the native and D is the denatured or partly denatured state and is given by the relation,

$$K = [\text{native}] / [\text{denatured}] \dots \dots \dots (7-3)$$

The ratio of the concentrations of the native and denatured states could be obtained from the relation,

$$K = (P_{eq} - P_n) / (P_d - P_{eq}) \dots \dots \dots (7-4)$$

where P is any property, which changes from the native (P_n) to the denatured (P_d) state. P_{eq} is the corresponding value at equilibrium. These properties in the case of proteins are the extinction coefficient, the secondary or globular structure, and other properties [32]. In the present study the ΔG values have been independently calculated for the reversible transitions by monitoring the changes in extinction coefficient and the percent helicity (secondary structure) values at different temperatures and the values are found to be consistent. The average ΔG values associated with the transitions are tabulated in Table 7.1. The free energy landscape of the protein BSA under thermal denaturation is shown in scheme 7.2. Our observations suggest that there are intermediate states associated with the thermal unfolding of BSA.



Scheme 7.2. The free energy landscape (not drawn to scale) of the protein BSA under thermal denaturation.

Table 7.1: Thermodynamic Parameters Associated with Temperature Induced Denaturation of BSA

Parameter	Transition 1 (Native→I1)*	Transition 2 (I1→I2)*	Transition 3 (I2→Unfolded)*
Temperature (⁰ C)	54	64	70
ΔH (KJ mol ⁻¹)	212	210	230
ΔG (KJ mol ⁻¹) (from extinction coefficient)	2.314	2.279	-
ΔG (KJ mol ⁻¹) (from CD)	1.797	1.951	-

* I1, I2 stand for intermediates 1 and 2 respectively.

Table 7.2: Solvation Correlation Function of the Dyes in BSA at Different Temperatures

Probe	Temperature = 25 ⁰ C			Temperature = 50 ⁰ C			Temperature = 75 ⁰ C		
	τ ₁ (ns)	τ ₂ (ns)	Shift (cm ⁻¹)	τ ₁ (ns)	τ ₂ (ns)	Shift (cm ⁻¹)	τ ₁ (ns)	τ ₂ (ns)	Shift (cm ⁻¹)
LDS	0.147 (52%)	0.687 (48%)	125	0.238 (100%)	-	062	0.393 (100%)	-	109
C500	0.489 (100%)	-	245	0.077 (53%)	0.987 (47%)	696	0.198 (100%)	-	157
DCM	0.235 (33%)	3.885 (67%)	560	0.236 (37%)	3.882 (63%)	825	0.790 (43%)	4.63 (57%)	350

To monitor the local dynamics of the protein and the nature of ligand binding in the different unfolded states, we have used three probes LDS, DCM and Coumarin 500 (C500). Figure 7.13(a) shows the temporal decay of the solvation correlation function associated with the probe LDS in BSA at temperatures 50⁰C and 75⁰C. The time constants and the spectral shift associated with the decay of solvation correlation function of the probe-BSA complex at the two different temperatures have been tabulated in Table 7.2. At 50⁰C the temporal decay of the solvation correlation function gives a time constant of 0.24 ns. The absence of the long component of ~0.70 ns associated with the protein residue/rigid water solvation [27] as evidenced at 25⁰C indicates that BSA swells up and accommodates more labile water molecules in its cavity. The spectral shift associated with the solvation shows that we are losing a considerable portion of ultrafast

solvation due to the labile water molecules in our instrumental resolution. The average time constants ($\tau_{av}=a_1\tau_1+a_2\tau_2$) associated with the decay of the solvation correlation functions for the probe decreases at 50⁰C compared to that at 25⁰C. At 75⁰C the solvation correlation associated with the probe-protein complex decays with a time constant of

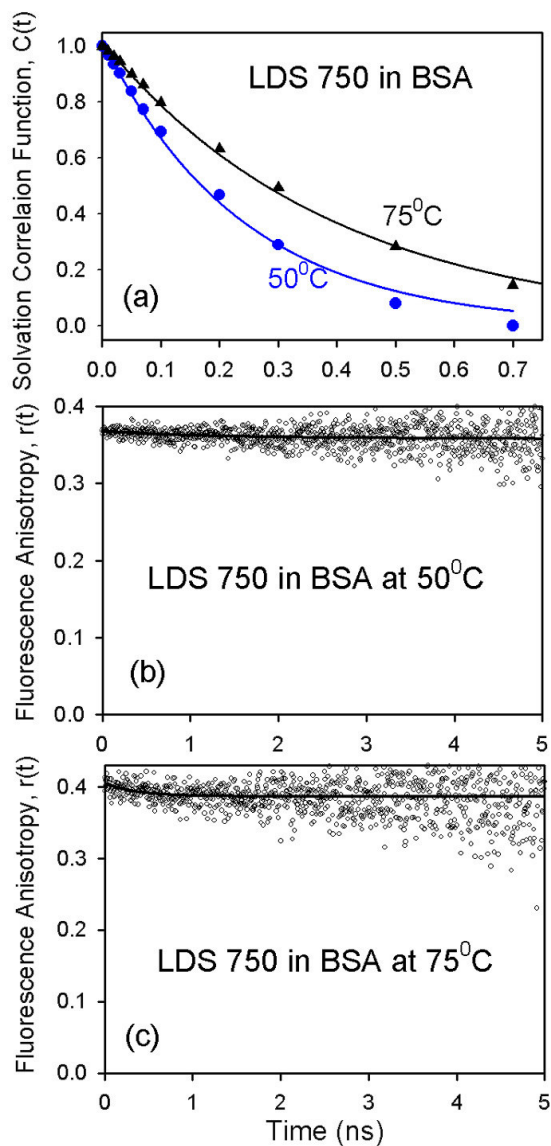


Figure 7.13. (a) The temporal decays of the solvation correlation function $C(t)$ of the probe LDS in BSA at 50⁰C and 75⁰C. The decay of fluorescence anisotropies, $r(t)$ of the probe LDS in BSA at 50⁰C (b) and 75⁰C (c).

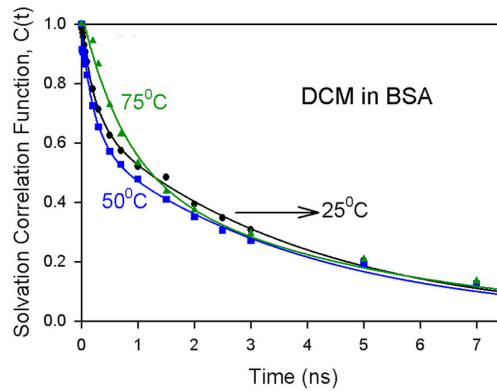


Figure 7.14. The temporal decays of the solvation correlation function, $C(t)$ of the probe DCM in BSA at different temperatures.

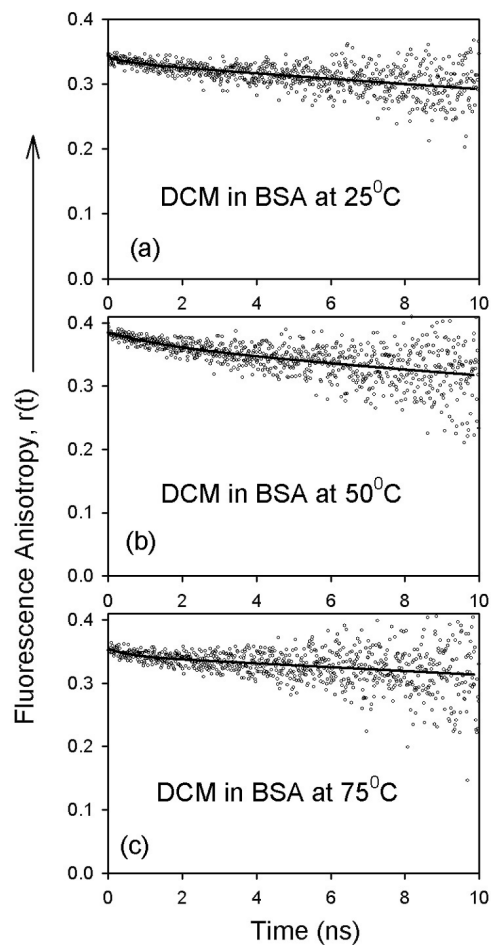


Figure 7.15. The temporal decays of fluorescence anisotropies $r(t)$ of the probe DCM in BSA at temperatures 25°C (a), 50°C (b) and 75°C (c).

0.393 ns. This increase in time constant along with the increase in the associated spectral shift (Table 7.2) show that the probe in this unfolded state is solvated by protein residues which are now more labile to reorient along the excited dipole of the ligand LDS. Figures 7.13(b)-(c) shows the decay of fluorescence anisotropy associated with the probe LDS at temperatures 50⁰C and 75⁰C, respectively. The time constants (Table 7.3) associated with the fluorescence anisotropies are consistent with the bigger size of the unfolded protein at the two temperatures [34]. The percentage of this long component does not decrease even at 75⁰C indicating that the probe is associated with the protein even in the unfolded state.

Figure 7.14(a) shows the decay of the solvation correlation function associated with the relaxation dynamics as experienced by the probe DCM bound to BSA at different temperatures. The time constants associated with the decay of the solvation correlation function (Table 7.2) of the DCM-BSA complex at 25⁰C show that the DCM molecule enters into the hydrophobic region of its binding site in the protein. This binding site of the protein is only slightly affected when the temperature is raised to 50⁰C. At 75⁰C the environment around the DCM molecule shows a change in the time constants of the C(t) decay. The longer time constants associated with the temporal decay of the solvation correlation function at 75⁰C suggest that there is increased solvation from the freely moving protein residues. The decrease in the spectral shift coupled with the red shift in the emission maximum at time=0 indicates that a considerable part of the ultrafast hydration is lost in our instrumental resolution. The observation is consistent with the fact that the binding site opens up, exposing the protein residues and admitting water molecules inside the pocket. The decays of the fluorescence anisotropies associated with the DCM-BSA complex at different temperatures have been shown in figures 7.15(a)-(c). The time constants associated with the decays (Table 7.3) suggest that the DCM molecule does not leave the unfolded protein even at 75⁰C.

Figure 7.16 shows the solvation correlation functions of the probe C500 in BSA at different temperatures. The time constants associated with the decays of the solvation correlation functions have been listed in Table 7.2. The temporal decay of the solvation correlation function gives a time constant of 0.487 ns consistent with the solvation due to rigid water molecules and/or polar residues of the protein [27]. The emission of the

Table 7.3: Fluorescence Anisotropy at Different Temperatures

Probe	Temperature = 25 ⁰ C		Temperature = 50 ⁰ C		Temperature = 75 ⁰ C	
	τ_1 (ns)	τ_2 (ns)	τ_1 (ns)	τ_2 (ns)	τ_1 (ns)	τ_2 (ns)
LDS		50.00 (100%)	0.84 (5%)	56.09 (95%)		74.01 (100%)
C500	0.31 (8%)	50.00 (92%)	1.07 (12%)	51.90 (88%)	0.24 (30%)	70.22 (70%)
DCM	-	50.00 (100%)	1.65 (5%)	55.10 (95%)	-	70.10 (100%)

probe in the protein complex at 25⁰C shows a maximum at 490 nm. Comparison of the emission of the probe in hydrophobic (n-heptane, emission maximum=436 nm) and polar (water, emission maximum=500 nm) solvents at 25⁰C suggests that the binding site of C500 in the protein is probably a crevice in close contact with water molecules. In this regard, the binding site of the probe is likely to be the binding site I located in sub-domain IIA of BSA molecule [35]. The emission maximum of the tryptophan residue located at the bottom of this binding site of structurally similar HSA shows a peak at

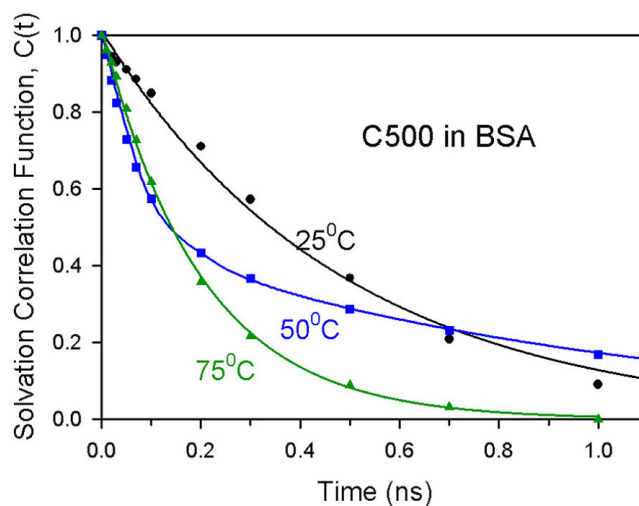


Figure 7.16. The temporal decays of the solvation correlation function $C(t)$ of the probe C500 in BSA at different temperatures.

338 nm consistent with a more bulk like environment [35]. The time constants associated with the solvation correlation function at 50⁰C suggest that the domain at which the probe resides changes considerably and due to opening of the crevice leaves the probe molecule exposed to the bulk solvent giving time constant of 0.077 ns(53%). The longer component of 3 ns(47%) associated with the solvation shows that the protein residue solvation is also a contributing factor. An increase in the spectral shift (Table 7.2) is also associated with the solvation at 50⁰C. At 75⁰C the binding site of the probe is completely destroyed [30] and C500 resides in a hydrophilic environment, indicated by the time constant of 0.114 ns of the temporal decay of the solvation correlation function, C(t). The residence of the probe in the hydrophilic environment is also evidenced from the red shift in the steady-state emission peak and TRES peak at zero time. A decrease in the shift value associated with the solvation suggests that we are losing a considerable portion of ultrafast solvation in our resolution. The dynamics reported by the probe C500 is consistent with the melting of domain II in the temperature range 50⁰C-60⁰C as reported in a previous study [30]. The temporal decays of the fluorescence anisotropies for the probe C500 are shown in figure 7.17(a)-(c). The time constants associated with the decay are consistent with the thermal unfolding of the protein at 50⁰C and 75⁰C. The time constants associated with the decay of fluorescence anisotropy for the C500-BSA complex at 75⁰C, shows a 0.24 ns component in addition to the longer 70 ns component associated with the overall tumbling of the unfolded protein. This suggests that the probe C500 is partially released into bulk buffer (since the average rotational time associated with the probe in bulk buffer is about 200 ps (data not shown)) after its binding site has been completely destroyed.

A comparison of the solvation characteristics along with the time constants associated with the temporal decay of fluorescence anisotropy of the three probes (C500, DCM and LDS) clearly shows that the probes DCM and LDS do not bind to the same binding site as C500. The analyses of the solvation correlation functions and the fluorescence anisotropies of the probe C500 at different temperatures are consistent with the binding of the probe at sub domain IIA (site I) [30]. The similarity in the nature of variation of the solvation correlation function and the fluorescence anisotropies of the two probes DCM and LDS at different temperatures suggest that the probes bind to the

same site in the protein. On the other hand, the difference in the variation of the solvation

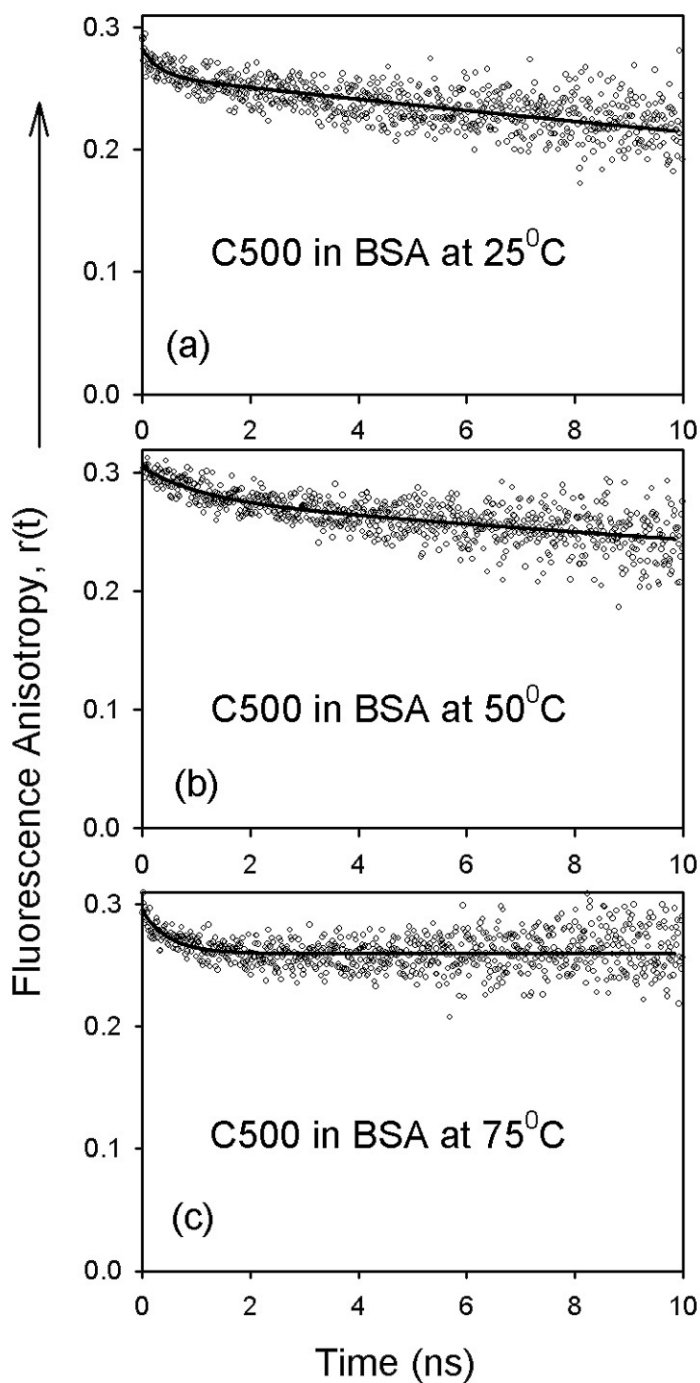


Figure 7.17. The temporal decays of fluorescence anisotropies $r(t)$ of the probe C500 in BSA at temperatures 25°C (a), 50°C (b) and 75°C (c).

correlation function and the fluorescence anisotropies of the two probes DCM and LDS at different temperatures with that of C500 suggest that these two probes does not bind to site I. This leaves the likely possibility that the probes bind to the second site II (sub domain IIIA) in the protein.

The picosecond resolved solvation studies on BSA with LDS and DCM at various temperatures show the similarity of the binding nature of LDS and DCM, indicating a possibility of binding of the ligands to similar sites in the protein. DCM is extremely hydrophobic and completely insoluble in water. In the protein it therefore occupies the binding site for hydrophobic residues and therefore, a possible location of the probe is in the binding site in domain IIIA [36]. On the other hand, LDS is a cationic dye with a large hydrophobic moiety. Early studies [1,37] of the binding of cationic surfactants having a hydrophobic alkyl chain explored the possible locations of the surfactants to be Sudlow I and Sudlow II regions [1], which are close to sub-domains IIA and IIIA, respectively. The binding affinity of LDS to Sudlow II regions (sub-domain IIIA) might direct the ligand to sub-domain IIIA, which is also the possible binding site of DCM [36]. Addition of excess LDS to the solution of DCM-BSA complex shows a significant red shift of 10 nm (data not shown) in the emission of DCM, reflecting the expulsion of DCM from BSA as a consequence of competitive binding with LDS. The observation indicates specific recognition of the ligand at a particular site (possibly the Sudlow region II or equivalently site II in sub-domain IIIA) of BSA, when one ligand occupies the site the other ligand cannot recognize the protein. In order to explore the further possibility of binding of the two ligands simultaneously in the protein, we have used FRET techniques. The significant spectral overlap of DCM emission with the absorption of LDS is expected to reveal inter-ligand distance, when they are in close proximity. To check the possibility of FRET between DCM and LDS, we study the FRET in CTAB micelles where both the ligands bind at the micellar surface. Figure 7.18(a) shows the normalized DCM (donor) emission and LDS (acceptor) absorption in CTAB micelles at room temperature. The figure 7.18(b) shows the emission of the donor and that of the donor acceptor complex. The figure 7.18(b) shows that the emission from the donor gets quenched due to absorption by the acceptor. This quenching of the donor emission is further evident from the faster lifetime associated with the donor-acceptor (DCM-LDS) complex compared to

that in donor (DCM) only in CTAB micelles (figure 7.18(c)). The Forster distance, R_0 for the donor and the donor-acceptor complex is calculated to be 2.8 nm. The distance between the probes is 2.4 nm. This distance corresponds to the length of the chord separating the DCM and the LDS molecules, both of which are located at the surface of the micelle having hydrodynamic diameter of 12 nm [38].

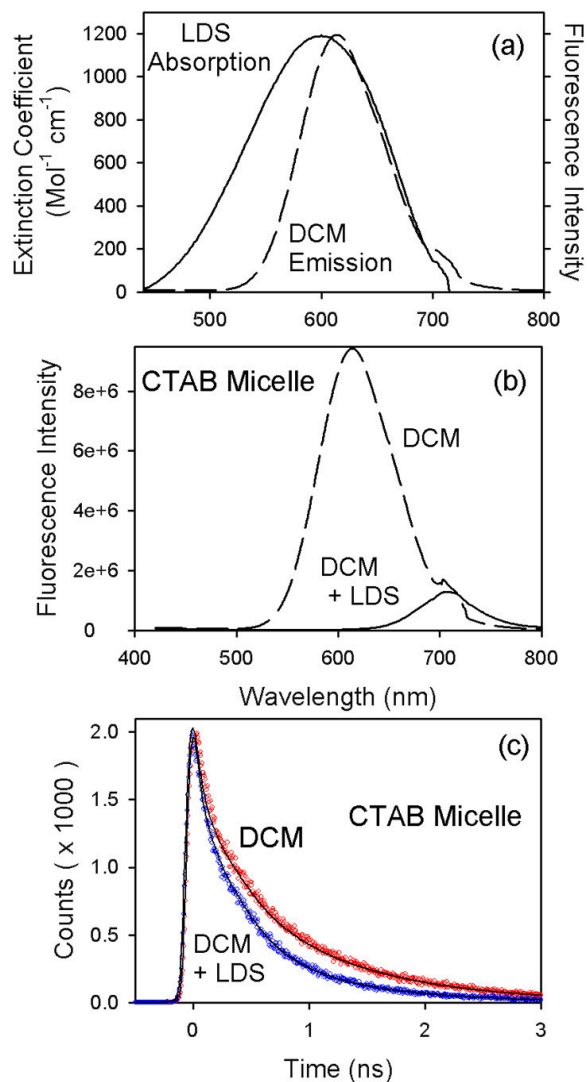


Figure 7.18. (a) The absorption spectrum of LDS and the emission spectrum of DCM in CTAB micelles. The emission spectra (b) and fluorescence transients (c) of DCM and DCM-LDS in CTAB micelles.

The R_0 value for the probes DCM and LDS in the protein solution at room temperature has been calculated to be 3.26 nm. The inter-domain distance in the protein has been estimated to be 3.18 nm (domain I and II), 2.58 nm (domain II and III) and 2.50 nm (domain I and III) [39]. Thus it is obvious that FRET is expected to reveal the inter-ligand distance if they are simultaneously bound to BSA. However, DCM in BSA solution in the presence of LDS at room temperature (25⁰C) does not show quenching of donor fluorescence in either steady-state or temporal decay of the donor molecules in the donor-acceptor complexes. The binding of DCM to the BSA solution containing both the probes (DCM and LDS) at room temperature has been borne out by the presence of a 50 ns component associated with the temporal decay of fluorescence anisotropy (figure 7.19(a)) indicating the global motion of the protein. The absence of longer components in the temporal decay of the fluorescence anisotropy of the probe LDS in the DCM-BSA complex, (figure 7.19(b)) show that the probe is not bound to the protein at room temperature. This clearly indicates that simultaneous binding and hence energy transfer does not take place between the probes in the protein at room temperature. This confirms that the probes DCM and LDS do not bind to the different domains in the protein. In other words the probes DCM and LDS compete for the same binding site in the protein. To study the effect of temperature on the specificity of binding, or in other words, to study the specificity of ligand binding in the different unfolded states associated with the temperature-induced denaturation of the protein, the energy transfer experiments are carried out at different temperatures. The binding of the DCM to the protein at different temperatures is borne out by the long component in the temporal decays of the fluorescence anisotropies at different temperatures. It is observed that the energy transfer between the donor (DCM) and acceptor (LDS) does not take place at intermediate temperatures of 50⁰C, 60⁰C or 70⁰C (data not shown), showing that the specificity of LDS binding is retained even when the structural integrity of the protein is substantially lost (as indicated in the DLS and CD profile). The observation indicates that even at 70⁰C, the protein is not completely unfolded, reflecting the existence of a

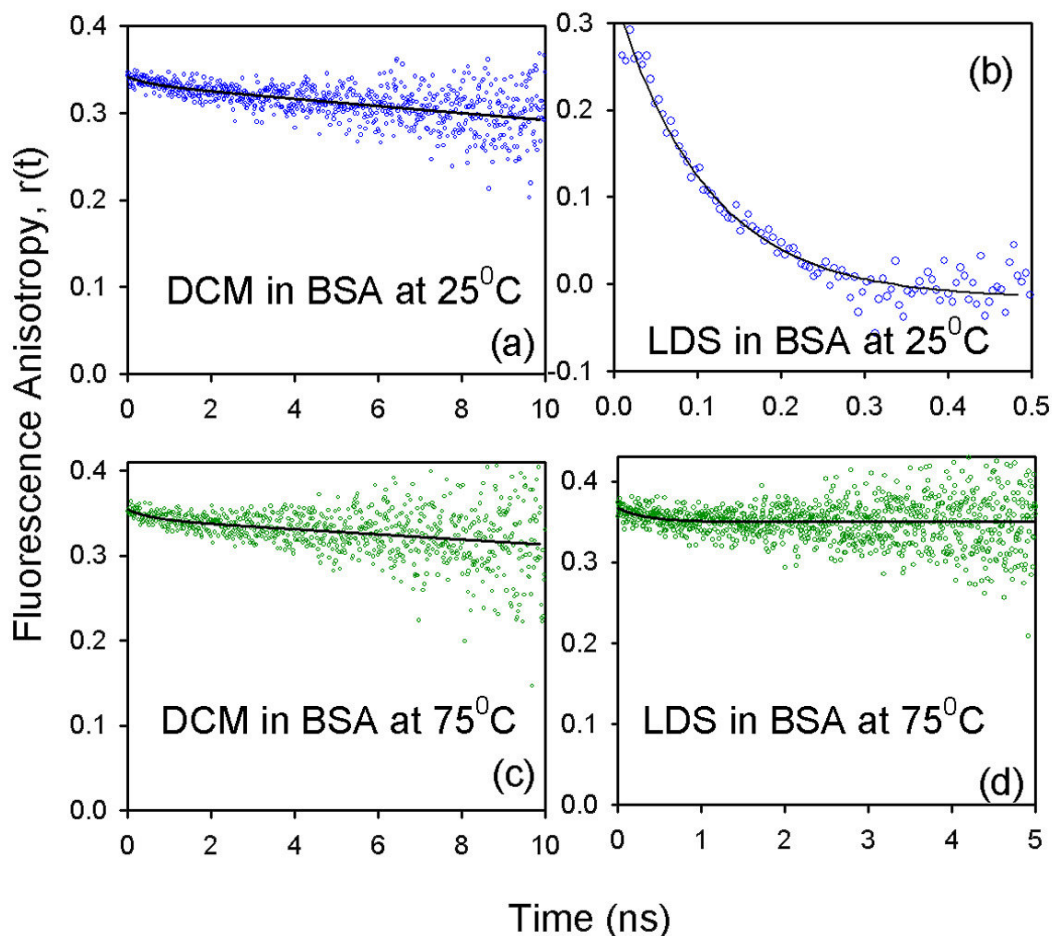


Figure 7.19. The temporal decay of fluorescence anisotropies, $r(t)$ of DCM and LDS in BSA solution containing both the probes at different temperatures.

transition temperature greater than 70°C . A transition temperature above 70°C is indicated from the deconvolution of the DLS, CD and DTA profiles to three-intermediate transitions. The energy transfer between the probes DCM and LDS finally takes place at 75°C .

The binding of both the ligands at the high temperature is indicated by a long component in the temporal decay of the fluorescence anisotropies (figures 7.19(c) and 7.19(d)). Figure 7.20(a) shows the normalized DCM (donor) emission and LDS (acceptor) absorption in BSA at 75°C . Figure 7.20(b) shows the quenching of the DCM (donor) emission in the DCM-protein and the DCM-LDS-protein complex at 75°C . The quenching of the donor fluorescence at 75°C is also reflected in the decrease in the

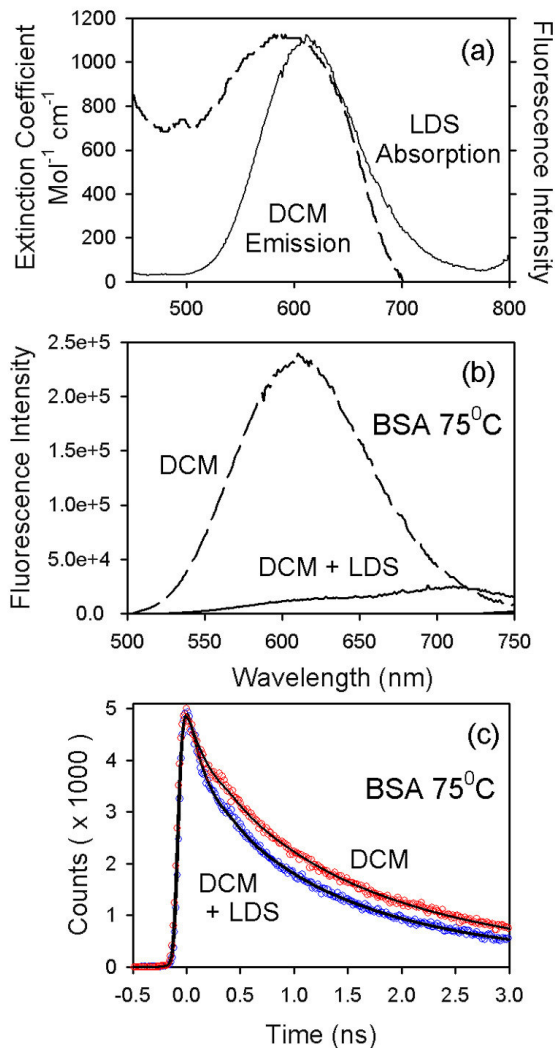


Figure 7.20. (a) The absorption spectrum of LDS and the emission spectrum of DCM in BSA at 75⁰C. The emission spectra (b) and fluorescence transients (c) of DCM and DCM-LDS in BSA at 75⁰C.

lifetime of the donor in the DCM-LDS -protein complex as shown in figure 7.20(c). The average lifetime of the donor in the protein at 75⁰C is 1.28 ns whereas that of the donor in the presence of acceptor is 0.882 ns. The R_0 distance associated with the energy transfer at this elevated temperature is 2.98 nm and the distance between the probes is 2.8 nm. The possibility of binding of LDS to a protein aggregate (hydrodynamic diameter=25 nm) at 75⁰C can be ruled out by the following control experiment. It is observed from DLS measurements that the hydrodynamic diameter of 25 nm does not return to that of the native protein (10 nm) upon cooling to room temperature. The observation is

consistent with the results obtained from another study on the thermal unfolding of the protein HSA [30]. The swelled protein (hydrodynamic diameter=25 nm), at room temperature is found to be unable to bind LDS. If the swelled protein is a protein aggregate, then it should be able to bind LDS. The lack of intramolecular energy transfer between DCM molecules in the swelled protein at room temperatures also stands against the aggregation at elevated temperature. The results clearly indicate that LDS binds to a non-specific site in the presence of DCM in the unfolded BSA at 75⁰C. This shows that the molecules DCM and LDS are simultaneously binding to BSA and that the binding has lost its specific nature. In other words the binding of ligands to BSA loses its specificity only when the protein is denatured.

7.3. Conclusion:

In the aforesaid studies, the effect of structural modifications in different molecular recognitions of two structurally related proteolytic enzymes trypsin and CHT by DAPI has been addressed. Steady-state, picosecond resolved fluorescence and polarization gated anisotropy have been used to characterize the binding of DAPI to CHT. The retention of enzymatic activity of CHT in the DAPI-CHT complex as well the simultaneous binding of the potent inhibitor PF and DAPI to CHT rules out the possibility of DAPI binding at the active site. Competitive binding studies with TNS in CHT show that TNS is expelled out from the enzyme with the progressive addition of DAPI indicating that DAPI binds at the TNS binding site. FRET studies between DAPI and PF indicates that DAPI is bound at the TNS binding site of the CHT in such geometry that the transition dipoles of PF and DAPI are nearly perpendicular to each other (scheme 7.1). The photophysics of the probe LDS and its efficacy to report unambiguously report environmental dynamics in both biomimetics and real biological systems like proteins have also been explored. Also, the specificity of molecular recognition of a transporter protein BSA in its various partially folded states has been addressed. We have prepared the partially folded states by using thermal denaturation to avoid the complications due to chemical denaturation. The thermal denaturation of BSA in phosphate buffer at pH=7 shows that three intermediate unfolded states are associated with the thermal unfolding. A comparison of the changes in the secondary (CD) and

globular tertiary (DLS) structure of the protein with the DTA studies suggests that the structural transitions take place around 50⁰C, 64⁰C and 75⁰C respectively. It is observed that the recognition by DCM and LDS is very specific at their particular binding site in BSA. Competitive binding studies on DCM and LDS to BSA and FRET reveal very specific nature of recognition of the protein; when one ligand is bound to BSA, the other can not get entry to the protein over a wide range of temperature. However, at higher temperatures the two ligands can be bound simultaneously, reflecting non-specific nature of recognition of BSA. Our studies show that the binding of ligands to BSA is specific, and the specificity is destroyed in the unfolded state of the protein.

References

- (1) T.J. Peters, All about albumin: Biochemistry, genetics and medical applications, *Academic Press*, San Diego, CA, 1996.
- (2) J. Ghuman, P.A. Zunszai, I. Petitpas, A.A. Bhattacharya, M. Otagiri, S. Curry, Structural basis of the drug-binding specificity of human serum albumin, *J. Mol. Biol.* 353 (2005) 38.
- (3) L. Hedstrom, J.J. Perona, W.J. Rutter, Converting trypsin to chymotrypsin: Residue 172 is a substrate specificity determinant, *Biochemistry* 33 (1994) 8757.
- (4) L. Graf, A. Jancso, L. Szilagyi, G. Hegyi, K. Pinter, G. Naray-Szabo, J. Hepp, K. Medzihradszky, W.J. Rutter, Electrostatic complementarity within the substrate-binding pocket of trypsin, *Proc. Natl. Acad. Sci. USA* 85 (1988) 4961.
- (5) D. Banerjee, S.K. Srivastava, S.K. Pal, Spectroscopic studies on ligand-enzyme interactions: Complexation of α -chymotrypsin with 4',6-Diamidino-2-phenylindole (DAPI), *J. Phys. Chem. B* 112 (2008) 1828.
- (6) M.L. Barcellona, E. Gratton, A molecular approach to 4',6-Diamidino-2-phenylindole (DAPI) photophysical behaviour at different pH values, *Biophys. Chem.* 40 (1991) 223.
- (7) M.L. Barcellona, G. Cardiel, E. Gratton, Time-resolved fluorescence of DAPI in solution and bound to polydeoxynucleotides, *Biochem. Biophys. Res. Comm.* 170 (1990) 270.
- (8) A. Mazzini, P. Cavatorta, M. Iori, R. Favilla, G. Sartor, The binding of 4',6-Diamidino-2-phenylindole to bovine serum albumin, *Biophys. Chem.* 42 (1992) 101.
- (9) R.D. Ludescher, L. Peting, S. Hudson, B. Hudson, Time-resolved fluorescence anisotropy for systems with lifetime and dynamic heterogeneity, *Biophys. Chem.* 28 (1987) 59.
- (10) T.K. Das, S. Mazumdar, Effect of Adriamycin on the boundary lipid structure of cytochrome c oxidase: pico-second time-resolved fluorescence depolarization studies, *Biophys. Chem.* 86 (2000) 15.

- (11) S.A. Bernhard, B.L. Lee, Z.H. Tashjian, On the interaction of α -chymotrypsin with chromophores: Proflavin binding and enzyme conformation during catalysis, *J. Mol. Biol.* 18 (1966) 405.
- (12) N.C. Maiti, M.M.G. Krishna, P.J. Britto, N. Periasamy, Fluorescence dynamics of dye probes in micelles, *J. Phys. Chem. B* 101 (1997) 11051.
- (13) D.L. Dexter, A theory of sensitized luminescence in solids, *J. Chem. Phys.* 21 (1953) 836.
- (14) J.D. Dow, Resonance energy transfer in condensed media from many particle viewpoint, *Phys. Rev.* 174 (1968) 963.
- (15) E. Casale, C. Collyer, P. Ascenzi, G. Balliano, P. Milla, F. Viola, M. Fasano, E. Menegatti, M. Bolognesi, Inhibition of bovine β -trypsin, human α -thrombin and porcine pancreatic β -kallikrein-B by 4',6-diamidino-2-phenylindole, 6-amidinoindole and benzamidine: A comparative thermodynamic and X-ray structural study, *Biophys. Chem.* 54 (1995) 75.
- (16) R.N. Smith, C. Hansch, Hydrophobic interaction of small molecules with α -chymotrypsin, *Biochemistry* 12 (1973) 4924.
- (17) W.O. McClure, G.M. Edelman, Fluorescent probes for conformational states of proteins. II. The binding of 2-p- toluidinonaphthalene-6-sulphonate to α -chymotrypsin, *Biochemistry* 6 (1967) 559.
- (18) J.D. Johnson, M.A. El-Bayoumi, L.D. Weber, A. Tulinsky, Interaction of α -chymotrypsin with the fluorescent probe 1-anilinonaphthalene-8-sulfonate in solution, *Biochemistry* 18 (1979) 1292.
- (19) P.B. Sigler, D.M. Blow, B.W. Matthews, R. Henderson, Structure of crystalline α -chymotrypsin. II. A preliminary report including a hypothesis for the activation mechanism, *J. Mol. Biol.* 35 (1968) 143.
- (20) D. Banerjee, S.K. Pal, Solvation dynamics of LDS 750 in micelles, reverse micelles and proteins, *Chem. Phys. Lett.* 451 (2008) 237.
- (21) J.T. Vivian, P.R. Callis, Mechanisms of tryptophan fluorescence shifts in proteins, *Biophys. J.* 80 (2001) 2093.

- (22) E.W. Castner, M. Maroncelli, G.R. Fleming, Subpicosecond resolution studies of solvation dynamics in polar aprotic and alcohol solvents, *J. Chem. Phys.* 86 (1987) 1090.
- (23) A.S.R. Koti, M.M.G. Krishna, N. Periasamy, Time-resolved area-normalized emission spectroscopy (TRANES): A novel method for confirming emission from two excited states, *J. Phys. Chem. A* 105 (2001) 1767.
- (24) S. Pal, S. Balasubramanian, B. Bagchi, Identity, energy, and environment of interfacial water molecules in a micellar solution, *J. Phys. Chem. B* 107 (2003) 5194.
- (25) H.G. Mahesha, S.A. Singh, N. Srinivasan, A.G.A. Rao, A spectroscopic study of the interaction of isoflavones with human serum albumin, *FEBS J.* 273 (2006) 451.
- (26) E.E. Sideris, M.A. Koupparis, P.E. Macheras, Effect of cyclodextrins on protein binding of drugs: the diflunisal/hydroxypropyl β -cyclodextrin model case, *Pharma. Res.* 11 (1994) 90.
- (27) A.K. Shaw, R. Sarkar, D. Banerjee, S. Hintschich, A. Monkman, S.K. Pal, Direct observation of protein residue solvation dynamics, *J. Photochem. Photobiol. A: Chem.* 185 (2007) 76.
- (28) D. Banerjee, S.K. Pal, Molecular recognition in partially folded states of a transporter protein: Temperature-dependent specificity of bovine serum albumin, *Photochem. Photobiol.* 84 (2008) 750.
- (29) C. Giancola, C. de Sena, D. Fessas, G. Graziano, G. Barone, DSC studies on bovine serum albumin denaturation: Effects of ionic strength and SDS concentration, *Int. J. Biol. Macromol.* 20 (1997) 193.
- (30) K. Flora, J.D. Brennan, G.A. Baker, M.A. Doody, F.V. Bright, Unfolding of acrylodan- labeled human serum albumin probed by steady state and time resolved fluorescence methods, *Biophys. J.* 75 (1998) 1084.
- (31) J.K.A. Kamal, L. Zhao, A.H. Zewail, Ultrafast hydration dynamics in protein unfolding: Human serum albumin, *Proc. Natl. Acad. Sci. USA* 101 (2004) 13411.
- (32) A. Cooper, Thermodynamics of protein folding and stability, *Protein: A Comprehensive Treatise* 2 (1999) 217.

- (33) J.F. Brandts, The thermodynamics of protein denaturation. I. The denaturation of chymotrypsinogen, *J. Am. Chem. Soc.* 86 (1964) 4291.
- (34) K. Takeda, K. Yamamoto, Fluorescence lifetime and rotational correlation time of bovine serum albumin-sodium dodecyl sulphate complex labeled with 1-Dimethylaminonaphthalene-5- sulphonyl chloride: Effect of disulphide bridges in the protein on the fluorescence parameters, *J. Prot. Chem.* 9 (1989) 17.
- (35) W. Qiu, L. Zhang, Y.Y. Okobiah, L. Wang, D. Zhong, A.H. Zewail, Ultrafast solvation dynamics of human serum albumin : Correlations with conformational transitions and site selected recognition, *J. Phys Chem. B* 110 (2006) 10540.
- (36) X.M. He, D.C. Carter, Atomic structure and chemistry of human serum albumin, *Nature* 358 (1992) 209.
- (37) V. Peyre, V. Lair, V. Andre, G. le Maire, U. Kragh-Hansen, M. le Maire, J.V. Moller, Detergent binding as a sensor of hydrophobicity and polar interactions in the binding cavities of proteins, *Langmuir* 21 (2005) 8865.
- (38) S.S. Berr, E. Caponetti, J.S. Johnson, J.R.R.M. Jones, L.J. Magid, Small-angle neutron scattering from hexadecyltrimethylammonium bromide micelles in aqueous solutions, *J. Phys. Chem.* 90 (1986) 5766.
- (39) N. Hagag, E.R. Birnbaum, D.W. Darnall, Resonance energy transfer between cysteine-34, tryptophan-214 and tyrosine 411 of human serum albumin, *Biochemistry* 22 (1983) 2420.

Chapter 8

Specific Interaction of a Small Ligand with an Enzyme: Relevance of Environmental Dynamics at the Active Site to Enzymatic Activity

8.1. Introduction:

The catalysis of substrates by enzymes are one of the most specific reactions in biology. It has been recently established that the protein conformational dynamics play an important role in enzyme catalysis. In a pioneering work, Kern et al. [1] have proposed that the intrinsic protein dynamics is associated with its catalytic efficiency. In the study, they have used NMR relaxation dispersion measurements to compare the motions of prolyl cis-trans isomerase cyclophilin-A in the native state with those during turnover. The results show that the dynamics of the protein which are crucial for the catalytic activity are also present in the native protein, and are hence the intrinsic dynamics of the protein. In another study [2] Loria et al. have shown that the conformational mobility of a histidine residue, distant from the active site of the enzyme α -lytic protease is essential in coordinating the motions involved in the rate-limiting enzymatic step. The role of collective motions in enzyme activity is also proposed in the study by Karplus et al. [3]. These have been followed by a recent theoretical study [4] on the effect of protein conformational dynamics on the enzyme catalyzed reactions, where two dimensional reaction free energy surfaces of the catalytic reaction have been constructed, using the protein conformational coordinate as an axis. In this chapter, we attempt to use fluorescence spectroscopic studies to explore the internal dynamics at the active site of a proteolytic enzyme α -chymotrypsin.

8.2. Results and Discussion:

8.2.1. Conformational Dynamics at the Active Site of α -Chymotrypsin and Enzymatic Activity [5].

The enzyme α -chymotrypsin (CHT) catalyses the hydrolysis of peptide bonds in the mammalian digestive systems. In the present study, we have studied the temperature dependent hydrolysis of the substrate peptide Ala-Ala-Phe-7-amido-4-methylcoumarin (AMC) by CHT. Figure 8.1 shows the k_{cat}/K_M value for the hydrolysis of AMC. k_{cat}/K_M is a measure of the catalytic efficiency of an enzyme. It is evident from figure 8.1 that the catalytic efficiency of the enzyme shows a maximum at 37°C coinciding with the normal body temperature of homeothermal animals. The rise and subsequent fall of the activity of CHT associated with the hydrolysis of N-acetyl-L-Tyrosine ethyl ester is reported [6]. In the study, the catalytic activity of the enzyme exponentially falls off after 40°C and is thought to be associated with the thermal denaturation of the protein. The catalytic

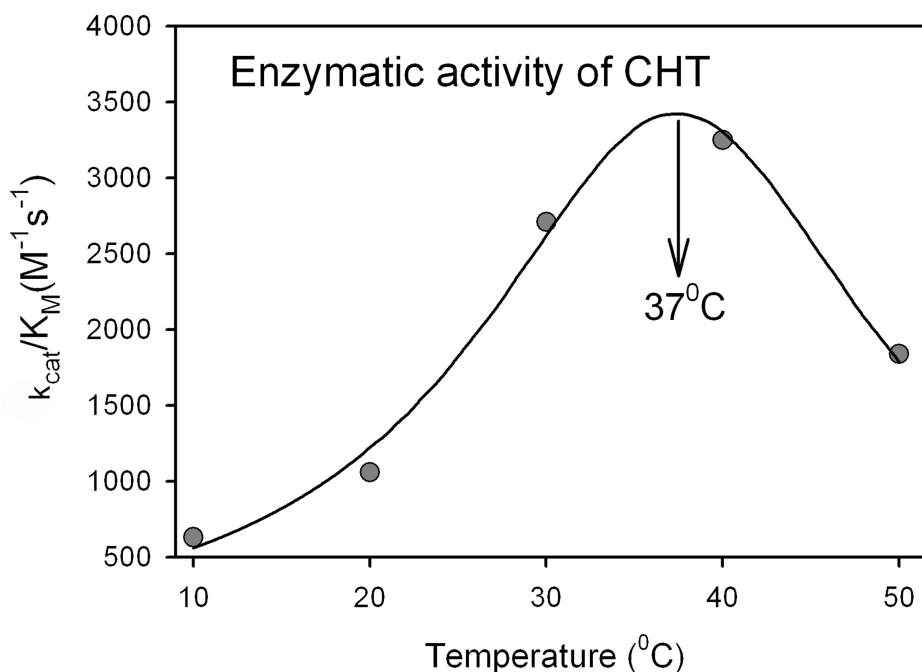


Figure 8.1. The variation of the catalytic efficiency of CHT with temperature. The solid line is a Gaussian fit.

parameters associated with the hydrolysis of AMC by CHT are tabulated in Table 8.1. It is seen that both the k_{cat} and K_{M} values associated with the enzyme catalysis increases upto 40⁰C and then falls. In enzyme catalysis, k_{cat} gives an idea of the turnover rate and K_{M} gives an indication of the formation of the enzyme-substrate complex. The inverse of the K_{M} is associated with the possibility of dissociation of the enzyme-substrate complex. The fall in the turnover rate and the increase in association possibility of the enzyme-substrate complex at 50⁰C suggest that at the higher temperatures, even when enzyme-substrate complex is formed favorably, product formation is hindered. The result might indicate conformational perturbation of the enzyme-substrate complex at higher temperatures.

Since proteins change their structure with temperature, the possible association of structural perturbations to the catalytic activity cannot be ruled out. In addition, proteolytic enzymes undergo autocatalysis in solution [7], the rate of which increases at higher temperatures. The fall in catalytic activity above 37⁰C can therefore be due to the decrease in the effective enzyme concentration as a result of autocatalysis. In order to explore the globular tertiary structures of the protein at different temperatures, and also the possibility of autocatalysis, we use dynamic light scattering (DLS) technique. DLS gives the hydrodynamic diameter of suspended particles in solution. The DLS studies are carried out with different initial concentrations of the protein ranging from 1 μM to 200 μM . The DLS experiments (figure 8.2(a)) reveal the hydrodynamic diameter of CHT to be ~6 nm, which agrees well with the dimensions of the hydrated protein [8]. The DLS measurements done with a high concentration of protein (>150 μM) shows a prominent peak at ~1 nm above 50⁰C. The size of 1 nm agrees well with the dimensions of an autocatalytic fragment of the CHT [7]. However, such fragments do not appear for lower concentration (<50 μM) of the protein (the concentrations which are used for the measurement of enzymatic activity), at any temperature. This indicates that the fall in enzymatic activity of the protein at high temperatures is neither due to the loss in effective enzyme concentration (due to autocatalysis) nor due to massive unfolding of the enzyme (characteristic of thermal denaturation).

Table 8.1: The Kinetics and Energetics of CHT Catalyzed Hydrolysis of AMC.

Temp	k_{cat}	K_M	k_{cat}/K_M	ΔG	ΔH	ΔS
($^{\circ}C$)	(s^{-1})	(mM)	($M^{-1}s^{-1}$)	(kJ/mol)	(kJ/mol)	(kJ/molK)
10	0.66	1.05	631	-5.54	54.68	0.21
20	04.1	3.91	1050	-6.94	45.18	0.18
30	12.8	4.73	2720	-9.46	35.36	0.15
40	21.7	6.79	3250	-10.17	25.21	0.11
50	08.1	4.37	1840	-	-	-

Figure 8.2(a) and Table 8.1 show the hydrodynamic diameter of CHT ($[CHT]=2 \mu M$) at different temperatures. It becomes evident from the inset of figure 8.2(a) that the average hydrodynamic diameter of the protein decreases from ~ 6 nm at $10^{\circ}C$ to ~ 5 nm at $50^{\circ}C$. The decrease in hydrodynamic diameter in proteins at the high temperature can be associated with the thinning of hydration shell corresponding to the loss of hydration waters at higher temperatures [9]. The change in number of hydration waters surrounding a protein is also reflected in the change in the partial apparent adiabatic compressibility (ϕ_k) of the protein solution at different temperatures. Figure 8.2(b) shows the ϕ_k at different temperatures. An increase in ϕ_k values at higher temperatures suggests progressive loss in the hydration waters with increasing temperature [9], resulting in the thinning of the hydration layer and concomitant decrease of the hydrodynamic diameter. However, the absence of scattering peaks at higher hydrodynamic diameters (inset of figure 8.2(b), representative of the denatured protein [8]) stands against a massive uncoiling of the protein at higher temperature. The DLS results thus confirm that there is no substantial change in the tertiary structure of the CHT which might be correlated with the temperature dependent change in the catalytic activity. In order to explore the secondary structure of CHT at different temperatures, the circular dichroism (CD) of the protein is monitored. The CD signal gives an idea about the overall secondary structure of the protein. The deconvolution of the CD signal at $20^{\circ}C$ reveals 10% helix, 32% β sheet and 33% random coils present in the protein (Table 8.2), which is consistent with earlier reports [10]. Figure 8.2(c) shows the optical rotation of the protein at different temperatures. The essential similarity (Table 8.2) of the CD spectrum of the protein at

different temperatures rules out the possibility of the contributions of major structural perturbations to its catalytic activity.

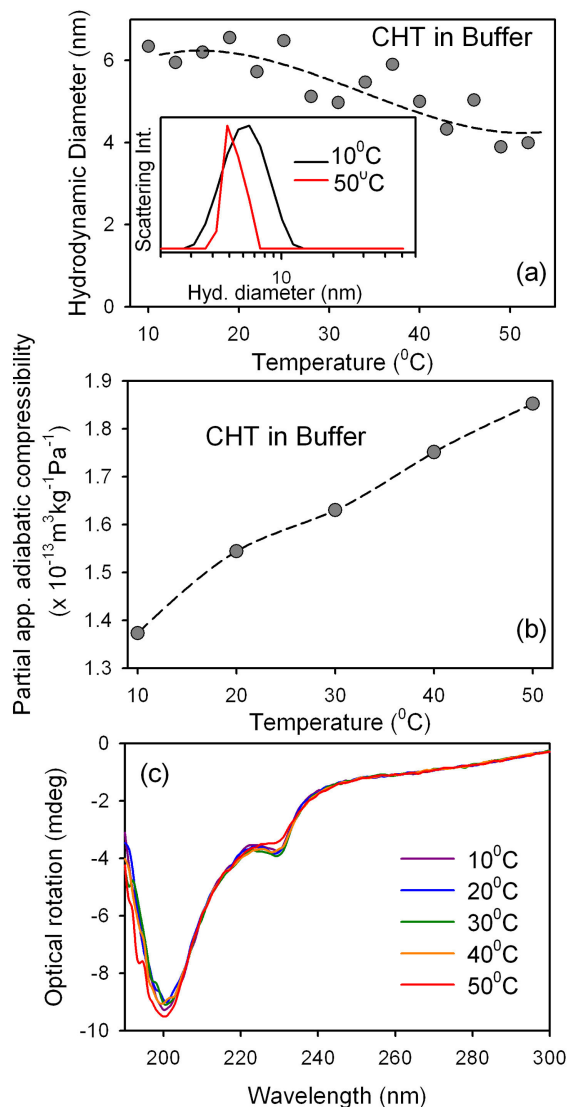


Figure 8.2. The hydrodynamic diameter and the partial apparent adiabatic compressibility of CHT at different temperatures are shown in (a) and (b) respectively. The broken lines are guides for the eye. The DLS profiles of CHT at two different temperatures (inset of (a)). (c) The CD spectra of CHT at different temperatures.

It is to be noted that a hydration layer, comprised of rigidly bound water molecules, surrounding the protein restricts its conformational flexibility [11]. The increase in the ϕ_k values at high temperatures (figure 8.2(b) and Table 8.2) suggests loss

of rigidly bound water molecules associated with the hydration layer. The loss of the rigidly bound hydration shell at higher temperatures is, therefore, associated with increased conformational flexibility of the overall protein. The conformational flexibility of the protein is likely to reflect itself in the dynamics of protein residues and substrates attached to the protein [12]. Since serine195, histidine57 and aspartate102 are associated with the catalytic activity of the enzyme, it seems logical that motions of these residues are involved in the enzymatic activity. It is to be noted that NMR of isotopically labeled proteins gives information about the local dynamics, is often not feasible due to the molecular size of the enzymes. The dynamics of covalently labeled fluorophores, estimated from fluorescence techniques, provides perhaps the best alternative for the

Table 8.2: Temperature Dependent Structure of CHT and anthraniloyl CHT (ANT-CHT)

Temp (⁰ C)	d_H^*		$\phi_k\#$ (M^3 $kg^{-1}Pa^{-1}$ ($\times 10^{-13}$)	Secondary Structure					
	CHT (nm)	ANT-CHT (nm)		CHT			ANT-CHT		
				α - helix %	β - sheet %	Ran dom %	α - helix %	β - sheet %	Ran dom %
10	6.34	5.98	1.37	10	32	33	11	33	28
20	6.55	6.01	1.54	10	32	33	11	32	28
30	4.97	5.02	1.63	10	32	33	11	32	28
40	5.00	5.20	1.75	10	32	33	11	32	28
50	3.89	4.02	1.85	08	33	33	10	33	29

* d_H =hydrodynamic radius, # ϕ_k = partial apparent adiabatic compressibility,

study of local dynamics in proteins. Here we have monitored the dynamics of the fluorescent anthraniloyl group covalently attached to the serine195 residue to study the dynamics of the serine residue using fluorescence anisotropy technique. The dynamics of the substrate is mimicked by proflavin (PF) in the active site of the protein. Figures 8.3(a) and (b) reflect the change in the fast and slow components of the rotational relaxation of PF at the protein active site. The slow component in the rotational dynamics of PF represents the microviscosity limited rotation of the probe in the protein cavity. This restricted rotation of PF has been used to calculate the microviscosity of the protein cavity according to the Stokes Einstein Debye equation [13]. The microviscosity at the active site of the protein is thus estimated to be 5 cp at 10⁰C. The corresponding viscosity

of buffer at the same temperature is 1.3 cp. At higher temperatures, the microviscosity decreases, manifesting in the faster rotation of PF. At 50⁰C, the microviscosity of the active site becomes buffer like and the PF tumbles off in a single rotational mode. It is to be noted that PF is not detached from the enzyme at this temperature. This is evidenced from the fluorescence lifetime of the probe in the protein at 50⁰C (~4 ns), which is much slower compared to that of the probe in buffer (<60 ps). The shorter (130 ps-30 ps) (Table 8.3) time component in the decay of fluorescence anisotropy of PF reflects the sub-slip rotational motion of the probe [13,14], which decreases monotonically with temperature.

The time constants associated with the decay of fluorescence anisotropy of anthraniloyl group are tabulated in Table 8.3. The anthraniloyl group is covalently attached to the serine195 residue and hence follows its motion. The slowest component at all temperatures (Table 8.3) reflects the global tumbling motion of the protein which varies with the viscosity of the solvent buffer according to the Stokes Einstein Debye equation as indicated by the solid black line in the figure 8.3(d). This long component is therefore not associated with enzyme activity. The fastest component of ~30 ps (Table 8.3) is similar in time scale with the normal modes of protein residues [15]. Recently, the role of picosecond dynamics in activity of a heme protein has been brought forward [16]. Normal mode analysis and molecular dynamics simulations of protein residues [15] have reported the existence of such low frequency normal modes with similar time constants in a chymotrypsin like serine protease. This mode remains constant in the temperature range 10⁰C to 40⁰C. However, at 50⁰C, this motion of the serine residue becomes slower (Table 8.3), indicating lower frequency of vibrations. The loss in catalytic activity at this temperature, coinciding with the slowing down of this component suggests that the fast dynamics of the serine residue is associated with enzymatic activity. In addition to this global motion of the protein and the normal mode dynamics, an additional motion having time constant of 12 ns (Table 8.3) is associated with the protein residue at lower temperature. The existence of this nanosecond component in the decay of rotational anisotropy of anthraniloyl CHT has already been reported [17]. The motion becomes faster (9 ns) (Table 8.3) at high temperatures, and vanishes after 30⁰C, where the protein activity is near maximum. This nanosecond component in the protein dynamics

represents an extremely low frequency mode of the protein, which perhaps lies outside

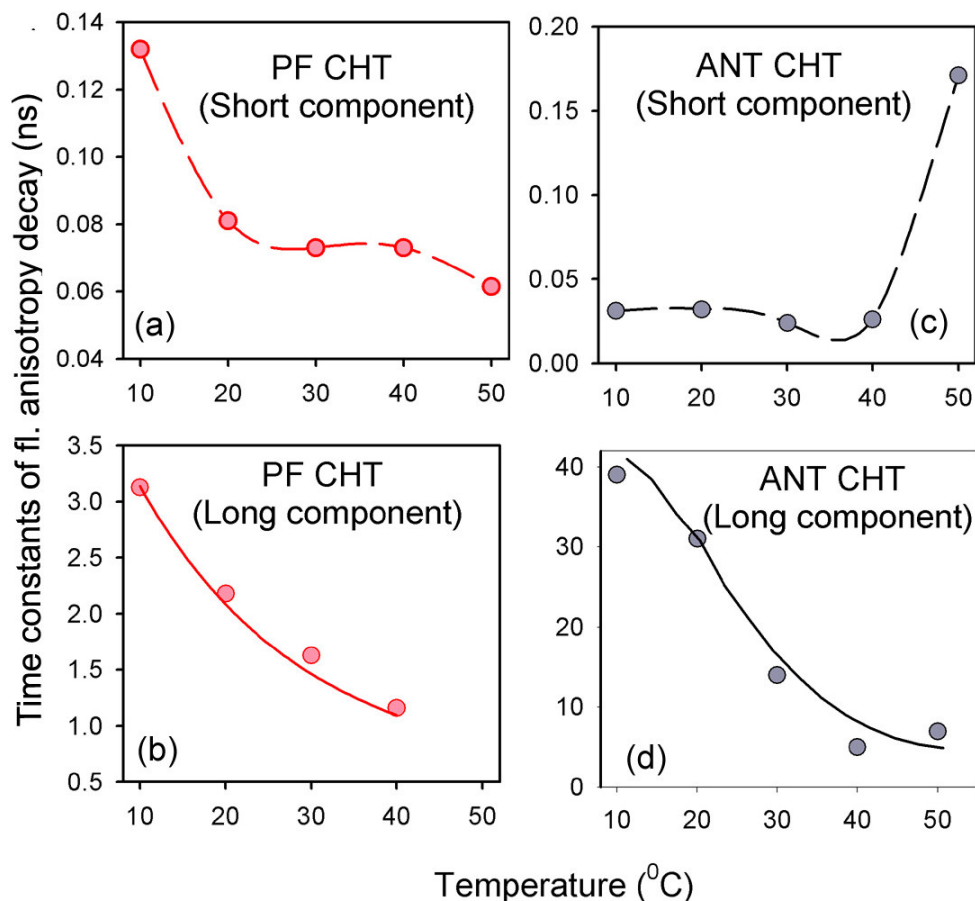


Figure 8.3. The rotational correlation times of fluorescence anisotropy of PF in CHT ((a) and (b)) and anthraniloyl-CHT (ANT-CHT) ((c) and (d)). The solid lines are the fits of the Stokes Einstein Debye equation; the broken lines are guides for the eye.

the purview of simulation and NMR studies. It is well known that the enzymatic activity is associated with the achievement of a critical active site conformation, which is effected through the conformational dynamics of the protein residues. It is also known that the active site conformation conducive to catalysis is pre-achieved by proteins at higher temperature. The nanosecond dynamics of the serine residue therefore, fits as a part of the critical conformational dynamics that effects the change of the conformation of the active site residues to the one most suited for the catalytic efficiency. The absence of this

component at higher temperatures suggests that the active site conformation, suitable for catalysis is pre-achieved by the protein at that temperature.

Table 8.3: The Fluorescence Anisotropies of CHT Bound Probes at Different Temperatures

Temp (^o C)	Rotation Correlation Time of anthraniloyl group			Rotational Correlation Time of PF	
	τ_1 (ns)	τ_2 (ns)	τ_3 (ns)	τ_1 (ns)	τ_2 (ns)
10	39	0.034	12	3.1	0.13
20	31	0.032	9	2.2	0.08
30	17	0.024	-	1.6	0.07
40	5	0.028	-	1.1	0.07
50	7	0.171	-	-	0.06

It is important at this stage to consider the structural consequences of the modification of CHT to its anthraniloyl derivative. In this regard we have monitored the secondary and overall globular tertiary structure of anthraniloyl CHT by CD and DLS techniques respectively. The similarity in the hydrodynamic radius of CHT and its anthraniloyl derivative (Table 8.2) suggests that the tertiary structure of the protein remains essentially the same on fluorescent labeling. Figure 8.4(a) shows the CD spectra of anthraniloyl CHT at different temperatures. A comparison with the temperature dependent CD spectra and the percentage secondary structures of the native CHT (figure 8.2(c) and Table 8.2) reveal that the overall secondary structure essentially remains the same, only a minor diminution of the 230 nm peak is observed, consistent with the CD spectrum of other acetylated chymotrypsin derivatives [10,18]. X-ray crystallographic studies on CHT reveal that in the active site, there exists an ion-pair between protonated isoleucine16 and aspartate194, (adjacent to the serine 195). The formation of this ion-pair is crucial for the substrate binding and hence activity of the enzyme. In this condition, the histidine57 and the serine195 are close enough to make hydrogen bonds with each other [19], which is essential for the catalytic activity. Structural studies have

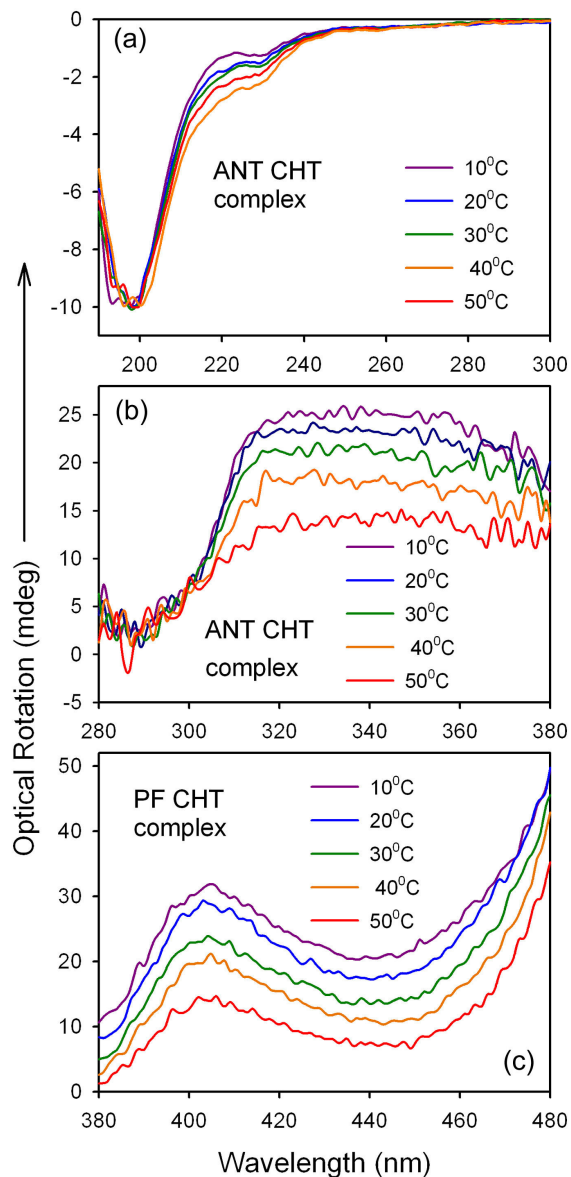


Figure 8.4. The CD (a) spectrum of ANT-CHT complex. The FDCD spectra of CHT using (b) anthraniloyl-CHT (ANT-CHT), and (c) proflavin (PF) as fluorescent probes.

also shown that the attachment of aromatic groups to the serine residue preserves the ion-pair in the active site [20]. Thus, it is expected that the attachment of anthraniloyl group to serine 195 preserves the active site conformation. Although the crystal structure of anthraniloyl CHT is not reported in literature, the comparison of the crystal structure of the tosyl derivative with that of the native enzyme [21] reveals that no significant differences in the active site conformation of CHT upon tosylation. Since the anthraniloyl

group remains attached to the active serine195 residue (the serine195 residue being directly involved in catalysis), direct measurement of the enzymatic activity of anthraniloyl CHT is not possible. However, considering the retention of the active conformation in anthraniloyl CHT [20], it is likely to assume that the rotational dynamics of the anthraniloyl group in the active site of CHT would closely resemble the protein residue dynamics of the native enzyme.

The consequences of the conformational dynamics to the active site structure at different temperatures are monitored through fluorescence detected CD (FDCD) studies. FDCD studies [22,23] have emerged as an efficient technique to probe the local structure of fluorescent probes in free state and when bound to macromolecules. The technique utilizes the different absorption of left and right circularly polarized light. Here, we have measured the FDCD of anthraniloyl CHT and PF. The fluorophores methyl anthranilate (mimic of the anthraniloyl group attached to CHT) and PF in buffer do not show circular dichroism. However, when bound in the active site of the protein, they adopt a fixed geometry as predicted by the geometry of the local environment. The bound molecules therefore show circular dichroism as shown in figures 8.4 (b)-(c). A chirality is thus, induced in the protein bound fluorophores. Figures 8.4(b) and 8.4(c) show the change in the optical rotation detected by the probes at different temperatures. The reduction in the optical rotation at higher temperatures clearly indicates a change in the active site conformation of the protein with increasing temperatures. The possibility that the loss in optical rotation is due to precipitation of the enzyme at high temperatures is ruled out from control absorption studies. The monotonic decreases in the FDCD signal with increasing temperatures suggest progressive decrease in induced chirality of the bound fluorophore. This loss in induced chirality of the fluorophore with increasing temperature suggests greater conformational flexibility of the protein at higher temperatures. The increased conformational flexibility at higher temperature assists the attainment of the critical active site conformation, reflected in the increase in the catalytic activity upto 40⁰C. The existence of active site conformations more suited for catalytic activity at high temperatures is reported [24]. The fall in the catalytic activity at 50⁰C, where there is least rigid binding of the substrate mimic/inhibitor due to the higher conformational flexibility of the protein, suggests the existence of a critical conformation for catalysis. In

this conformation, the normal mode dynamics of the serine residue becomes slower, as discussed earlier, altering the catalytic activity. Thus, the interplay between the two shorter dynamics associated with the motion of anthraniloyl serine 195 plays a crucial role in the determination of active site conformational changes and also controls the catalytic efficiency at different temperatures.

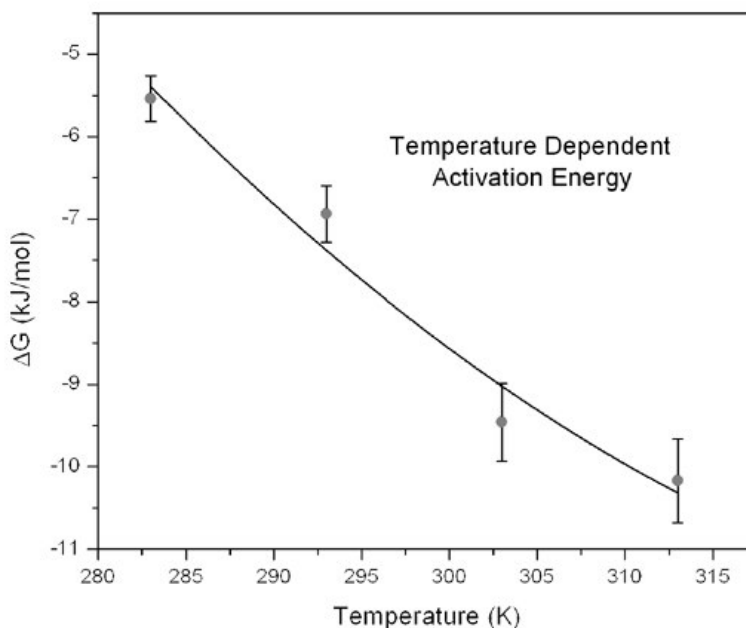


Figure 8.5. The plot of ΔG against temperature. The solid line is the second order polynomial fit.

It is interesting to observe the implication of the conformational dynamics of the protein to the energetics of catalysis. The overall free energy of activation for the enzymatic catalysis can be estimated from the catalytic efficiency (k_{cat}/K_M) according to the relation, $\Delta G = -RT \ln (k_{\text{cat}}/K_M \times h/k_B T)$ [25], where h and K_B are Planck and Boltzmann constants, respectively, and T is the absolute temperature. The decrease in the ΔG values with increase in temperature suggests that the enzymatic activity is thermodynamically more favourable at higher temperatures. A possible reason for the observed decrease in ΔG can be due the easier achievement of the transition state conformation through motions along the conformational coordinates at elevated temperatures, as discussed earlier. The enthalpy of the process is obtained from the nonlinear dependence of the ΔG

on T (figure 8.5) in terms of a two degree polynomial equation [26] where a, b, c are constants and T is the absolute temperature.

$$\Delta G = a + bT + cT^2 \quad (8-1)$$

$$\Delta H = \frac{d\left(\frac{\Delta G}{T}\right)}{d\left(\frac{1}{T}\right)} = a - cT^2 \quad (8-2)$$

Figure 8.5 shows the variation of ΔG with T. From the second order polynomial fit, we obtain the values of a, b and c and put them in equation 2 to calculate the values of ΔH at different temperatures (Table 8.1). As is observed from Table 8.1, there occurs a considerable decrease in the ΔH value as the temperature is raised. The increase in substrate affinity to reach the transition state is associated with a decrease in enthalpy, which might have its origin in the formation of new electrostatic and hydrogen bonding interactions, that can act synergistically [27]. The result is consistent with the fact that the affinity of an enzyme-substrate complex to proceed from the ground state to the transition state is largely enthalpic in origin [28]. It could be noted that when water molecules are involved as a substrate in the course of the reaction, the contribution of water to the energetics is significant [29]. In the present system also, the water present in the hydrophobic cavity of the enzyme might contribute to the observed decrease in ΔH . It is to be noted that the decrease in ΔH at different temperatures, is *not* associated with a corresponding increase in ΔS , which can be expected in cases where the ΔG itself changes with temperature. Examination of Table 8.1 reveals that the ΔS values remain more or less constant, suggesting that the entropic contribution is less significant in the present process. The observation clearly indicates the role of conformational dynamics at high temperatures to assist the protein catalysis by lowering the energy of the transition state.

8.3. Conclusion:

The dynamics of a specific protein residue in the active site of the proteolytic enzyme α -chymotrypsin (CHT) has been correlated with its temperature dependent catalytic efficiency. The catalytic efficiency k_{cat}/K_M of the enzyme at different temperatures show

a maxima at 37⁰C, coinciding with the normal body temperature of homeothermals. The overall secondary structure of the protein determined from circular dichroism and globular tertiary structure from dynamic light scattering however shows no significant change in the studied temperature range, ruling out the possibility of massive structural reorientation of the overall protein responsible for the altered catalytic activity. The temperature dependent rotational dynamics of the protein and probe at the active site of CHT projects out the crucial dynamics of active site serine195 residue responsible for catalysis. The minor structural perturbations at the active site due to conformational flexibility at high temperature are also evidenced from FDCE studies. The energetic parameters associated with the catalytic processes at different temperatures indicate that the conformational dynamics enhances the catalytic activity at higher temperatures by lowering the transition state energy.

References

- (1) E.Z. Eisenmesser, O. Millet, W. Labeikovsky, D.M. Korzhnev, M. Wolf-Watz, D.A. Bosco, J.J. Skalicky, L.E. Kay, D. Kern, Intrinsic dynamics of an enzyme underlies catalysis, *Nature* 438 (2005) 117.
- (2) E.D. Watt, H. Shimada, E.L. Kovrigin, J.P. Loria, The mechanism of rate-limiting motions in enzyme function, *Proc. Natl. Acad. Sci. USA* 104 (2007) 11981.
- (3) M. Karplus, J. Kuriyan, Molecular dynamics and protein function, *Proc. Natl. Acad. Sci. USA* 102 (2005) 6679.
- (4) W. Min, X.S. Xie, B. Bagchi, Two-dimensional reaction free energy surfaces of catalytic reaction: Effects of protein conformational dynamics on enzyme catalysis, *J. Phys. Chem. B* 112 (2008) 454.
- (5) D. Banerjee, S.K. Pal, Conformational dynamics at the active site of α -chymotrypsin and enzymatic activity, *Langmuir* 24 (2008) 8163.
- (6) P. Lozano, T. De Diego, J.L. Iborra, Dynamic structure/function relationships in the α -chymotrypsin deactivation process by heat and pH., *Eur. J. Biochem.* 248 (1997) 80.
- (7) N. Singh, T. Jabeen, S. Sharma, I. Roy, M.N. Gupta, S. Bilgrami, R.K. Somvanshi, S. Dey, M. Perbandt, C. Betzel, A. Srinivasan, T.P. Singh, Detection of native peptides as potent inhibitors of enzymes: Crystal structure of the complex formed between treated bovine α -chymotrypsin and an autocatalytically produced fragment, Ile-Val-Asn-Gly-Glu-Glu-Ala-Val-Pro-Gly-Ser-Trp-Pro-Trp, at 2.2 Å resolution, *FEBS J.* 272 (2005) 562–572.
- (8) A.K. Shaw, R. Sarkar, D. Banerjee, S. Hintschich, A. Monkman, S.K. Pal, Direct observation of protein residue solvation dynamics, *J. Photochem. Photobiol. A: Chem.* 185 (2007) 76.
- (9) R.K. Mitra, S.S. Sinha, S.K. Pal, Temperature-dependent hydration at micellar surface: Activation energy barrier crossing model revisited, *J. Phys. Chem. B* 111 (2007) 7577.
- (10) J. McConn, G.D. Fasman, G.P. Hess, Conformation of high pH form of chymotrypsin, *J. Mol. Biol.* 39 (1969) 551.

- (11) S.K. Pal, J. Peon, A.H. Zewail, Ultrafast surface hydration dynamics and expression of protein functionality: α -chymotrypsin, *Proc. Natl. Acad. Sci. USA* 99 (2002) 15297.
- (12) D. Banerjee, S.S. Sinha, S.K. Pal, Interplay between hydration and electrostatic attraction in ligand binding: Direct observation of hydration barrier at reverse micellar interface, *J. Phys. Chem. B* 111 (2007) 14239.
- (13) S.S. Narayanan, R. Sarkar, S.S. Sinha, F. Dias, A. Monkman, S.K. Pal, Luminescence depolarization dynamics of quantum dots: Is it hydrodynamic rotation or exciton migration?, *J. Phys. Chem. C* 112 (2008) 3423.
- (14) S.R. Inamdar, J.R. Mannekutla, B.G. Mulimani, M.I. Savadatti, Rotational dynamics of nonpolar laser dyes, *Chem. Phys. Lett.* 429 (2006) 141.
- (15) P. Dauber-Osguthorpe, D.J. Osguthorpe, P.S. Stern, J. Moul, Low frequency motions in proteins Comparison of normal mode and molecular dynamics of streptomyces griseus protease A, *J. Comput. Phys.* 151 (1999) 169.
- (16) M. Brunori, F. Cutruzzola, C. Savino, C. Travaglini-Allocatelli, B. Vallone, Q.H. Gibson, Does picosecond protein dynamics have survival value?, *Trends in Biochem. Sc.* 24 (1999) 253.
- (17) J. Broos, A.J.W.G. Visser, J.F.J. Engbersen, W. Verboom, A. van Hoek, D.N. Reinhoudt, Flexibility of enzymes suspended in organic solvents probed by time-resolved fluorescence anisotropy: Evidence that enzyme activity and enantioselectivity are directly related to enzyme flexibility, *J. Am. Chem. Soc.* 117 (1995) 12657.
- (18) M. Volini, P. Tobias, Circular Dichroism Studies of Chymotrypsin and Its Derivatives: Correlation of changes in dichroic bands with deacylation, *J. Biol. Chem.* 244 (1969) 5105.
- (19) B.W. Matthews, P.B. Sigler, R. Henderson, D.M. Blow, Three-dimensional structure of tosyl α chymotrypsin, *Nature* 214 (1967) 652.
- (20) P.B. Sigler, D.M. Blow, B.W. Matthews, R. Henderson, Structure of crystalline α -chymotrypsin. II. A preliminary report including a hypothesis for the activation mechanism, *J. Mol. Biol.* 35 (1968) 143.

- (21) J.J. Birktoft, D.M. Blow, The structure of crystalline α -chymotrypsin: V. The atomic structure of tosyl- α -chymotrypsin at 2\AA resolution, *J. Mol. Biol.* 68 (1972) 187.
- (22) T. Ikkai, T. Aarii, K. Shimada, Eximer fluorescence as a tool for monitoring protein domain dynamics applied to action conformation changes based on circularly polarized fluorescence spectroscopy, *J. Fluoresc.* 16 (2006) 367.
- (23) F. Meadow, N. Narayanan, G. Patonay, Determination of protein-dye association by near infrared fluorescence-detected circular dichroism, *Talanta* 50 (2000) 1149.
- (24) D. Mazumder-Shivkumar, K. Kahn, T.C. Bruice, Computational study of the ground state of thermophilic indole glycerol phosphate synthetase: Structural alterations at the active site with temperature, *J. Am. Chem. Soc.* 126 (2004) 5936.
- (25) J.K.A. Kamal, T. Xia, S.K. Pal, L. Zhao, A.H. Zewail, Enzyme functionality and solvation of subtilisin carlsberg: From hours to femtoseconds, *Chem. Phys. Lett.* 387 (2004) 209.
- (26) S.K. Hait, S.P. Moulik, Interfacial composition and thermodynamics of formation of water/isopropyl myristate water-in-oil microemulsions stabilized by butan-1-ol and surfactants like cetyl pyridinium chloride, cetyl trimethyl ammonium bromide, and sodium dodecyl sulfate, *Langmuir* 18 (2002) 6736.
- (27) W.M. Kati, R. Wolfenden, Contribution of a single hydroxyl group to transition-state discrimination by adenosine deaminase: Evidence for an "entropy trap" mechanism, *Biochemistry* 28 (1989) 7919.
- (28) R. Wolfenden, M. Snider, C. Ridgway, B. Miller, The temperature dependence of enzyme rate enhancements, *J. Am. Chem. Soc.* 121 (1999) 7419.
- (29) F.W. Westheimer, Mechanisms related to enzyme catalysis, *Adv. Enzymol.* 24 (1962) 441.

Chapter 9

Role of Hydration Barrier in the Biomolecular Recognition by Small Ligands

9.1. Introduction:

The interface between biological molecules (bio-interface) and its immediate environment has attracted researchers over a decade [1-9]. Many biologically important processes take place at bio-interfaces. These include transport, oxidation and reduction of molecules at cell membranes and the recognition of proteins and DNA by drugs. Since biomolecules are functionally active in their hydrated state [10], the hydration at the biological interface has received due attention [1,2,5-9]. Theoretical [6,7] and experimental [1,2,8,9] studies on hydration at bio-interfaces have revealed that the interfacial water molecules possess unique structure and dynamics. The interfacial waters are hydrogen bonded to the biomolecular interface and show slower dynamics than that of free water [7,8,11,12]. There exists a dynamic equilibrium between bound and free waters at a bio-interface [6,8]. This dynamic equilibrium is extremely sensitive to the external environment such as temperature and pressure. The slow component of solvation, τ_{solv} can be expressed as a function of temperature (Arrhenius equation) as,

$$\frac{1}{\tau_{\text{solv}}} \approx k_{\text{bf}} = \frac{k_{\text{B}} T}{h} e^{-\Delta G_{\text{bf}}^{\circ} / RT} \quad (9-1)$$

k_{bf} and $\Delta G_{\text{bf}}^{\circ}$ are the rate constant and binding energy for bound to free water interconversion, respectively, k_{B} , h are the Boltzmann and Plancks constants and T the absolute temperature. This equilibrium is responsible for the slow dynamics associated with the biomolecular interfaces, which play an important role in molecular recognition of the biomolecule by ligands [13,14].

It is relevant to mention in this regard that many naturally occurring bio-interfaces contain charged molecules with compensating counterions dissolved in adjacent aqueous phase. Classical examples are the cell membrane and the DNA. It is to be noted that

although dynamics of hydration plays an important role in molecular recognition of biological interfaces [8], favorable charge interactions also dictate molecular recognition at a charged bio-interface. The interaction of DNA with the protein histone [15], the interaction of anticancer and antihelmenthic minor groove binding drugs daunomycin and Hoechst 33258 (H258) [13] with DNA are important examples. Thus, there is interplay between electrostatic interactions and hydration at a bio-interface. The charge at the bio-interface leaves impression on the hydration structure [5] and dynamics [16]. In turn, the hydration at the biomolecular interface dilutes the electrostatic interaction between the charged interface and the oppositely charged ligand, preventing the approach of the latter towards the interface. The ligand thus resides in the hydration layer of the interface and reports environmental dynamics associated with the equilibrium between water molecules in different energy states. Although the effect of interfacial charge to surface hydration have been studied [5,16], but the interplay of charge and hydration in molecular recognition remains unexplored.

In this chapter, we explore the environmental dynamics reported by positively charged H258, which acts both as the model ligand and fluorescence reporter in negatively charged AOT reverse micellar interface at different temperatures to characterize the dominant forces in molecular recognition. Picosecond resolved fluorescence and polarization gated anisotropy have been used to characterize the binding of the H258 to the interface at different temperatures. The dynamics at the interface have been constructed from time resolved emission spectrum (TRES) at different temperatures.

9.2. Results and Discussion:

9.2.1. Interplay between Hydration and Electrostatic Attraction in Ligand Binding: Direct Observation of Hydration Barrier at Reverse Micellar Interface [17].

Figure 9.1 shows the hydrodynamic diameter of the AOT/isooctane reverse micelles (RMs) having $w_0=5$ at 20⁰C obtained from DLS experiments. The hydrodynamic diameter remains constant over a wide range of temperature (inset of figure 9.1). This suggests that the structural integrity of the RMs is retained even at higher temperatures

used in our study. H258 is a positively charged dye at neutral pH. The dye binds to the

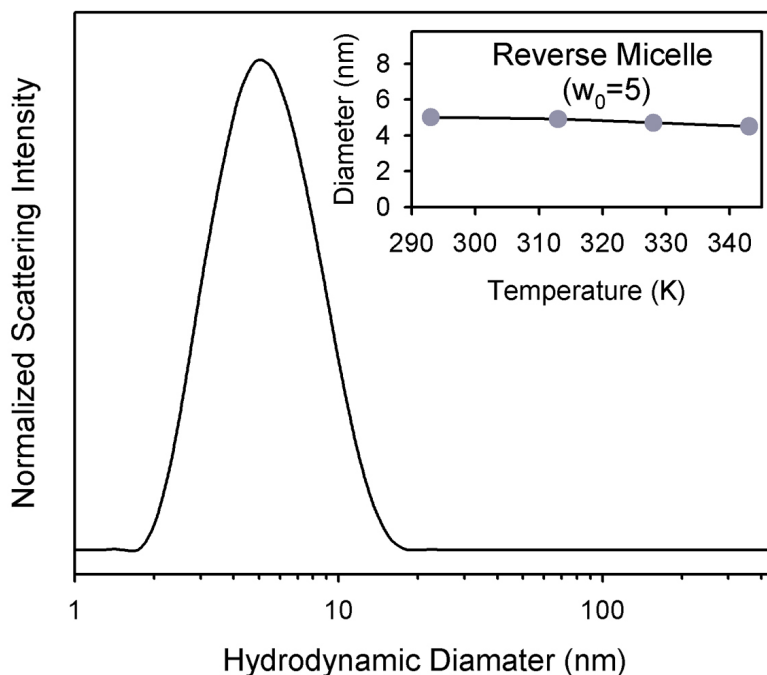


Figure 9.1. The DLS profile of reverse micelles ($w_0=5$) at 20°C and at different temperatures (inset). The black line in the inset is a guide to the eye.

negatively charged surface of SDS micelles and reverse micelles [18]. Figure 9.2(a) shows the absorption spectrum of the dye in reverse micelles with $w_0=5$ at different temperatures. It is seen from figure 9.2(a) that the peak corresponding to maximum absorption shows progressive blue shift with increasing temperature. The result is indicative of the fact that H258 moves towards the interface with increasing temperature. The location of the absorption dipole moment of the probe molecule makes it insensitive to the increased electrostatic interactions. The emission maximum remains constant in the temperature range 25°C - 45°C but become blue shifted at higher temperatures (figure 9.2(b)). This indicates that the excited state of the dye is destabilized at higher temperatures due to the decreased environmental polarity. In order to rationalize the results of the steady-state spectral measurements, it is essential to show that the dye remains in the reverse micelle at higher temperatures. H258 in bulk buffer, shows a

rotational lifetime, τ_{rot} of 500 ps, indicative of the free rotational motion [18]. At the interface of the reverse micelle, the twisting dynamics of H258 is frozen and the τ_{rot}

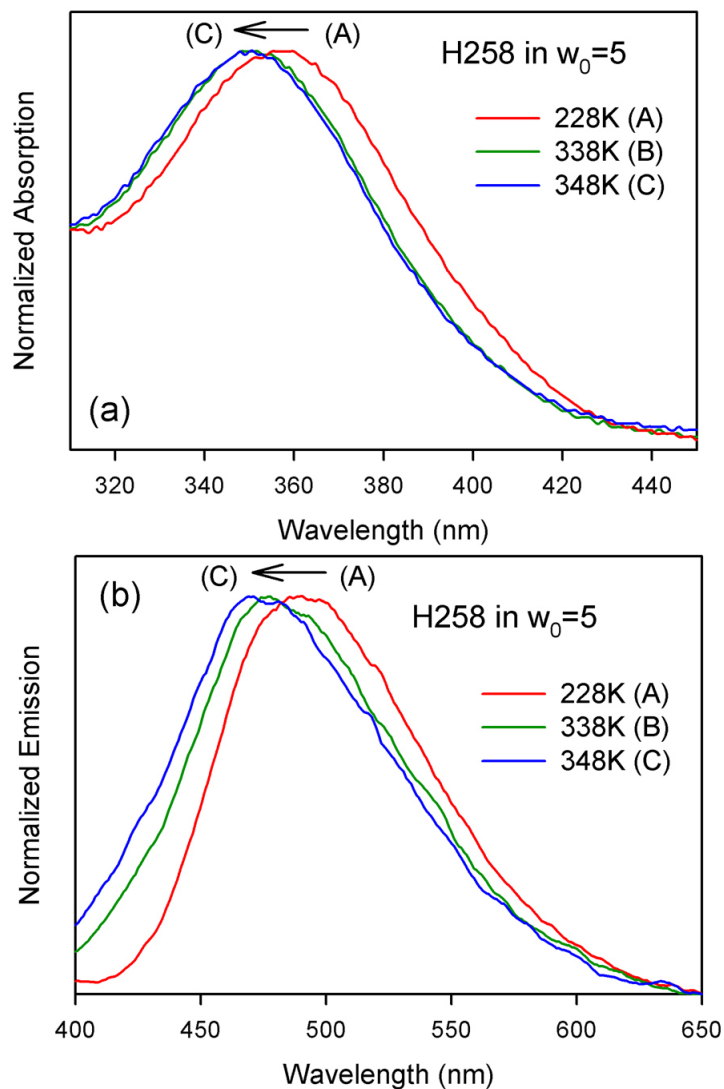


Figure 9.2. The absorption (a) and emission (b) spectra of H258 in reverse micelles at different temperatures.

obtained reflects the overall rotational dynamics of the reverse micelles [18]. At 15⁰C, (figure 9.3(a)) the global tumbling time associated with the reverse micelle is 5.10 ns. With increasing temperature, the rotational dynamics becomes faster. Figure 9.3(b) and Table 9.1 show the observed rotational lifetimes reported by the probe at higher

temperatures. The rotational lifetimes of AOT reverse micelles is independently calculated (Table 9.1) using the Stokes- Einstein -Debye equation,

$$\tau_{\text{rot}} = \eta V / kT \quad (9-2)$$

where η , V , k and T represents the viscosity coefficient, effective volume of the rotating species (here the reverse micelles), Boltzmann constant and absolute temperature respectively. The hydrodynamic radius (r_H) of the reverse micelles (used for the theoretical calculations) has been obtained from the relation $r_H = 0.2w_0 + \text{length of the surfactant chain}$ [19]. The calculated hydrodynamic radius, considering the length of the surfactant chain to be 1.1 nm [19], comes out to be 2.1 nm. The hydrodynamic radius of the RM obtained from DLS experiments (2.0 nm) is in close agreement with that of the estimated value. The viscosity coefficients of isooctane at different temperatures have been obtained from experimentally reported η values at different temperatures [20]. The good agreement of the experimental and theoretical values (Table 9.1, figure 9.3(b)) of rotational relaxation time constants suggest that H258 remains as an integral part of the RM at higher temperature and successfully reports its dynamics.

To explore the environmental dynamics of H258 at different temperatures, the temporal decay of the solvation correlation function, $C(t)$ is constructed. Figure 9.4(a) shows the $C(t)$ decay at 15⁰C. The average solvation correlation time, τ_{solv} (defined by $\tau_{\text{solv}} = a_1\tau_1 + a_2\tau_2$, where a_1 , a_2 represent the relative concentrations corresponding to

Table 9.1: Average Solvation Correlation Time, τ_{solv} and Rotational Time Constants, τ_{rot} at Different Temperatures

Temp (K)	τ_{solv} (ns)	τ_{rot} (experimental)(ns)	τ_{rot} (Stokes-Einstein-Debye equation) (ns)
288	1.66	5.10	4.51
298	1.46	4.08	3.84
308	1.33	3.52	3.39
318	1.24	3.27	2.97
328	1.25	2.55	2.64
338	1.40	2.51	2.42
348	1.57	2.45	2.21

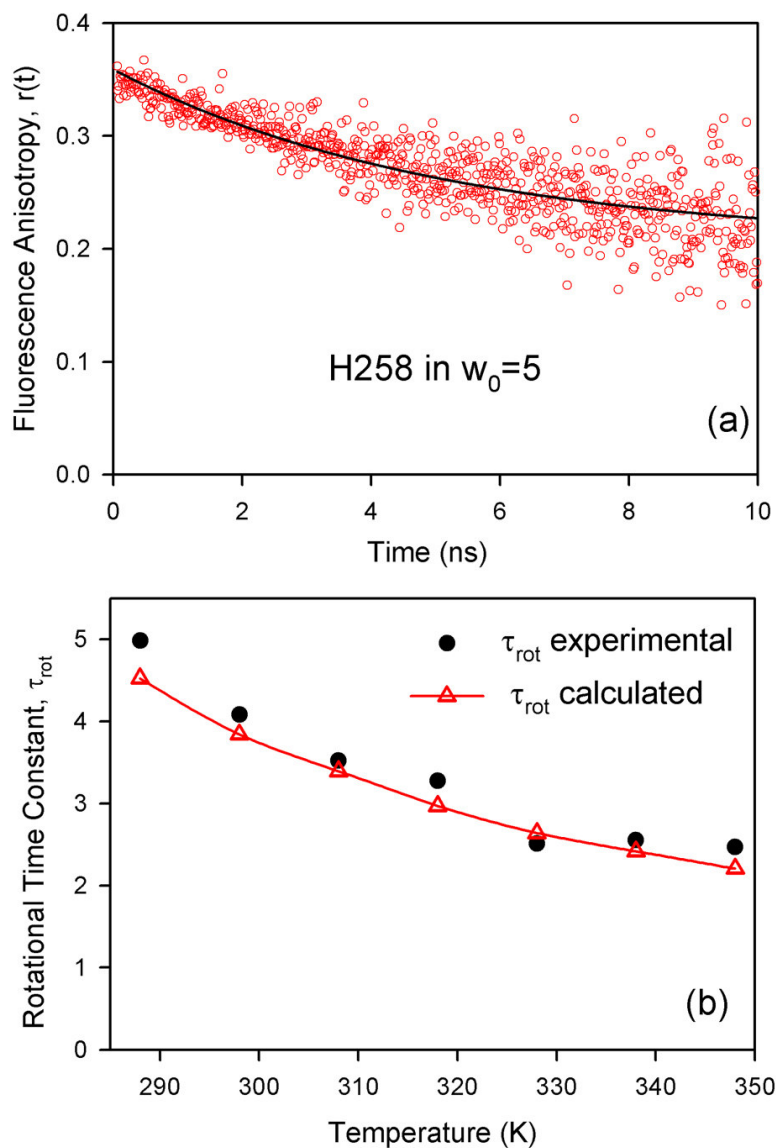


Figure 9.3. (a) The temporal decay of rotational anisotropy at 15°C. (b) The experimental (circles) and calculated (triangles) values of τ_{rot} of H258 in reverse micelles at different temperatures. The red line is a guide to the eye.

solvation times τ_1 and τ_2) associated with the decay is 1.69 ns, consistent with the slower dynamics of water at the reverse micellar interface [21]. With increase in temperature, upto 45°C, τ_{solv} becomes faster and reaches a plateau in the range 45°C-55°C. After 55°C, the τ_{solv} becomes progressively slower (Table 9.1). A plot of $1/\tau_{solv}$ against $1/T$, where T denotes the temperature in absolute scale is shown in figure 9.4(b). It is evident from the figure that upto 45°C the data agree well with the activation energy barrier model

(governed by the Arrhenius equation) for the dynamical equilibrium [6,22] between bound and free-type water molecules. The corresponding energy barrier of 1.9 kcalmol^{-1} is close to the value of $1.18 \text{ kcalmol}^{-1}$ for dynamical transition between head group bound water and interfacially bound water, obtained from simulation studies [22]. The result indicates that H258 is located in the hydration shell at the interface of the reverse micelle and the excited state relaxation of H258 essentially involves the transition between interfacially bound waters.

Table 9.2: Apparent Specific Volume, (ϕ_v) and Partial Apparent Adiabatic Compressibility, (ϕ_k) of Solubilized Water at Different Temperatures

Temperature (K)	$\phi_v (\text{m}^3\text{kg}^{-1})$	$\phi_k (\text{Pa}^{-1}\text{m}^3\text{kg}^{-1})$
293	8.63×10^{-2}	7.5×10^{-13}
303	8.69×10^{-2}	7.6×10^{-13}
313	8.78×10^{-2}	7.8×10^{-13}
323	8.93×10^{-2}	8.4×10^{-13}
333	9.10×10^{-2}	9.6×10^{-13}
343	9.30×10^{-2}	16.0×10^{-13}

In order to rationalize the deviation from the barrier crossing dynamics, it is essential to visualize the hydration shell at high temperatures. At higher temperatures, an increased fraction of the bound water molecules at the interface crossover an activation energy barrier to a less bound state. Densimetric and acoustic studies on the reverse micelles at different temperatures show that the apparent specific adiabatic compressibility, ϕ_k of solubilized water molecules in the reverse micelles increase drastically after 40°C (Table 9.2, inset of figure 9.4(a)). To estimate ϕ_k , we have used the effective medium theory [19] where solubilized water (corresponding to $w_0=5$) has been considered as a solute in AOT/isooctane environment. The increased compressibility of hydration water at higher temperatures is also observed at the interface of anionic SDS micelles [23]. The observations suggest that both the rigidity and the number of bound

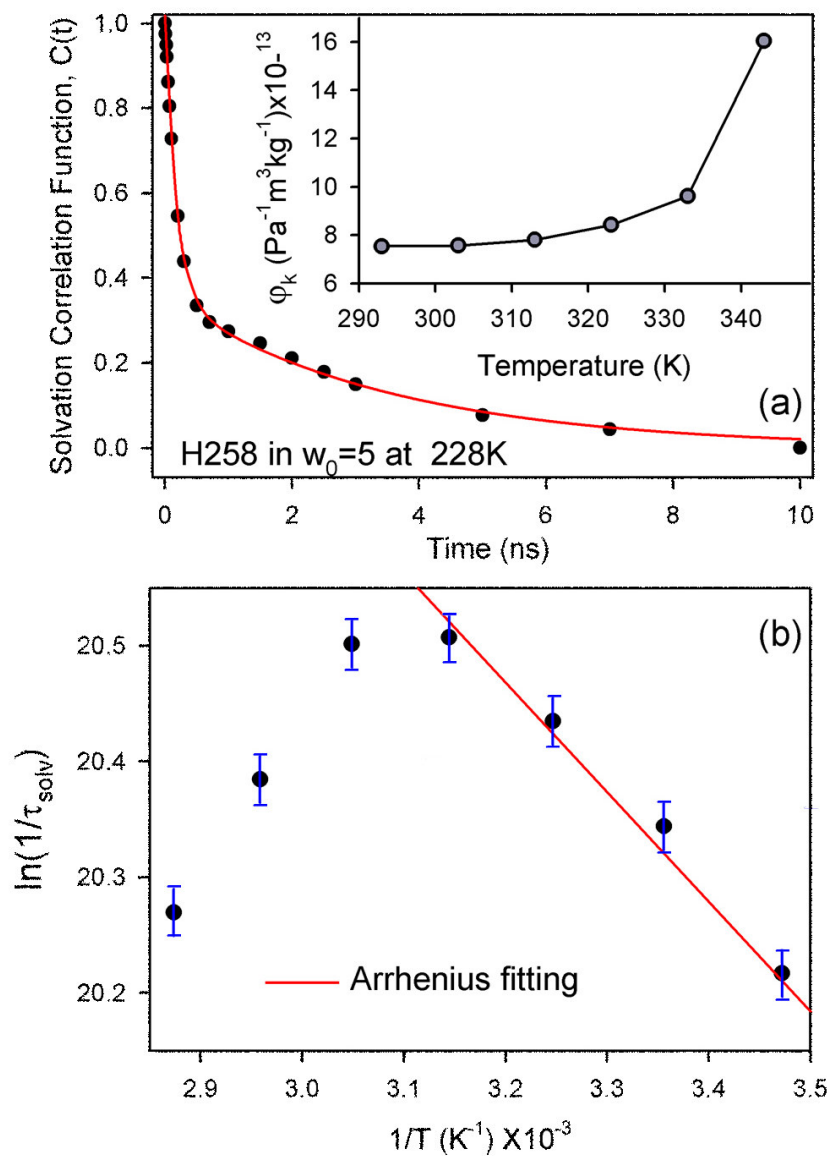


Figure 9.4. (a) The temporal decay of the solvation correlation function at 15°C . (inset) The variation of ϕ_k with temperature, the black line is a guide to the eye. (b) The plot of $1/\tau_{\text{solv}}$ against $1/T$, the red line is a fitting to the Arrhenius equation.

waters in the interfacial hydration shell are lost at higher temperatures. The hydration shell, thus, becomes soft at higher temperatures.

At this point, the role of hydration shell surrounding a charged ion needs to be discussed. The simplest example in this regard is the solvation of an isolated ion. Using femtosecond mid-infrared spectroscopy, Bakker et al. [24] studied the reorientation time of water in aqueous solutions with different concentrations of dissolved salt. They have

found out that the viscosity of an aqueous solution of MgClO_4 shows 30% increase compared to that in bulk water. The observed change in viscosity of the solution agrees well with the model that individual ions along with their first solvation shells are like rigid spheres rotating in bulk water. The reorientation time of water in the solvation shells is 7.6 ps which is slower than that of the bulk water (reorientation time = 2.5 ps). This observation very subtly gives the information that the influence of the charge of the central ion is discernible till its first solvation shell. In other words, the water in the first solvation shell screens the charge of the central ion. With this information, we can rationalize the behavior of the hydration shell at different temperatures. At lower temperatures, the intact hydration shell surrounding the charged surface screens the charge at the interface and effectively dilutes the electrostatic interaction between H258 and the oppositely charged interface. However, at higher temperatures, the soft hydration shell improperly screens the charge of the interface. The increased electrostatic attraction between the charged interface and the probe causes the probe to diffuse towards the interface. The diffusion of H258 to more hydrophobic regions of the interface is borne out by the spectral shifts associated with the steady-state spectra. The motions of the surfactant head groups contribute towards the solvation stabilization of the probe at high temperatures, when the probe is located closer to the interface. Thus, at higher temperatures, the motions of the charged head groups at the reverse micellar interface essentially overwhelm the dynamics reported by H258. The observed dynamics, therefore deviates from the Arrhenius model, which depicts the transformation of head group-bound water to interfacially bound water.

9.3. Conclusion:

In the present study the interplay between electrostatic attraction and dynamics of hydration in molecular recognition of negatively charged reverse micellar interface by positively charged H258 has been addressed. Upto 45⁰C, the environmental dynamics reported by the interface-binding probe H258 becomes progressively faster with increasing temperature and follows the Arrhenius equation. Above 45⁰C, the observed dynamics slows down with increasing temperature, thus deviating from the Arrhenius equation. The slower dynamics at higher temperatures is due to increasing contributions

from the motions of the surfactant head groups, indicating that the probe is closer to the interface at higher temperatures. This suggests an increasing electrostatic attraction between the ligand and interface at higher temperatures and is attributed to the change in hydration. Densimetric and acoustic studies, indeed, show a drastic increase in the apparent specific adiabatic compressibility of the water molecules present in RMs after 45⁰C, suggesting the existence of a softer hydration shell at higher temperatures. Thus, deviation from the Arrhenius equation has been monitored to understand the role of the hydration barrier to electrostatic attraction at the interface. Our studies indicate that the hydration layer at a charged interface act both as a physical and energetic barrier to electrostatic interactions of small ligands at the interface. Control of electrostatic interaction and hence molecular recognition at the interface of real biomolecules can also be developed by the design of other appropriate methods to alter the compressibility of the hydration shell.

References

- (1) S.K. Pal, J. Peon, A.H. Zewail, Biological water at the protein surface: Dynamical solvation probed directly with femtosecond resolution, *Proc. Natl. Acad. Sci. USA* 99 (2002) 1763.
- (2) S.K. Pal, J. Peon, B. Bagchi, A.H. Zewail, Biological water: Femtosecond dynamics of macromolecular hydration, *J. Phys. Chem. B* 106 (2002) 12376.
- (3) F.T. Burling, W.I. Weis, K.M. Flaherty, A.T. Brunger, Direct observation of protein solvation and discrete disorder with experimental crystallographic phases, *Science* 271 (1996) 72.
- (4) X. Cheng, B.P. Schoenborn, Neutron diffraction study of carbonmonooxymyoglobin, *J. Mol. Biol.* 220 (1991) 381.
- (5) V.M. Dadarlat, C.B. Post, Decomposition of protein experimental compressibility into intrinsic and hydration shell contributions, *Biophys. J.* 91 (2006) 4544.
- (6) N. Nandi, B. Bagchi, Dielectric Relaxation of Biological Water, *J. Phys. Chem. B* 101 (1997) 10954.
- (7) S. Pal, P.K. Maiti, B. Bagchi, Exploring DNA groove water dynamics through hydrogen bond lifetime and orientational relaxation, *J. Chem. Phys.* 125 (2006) 234903.
- (8) S.K. Pal, A.H. Zewail, Dynamics of water in biological recognition, *Chem. Rev.* 104 (2004) 2099.
- (9) G. Otting, K. Wuethrich, Studies of protein hydration in aqueous solution by direct NMR observation of individual protein-bound water molecules, *J. Am. Chem. Soc.* 111 (1989) 1871.
- (10) L. Zhao, S.K. Pal, T. Xia, A.H. Zewail, Dynamics of ordered water in interfacial enzyme recognition: Bovine pancreatic phospholipase A₂, *Angew. Chem. Int. Ed.* 43 (2004) 60.
- (11) X.J. Jordanides, M.J. Lang, X. Song, G.R. Fleming, Solvation dynamics in protein environments studied by photon echo spectroscopy, *J. Phys. Chem. B* 103 (1999) 7995.
- (12) M. Marchi, F. Sterpone, M. Ceccarelli, Water rotational relaxation and diffusion in hydrated lysozyme, *J. Am. Chem. Soc.* 124 (2002) 6787.

- (13) S.K. Pal, L. Zhao, A.H. Zewail, Water at DNA surfaces: Ultrafast dynamics in minor groove recognition, *Proc. Natl. Acad. Sci. USA* 100 (2003) 8113.
- (14) S.V. Ruffle, I. Michalarias, J.-C. Li, R.C. Ford, Inelastic incoherent neutron scattering studies of water interacting with biological macromolecules, *J. Am. Chem. Soc.* 124 (2002) 565.
- (15) D. Zhong, S.K. Pal, A.H. Zewail, Femtosecond studies of protein-DNA binding and dynamics: Histone I, *CHEMPHYSCHEM* 2 (2001) 219.
- (16) A.V. Benderskii, K.B. Eisenthal, Aqueous solvation dynamics at the anionic surfactant air/water interface, *J. Phys. Chem. B* 105 (2001) 6698.
- (17) D. Banerjee, S.S. Sinha, S.K. Pal, Interplay between hydration and electrostatic attraction in ligand binding: Direct observation of hydration barrier at reverse micellar interface, *J. Phys. Chem. B* 111 (2007) 14239.
- (18) D. Banerjee, S.K. Pal, Ultrafast charge transfer and solvation of DNA minor groove binder: Hoechst 33258 in restricted environments, *Chem. Phys. Lett.* 432 (2006) 257.
- (19) A. Amararene, M. Gindre, J.-Y. Le Huerou, W. Urbach, D. Valdez, M. Waks, Adiabatic compressibility of AOT [sodium bis(2-ethylhexyl) sulphosuccinate] reverse micelles: Analysis of a simple model based on micellar size and volumetric measurements, *Phys. Rev. E.* 61 (2000) 682.
- (20) A.A.H. Padua, J.M.N.A. Fareleira, J.C.G. Calado, W.A. Wakeham, Density and viscosity measurements of 2,2,4-Trimethylpentane (isooctane) from 198 K to 348 K and up to 100 MPa, *J. Chem. Eng. Data* 41 (1996) 1488.
- (21) H. Tan, I.R. Piletic, R.E. Riter, N.E. Levinger, M.D. Fayer, Dynamics of water confined on a nanometer length scale in reverse micelles: Ultrafast infrared vibrational echo spectroscopy, *Phys. Rev. Lett.* 94 (2005) 057405(1).
- (22) S. Pal, S. Balasubramanian, B. Bagchi, Identity, energy, and environment of interfacial water molecules in a micellar solution, *J. Phys. Chem. B* 107 (2003) 5194.
- (23) R.K. Mitra, S.S. Sinha, S.K. Pal, Temperature-dependent hydration at micellar surface: Activation energy barrier crossing model revisited, *J. Phys. Chem. B* 111 (2007) 7577.

- (24) A.W. Omta, M.F. Kropman, S. Woutersen, H.J. Bakker, Negligible effect of ions on hydrogen bond structure in liquid water, *Science* 301 (2003) 347.

List of Publications

1. **Debapriya Banerjee** and Samir Kumar Pal
“Excited State Solvation and Proton Transfer Dynamics of DAPI in Biomimetics and Genomic DNA”
J. Phys. Chem. A (2008) 7314.
2. **Debapriya Banerjee** and Samir Kumar Pal
“Conformational Dynamics at the Active Site of α -Chymotrypsin and Enzymatic Activity”
Langmuir 24 (2008) 8163.
3. **Debapriya Banerjee** and Samir Kumar Pal
“Molecular Recognition in Partially Folded States of a Transporter Protein: Temperature-Dependent Specificity of Bovine Serum Albumin”
Photochem. Photobiol. 84 (2008) 750.
4. **Debapriya Banerjee**, Sachin Kumar Srivastava and Samir Kumar Pal
“Spectroscopic studies on Ligand-Enzyme Interactions: Complexation of α -Chymotrypsin by 4',6-Diamidino-2-phenylindole (DAPI)”
J. Phys. Chem. B 112 (2008) 1828.
5. **Debapriya Banerjee** and Samir Kumar Pal
“Dynamics in the DNA Recognition by DAPI: Exploration of the Various Binding Modes”
J. Phys. Chem. B 112 (2008) 1016.
6. **Debapriya Banerjee** and Samir Kumar Pal
Solvation Dynamics of LDS 750 in Micelles, Reverse Micelles and Proteins”
Chem. Phys. Lett. 451 (2008) 237.

7. **Debapriya Banerjee**, Sudarson Sekhar Sinha and Samir Kumar Pal
“Interplay between Hydration and Electrostatic Attraction in Ligand Binding: Direct Observation of Hydration Barrier at Reverse Micellar Interface”
J. Phys. Chem. B 111 (2007) 14239.
8. **Debapriya Banerjee** and Samir Kumar Pal
“Direct Observation of Essential DNA Dynamics: Melting and Reformation of the DNA Minor Groove”
J. Phys. Chem. B 111 (2007) 10833.
9. **Debapriya Banerjee** and Samir Kumar Pal
“Simultaneous Binding of Minor Groove Binder and Intercalator to Dodecamer DNA: Importance of Relative Orientation of Donor and Acceptor in FRET”
J. Phys. Chem. B 111 (2007) 5047.
- *10. Ajay Kumar Shaw, Rupa Sarkar, **Debapriya Banerjee**, Susanne Hintschich, Andy Monkman and Samir Kumar Pal
“Direct Observation of Protein Residue Solvation Dynamics”
J. Photochem. Photobiol. A 185 (2007) 76.
11. **Debapriya Banerjee** and Samir Kumar Pal
“Ultrafast Charge Transfer and Solvation of DNA Minor Groove Binder: Hoechst 33258 in Restricted Environments”
Chem. Phys. Lett. 432 (2006) 257.

* Not included in thesis.